ANALYSIS OF AOSERP

PLUME SIGMA DATA

by

D. S. DAVISON

E. D. LEAVITT

Intera Environmental Consultants Ltd.

for

ALBERTA OIL SANDS ENVIRONMENTAL RESEARCH PROGRAM

ME 3.8.3

December 1979

TABLE OF CONTENTS

TABLE OF CONTENTS (CONTINUED)

TABLE OF CONTENTS (CONTINUED)

TABLE OF CONTENTS (CONCLUDED)

LIST OF TABLES

LIST OF TABLES (CONCLUDED)

LIST OF FIGURES

LIST OF FIGURES (CONTINUED)

LIST OF FIGURES (CONTINUED)

LIST OF FIGURES (CONCLUDED)

ABSTRACT

This analysis of AOSERP sigma data is an attempt to synthesize the available plume dispersion data from the AOSERP study region to derive a useful procedure for predicting the plume sigma values. The report includes a critical review of many of the more widely known sigma specification schemes and an analysis of the characteristics of the sensor systems used to collect the data. With such a background, the discrepancies which existed between the measured plume sigma values and the predicted values were more understandable.

The plume dispersion process was treated as a two-stage process with a source-dominated phase and an environmentally dominated phase. In the source-dominated phase, the plume rise and plume geometry are intimately related. It was found that the more recent formulations suggested by Briggs (1975) worked adequately for averaged values. The transition point from the source-dominated to environmentally dominated phases of dispersion (the sigma transition) could be clearly specified theoretically but would be difficult to do reliably in an operational or climatological mode.

For the environmentally dominated phase of dispersion, procedures were recommended for plume sigma specification. The Pasquill (1976) and the Draxler (1976) schemes were recommended for lateral dispersion. For vertical dispersion, the TVA scheme was recommended for stable and neutral conditions; the Draxler scheme was tentatively recommended for unstable conditions.

The effects of wind direction shear were carefully reviewed and were found to include centerline displacement, distortion of plume shape and shear-enhanced dispersion. All of these effects can be reflected in the time and space scales of the ground level concentrations.

The major areas of uncertainty which are of concern for sigma specification were identified as: prediction of mixing heights and lapse rates, the plume geometry in the range of 1 to 3 km downwind, the specification of plume geometry in the vertical in unstable conditions, and the significance of surface absorption of SO_2 upon ground

level concentrations. Specific recommendations were made for improved co-ordination for any future intensive field program.

ACKNOWLEDGEMENTS

This research project ME 3.8.3 was funded by the Alberta Oil Sands Environmental Research Program, a joint Alberta-Canada research program established to fund, direct, and co-ordinate environmental research in the Athabasca Oil Sands area of north-eastern Alberta.

1. INTRODUCTION

1.1 CONTEXT OF THIS STUDY IN AOSERP

The Terms of Reference for this study indicated that Gaussian models will be used for the first estimates of ground level concentrations in the Alberta Oil Sands Environmental Research Program (AOSERP) study area. Three intensive field programs have been undertaken to date (March 1976, February 1977 and June 1977). Much of the data from these studies have become available in AOSERP reports. The objective of this study was to utilize the available data set to generate a practical scheme for the specification of Gaussian plume sigma values in the AOSERP region. Thus, this study was the first synthesis of the data set and the first comprehensive review of the applicability of various sigma specification schemes to the AOSERP study region.

The specific tasks in the outline of work presented in the contract Terms of Reference are presented below:

> Obtain and examine all data relevant to plume dispersion which have been acquired in the study area such as:
>
> (a) direct plume spread measurements by aircraft
> (b) vertical plume spread measurements by photography
> (c) horizontal plume spread measurements by correlation spectrometer.
> (d) boundary layer turbulence measurements from a tethersonde.
> (e) bivane measurements from a 150 m tower.
> (f) turbulence measurements from instrumented aircraft.
>
> Derive sigma values from these data.
>
> Determine the means by which σ_y and σ_z values can be organized into a practical system for specifying Gaussian dispersion parameters.
>
> Assess the degree to which currently used diffusion typing schemes of Pasquill-Turner, Pasquill-Smith,

Brookhaven National Laboratory, Tennessee Valley Authority and Cramer can be used to parameterize these data when the required support data are available.

Intercompare simultaneous sets of data and assess the degree to which these data can be handled to support the interpolation schemes of Draxler and Briggs.

Develop the most promising approach into a useful procedure for predicting Gaussian dispersion parameters for use in plume modeling in the Alberta Oil Sands Environmental Research Program study area.

Recommend alternative programs of measurements which could be carried out in the AOSERP study area (a) on a field study basis and (b) on an intermittent or continuous basis which will enable the refinement of sigma calculations.

1.2 STRUCTURE OF THIS REPORT

This report has four major sections. The first section (Chapters 2, 3 and 4) is a review section presenting outlines of the major theoretical frameworks used in dispersion modeling, of commonly used specification procedures for dispersion parameters (Gaussian sigma values in particular), and of two mixing mechanisms that need special attention: initial plume-induced dilution and wind shear effects. The second section (Chapter 5) is a detailed examination of the inherent sampling characteristics and specific analysis techniques utilized for each data set considered in this study. In the third section (Chapters 6, 7 and 8) the observed data is compared to the various sigma specification schemes and the evidence of shear effects and directional dependencies of the sigmas is evaluated. The fourth section of the report (Chapters 9 and 10) outlines a recommended procedure for the calculation of

plume sigmas. It also presents specific recommendations for the measurement of routine data needed for the sigma specifications, for the design of objectives and organization of future field studies, and for specific modeling efforts needed for routine sigma specification. The highlights of the report are summarized in the Conclusions presented in Chapter II.

2. CHARACTERIZATION OF THE DIFFUSION PROCESS

2.1 THEORETICAL FRAMEWORKS FOR DISPERSION FORMULATIONS

A discussion of the major theoretical frameworks for dispersion leads to a better understanding of the approximations inherent in a Gaussian formulation and in some of the more theoretically based sigma specification schemes. Pasquill (1974) has presented a fairly comprehensive survey of the theoretical framework for dispersion formulations. In the following sections, a brief review is presented with emphasis on the level of theoretical support for commonly used approaches.

Pasquill (1974, p. 101 ff) identifies three major frameworks for the theoretical analysis of dispersion:

(a) gradient transfer
(b) Taylor's statistical theory
(c) similarity theory

The gradient transfer (k-theory) formulation is based upon the diffusion equation and upon the assumption that the eddy flux terms can be represented by a diffusion coefficient and a local gradient of concentration. It is based upon a particular physical model of mixing.

Taylor's statistical theory is a kinematic approach in which the behaviour of marked elements of the turbulent fluid is described by statistical properties of the fluid motion. It is based upon Taylor's solution for isotropic, homogeneous turbulence which involves the Lagrangian velocity correlation coefficients.

Similarity theory has developed from Monin-Obukhov similarity theory in the surface stress layer and is being extended by a number of groups into the whole mixed layer using Rossby number similarity and free convection scaling.

Pasquill has argued (see Pasquill 1975 p.5 and p.30) that the statistical theory is the only theory which can represent lateral dispersion for both a surface and elevated release. For a ground source, a gradient transfer approach and a similarity

approach (with some restrictions) can simulate vertical dispersion. For an elevated source, Taylor's theory is useful for vertical dispersion prior to impingement; the gradient-transfer relationships are adequate at larger distances, but no theory is adequate during the first stages of impingement (Pasquill's stage 2). However, it must be emphasized that these limitations are based upon the adequacy of rigorous theoretical developments. There is still considerable experimental guidance available and the numerical models can often be formulated to effectively utilize the experimental evidence over ranges in which there is little theoretical guidance.

2.2 TAYLOR'S STATISTICAL THEORY

Taylor's statistical theory is the only theoretical framework which has validity (according to Pasquill) for lateral spreading. In addition it is the basis of the most recently recommended procedures for determining σ_y (Hanna et al. 1977). However, the large diffusion time power law prediction, $(X^{\frac{1}{2}})$, can be shown to be representable in terms of an effective eddy diffusion coefficient for use in gradient-transport models. Thus it is appropriate to briefly review the basis of the theory.

The statistical theory of turbulent diffusion was largely developed by Taylor in the 1920's, who developed an expression relating particle displacements to the autocorrelation function for homogeneous, stationary turbulence;

$$\sigma_y^2 = 2\sigma_v^2 \int_o^T \int_o^t R(\xi)\, d\xi\, dt \qquad (2.1)$$

where T is the dispersion time and where R is the Lagrangian autocorrelation function of the appropriate velocity component. A similar equation relates σ_z to σ_w. At very short dispersion times, the Lagrangian autocorrelation coefficient is approximately unity and so

$$\sigma_y^2 = \sigma_v^2 \, T^2 \tag{2.2}$$

For large dispersion times, T, equation (2.1) reduces to

$$\sigma_y^2 = 2 \, \sigma_v^2 \, t_L \, T \tag{2.3}$$

where t_L is the Lagrangian integral time scale given by

$$t_L = \int_o^\infty R \, (\xi) \, d \, \xi \tag{2.4}$$

Thus the statistical theory predicts a large dispersion time behaviour of $\sigma_y \propto x^{\frac{1}{2}}$.

The physical basis for the change in the power law from X^1 to $X^{\frac{1}{2}}$ for increasing downwind distances, X, is based upon the increasing importance of the larger scales of motion for increasing downwind distances. At short times, all frequencies of turbulent motion contribute to the time-averaged dispersion. However, at larger times when the plume spread is large, the small scales of motion tend to be less and less effective at changing concentrations.

The form of the Lagrangian autocorrelation function for velocities is not well known. One of the major problems is the difficulty of obtaining Lagrangian (following the motion) measurements or of interpreting Eulerian (fixed point) measurements in terms of Lagrangian statistics. Pasquill (1974 p. 131) suggested that the problem of knowing the exact shape of the Lagrangian autocorrelation function was not too serious based upon an investigation of a range of possible forms. However, in a more recent evaluation, Pasquill (1975, p. 7 ff) suggests that a wider range of forms needs to be considered. In spite of these problems, several practical dispersion schemes have been developed from the statistical theory and will be discussed in a later chapter.

2.3 FORMULATIONS BASED UPON THE DIFFUSION EQUATION

2.3.1 Development of the Gaussian Formulations

The diffusion equation has been the starting point of most mathematical approaches and represents a generalization of the classical equation for conduction of heat in a solid. For an incompressible fluid (see for example Pasquill 1974 p. 108 ff)

$$\frac{\partial \overline{C}}{\partial t} + \overline{u}\frac{\partial \overline{C}}{\partial x} + \overline{v}\frac{\partial \overline{C}}{\partial y} + \overline{w}\frac{\partial \overline{C}}{\partial z} =$$

$$- \left[\frac{\partial \overline{(u'C')}}{\partial x} + \frac{\partial \overline{(v'C')}}{\partial y} + \frac{\partial \overline{(w'C')}}{\partial z}\right] \qquad (2.5)$$

where C is concentration and primed quantities are fluctuations about the mean (denoted by an overbar). Using a simple gradient-transfer assumption,

$$\frac{\partial}{\partial x}\overline{(u'c')} = \frac{\partial}{\partial x}\left(K_x \frac{\partial C}{\partial x}\right) \qquad (2.6)$$

If the K's are constant, independent of x, y, or z, then the diffusion process is called Fickian. For a steady source with a constant wind speed, $\overline{u}$, (2.5) can be written (see Sutton 1953 p. 134 ff)

$$u\frac{\partial C}{\partial x} = K_y \frac{\partial^2 C}{\partial y^2} + K_z \frac{\partial^2 C}{\partial z^2} \qquad (2.7)$$

The solution to (2.7) is

$$C\ (x,y,z) = \frac{Q}{4\Pi x\ (K_y K_z)^{1/2}} \quad \exp\left[-\frac{\bar{u}}{4x}\left(\frac{y^2}{K_y} + \frac{z^2}{K_z}\right)\right] \tag{2.8}$$

The solution can be written in terms of sigmas of the Gaussian distribution.

$$C\ (x,y,z) = \frac{Q}{2\Pi\ \sigma_y\ \sigma_z u} \quad \exp\left\{-\frac{1}{2}\left[\left(\frac{y}{\sigma_y}\right)^2 + \left(\frac{z}{\sigma_z}\right)^2\right]\right\} \tag{2.9}$$

where

$$\sigma_y = \left(\frac{2x}{\bar{u}} K_y\right)^{1/2} \tag{2.10}$$

However, experimental data on the atmosphere showed that the implied values of K varied with time of travel, position and with the scale of the diffusion process. Thus values of the sigmas have usually been specified empirically and so the Gaussian solution is not in general directly related to the Fickian form of the diffusion equation in (2.7).

An alternative derivation of the Gaussian equation arises out of the statistical theory (see for example Gifford 1975). If the form of the distribution of diffusing particles is normal or Gaussian, even if anisotropic, then the Gaussian distribution immediately follows. In this way the Gaussian distribution does not need to be related to the gradient transfer approach which is questionable for travel times which are not much larger than the Lagrangian integral time scale.

For practical applications, the Gaussian model must utilize some rather gross approximations. The formulation for an elevated source is only moderately more complicated than (2.10). However, after the plume impinges on the ground or reaches a trapping inversion, then fictitious virtual sources must be used (see Turner 1970 for example), to stimulate these boundary effects. The plume geometry is totally specified at any downwind distance

by two perameters. Thus the model cannot represent any profile other than an elliptical one in the YZ plane. Inspection of isopleths reveals that this is often not very accurate. Perhaps the major drawback is that stability, which defines the sigma values, must be specified in terms of a single stability class for the entire plume. Very often in the AOSERP region, the local stability varies with height through the vertical region in which the effluent plumes are found. This makes the selection of the appropriate σ_y and σ_z values from any formulation uncertain. Shears in wind speed in particular would be difficult to handle for any conceivable sigma specification scheme.

In spite of limitations as outlined above, the Gaussian model has seen wide application in industrial dispersion problems. Presumably this is due to its simplicity and economy of operation. Nevertheless, for many practical applications, "the Gaussian formula properly used, is peerless as a practical diffusion modeling tool" (Gifford 1975 p. 40). However, it is important to recognize that for many specific situations the Gaussian model is inadequate.

2.3.2 Application of K-theories

Considerable work has been done in the use of the gradient-transfer relationship in dispersion formulations. Corrsin (1974) provided a detailed review and stated that "the partial success of gradient transport models in turbulence is largely fortuitous and certainly surprising". The major obstacle to the application of the gradient-transfer hypothesis for practical dispersion problems is related to the changes with downwind distance in the size scales of the eddies which are effective in the mixing of the effluent.

A related concept is clear from the mathematics of the statistical theory, in which the contribution of various spectral ranges to the average particle displacement depends upon diffusion time, viz. (Pasquill 1974 p. 125):

$$\overline{X^2} = \overline{u'^2}\,\overline{T^2} \int_0^\infty F_L(n)\,\frac{\sin^2(\pi nT)}{(\pi nT)^2}\,dn \qquad (2.11)$$

where X is the deviation of a typical particle

T is the available dispersion time

$F_L(n)$ is the Lagrangian spectrum function for frequency n

The integral in equation (2.11) is a weighting function operating upon the turbulent velocity variance. The weighting function is the equivalent of averaging over a time, T, prior to computing the variance. The effect of higher frequencies becomes less and less important for larger dispersion times. The specification of the mixing of the plume, thus, depends upon how long the plume has had to disperse or equivalently, upon how large the plume is.

The classical gradient-transfer hypothesis may represent a slightly different limitation. The gradient-transfer hypothesis in the diffusion equation is of the form

$$\overline{v'C'} = K_y \frac{\partial C}{\partial y} \qquad (2.12)$$

One of the problems with the above hypothesis, is that the size scale of the gradient of the concentration is not large compared to the size scales responsible for the mixing. Thus one of the assumptions involved in the mixing length approach has not been met. Pasquill (1974) argues that fluctuations which are of a similar or larger scale than the material distribution will exert action such as convolution, systematic distortion and bodily movement and so it is inappropriate to represent such motions as a simple diffusion process. This physical arguement is not convincing if the time-averaged concentrations are considered. The larger size scales are important for the time-averaged concentrations as is shown by the statistical theory. Thus, their inclusion in a K-theory cannot be considered inappropriate.

The relationship in (2.12) can be valid at longer distances simply on dimensional grounds. Pasquill (1974, p. 126) indicates that the statistical theory can be properly represented by an "effective eddy diffusivity" of the form

$$K_x = \overline{u'^2}\, t_L \qquad (2.13)$$

for large diffusion times. It is clear from the statistical theory that the use of (2.13) for small diffusion times would be equivalent to neglecting the additional effects of the small scale eddies.

From an operational point of view, a K-theory model could work even if the gradient-transport hypothesis is questionable so long as the dispersive nature of the turbulence could be specified as a field variable independent of the source. However, as was seen above, the relative importance of size scales changes as the size of the plume changes. Thus close to the source a K-theory model may have serious problems. In many practical problems, however, the region close to the source is the region in which plume buoyancy effects are significant. Thus, for these situations no passive diffusion formulation is adequate and an initial dilution formulation following, perhaps, Briggs' (1975) approach is required.

Pasquill (1974 p. 103) reports on an independent derivation of the flux-gradient relation for momentum transfer by Monin (1965) based upon the Friedman-Keller equations. It was not clear on the physical interpretation of some of Monin's parameters outside of the surface-stress layer; however, Pasquill considers that the work represents a significant step in that it by-passes the necessity for a mixing length hypothesis in establishing a flux gradient relationship.

In summary, then, the constant-K or Fickian approach has been found to be inadequate and led to the development of the Gaussian formulation in which sigmas had to be specified as

functions of stability, source height (sometimes) and distance downwind. The assumptions normally required for a gradient-transfer relationship through a mixing length model are not met close to the source. The statistical theory, however, indicates that the large scale eddies contribute to the time-averaged concentration at all downwind distances and it is only the small scale eddies which become progressively less important for longer downwind distances. The large downwind distance limit of Taylor's statistical theory can be properly represented by an effective eddy diffusivity. Thus the use of K-theory models may be inappropriate only close to the source; in these situations source-dominated initial dilution is probably important, rendering any passive dispersion formulation inappropriate. There is an important distinction here between the use of the flux-gradient relationship in a numerical model (K-theory model) and the validity of a mixing length hypothesis.

The above discussion has only touched upon some of the developments in the gradient-transfer relationships. Calder (1965) showed that the K's should really be treated as second order tensors. A similar argument is presented by Pasquill (1974 p. 162) who suggests that the additional terms cannot necessarily be neglected. Other workers have discussed whether the K's for material diffusivity are closer to those for momentum or heat or water vapor. Thus the gradient-transfer approach is still in an ongoing stage of development.

2.3.3 The Role of the Gaussian Model

An important point in this brief review is that the Gaussian model involves many simplications and approximations. It is very unlikely that any simple analytical solution will be developed that accurately describes dispersion. The use of a Gaussian model is perhaps adequate for many purposes, especially if it can be verified with real data in the AOSERP region. The

selection of the appropriate sigmas can be guided by theoretical developments, experience in other areas, and the available AOSERP data base. The simplicity and economy of operation will probably mean that the Gaussian model will always have a role at least for computation of long term, average concentrations.

3. COMPLICATIONS FOR REAL SOURCES IN THE ATMOSPHERIC BOUNDARY LAYER

3.1 WIND DIRECTION SHEAR EFFECTS

A variation with height of the mean wind direction will have a distorting effect on the development of a plume. The first and most obvious effect is that the plume centerline projected on a horizontal plane appears curved. This displacement of the lateral position of the centerline can be important for computing locations of maximum ground level concentrations. As discussed in Slawson et al (1978) the displacement of the plume centerline may introduce an error in the determination of plume rise and plume σ_z determined from photography data. The magnitude of this error is discussed in a later section.

As the plume grows in the vertical direction, the lateral shear will cause a tilt in the plume with height. This shear or tilt in the plume combined with vertical mixing will lead to an enhanced lateral rate of growth of the plume. G.I. Taylor (1953) discussed the importance of this effect in relation to diffusion in pipe flow. Saffman (1962) used the methods of moments to solve the diffusion equation for the effect on longitudinal dispersion of $\partial\bar{u}/\partial z$. Pasquill (1969) considered Swedish data (from Hogstrom 1964) and concluded that the shear induced spread at X = 5 km was 14 % in neutral conditions and 22% in stable conditions. Hogstrom (1964) attempted to solve the problem by considering the affect of a mean velocity shear on the statistical behaviour of a typical particle. This work was extended by Smith (1965) whose results are discussed below. Using Smith's theory, Pasquill (1974) calculated downwind distances at which shear enhancement would become important for different values of the mean shear. He concluded that the typical minimum distance is around 10 km. This relatively large distance partially explains why very few observations of true shear enhancement have been made. In the following sections the effects of shear are discussed in terms of centerline displacement,

distortion of the plume cross-sectional shape and shear-enhanced dispersion. The data from AOSERP will be discussed in a later chapter.

3.1.1 Centerline Displacement

The most obvious effect of direction shear in the mean wind is the displacement of the center line as shown in Figure 1 The calculation of the displacement is straight-forward if the vertical profile of the horizontal wind field is known. From Smith (1965) the displacement of the plume centerline, y_c, during plume rise is given by:

$$y_c = \frac{1}{2} \Psi ZT + \overline{v'w'} Z/\sigma_w^2 \qquad (3.1)$$

where it is assumed that the lateral velocity v(Z) (= ΨZ) varies linearly with height and where $\psi = d\bar{v}/dz$. The second term on the RHS of the equation reflects the failure of a particle to adjust instantaneously to the mean velocity at the new level. Notice the correlation between v' and w' will be opposite to the direction of the wind shear. See Pasquill (1974) for a more complete discussion.

For long dispersion times, the second term can be neglected and since $T = X/\bar{u}$

$$y_c = \frac{1}{2} \frac{\Psi Z}{\bar{u}} X \qquad (3.2)$$

Substituting $\Psi Z/\bar{u} = \tan \alpha$ where α is the change in wind direction over the depth Z this expression becomes

$$y_c = \frac{1}{2} \tan \alpha \; X \qquad (3.3)$$

(a)

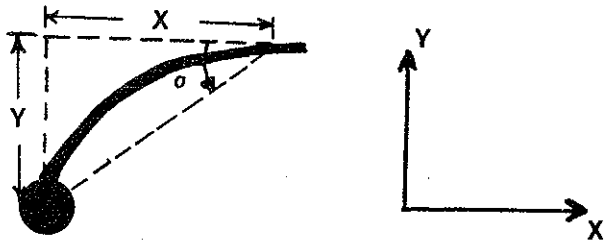

(b)

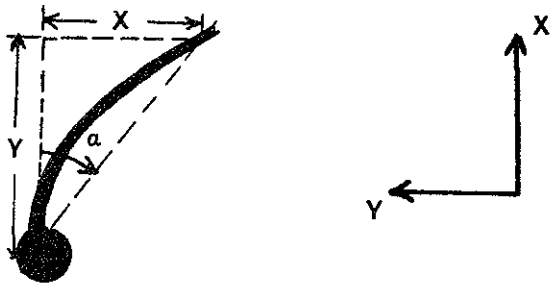

Figure 1 Plan views of centerline displacement. The formulation of (3.1) is independent of whether the X-direction (U-direction) is chosen based upon the wind direction at effective plume height (a) or at stack height (b).

For X = 1 km and $\alpha = 30°$ over the plume rise depth, the value of y_c is 290 m. This discussion assumed a linear plume rise in a constant shear layer.

3.1.2 Distortion of the Plume by Shear

At any downwind distance, the upper and lower edges of the plume will have different directions of motion in the presence of wind direction shear. This effect is analogous to the centerline change in direction with height and leads to a distortion of the plume in the form of a tilt of the plume cross-section.

If the plume thickness varies linearly with X and $v(Z) = \alpha Z$ the shear-induced tilt can be expressed as

$$\Delta y = \frac{1}{2} \tan \alpha \, X \qquad (3.5)$$

where Δy is the lateral displacement of the plume from the plume centroid at a vertical distance of ΔZ and α is the change in wind direction over the same vertical distance. This expression is identical to the expression for centerline displacement since the displacement ΔZ with respect to the plume centroid is analogous to the changing plume rise under the simplifying assumptions used here.

Measurements in shear conditions at large downwind distances are very rare. Brown and Michael (1974) reported on aircraft particulate concentration measurements from a power plant in shear conditions to a downwind distance of 26 km. In one case they measured the plume tilt at downwind distances of 3.6, 20.0 and 26.0 km under very stable conditions with a wind shear averaging 12° from the bottom to the top of the plume. The measured tilt can be represented as

$$m = \frac{\Delta Z}{\Delta Y} \qquad (3.6)$$

where m is the tilt,

ΔZ is the vertical extent of the plume, and

ΔY is the lateral distance between the centers of mass for the top and bottom traverses of the plume.

Since the wind information was presented in terms of an average wind turning through the average depth of the plume , then equation (3.5) can be written

$$mX = \frac{2\ \Delta Z}{\tan \alpha} \tag{3.7}$$

where average values of ΔZ and α (the total turning angle) are used in the right-hand-side of (3.7). The value of mX would then be considered as being constant with downwind distance. The comparison is shown in Table 1. The two values of mX at 20 and 26 km downwind are similar; however, the value at 3.6 km is much larger. There are several possible explanations for this discrepancy. At 3.6 km, the ΔY value is small and so errors in the position recovery system could result in significant errors in the value of m. In the very stable conditions of the measurements, the wind shear is probably variable in time and nonlinear with height. Thus the approximations involved in equation (3.7) may not be valid. Brown and Michael (1974) also calculated a "total σ_y" by combining the average single-level variance with the variance contribution from the tilt of the centers of gravity. This "total σ_y", however, should not be considered as an appropriate σ_y for a Gaussian formulation since it would generate a much larger volume than the volume of the tilted plume particularly at large downwind distances (see Figure 2).

A similar consideration is important in the use of σ_y values obtained from the COSPEC. The vertically-integrated COSPEC values are equivalent to Brown and Michael's total σ_y. Some of the analysis techniques (such as were used for the LIDAR) also led to σ_y's equivalent to vertically integrated values. The applicability

Table 1. Plume tilt under stable high-shear conditions as a function of downwind distance using data from Brown and Michael (1974)

Downwind Distance X (km)	Plume Depth ΔZ (m)	Plume Tilt m	mX (m)
3.6	195	0.40	1440
20.0	240	0.03	600
26.0	210	0.02	520

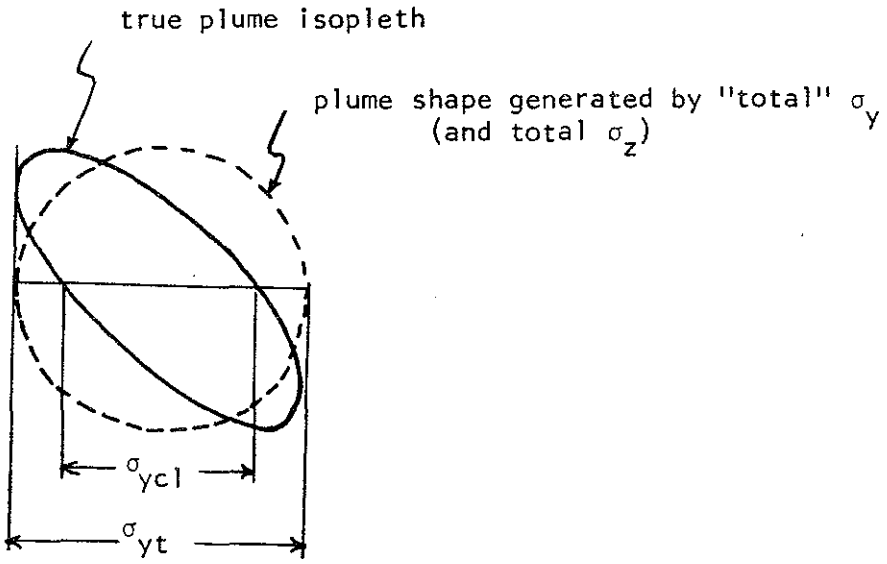

Figure 2. A comparison of the plume cross-rectional shape under shear conditions with a generated shape (dotted line) if Brown and Michael's "total σ_y" were used in a Gaussian formulation (along with an analogously defined total σ_z). An immersion sensor (e.g. an aircraft) would measure σ_{ycl} at the centerline compared to the total σ_y (σ_{yt}).

of these values will partly depend upon the importance of shear effects and will be discussed in a later chapter.

Another consideration in the Brown and Michael approach (see also Brown, Cohen and Smith 1972) is the appropriateness of taking average σ_y's from a variety of levels. If the cross-wind distribution were truly Gaussian, at every height, and if the turbulent mixing mechanisms were invariant with height, then the σ_y values at all levels would be the same even though the maximum concentrations varied with height. However, the actual cross-wind distribution will be a truncated form of Gaussian and any measurement system will have noise requiring the adoption of a noise limiter to truncate the measurement. These two effects will result in calculated σ_y values being less at the upper and lower limits of the plume. If the σ_y values were calculated at all levels by a second moment technique out to a fixed concentration isopleth (as suggested by Figure 18 in Brown et al. 1972), then the non-centerline σ_y values would be too small. The above effect may not always be large compared to the statistical sampling problem: however the "simple" σ_y variation with height in Figures 6, 7 and 8 of Brown and Michael (1974) suggests that it probably is important for that case study.

3.1.3 Shear-Enhanced Dispersion

As mentioned above the vertical tilt induced in the plume by the wind shear gives rise to enhanced horizontal spread due to the interaction between vertical mixing and the velocity shear. This interaction is most obvious if we consider what occurs to a plume during the transition from a stably stratified to an unstably stratified boundary layer. Due to the rapid mixing that occurs in the vertical during fumigation, it is apparent that a sheared plume will be mixed over a greater lateral distance and ground level concentrations will be lower than for an unsheared plume.

In the more general case, with limited vertical mixing, it is apparent that the shear-enhanced dispersion depends on the variation of shear with height and the variation of the vertical diffusivity along the path of the plume. Unless simplifying assumptions are made, solution of the problem will require use of relatively sophisticated numerical solutions of the diffusion equation.

One approach is that of Smith (1965) who applied the Taylor statistical treatment assuming homogenous turbulence and a linearly varying lateral velocity equal to Ψz. Smith developed the following expression for a shear flow bounded on the lower side and free on the upper side:

$$\sigma_y^2 = 2\,\sigma_v^2\,T\,t_{vL} + \frac{1}{6}\,\Psi^2\,\sigma_w^2\,t_{wL}\,T^3 \qquad (3.8)$$

where the first term is the long diffusion time statistical theory prediction for homogeneous turbulence and the second term is the effect of the wind shear. Since the second term varies as T^3 the shear term will eventually dominate and σ_y will then increase at a rate of $T^{1.5}$. Writing $\Psi = \bar{u} \tan \alpha/\Delta Z$, then, from (3.8),

$$\left(\frac{\sigma_s}{\sigma_t}\right)^2 = \frac{1}{12}\left(\frac{\tan^2 \alpha}{(\Delta Z)^2}\right)\left(\frac{\sigma_w}{\sigma_v}\right)^2\left(\frac{t_{wL}}{t_{vL}}\right)x^2 \qquad (3.9)$$

where $(\sigma_s/\sigma_z)^2$ is the ratio of the shear to turbulence contributions to the variance σ_y^2 as formulated in (3.8). Table 2 presents values of the ratio $(\sigma_s/\sigma_t)^2$ as a function of wind turning and downwind distance. The calculations in Table 2 assumed $\sigma_w = 0.6\,\sigma_v$ and $t_{vL} = t_{wL}$, following Pasquill (1974 p. 164). Although this ratio of σ_w/σ_v may be reasonable for surface layer turbulence, it may be inappropriate for typical plume heights. For stable conditions, σ_v should contain the contributions from the quasi two-dimensional eddies. The σ_w values may be very small

Table 2. Predicted values of the ratio of shear to turbulence contributions to the variance, $(\sigma_s/\sigma_t)^2$ using Smith's formulation and assuming $\sigma_w = 0.6\ \sigma_v$, and $t_{vl} = t_{wl}$.

Turning Angle α (degrees/100 m)	Downwind Distance (km) X: 1	3	10	30
2.5	0.01	0.05	0.58	5.2
5	0.02	0.21	2.31	20.
10	0.90	0.83	9.18	83.

in such cases. Thus the values in Table 2 may significantly overestimate the importance of shear enhanced dispersion. Further discussion of the variation of σ_s/σ_t is given by Pasquill. Table 2 suggests that for typical values of shear, a downwind distance of about 10 km is required for σ_y to be increased significantly over the turbulence value.

As mentioned above, solutions for more complicated boundary layer wind profiles require numerical solutions of the diffusion equation; see for example Csanady (1969) and Kumar (1978a). All of these reports suggest that shear effects can become important when X is of order 10 km. Kumar in particular finds that for elevated releases in neutral-stable stratification, the shear term can be dominant for X > 10 km. Note that all these models are applications of K-theory and the results will be sensitive to the selected profiles of velocity and eddy diffusivity.

In general, data to compare with the theory is very scarce. Randerson (1972) reports the observed spread of a nuclear debris cloud. The cloud spread approximately at $T^{0.5}$ for about 30 minutes after detonation. For approximately the next 12 hours puff spread was proportional to $T^{1.2}$ after which it again spread at $T^{0.5}$. The initial change in slope to a $T^{1.2}$ behaviour occurred approximately 15 km downwind of the detonation site. The wind shear was approximately 5°/100 m; comparison with Table 2 indicates some confirmation of the results of the above theoretical approximations.

It is interesting to note that the second transition to a $T^{0.5}$ behaviour was predicted by Csanady (1969) based upon the limitation of the wind shear in the vertical in the Ekman layer for dispersion times of the order of a couple of days. Both Csanady and Randerson quote the Randerson data in support of Csanady's model. However the wind sounding data taken during the experiment indicate that there was significant turning in the wind profile for about the first 18 hours after which the wind direction

was approximately constant through most of the cloud depth. So the decrease in slope to approximately the turbulence prediction may have been simply the result of the decreased wind shear. This emphasizes the limited experimental validation of shear effects.

The Brown and Michael (1974) work discussued earlier provides some observations of shear-enhanced dispersion. They divided their data into high shear and low shear cases. For the high shear cases ($\partial\alpha/\partial z \simeq 10°/100$ m), σ_y varied as $X^{0.88}$; for the low shear cases ($\partial\alpha/\partial z$ f $4°/100$ m), σ_y varied as $X^{0.79}$. However, they used the total σ_y of the sheared plume, including the affect of the vertical tilt of the plume. Thus the above power laws do not reflect a true shear-enhanced dispersion at a given height. There is one case study shown in the Brown and Michael paper which permits an evaluation of the true shear-enhanced dispersion. The values of "simple σ_y" are plotted in Figure 3. They have a power law dependence of $X^{1.3}$; the average wind shear through the plume depth was $6°/100$ m. If we assume that the transition to shear dominated dispersion occurred at about 6-10 km, then the two values at 20 and 26 km would have a power law-dependence closer to $X^{1.5}$ as predicted by Smith's theory.

In summary, there exists a theoretical framework from which the effects of shear can be estimated. There is some experimental validation of the theory. However, it must be noted that the conditions required to generate an $X^{1.5}$ power law for σ_y (linear change of the lateral wind component with height) may not often be met exactly in practice. Thus some variation from the 1.5 exponent can be expected.

3.2 PLUME RISE AND INITIAL DILUTION

It is widely recognized that the initial stages of plume dispersion are dominated by the source characteristics (Hanna et al. 1977). Thus any attempt to derive realistic estimates of plume sigma values and ground level concentrations must include a consideration of the initial source effects. The plume rise and

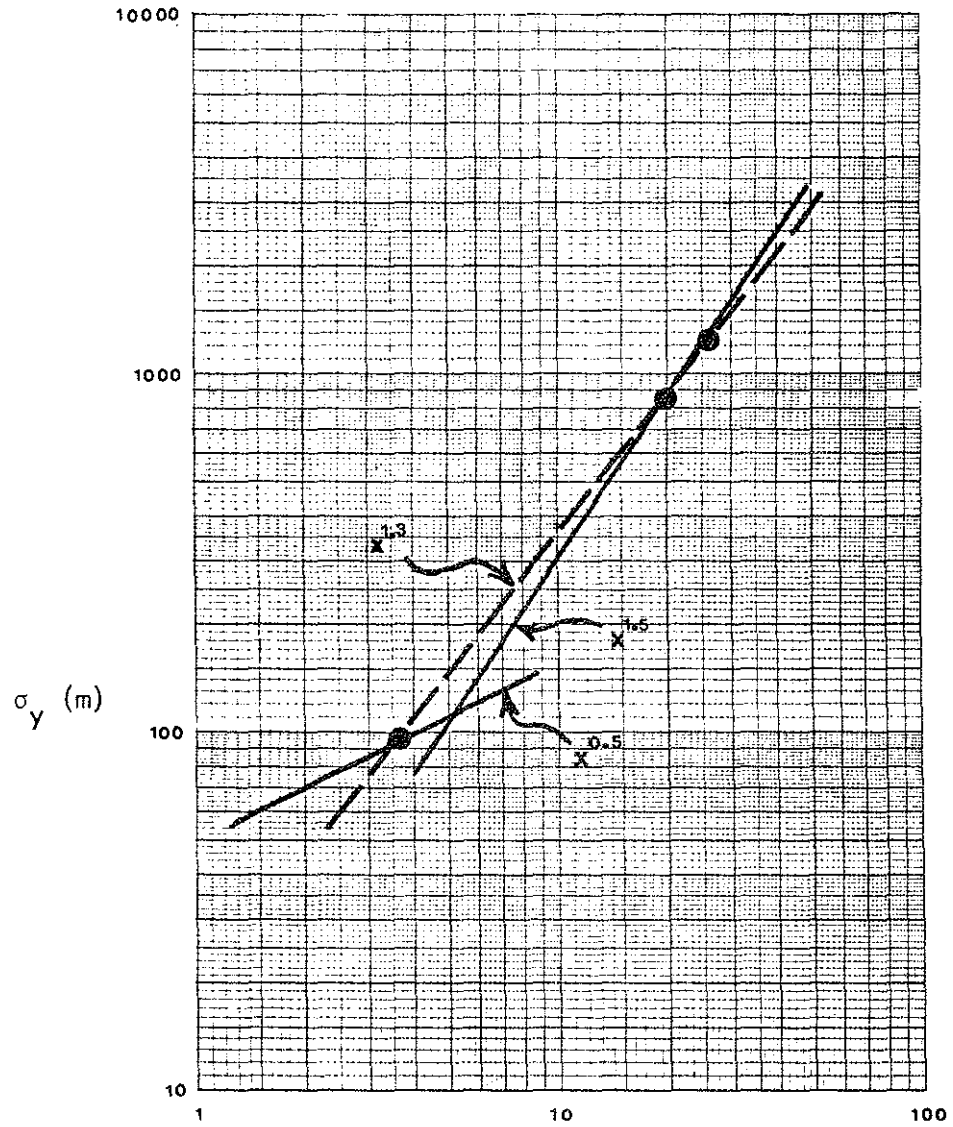

Figure 3. Data from Brown and Michael (1974) which show the effect of shear enhanced dispersion. A slope of $X^{1.5}$ is predicted by Smith (1965) for shear dominated dispersion. A slope of $X^{0.5}$ is the large-X power law dependence for Taylor's statistical theory (no shear effects). Smith predicts shear effects may become dominant for $X \geq 10$ km.

the plume dimensions during the initial plume-dominated stage of dispersion are intimately related. The rate of entrainment of ambient air determines both the plume cross-sectional size and to a large extent the plume rise. In any type of dispersion, the plume rise critically affects the ground level concentrations. Plume rise may also determine the strength of the dispersive mechanisms in a non-homogeneous boundary layer. In the following sections a brief review of plume rise and initial dilution theories is presented to provide a framework for the AOSERP measurements discussed in a later chapter.

3.2.1 Plume Rise from Conservation Equation Models

The study of plume rise and of the plume dimensions at short downwind distances was carefully reviewed recently by Briggs (1975) providing an updated reference from his earlier work (Briggs 1969). The review by Briggs indicates that plume rise theory has usually treated the effluent plume as an entity within a turbulent environment. Conservation equations and various closure assumptions were considered following the classical work by Morton, Taylor and Turner (1956). Only a brief summary of points pertinent to this study will be outlined below.

For a buoyant bent-over plume in neutral conditions, in the buoyancy-dominated phase of plume rise, Briggs (1975) recommends

$$\Delta H = C_1 \, F^{1/3} \, U^{-1} \, X^{2/3} \qquad (3.10)$$

where C_1 is an empirical constant with a recommended value of about 1.6, and where F is the buoyancy flux of the source given by

$$F = \frac{g}{To} \, (To - Ta) \, Vo \qquad (3.11)$$

where To is the absolute temperature of the efflux, Ta is ambient temperature and Vo is the source volume flux divided by Π.

Briggs (1975) discussed the concept of an effective volume flux in order to compensate for the motion of the air which is displaced by the rising effluent plume. In particular, he suggests that the plume has an effective radius, r, which is different from the visual radius. The numerical coefficient in (3.10) is derivable from theory relating back to plume radius,

$$C_1 = \left(\frac{3}{2\beta^2}\right)^{1/3} \tag{3.12}$$

where β is a parameter relating plume radius to plume rise, ΔH,

$$\beta = \frac{r}{\Delta H} \tag{3.13}$$

Briggs (1969) suggested a value of $\beta = 0.50$ based upon a review of observations, Bringfelt (1969) suggested a value of $\beta = 0.53$. However these experimental values refer to visual plume radii and not effective plume radii. These values of β lead to $C_1 = 1.82$ and 1.75 respectively.

Briggs suggests that the use of an effective value of r which is larger than the visual r, would lead to a larger value of β_{eff} and thus better agreement with plume rise observations. However, Briggs suggested value of $\beta = 0.6$ would correspond to a modified volume flux of only about 1.4 the unmodified flux. Thus the suggested change in the effective volume flux of a factor of 2.3 appears to be too large. The present authors feel that the wide variation in the experimental values of the coefficient, C_1, does not permit confidence in the specification of an effective value of β significantly different from the observed values, particularly since no consideration has been made of the Y/Z plane asymmetry (i.e. the eccentricity of the plume cross-section).

For a buoyant bent-over plume in stable conditions, Briggs shows that the conservation equations lead to a momentum

flux equation of the form of a damped harmonic oscillator. For calculations up to the point of maximum rise, Briggs (1975 p. 82) suggested

$$\Delta H = \left(\frac{3}{\beta^2 U s'}\right)^{1/3} \left[(\omega' F_m \sin(\omega' t) + F(1 - \cos(\omega' t))\right]^{1/3} \tag{3.14}$$

and

$$\Delta H_{max} = \left(\frac{3F}{\beta^2 U s'}\right)^{1/3} \left(1 + \left[1 + \left(\omega' \frac{F_m}{r}\right)^2\right]^{1/2}\right)^{1/3} \tag{3.15}$$

where s is an ambient stability parameter defined by

$$s = \frac{g}{\Theta_a} \frac{\partial \Theta_a}{\partial z} = \omega^2 \tag{3.16}$$

where Θ_a is the ambient potential temperature and ω is the Brunt-Vaissala frequency. F_m and F are the momentum and buoyancy fluxes of the source respectively, β is an empirical constant ($\simeq 0.6$) and primes on ω and s indicate that these quantities have been modified by the Briggs (1975) concept of effective momentum flux. (See Briggs 1975 for more details). Equation 3.15 presents an estimate of the height of the "overshoot" which is often observed in stable conditions. The final height of the plume in stable conditions was estimated by Briggs as $0.79\ Z_{max}$. The final plume rise, ΔH_f, from actual observations in stable conditions is (Briggs 1975),

$$\Delta H_f = C_2 \left(\frac{F}{Us}\right)^{1/3} \tag{3.17}$$

where C_2 is an empirical constant. The value of C_2 has a range of 1.8 to 3.1 (see Table 4 in Briggs 1975) and has a recommended value (Briggs 1975) of about 2.6.

The downwind distance to the point of maximum plume rise for the main GCOS powerhouse stack can be calculated from (3.14) for typical stable conditions. Equation (3.14) can be written as

$$\Delta H = \left(\frac{3F}{\beta^2 Us'}\right)^{1/3} \left((1 - \cos(\omega' t) + \frac{\omega' F_m}{F} \sin(\omega' t)\right)^{1/3} \tag{3.18}$$

If we choose a potential temperature gradient of 3°C/100 m and an average wind speed through the region of plume rise of 5 m/sec. then the downwind position of maximum plume rise for the GCOS powerhouse plume would be about 300 m. For a less stable situation (potential temperature gradient of 1°C/100m) with the same wind speed of 5 m/sec, the point of maximum rise is predicted to occur at about 550 m downwind. Thus for stable conditions, the plume rise associated with the GCOS powerhouse plume will be complete fairly close to the stack.

Briggs (1975) discussed plume rise for common stability situations found in real atmospheres. He approximated the plume cross-sectional structure by a rectangle and used this to consider partial penetrations of elevated inversions and rise through stable layers with arbitrary density profile. Such conditions are not unusual in the AOSERP region.

In convective conditions, there is some uncertainty as to how to define an effective stack height. Briggs has adopted a reasonable criterion in defining effective stack height as the plume height corresponding to maximum ground level concentrations. Note that this definition is strongly application-oriented and does not relate to a physical limitation of plume rise. Briggs

suggested that in convective conditions, the downward velocities which will determine ground impingement will scale with the convective scaling velocity

$$w_* = (H\, Z_i)^{1/3} \tag{3.19}$$

where Z_i is the height of the mixed layer and H is the product of heat flux and the buoyancy parameter

$$H = \frac{g}{T_a} \overline{w'T'} \tag{3.20}$$

With the assumption that the dissipation is determined solely by buoyant production and with the use of some approximate empirical values, Briggs suggested for effective plume rise in convective conditions,

$$\Delta H = 4.3 \left(\frac{F}{U}\right)^{3/5} (H)^{-2/5} \tag{3.21}$$

Although the model for convective conditions is very speculative, Briggs notes that it does indicate that convective turbulence is very important in limiting plume rise in only moderately unstable conditions. The transition to environmentally dominated dispersion will be discussed more fully later.

Although Briggs (1975) review is probably the most complete and balanced review available, there are other formulations for plume rise which are frequently used. Montgomery et al. (1972) presented an empirical formulation, often called TVA (1972), based upon the experience of the Tennessee Valley Authority. Another commonly-used empirical formulation is that by Holland (1953). Both the TVA and Holland formulations predict final plume rise only. One of the problems with such a formulation is that it is often difficult to determine experimentally when the plume has reached its final height.

3.2.2 Plume Dimensions during the Plume Entrainment Stage of Dispersion

Plume geometry, and in particular plume sigma values, close to the stack are largely determined by the mixing generated by the buoyant plume itself. The Pasquill-Gifford curves for Gaussian sigma values, on the other hand, are based upon data from the dispersion of passive tracers. The Pasquill-Gifford and most other dispersion curves reflect environmentally dominated dispersion at all downwind distances. Thus, it is important to understand and quantify the source-dominated phase of dispersion in order to generate a useful procedure for specifying dispersion coefficients.

The entrainment hypothesis which was used as the closure hypothesis for the conservation equations by Morton et. al. (1956) and by many others (see Briggs 1975, Table 1), was that the entrainment velocity, v_e, scaled with the mean vertical velocity of the plume, $\overline{w}_p$:

$$v_e = \beta \overline{w}_p \tag{3.22}$$

This assumption leads to

$$\frac{dr}{d\Delta H} = \beta \tag{3.23}$$

where r is the plume radius and β is an entrainment constant. The above relationship was confirmed by Briggs (1969) and Bringfelt (1969) who both found that the integration constant in 3.23 was small and that $\beta \simeq 0.5$ (Bringfelt, 0.53). Thus, the plume radius can be expected to scale with plume height and hence with $X^{2/3}$ in the plume-dominated phase of dispersion in neutral conditions:

$$\begin{aligned} r &= \beta \Delta H \\ &= \beta \left[\frac{3}{2\beta^2} \frac{F}{U} \right]^{1/3} t^{2/3} \\ &\doteq 1.0\, F^{1/3}\, U^{-1}\, X^{2/3} \end{aligned} \tag{3.24}$$

Briggs (1975) recommends the use of $r = \beta\Delta H$ for the stable case as well, noting that many of the more recent models use $v_e = \beta w$ to account for continued growth in the oscillatory stage after the maximum plume rise (e.g. Slawson and Csanady 1971). Note that since plume rise approaches its limit quite rapidly in stable conditions, this would mean that a simple power law for plume radius is inappropriate. The validity of the concept of entrainment, after the maximum rise rate is somewhat questionable and so the specification of plume radius by plume rise models at that stage of dispersion may not be appropriate. This point is discussed in more detail in the next section. For the purpose here, a reasonable approximation for stable conditions still appears to be $r = \beta\Delta H$.

There is still some uncertainty in the specification of σ_y and σ_z during the source-dominated phase of dispersion even if the visible plume depth can be estimated. Most plume rise models have used a plume radius without much consideration of the concentration profile within the plume. Briggs (1975) has suggested the presence of two counter-rotating vortices but none of the models simulates such a mechanism. The AES LIDAR images available for this study did not show such a structure even at a downwind distance of only 230 m. Thus the twin vortices are probably not always present. Bringfelt (1969) suggested a σ_y/σ_z ratio of about 2 even in the initial stages but his suggestion appeared to be based upon Hogstrom's (1964) work which was for a passive tracer cloud. Briggs (1975) has proposed an effective volume flux to include the air which must get out of the way of the rising plume; his suggested value for the ratio of the effective to actual volume flux, based upon Richards (1963), is 2.3. Possibly some of the discrepancy Briggs reports between the effective plume radius and the visual plume radius is due to an elliptical cross-section of the plume during the source-dominated phase of dispersion.

The identification of σ_z from the visible plume depth is also a problem. Most plume modelers have assumed a "top-hat" profile for the plume concentrations. For such a profile, the second moment standard deviation, σ_{TH}, is related to the total visual depth, D, of the plume by

$$D = 3.46\ \sigma_{TH} \tag{3.25}$$

The top-hat profile is perhaps not unreasonable for the well-mixed plume dominated by self-induced turbulence.

Interpreters of plume photography have often used the rather arbitrary 10% criterion. In this technique, the plume is assumed to have a Gaussian distribution and the visible plume edge is assumed to represent 10% of the centerline concentration. This assumption leads to

$$D = 4.3\ \sigma_G \tag{3.26}$$

where D is the visual plume depth and σ_G is the standard deviation using the 10% criterion. Pasquill (1974 p. 173 ff) has reviewed the evidence for a Gaussian shape of the plume at short distances for a passive tracer. He quoted Cramer (1957) to show that the standard deviation (second moment) and the plume edge as defined by the 10% criterion, on the average implied a Gaussian distribution. Note, however, that this did not imply that the visual edge was 10% of the centerline concentration. Gifford [in Slade, ed. (1968), p. 103 ff] outlined in some detail the procedures for photographic interpretation of plume photography in terms of opacity theory. Hogstrom (1964) adopted a similar approach for analysis of his plume photography data (for both σ_y and σ_z), but unfortunately his data were exclusively for passive tracers.

In summary, there is reasonable experimental evidence that visible plume thickness and plume rise have a constant ratio for both neutral and stable conditions for much if not all of the downwind distance to the transition point to environmentally dominated dispersion. The concentration profile during the

source-dominated stage of dispersion is not convincingly documented; Briggs' suggestion of counter-rotating vortices is not documented by the limited amount of LIDAR data available to this study. There is some uncertainty as to the specification of σ_z from visible plume thickness measurements; (this point will be considered in further detail in the discussion of plume photography data). There is little experimental evidence as to the ratio of σ_y to σ_z during the initial dilution phase; although Briggs' suggestion of an "effective radius" equal to about 1.5 of the visible radius suggests that σ_y may be larger than σ_z by as much as a factor of 2.3.

3.2.3 The Transition to Environmentally Dominated Dispersion

3.2.2.1 Sigma Transition and the Dissipation Criterion. For a practical scheme to specify dispersion coefficients, the transition point between dispersion dominated by plume buoyancy effects and environmentally determined dispersion must be specified. There has been considerable work directed towards determining the limitation of plume rise. This information is important for the determination of an effective stack height in dispersion models. The transition point for the change in dominance from the plume-generated mixing to ambient turbulence mixing (let us call this the sigma transition) is probably at a different downwind distance than the plume rise transition (or leveling-off) point. Very little experimental work has been directed towards determining the sigma transition; however some theoretical guidance is available.

The limits to plume rise have been reviewed by Briggs (1975). He suggested that in spite of numerous reports in the literature, there is no evidence that plume rise is limited in neutral conditions. Specifically, many workers have suggested termination of rise at some downwind distance x/L_b where L_b is a buoyancy length scale ($L_b = F/U^3$). Briggs claimed that data do not support this rise limitation in neutral conditions.

Slawson and Csanady (1967) suggested a three stage plume rise in which plume entrainment reflected changes in the turbulent spectrum dominating dispersion. In their second and third stages, the closure hypotheses for the conservation equations were assumptions relating the rate of plume radius growth to ambient turbulence characteristics. Briggs (1964) (and again in Briggs' 1969 review) had an equivalent procedure utilizing an inertial subrange relative dispersion formulation (Pasquill's 1974 "accelerated growth" phase). Briggs (1975 p. 75) now considers that the above entrainment assumptions predict too gradual a transition and recommends an end to the self-structured plume rise when the dissipation inside the plume equals ambient dissipation.

The concept of entrainment as applied to plume models has physical limitations, which Briggs' earlier work and the Slawson/Csanady model do not recognize. The concept of a plume entraining ambient air is reasonable only if the plume has a distinctive structure and a dynamic boundary. The plume will rather quickly assume the low frequency motions of the wind spectrum. It is only at the size scales of the plume itself that a comparison of ambient and internal plume motions is useful. The turbulence generated in the plume will arise from vertial velocity shears at the plume boundaries and by internal thermal inhomogeneities in the plume. As the rate of plume rise decreases the energy source for plume turbulence will be less and less. Thus eventually, the level of turbulent energy production in the atmosphere will equal and then exceed the turbulent energy production in the plume. At this point, the turbulent eddies in the atmosphere will be as vigorous as the dominant eddies of the same size in the plume. The plume will be unable to sustain any internal circulation and will not even be distinguishable in terms of eddy structure. The plume may still be identifiable by a slight heat excess and by gas constituent differences but dispersion at this time will be determined by ambient turbulence. Beyond this sigma transition point, it is inappropriate to use an entrainment concept.

Entrainment is really dispersion and at this point the plume is no longer a distinct entity as far as dispersion is concerned.

Briggs (1975) applied the dissipation criterion to determine plume "break-up" and the termination of the self-structured phase of plume rise. The same dissipation criterion is used by Briggs for both neutral and convective situations. The only difference is that the dissipation, ε, is determined in the neutral case by mechanical turbulent energy production and in the convective case by convective turbulent energy production. There is some question as to the validity of applying a convective formulation close to the ground except in very low wind speed cases and also to the validity of neglecting other terms in the turbulent energy equation. However, the principle of comparing dissipation inside the plume to the ambient value is probably useful for the specification of the sigma transition.

3.2.3.2 Dissipation Levels in the Atmosphere. Dissipation is often considered to be a measure of the total amount of turbulent energy in the field. Dissipation appears in the energy equation as in the following approximate equation:

$$\left[\begin{array}{l}\text{Time rate of}\\ \text{change of}\\ \text{turbulent}\\ \text{energy}\end{array}\right] = \left[\begin{array}{l}\text{Mechanical}\\ \text{energy}\\ \text{production}\end{array}\right] + \left[\begin{array}{l}\text{Thermal energy}\\ \text{production or}\\ \text{sink}\end{array}\right] + \left[\begin{array}{l}\text{Vertical}\\ \text{divergence}\\ \text{of turbulent}\\ \text{energy}\end{array}\right] + \left[\text{Dissipation}\right]$$

More detailed descriptions are available in any standard atmospheric turbulence text such as Lumley and Panofsky (1964) or Tennekes and Lumley (1972). At AOSERP, at typical plume heights, the time rate of change was generally small except near the edge of the mixed layer. Within the mixed layer, dissipation, ε, has often been found to be nearly constant (Lenschow 1970 , Kaimal et al. 1976) for fully convective boundary layers. This implies that the vertical divergence of turbulent kinetic energy changes with height to balance the decrease of heat flux with height associated

with boundary layer heating. However, at AOSERP, at typical plume heights, dissipation was usually found to decrease with height (Davison and Grandia 1978). This decrease of dissipation with height was reproducible and showed significant and consistent temporal changes throughout the day (see for example Figure 24 in Davison and Grandia 1978 for a clear sunny midday run on June 19 1977). These data suggest that free convection scaling may occur only rarely in the AOSERP region. Pasquill (1975 p. 27) reviews recent data by Caughey and Readings (1974) which suggests that it would be inappropriate to neglect roughness effects on σ_z until a height Z_c given by $Z_c = 10L$ where L is the Monin-Obukhov length. Deardorff and Willis (1975) adopted the criterion that 9/10 of the mixed layer should be above Z_c in order to apply free convective scaling. Thus the criterion on height of the mixed layer for free convection scaling becomes

$$Z_i \geq 10\, Z_c \doteq 100\, L \qquad (3.28)$$

Although there were no reliable measurements of the surface Monin Obukhov length, L, a reasonable estimate based upon the aircraft turbulence statistics for the June 19 afternoon case would be about 30 to 40 m. There were no measurements of the mixing height (it was greater than the limit of minisonde data and aircraft traverses); however, it is likely that Z_i did not reach 3 to 4 km. Thus the Willis and Deardorff criterion would suggest that the effects of mechanical turbulence were not negligible, in agreement with the aircraft dissipation measurements. The Caughey and Readings criterion would suggest that for the June 19 case, the plume sigmas would also be affected by mechanical turbulence.

It is clear then that the specification of dissipation in the atmospheric will almost always involve both mechanical and thermal contributions. For a purely mechanically mixed neutral surface boundary layer (see for example Lumley and Panofsky 1964)

$$\varepsilon \simeq \frac{u_*^3}{kz} \tag{3.29}$$

where u_* is the friction velocity and k is Von-Karman's constant ($\simeq 0.4$). By use of a drag coefficient we can estimate a neutral value of ε

$$\varepsilon_n \simeq \frac{(C_D \overline{U}_{100}^2)^{3/2}}{kz} \tag{3.30}$$

where the subscript 100 refers to values at 100 m AGL and where C_D is a drag coefficient evaluated at 100 m. Equations (3.29) and and (3.30) imply a balance between local production of kinetic energy which would only be approximately valid in the constant flux surface layer of a neutral atmosphere. At typical plume heights the vertical divergence of kinetic energy would probably be important and dissipation values might be less than predicted by (3.29) and (3.30). Briggs quotes Herbert (1971) in which ε was observed to decrease linearly with height for near neutral conditions from heights of 150 m to 1200 m.

For free convective scaling, the dissipation, ε_c is given by

$$\varepsilon_c \simeq 0.04\ H \tag{3.31}$$

where

$$H = \frac{g}{T_a} \overline{w'T'} \tag{3.32}$$

In stable conditions, the dissipation, ε, will decrease quite rapidly with height. Complete turbulent energy budgets are very rare for typical plume heights under stable conditions and so no explicit analytical expression is available.

The above discussion indicates that the specification of environmental dissipation values at plume height is uncertain. The theoretical formulations for neutral and free convection do provide some guidance. In addition the aircraft measurements of dissipation (Davison and Grandia 1978) can be used in specific case studies to roughly test the validity of the dissipation criterion. Fortunately, the plume's internal dissipation tends to decrease rapidly with distance and so quite large uncertainties in the

environmental value of dissipation will not lead to large uncertainties in the sigma transition point.

3.2.3.3 Dissipation Levels in the Plume. The dissipation value inside the plume can be estimated from a potential energy approach. The buoyant potential energy production per unit mass when the parcel moves over a vertical distances Δz is

$$PE = \frac{\rho'}{\rho} g \quad \Delta z \tag{3.33}$$

where ρ' is the density differential of the effluent compared to ambient. For a plume, at a given downwind distance, the buoyant energy production rate, P_c, per unit mass, is given by

$$P_c = \frac{T'}{T_a} \quad g \; W \tag{3.34}$$

where T_a is ambient temperature and W is the local vertical velocity of the plume with temperature excess T'.

For a neutral atmosphere, dilution and temperature excess of the diluted plume will vary linearly. Thus for the total plume the product of temperature excess and volume flux will be a constant. For the total plume, the buoyant energy production rate per unit mass is

$$P_c = \frac{F \; W}{V} \quad \left(\frac{T_o}{T_a}\right) \tag{3.35}$$

where F is the initial buoyancy flux, W is the local rise rate, V is the local volume flux and T_o/T_a is the ratio of effluent (at the source) to ambient temperatures. Note that the definitions of F and V could both include factors of π unlike Briggs' definition of F or V, but these will cancel out.

Equation (3.35) can be simplified using the $X^{2/3}$ law for plume rise to evaluate W:

$$\Delta H = 1.6\, F^{1/3}\, \bar{U}^{-1}\, X^{2/3} \tag{3.36}$$

$$W = 1.07\, F^{1/3}\, X^{-1/3} \tag{3.37}$$

The local volume flux can be written (without the Π factor)

$$V = r^2\, \bar{U}$$

$$= \beta^2 (\Delta H)^2\, \bar{U}$$

$$= \beta^2\, (1.6)^2\, F^{2/3}\, U^{-1}\, X^{4/3} \tag{3.38}$$

where use has been made of the expression

$$r = \beta\, \Delta H \tag{3.39}$$

Equation (3.35) can now be written

$$P_c = \frac{1.07}{\beta^2\, (1.6)^2} \quad \frac{T_0}{T_a} \quad F^{2/3}\ \bar{U}\ X^{-5/3} \tag{3.40}$$

An assumption must now be made as to what fraction, K_1, of the buoyant potential energy is available for turbulence production. Briggs (1975 p. 75) suggests a value of 0.7 following Richards (1963). Then if we can assume that the dissipation in the plume ε_p, is equal to the local rate of buoyant production, then

$$\varepsilon_p = \frac{K_1\ \ 1.07}{\beta^2\, (1.6)^2} \quad \frac{T_o}{T_a} \quad F^{2/3}\, \bar{U}\ X^{-5/3} \tag{3.41}$$

The value of β recommended by Briggs (1975) is 0.6 based upon a comparison of plume rise predictions to observations. Values of β based upon visual plume thickness average about 0.5 (Briggs 1969) to 0.53 (Bringfelt 1969).

Adopting $\beta = 0.6$ and $K_1 = 0.7$, the prediction for dissipation inside the plume becomes

$$\varepsilon_p = 0.81 \frac{T_o}{T_a} F^{2/3} \bar{U} X^{-5/3} \quad (3.42)$$

Briggs (1975) recommended another expression for ε_p based upon scaling arguments:

$$\varepsilon_p = \eta \frac{\bar{w}^3}{\Delta H} \quad (3.43)$$

where η is an empirical constant.

When the plume rise expressions for neutral stability is used, this becomes

$$\varepsilon_p = 0.77 \eta F^{2/3} \bar{U} X^{-5/3} \quad (3.44)$$

Briggs evaluated the constant η using a potential energy argument similar to the one leading to equation (3.42) with some additional speculation on the distribution of energy within the plume; Briggs suggested η=1.44 leading to a numerical coefficient of 1.1 in equation (3.44). For the GCOS stack $T_o/T_a \simeq 2$; this levels to a numerical coefficient in (3.42) equal to 1.6. The discrepancy between these two numerical values is an indication of the sensitivity of the result to minor changes in the assumptions needed to derive expressions for in-plume dissipation estimates.

There is one experimental value which can be used to test the above estimates for in-plume dissipation values for the GCOS powerhouse plume. On June 22 1977, in the early evening run, the aircraft traverse of the plume indicated substantially larger dissipation values inside the plume than in the ambient air (see Davison and Grandia 1978). Surface convective support had ceased and so ambient conditions were near neutral with low turbulence values. Two consecutive traverses through the plume at 3.6 km

indicated in-plume ε values of 52 and 65 (cm^2 sec^{-3}) compared to ambient values of about 13 ± 2 (cm^2 sec^{-3}) (error indicates standard deviation of the mean value of 12 blocks). Evaluating the expression for ε_p from (3.42), $\varepsilon_p \simeq 23$ ($cm^2 sec^{-3}$). Allowing for 10% uncertainties in wind speed and downwind distances, then the predicted ε_p is still less than about 30 (cm^2 sec^{-3}). The plume showed no apparent increased dissipation values at 8.0 km on the same runs. For an $X^{-5/3}$ decay rate, the 3.2 km observed values would be predicted to be about 13 cm^2 sec^{-3} at 8.0 km which is the ambient value. Thus the 8.0 km value is of no help in validating the theoretical estimate of ε_p. Thus the one experimental value suggests that the dissipation formulations may be underestimating the in-plume dissipation by as much as a factor of 2. Agreement with the observed ε value would require $\beta_1 = 0.36$ (allowing for implicit β dependence in the 1.6 and 1.07 factors) which would lead to a C_1 coefficient for plume rise of 2.3, which is larger than found by most investigators. Considering the crudeness of the handling of the turbulence terms in the conservation equations for plume rise and the simplicity of the assumed geometry, the apparent discrepancy is not too surprising. More than one fortuitous case of in-plume dissipation levels are needed, however, to substantiate the possible shortcomings of the theoretical approach.

3.2.3.4 Specification of the Transition to Environmentally Dominated Dispersion. The previous sections have presented arguments, largely based upon Briggs (1975), that the transition point to environmentally dominated dispersion is determined by the relative magnitudes of the in-plume to ambient dissipation. Departing from Briggs and Slawson and Csanady (1967), the present authors have argued that the entrainment concept is invalid beyond this transition point. The specification of the ambient dissipation values at typical plume heights was seen to be theoretically simple for the mechanical mixed atmosphere and for free convection scaling.

However, for many practical situations, atmospheric dissipation is not easy to specify.

The specification of the in-plume dissipation levels were sensitive to the details of the assumed conditions for their calculation. The one experimental value available suggested that the predicted in-plume dissipation values were about a factor of 2 or 3 too small.

The above summary suggests that even through the specification of the sigma transition in terms of dissipation values is appealing theoretically, it may be difficult to specify it reliably in many practical situations. It should be possible to determine the in-plume dissipation values by measurements under a variety of stability conditions. This could be done by aircraft or acoustic doppler radar. Except for stable conditions, a rough estimate of the ambient dissipation value can be made from an approximate energy balance equation. In stable conditions, the ambient dissipation values will be small. In these situations, the low frequency, nearly two-dimensional, oscillations in wind direction and wind speed will be the important mixing parameters for elevated plumes. In most of the stable situations, significant ground level concentrations would occur only during fumigation and inversion break-up when the neutral or convective schemes might apply. Thus the limitations for environmental dissipation specification on stable conditions may not be too severe for practical purposes.

Typical values for the sigma transition point for neutral mechanically-mixed conditions and for free convective conditions can be calculated. Table 3 shows a range of predicted values of the ambient dispersion and the transition distance ($\varepsilon_{plume} = \varepsilon_{environment}$) as a function of wind speed for neutral, mechanically mixed conditions. The ambient values of dissipation were calculated applying (3.30) for heights of 100 and 300 m. The drag coefficient was evaluated using a logarithmic wind profile to 100 m for roughness lengths of 10 and 50 cm.

Table 3 Transition points based upon calculated dissipation values for two heights in a mechanically mixed atmosphere

Roughness Z_o (cm)	Wind Speed $\bar{U}$ (m/sec)	Ambient Dissipation ε_a (cm^2 sec^{-3})		Transition Point X_t (km)	
		Z = 300m	Z = 100m	Z = 300m	Z = 100m
10	5	2	6	8.3	4.3
	10	17	50	3.6	1.9
	15	60	170	2.2	1.1
	20	130	400	1.6	0.8
50	5	5	13	5.2	2.7
	10	36	110	2.3	1.2
	15	120	360	1.4	0.7
	20	290	860	1.0	0.5

The roughness length of 10 cm is the same as the Round Hill experimental site used by Cramer (1957). However, the variation of type and height of vegetative cover in the AOSERP region (see Thompson et al. 1978) suggests that a value of Z_o larger than 10 cm might be appropriate. A detailed analysis of wind profiles would be needed to estimate an aerially averaged value of Z_o.

The measured values of dissipation (Davison and Grandia 1978) in June 1977 showed marked thermal effects. Most of the cases showed major differences depending upon the inversion level and fairly significant temporal changes even around mid-day. Typical values for dissipation in the mixed layer in June 1977 were 50 to 100 cm^2 sec^{-3} which are reasonably consistent with the range of calculated values in Table 3.

Although the values of the sigma transition distance in Table 3 are only estimates, it can be seen that for a mixed boundary layer the first one or two kilometers of plume travel can be expected to be affected by plume induced mixing. Thus interpretation of plume photo and LIDAR data must account for these initial plume effects.

3.3 SURFACE HETEROGENEITY EFFECTS

Most dispersion theories assume very simple surface characteristics. Usually flat homogeneous terrain is adopted. However for any practical application, the effects of topography and land cover characteristics and variations need to be considered. The effects of topography are evident in the distortion of the wind field. To account for this terrain effect, a variety of techniques have been developed (see for example a review by Egan 1975). A Gaussian model has severe limitations whenever terrain is important. A more useful approach has been to use potential flow theory to compensate for terrain; this approach is usually combined with some type of K-theory dispersion formulation.

Land cover characteristics and variations present a more serious problem for numerical modellers. For a reasonably homogeneous land cover, the roughness and albedo of the surface will tend to be homogeneous even though different from other sites. This site specificity will change the rate of dispersion (the Gaussian sigmas) for given meteorological conditions compared to different sites. A classic example of site differences was present by Cramer (1957) and Cramer et al. (1959) in a comparison of diffusion data from the O'Neill site (flat smooth Nebraska plains, $Z_o \leq 1$ cm) to data from the Round Hill site ($Z_o \geq 10$ cm). The cloud width for a passive tracer was found to scale with wind direction fluctuations in the same fashion at both sites. However, the sigmas were inconsistent if plotted as functions of a stability parameter because in neutral conditions the standard deviation of the wind azimuth at Round Hill is approximately double that at O'Neill. Part of the site differences is undoubtedly due to more topographical relief at Round Hill but part of the site differences are due to roughness differences.

The presence of variations in land cover further complicates the dispersion modeling. If the size scale of the variations is small, then an effective roughness length can be estimated. However, if the land cover variations are of the size scale of perhaps 0.5 km or large, then significant dispersion effects may result. A well-documented extreme case is the change in dispersion characteristics across a land water interface (see, for example, Gifford 1968 p.107). Similar types of changes although probably less severe can occur across changes in land cover. An example pertinent to AOSERP is the changes from open muskeg to land cover dominated by tall black spruce. There are marked changes in surface roughness and also changes in albedo especially in winter.

Some very preliminary work on surface heterogeneity effects on turbulence characteristics was presented by Davison et al. (1977) and Davison and Grandia (1978). Turbulence runs in an instrumented aircraft were made on a few occasions to attempt to detect significant spatial variability in the turbulence parameters at typical plume height. Although the data were sparse, tentative conclusions were that the Athabasca River valley did not have a significant effect upon the turbulence levels at plume height; however, there was some indication that land cover variations on the east side of the river did have significant effects.

There is considerable evidence, however, that there is a pronounced valley effect on the temperature and wind fields. Flow separation and complex stability structures have been documented in the Athabasca River valley by Mickle et al. (1978) and Kerman and Turner (1978). Although the valley effects are real, they may only be of importance for low level and fugitive emissions and not for the main stack effluents.

A comparison of simultaneous minisonde releases shows that there were often significant differences between sites. These data are discussed in more detail in the section below on the characteristics of the minisonde data. It appears that the apparent differences may be mostly attributable to statistical sampling and analysis limitations. This interpretation would imply that the differences from minisonde sites are due less to systematic spatial variations than to short term fluctuations which are advecting with the mean wind. An examination of some of the tethersonde data suggests that significant low frequency energy exists in the wind field; this suggests that much of the spatial differences may be of short duration.

A way of testing the sensitivity of surface heteorogeneity effects is to determine if any directional dependence exists for the measured plume sigma values. This directional dependence

testing is discussed in detail in a later chapter. In brief, there did not appear to be any obvious directional dependence on the average plume sigmas. If this is correct then surface heteorogeneity may not be a major problem at typical plume heights near the GCOS site.

3.4 SAMPLING AND AVERAGING CONSIDERATIONS

3.4.1 Eulerian and Relative Dispersion

Dispersion has often been treated as a two stage process. One part of dispersion is the growth of a cloud or of a plume cross-section with respect to the center of mass; this is relative dispersion. The second part of dispersion is associated with the changes in the center line position due to lower frequency oscillations of the whole plume. The total dispersion is the sum of the two effects (actually the sum of the variances) and is referred to as Eulerian or time-averaged dispersion. Thus, Eulerian dispersion is always larger than relative dispersion; although for long diffusion times they approach the same limit as the oscillations of the center line become small compared to the total dispersion.

3.4.2 The Effects of Averaging Time

Eulerian dispersion clearly is a function of averaging time. For longer averaging times, lower frequency meanders continue to decrease the average concentrations at any given position. Gifford (1975 p.42) reviewed work from several sources and recommended the following formulation,

$$\frac{C_A}{C_B} = \left(\frac{t_B}{t_A}\right)^p \qquad (3.45)$$

where C_A is the average concentration over an averaging time t_a and p is a constant. The above formulation is based upon the idea that $\sigma_y \propto \sigma_\theta$. Csanady (1973) recommended

$$\frac{\sigma_{yA}}{\sigma_{yB}} \simeq \frac{\sigma_{\theta A}}{\sigma_{\theta B}} \simeq \left(\frac{t_A}{t_B}\right)^q \qquad (3.46)$$

where q has a value of about 0.25 to 0.3 for time periods from 1 hour to about 100 hours. Similar considerations might apply to σ_z for downwind distances of less than a few kilometres (i.e. before the effects of limited mixing. Thus close to the source, the value of p in (3.45) would be about 0.5 (Hino 1968) for time periods of 1 to 100 hours. Further downwind, when σ_z is approximately constant, and when there are no significant shear effects, $p \simeq 0.25$ to 0.3 for $t > 1$ hr. For averaging times from a few minutes to an hour, Gifford recommends a value of $p \simeq 0.2$.

Although the above formulations for the effect of averaging time are often useful, they have practical limitations. Pasquill (1974 p.26 ff) outlined the effects of averaging time in a more rigorous fashion in terms of spectral contributions to variances. It is clear that the above power laws assume a very simple shape for the wind direction spectrum. It is well known that the shape of the low frequency wind direction spectrum is sensitive to local variations of topography and roughness (Panofsky 1973 p. 166). Thus the above power laws must be recognized as only rough approximations which may vary from site-to-site and with meteorological conditions. An example from the AOSERP study area was presented by Fanaki et al. (1978a p. 35). The effects of smoothing the wind direction data prior to the calculation of σ_θ, were shown to vary with time of day even though the absolute value of σ_θ for a small smoothing time was similar. This result reflects the changing shape of the wind direction spectrum at lower frequencies. Fanaki considered averaging times up to only about 2 minutes. Thus his data cannot be used to directly evaluate q in (3.46), but the

principle is the same. The use of extrapolation formulas, such as (3.45) and (3.46), to account for different averaging times must be viewed with considerable reservation.

3.4.3 Plume Traverses as Measures of Relative Dispersion

A measurement system which involves a traverse of the plume has specific sampling characteristics. If a helicopter, aircraft, LIDAR or COSPEC is used to sample across a plume, then that single measurement is a measure of relative dispersion. The speed of the traverse is largely irrelevant because no Eulerian averaging is being done on the entire plume. A very rapid traverse will capture this instantaneous dispersion accurately. A very slow traverse will mean that one side of the plume may have meandered in or out during the traverse; thus slow traverses would generate a scatter about the true instantaneous relative dispersion estimates.

Often researchers have attempted to assign an averaging time for a traverse of a plume based upon the speed of traverse, and then use the averaging time extrapolation formulas discussed in the previous section. This is an incorrect practice. Any plume traverse is a measure of relative dispersion. The difference between relative dispersion and time-averaged or Eulerian dispersion is a function of downwind distance from the source and can be estimated as shown in the following section.

When repeated plume traverses are averaged, then the averaging procedure determines the type of dispersion measurement. If the averaging is performed with respect to each traverse's center of mass, then the result is an ensemble average of relative dispersion. If the averaging is performed with respect to the ground, then an Eulerian average results. The equivalent time-basis for a series of Eulerian-averaged measurements of relative dispersion would be the total time separating the traverses if sufficient numbers of traverses are made to avoid serious aliasing effects (see Blackman and Tukey 1959) or to generate a representative population distribution.

3.4.4 Quantitative Differences Between Relative and Eulerian Dispersion

Pasquill (1974 p. 142-45) developed an expression for relative dispersion of the form

$$\frac{d\sigma}{dx} = 2\,\beta_t i^2 \int_0^\infty \frac{n_2}{(1+n^2)^2} \quad \frac{1 - e^{-r^2 n^2}}{nr}\, dn \qquad (3.47)$$

where σ is the standard deviation of the cluster of particles about the center of mass

i is the intensity of the turbulence; $i \simeq \sigma_v/\overline{u}$

$r = \sigma/\ell$

$n = k/\ell$, a non-dimensional frequency or wave number

ℓ = integral length scale

β_t is the assumed time scaling factor between Lagrangian and Eulerian statistics.

For initially small clusters, ($\sigma_o \leq 0.1\ \ell$), (3.47) can be numerically integrated to yield a "virtually universal curve" in terms of σ/ℓ as a function of x/ℓ, (see Figure 4). All length scales are normalized by ℓ and so changes in ℓ can be compensated for linearly.

The intensity of turbulence is a simple scaling parameter for the rate of spread in (3.47). Hence changes in i can be easily accounted for in σ. The value of i increases markedly with increasing instability, see for example Panofsky (1973 p. 165). Note also that although relative dispersion varies with i^2 during a nearly-linear phase of dispersion (the lower curve plotted in Figure 4), time-averaged dispersion varies as i (Pasquill 1974 p. 145). This means that if i is twice as large, then the same discrepancies between relative and time-averaged dispersion are found twice as close to the source. Thus in unstable conditions, smaller discrepancies can be anticipated between relative and time-averaged dispersion.

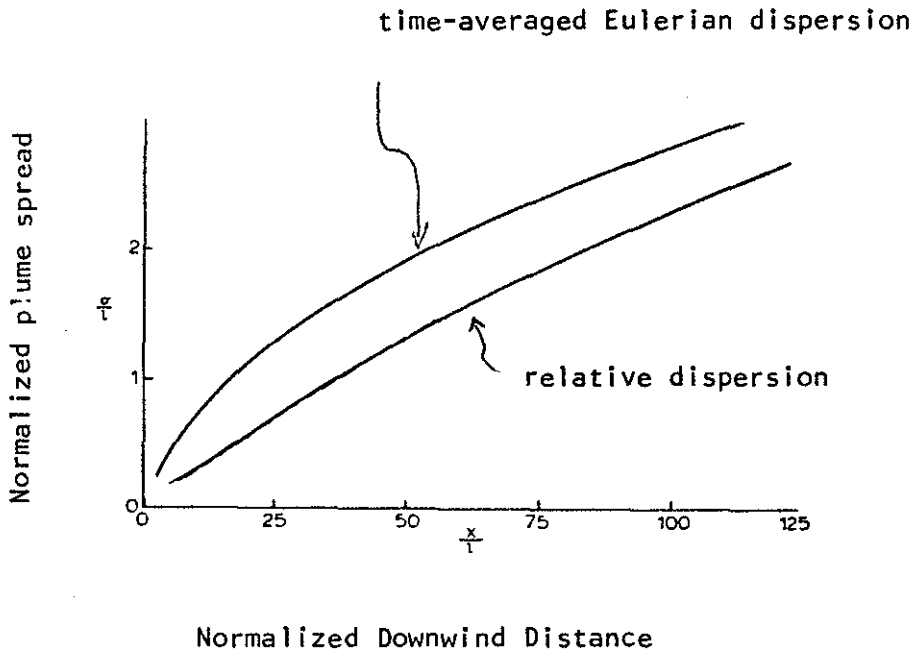

Figure 4 A comparison of time-averaged Eulerian dispersion to relative dispersion. This sketch is adapted from a comparison of puff dispersion to Eulerian dispersion from a continuous source as discussed by Pasquill (1974 p.144). The normalization parameter is the integral length scale, ℓ.

The above formulations have not considered the fact that the plume itself will dominate dispersion for typically the first kilometre. However, this plume-dominated region refers only to relative dispersion. The plume will still follow the lower frequency wind field oscillations and so the concepts of relative and time-averaged dispersion are still valid. The numerical ratios, from Figure 4, however, may be inappropriate.

Fortunately the COSPEC data from the March 1976 field study (Hoff et al. 1978) provided a means of evaluating the difference between relative and Eulerian dispersion. Six series of four traverses each were made by the COSPEC underneath the GCOS plume. The percentage difference between relative and time-averaged σ_y values was $7 \pm 5\%$ for downwind distances between 3.6 and 4.0 km. These data indicate that the discrepancies between averaged (30 minute) relative and Eulerian dispersion values were not large.

3.4.5 Representative Sampling

A final problem to recognize is the difficulty in obtaining representative measurements. This is an especially serious problem close to the source and in unstable conditions. The various theoretical formulations have assumed that representative or ensemble-averaged measurements are available. In practice, there is a large variance in the population of relative dispersion values close to a stack. The photographs shown in Figure 5 demonstrate this effect graphically. Close to a source and in unstable conditions obtaining representative plume profiles by a series of vertically stacked traverses by an aircraft (or LIDAR) is very difficult. A large number of repeated measurements at one downwind distance can partly compensate but only at the cost of increased lack-of-stationarity effects.

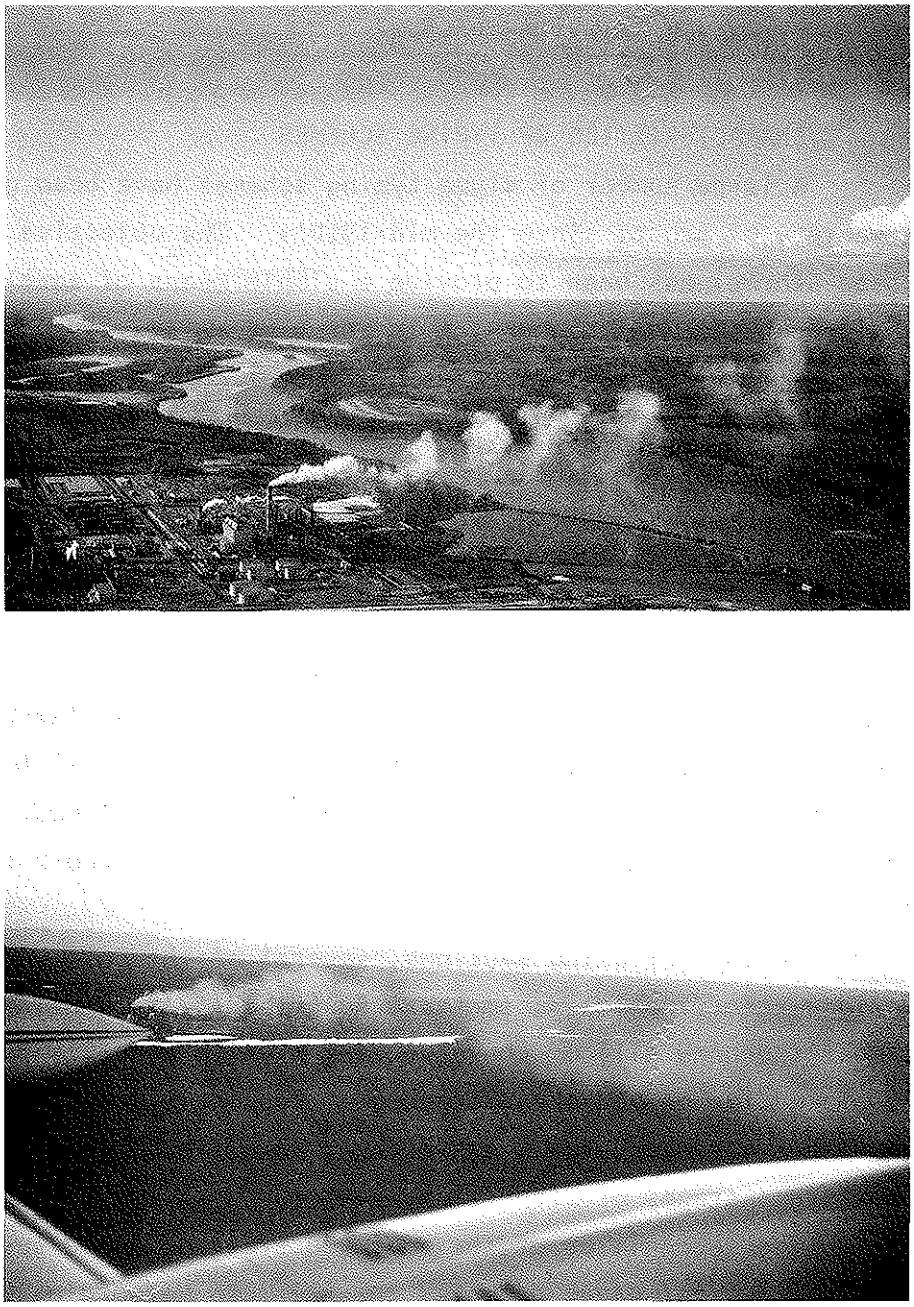

Figure 5 Examples of the intermittency of plume structure. The upper photograph taken at 1923 MST on June 22, 1977 shows the puffiness often exhibited by the plume close to the source. The lower photograph was taken at 2245 MST on June 22, 1977 at a downwind distance of 8 km. Problems in obtaining representative plume traverses exist even under non-convective situations.

4. SIGMA SPECIFICATION SCHEMES

4.1 CHARACTERISTICS OF TYPING SCHEMES

A large number of sigma typing schemes have been generated by a variety of groups since the mid-1950's. The objective of all of these schemes has been to provide a simple means of specifying lateral and horizontal dispersion in terms of relatively easily measured meteorological parameters. The most common dispersion parameters specified have been the Gaussian σ_y and σ_z as functions of downwind distance and of some measure of the mixing potential of the atmosphere. As was discussed in the previous chapters, the real mixing process is a very complex turbulent process with different size scales and mixing mechanisms important at different stages. Also the characteristics of the source are very important especially for industrial plumes. In spite of the complexity of the dispersion process, practical estimates are essential for air quality management. Thus the diffusion typing schemes must be viewed in terms of a practical necessity recognizing their theoretical limitations.

In the following sections, several of the most widely used sigma specification schemes are described. It is evident that most (perhaps all) of these schemes have in practice been extrapolated far beyond the distances of supporting measurements often with a disregard for the different power laws expected for the different stages of dispersion.

The recognition of the confused state of sigma specification in practical usage prompted the American Meteorological Society to convene a Workshop on Stability Classification Schemes and Sigma Curves in June 1977. The Workshop consisted of 25 invited attendees including many of the most experienced researchers in turbulent dispersion. The report of the Workshop (Hanna et al. 1977) summarized the problems associated with stability and

sigma specification and partially outlined recommended procedures. The recommended lateral dispersion formulation involved Pasquill's approximation of Taylor's theory (Pasquill 1976 , Draxler 1976) which is discussed in a separate section below. The vertical dispersion formulation was still considered to be in a poor state of knowledge. Perhaps the failure of specification schemes for the vertical dispersion represents a limitation in the representation of mixing at different heights by a single parameter.

4.2 EMPIRICAL SIGMA SPECIFICATION SCHEMES

Many empirically based sigma specification schemes have been developed over the past two decades. Some of the schemes have minor changes compared to a few widely used schemes often relating to the specifications of the turbulent mixing class. The turbulent mixing class is often referred to as stability class and will be done so in this report for convenience. However, it is recognized that a true stability measurement should involve a ratio of mechanical to convective energies which many of these stability schemes do not have. A number of review articles outlining many of the typing schemes have appeared in the literature, notably Islitzer and Slade (1968) Gifford (1975) and Weber (1976). A summary review of the major typing schemes is presented below with an emphasis on the data base from which each scheme was developed.

4.2.1 Pasquill-Gifford Scheme

The Pasquill-Gifford scheme is probably the most widely used sigma specification scheme and so its experimental basis will be examined carefully. The data base of the original scheme developed by Pasquill is well described in Pasquill (1961); although the original scheme was presented earlier. The system involved the specification of the total angular width, θ, and depth, h, of the visible plume from a ground source as defined (somewhat arbitrarily)

as the 10% concentration level. For a Gaussian distribution $\Theta = 4.30\ \sigma_y$ and $h = 2.15\ \sigma_z$. The data base consisted of the Porton experiments of the 1920's and 1930's, Project Prairie Grass as summarized by Cramer (1957) and measurements by Bowne and Islitzer at the National Reactor Testing Establishment in Idaho Falls. Pasquill (1961) stated that the specification of angular spread was based upon measurements for downwind distances of less than 1 km and that for longer ranges "the method is open to question". There were 3 data points at 75 km taken under conditions of vigorous mixing over a depth of 1000 m (i.e., probably small shear effects). The duration of the source in the dispersion tests was usually less than 10 minutes. For the vertical depth of the plume most of the data base was similarly limited to ranges of less than 1000 m. Values of h for longer ranges were based upon estimations from the Hay-Pasquill (1959) modification of Taylor's statistical theory with some experimental data for neutral to moderately unstable conditions.

Pasquill recognized that wind fluctuation data would not always be available and so he generated stability categories based upon wind speed and solar insolation (see Table 4). Note that in this case both mechanical and convective energies are being considered and so Pasquill's classes are true stability approximations. Turner (1970) generalized Pasquill's turbulence typing by specifying surface insolation in terms of the solar elevation angle and cloud height as well as the amount of cloudiness.

To allow for elevated sources, Pasquill (1961) proposed correction factors based upon the Gaussian formulation. The only experimental testing for this procedure were 13 values from Bowne and Islitzer for a source at a height of 50 m for the position of maximum ground level crosswind integrated concentrations. The ratio of calculated to observed distances (using wind fluctuation data and a Gaussian formulation) ranged from 0.76 to 1.82, which

Table 4 Stability Classifications According to Pasquill (1961)

Surface Wind Speed m/sec	Daytime Insolation			Night-time Conditions	
	Strong	Moderate	Slight	Thin overcast or $\geq$ 4/8 Cloudiness*	$\leq$ 3/8 Cloudiness
<2	A	A-B	B		
2	A-B	B	C	E	F
4	B	B-C	C	D	E
6	C	C-D	D	D	D
>6	C	D	D	D	D

D-stability is used for heavy overcast, day or night.

* The degree of cloudiness is defined as that fraction of the sky above the local apparent horizon which is covered by clouds.

Pasquill considered to be a reasonable validation of the approach. Thus the allowance for elevated sources is largely developed using a Gaussian formulation.

Gifford (1961) converted Pasquill's θ and h valves into families of curves of σ_z and σ_y assuming a Gaussian distribution. Note that Gifford assumed that the lateral width represented the 10% of axial concentration level. The resultant curves, the so-called Pasquill-Gifford curves, are plotted in Figure 6.

Attempts have also been made to relate these stability types to specific measured parameters such as the lapse rate and surface Richardson number (see for example, Gifford 1975). The lapse rate specification and surface Richardson number require representative near-surface measurements. In a heteorogeneous terrain such as in the vicinity of the Athabasca Oil Sands Study Area, reliable and representative near surface statistics would be very difficult to obtain especially on an on-going basis. The U.S. Nuclear Regulatory Commission requires the selection of stability in terms of temperature differences between the 10 and 60 m levels (NRC Regulatory Guide 1.23, 1972); these stability criteria are presented in Table 5. Although this selection procedure is probably not suitable for AOSERP, this procedure was tested for stable conditions using the temperature gradient over the region of plume rise.

4.2.2 Tennessee Valley Authority Scheme

The Tennessee Valley Authority carried out an extensive program of observations of dispersion of stack gases from coal fired power plants (Carpenter et al. 1971). They categorized the different dispersion situations as coning, fanning and inversion break-up, looping and trapping.

For small plants the coning periods were identified with maximum surface concentrations. In this case the effluent plume is

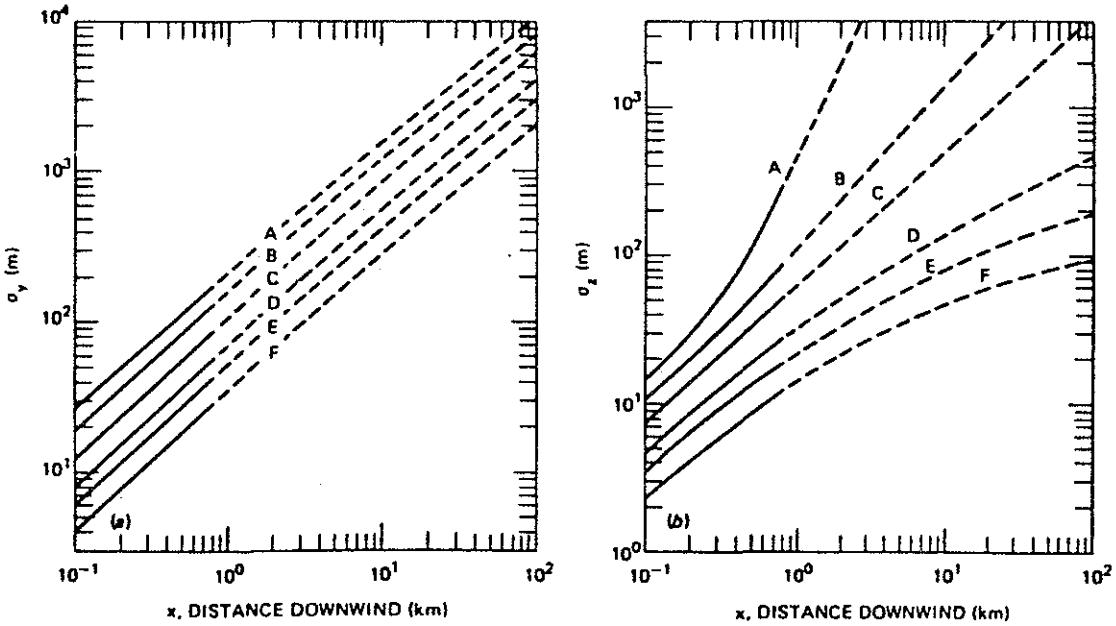

Figure 6 The Pasquill - Gifford sigma curves. The dotted lines emphasize the very limited empirical data base beyond a downwind distance of 800 m.

Table 5 Stability Classifications According to USAEC Guide 1.23

Stability Classification	Pasquill Categories	Temperature change with height (^{o}C/100 m)
Extremely unstable	A	< -1.9
Moderately unstable	B	-1.9 to -1.7
Slightly unstable	C	-1.7 to -1.5
Neutral	D	-1.5 to -0.5
Slightly stable	E	-0.5 to 1.5
Moderately stable	F	1.5 to 4.0
Extremely stable	G	> 4.0

shaped approximately like a horizontal cone. This situation most typically occurs with near-neutral stability conditions and moderate to high wind speeds. The level and location of maximum surface concentrations are primarily dependent on effective plume rise, wind speed and stability.

Fanning and inversion break-up occur when the plume is emitted into a stable atmosphere and is transported downwind with minimum vertical dispersion until heating from below erodes the inversion layer. This produces an intense but short duration (30-45 min) burst of maximum surface concentration at distances up to 30 km from the source.

Looping was observed to occur infrequently for plumes with the heat content and the high rise rates of the TVA power plant plumes and was not studied very intensively.

As plant size increased TVA found that the inversion-trapping case became relatively more important. This typically occured when an unstable or neutral boundary layer was topped by a relatively low-level subsidence inversion below 1200 m. In this case the SO_2 concentrations were more or less uniformly mixed throughout the boundary layer and surface concentrations were typically larger than for the coning model.

For the coning dispersion situation, Carpenter et al. (1971) presented the data as functions of the potential temperature lapse rate, $\Delta\theta/\Delta Z$, and distance from the source (see Table 6 and Figure 7).

The measurement technique for the TVA dispersion program from 1957 to 1962 has been summarized by Islitzer and Slade (1968 p. 130 ff). In brief, measurements were made of SO_2 concentrations by means of series of vertically stacked helicopter traverses in the crosswind direction at downwind distances of 0.8 to 3.2 km for neutral conditions, and of 0.8 to 16 km for stable conditions. Islitzer and Slade attribute an "averaging time" of a few minutes

Table 6 Turbulence Types for TVA

Type	$\Delta\theta/\Delta Z$ ($^{o}K/100$ m)	
A	0.00	Neutral
B	0.27	Slightly Stable
C	0.64	Stable
D	1.00	Isothermal
E	1.36	Moderate Inversion
F	1.73	Strong Inversion

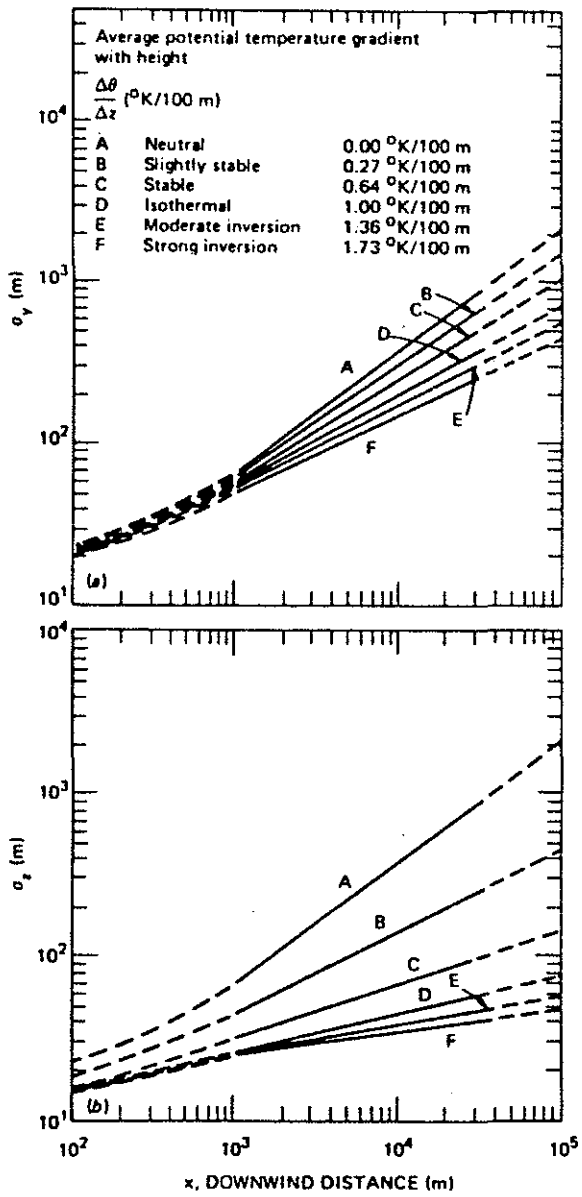

Figure 7 The TVA curves presented by Carpenter et al. (1971). The data for neutral conditions extended to 3.2 km downwind; for stable conditions, to 16 km downwind.

to this technique. However, it is clear that the measurements are of relative dispersion and that the discrepancy between these measurements and a time-averaged measurement depends upon distance from the source as discussed in an earlier chapter of this report.

It is interesting to note that Islitzer and Slade attributed the large σ_z values to "strong vertical mixing as the hot plume is ejected from the stack". This emphasizes the significance of the TVA data in that they reflect dispersion from full-scale industrial sources with significant plume rise and initial dilution effects present. For neutral stability, the σ_y curve has a slope of about $X^{2/3}$ which is the Briggs prediction for initial plume-dominated expansion. Such initial effects would be expected to be important over the range of downwind distances examined for neutral stability; it is also consistent with the gradual change from X^1 to $X^{1/2}$ predicted by Taylor's theory. For stable conditions, the TVA σ_y curves have slopes closer to $X^{1/2}$ which is also consistent with initial dilution and Taylor's theory for the longer downwind distances sampled.

The TVA curves were extrapolated in both directions with dashed lines (Figure 4 and 5 in Carpenter et al. 1971). We feel that this extrapolation is unwarranted since the long-dispersion-time power law behaviour predicted by Taylor's statistical theory has been ignored. The $X^{1/2}$ predicted by Taylor's theory has recently been recognized as the appropriate large X behaviour, (Hanna et al. 1977).

For the AOSERP data, the TVA curves can be tested using the minisonde temperature profiles for stability classifications. It must be noted however that TVA found that looping plumes did not occur often and so their curves may not handle the looping plumes observed at AOSERP. In any case, the TVA stability classification scheme, being based upon elevated lapse rates, cannot distinguish between neutral and convective conditions.

TVA identified a trapping mode and adopted the approximation of uniform dispersal vertically throughout the mixed layer. Dispersion in the lateral direction was presumably the same as for the coning mode. For the AOSERP data, these cases of limited mixing will still be compared to the TVA σ_y and σ_z curves with some case by case discussion as seems appropriate.

4.2.3 Brookhaven National Laboratory

In the BNL scheme, (Singer and Smith 1966) the turbulence types are based on the range of the wind direction fluctuations measured over a 1 hour period at 108 m above the ground. Five categories were defined:

A Peak to peak fluctuations of the horizontal wind exceed 90°.

B_2 Fluctuations range from 40° to 90°.

B_1 Fluctuations range from 15° to 45°.

C Distinguished by the unbroken solid core of the trace through which a straight line can be drawn without touching open space.

D The trace approximates a straight line with short term fluctuations less than 15°.

The BNL turbulence scheme has also been related to the temperature gradient from the surface to 123 m and the wind speed at 108 m (see Table 7). Although the temperature gradient and wind speed groupings have overlap between classes, they do provide an approximate means of stability classification in the absence of gustiness data and help to resolve the differences between the B_1 and C classes.

Table 7 Properties of the BNL Turbulence Types

Type	Seasonal Frequency, %	$\Delta T/\Delta Z$ per 123 m, ^{o}C	Average Wind Speed at 108 m, m/sec	σ_y,m	σ_z,m	Average Wind Speed at 9 m, m/sec
A	1	-1.25 ± 7*	1.8 ± 1.1*			
B_2	3	-1.6 ± 0.5	3.8 ± 1.8	$0.40_x^{0.91}$	$0.41_x^{0.91}$	2.5
B1	42	-1.2 ± 0.65	7.0 ± 3.1	$0.36_x^{0.86}$	$0.33_x^{0.86}$	3.4
C	14	-0.64 ± 0.52	10.4 ± 3.1	$0.32_x^{0.78}$	$0.22_x^{0.78}$	4.7
D	40	$+2.0 \pm 2.6$	6.4 ± 2.6	$0.31_x^{0.71}$	$0.06_x^{0.71}$	1.9

* Standard deviation

As shown in Table 7 values of σ_z and σ_y are expressed as power laws with both having the same exponent but different proportionality constants for a given turbulence type. The BNL curves are plotted in Figure 8.

The diffusion trials used to develop this scheme included:

(a) Short-range (less than 100 m) observations of uranine dye released at 2 m height,
(b) observations of oil-fogs released at 110 m height and tracked to intermediate ranges using ground based samplers and
(c) aircraft observations of Argon 41 released at 110 m height and tracked out to 50 km or more from the source.

Except for the aircraft sampling, concentration mean values were obtained over periods ranging from 30 minutes to 90 minutes. The lateral sigma values except for the aircraft value were all calculated from ground level concentration measurements. Values of σ_z were calculated from the ground level concentration measurements assuming a Gaussian distribution.

One limitation of the BNL scheme is that a single power law is fitted to all data in each turbulence type for the entire range of X, from less than 100 m to almost 100 km. This approach is inconsistent with Taylor's statistical theory, wind initial dilution effects for real stacks, with shear effects and with many other data sources. Singer and Smith (1966) presented a plot of some of the data used to generate the σ_y curves. Figure 9 shows these data together with a series of dashed lines showing the X^1 and $X^{1/2}$ power law behaviour predicted by Taylor's theory for short and long downwind distances. It can be seen that most of the data beyond the first couple of kilometres downwind from the source could fit on $X^{1/2}$ power law better than the BNL curves. The two sets of aircraft sampled data in particular each show an $X^{1/2}$ power law. Only by combining these data with each other and with other data of the same gustiness class at shorter downwind distances can a single power law seem reasonable. Thus it appears

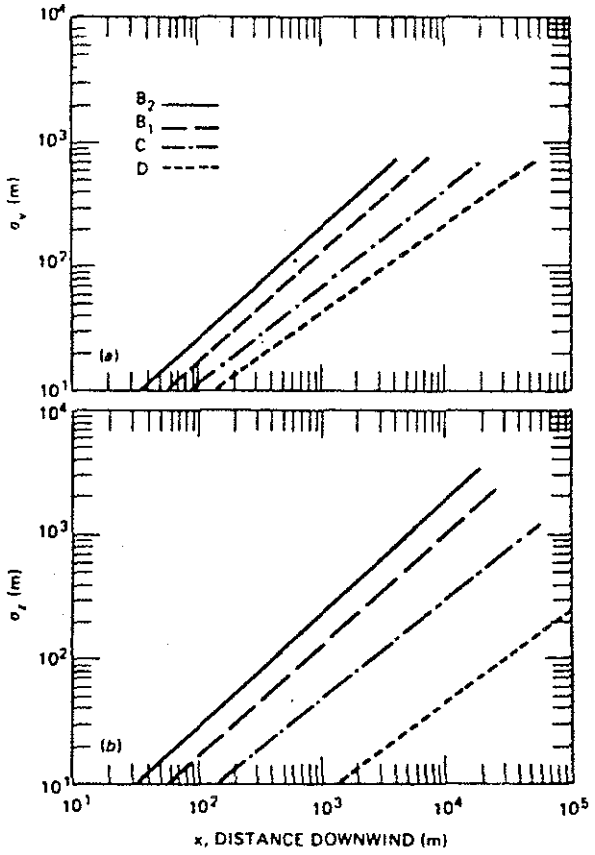

Figure 8 The BNL curves developed by Singer and Smith (1966). The stability classes are defined in terms of the characteristics of the wind direction fluctuations as measured by an aerovane at 103 m.

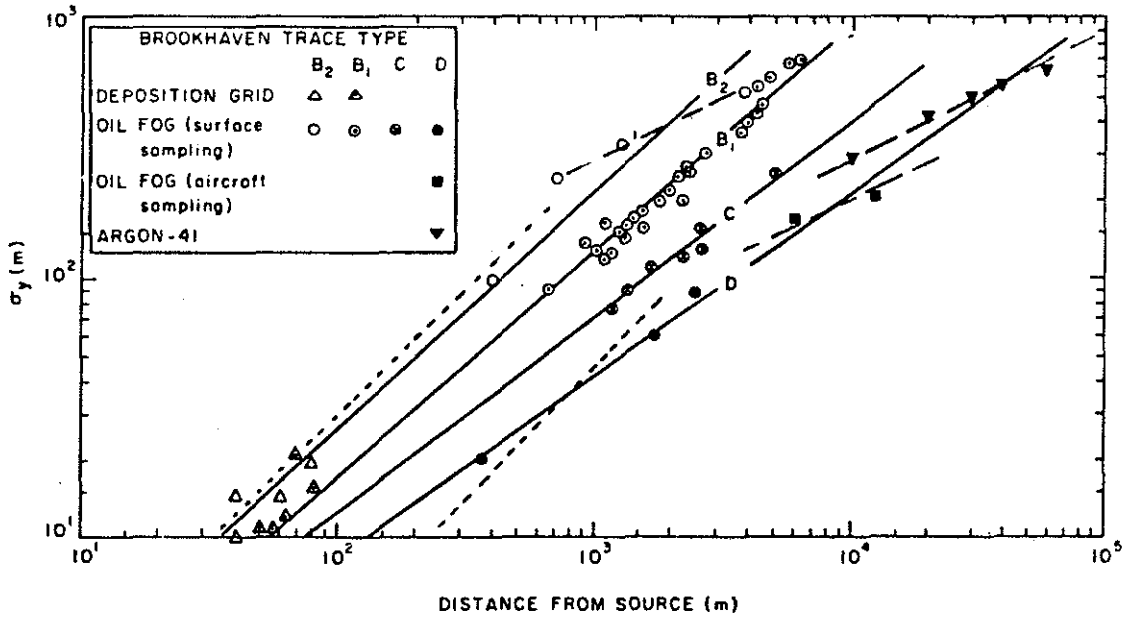

Figure 9 Sample data for the BNL curves (Singer and Smith 1966). The solid lines are the BNL classes. The short dash lines are X^{1} power laws (the short dispersion time prediction of Taylor theory). The long dash lines are $X^{1/2}$ power laws (the long dispersion time prediction of Taylor theory).

that the combination of data for very short downwind distances of the deposition grid data with data for the intermediate range (mostly 1 to 10 km), generated a single power law which is perhaps inappropriate for the intermediate range.

The BNL curves are widely used curves and so it is appropriate to compare the AOSERP data base with them. According to Weber (1976), "the dispersion curves recommended by the American Society of Mechanical Engineers, Smith (1968), are based on the Singer-Smith formulation and the recommended dispersion parameters are exactly the same". Note that the BNL scheme has no allowance for any initial dilution effects due to the plume-induced mixing. The data have been collected for a passive tracer.

The BNL gustiness classes were originally defined in terms of the wind direction trace as recorded by a Bendix-Friez aerovane located at 108 m on the BNL tower. For AOSERP applications, the BNL classes were chosen in the following ways:

(a) if σ_θ data were available from the tethersonde at the plume height, then the "fluctuations" of the BNL scheme were taken to be $\pm$ 3 σ_θ. For resolving the ambiguity between classes B and C, lapse rate and wind speed information were used.

(b) if σ_θ data were available from the tethersonde in the mixed layer and the plume was in the mixed layer, then $\bar{u}\sigma_\theta$ was taken as a constant with height following the recommendations of Singer and Smith (1966); then procedure (i) was followed.

(c) if σ_θ data were unavailable or available at times not coincident with plume dispersion measurements, then the temperature lapse rate over the region of plume rise combined with the wind speed were used to estimate the BNL turbulence type according to Table 7.

4.2.4 Cramer

Cramer developed a sigma specification scheme in terms of wind direction fluctuations based upon the Prairie Grass and Round Hill experiments from 1956 to 1959. A summary of their results was presented by Islitzer and Slade (1968 p. 133 ff); more

detail on the exact experimental procedures used were presented in Cramer et al. (1959).

The data are based upon emissions from passive, near-surface sources (typically at a height of less than 1 m) with measurements made to downwind distances of 800 m. A series of bivanes ensured representative measurements of wind direction fluctuation over the region of dispersion.

Cramer found that although the two sites were markedly different in roughness, the same relationship between σ_y and σ_θ was valid for both sites over a wide range of σ_θ values at a downwind distance of 100 m. Cramer represented the sigma values as power law functions of X (i.e. $\sigma_y = \sigma_\theta X^p$). Pasquill (1974 p. 185) notes that in their final report (Cramer et al. 1959) the power law exponent, p, was considered invariant with distance with values as follows:

Unstable conditions	0.8 - 0.9
Near-neutral conditions	0.8
Stable conditions	0.6

The above values can be compared with the Pasquill Gifford (Turner) power law of about 0.87 for all stabilities. Islitzer and Slade (in Slade 1968, p. 134) quoted later work by Cramer et al. (1964) where the exponent, p, has a range of 0.45 to 0.85 as a function of σ_θ (see Table 8). Note also that σ_z is written as a function of horizontal not vertical wind direction fluctuations.

The representation of σ_z as a function of σ_θ needs to be treated with great caution for elevated sources. Very close to the ground, there will virtually always be mechanical turbulent mixing. However, in stable elevated layers, the lower frequency wind direction fluctuations may be large without there being appreciable vertical mixing. Fanning of a plume is an example of such a situation.

Table 8 Distance dependency of diffusion coefficients based on project prairie grass data* in which $\sigma_y = \sigma_\theta x^p$ and $\sigma_z = \sigma_\theta x^q$

σ_θ, deg	p (200 to 800 m)†	q (50 to 800 m)†
3	0.45	0.86
4	0.56	0.86
5	0.64	0.88
6	0.71	0.91
7	0.80	0.96
8	0.85	1.13
10	0.85	1.29
12	0.85	1.55
20	0.85	1.74
25	0.85	1.89

* From Cramer et al. 1964

† Distance interval on which the estimates are based

The Cramer specification scheme can be written as

$$\frac{\sigma_y}{\sigma_\theta X} = X^{p-1} \qquad (4.1)$$

The Cramer scheme is, thus, a particular case of Pasquill's universal expression as discussed in the 1977 AMS Workshop, Hanna et al. (1977), and so can be tested along with the more recent developments of the same form.

4.2.5 Briggs Interpolation Scheme

In 1973, Briggs presented a sigma specification scheme (see Weber 1976) designed for the calculation of ground level concentrations from tall stacks. Briggs was guided by the sigma specification schemes of Pasquill-Gifford, TVA and BNL. In addition, his formulation recognized the predictions of Taylor's statistical theory (i.e. $\sigma_y \propto X^{1/2}$ at large X). Briggs recommended formulas for "open country" are shown in Table 9 and in Figure 10. Note that Brigg's scheme utilizes the Pasquill type of stability classification.

Weber (1976) comments that Briggs felt the PG curves were most accurate at short ranges. BNL curves were "appropriate" at intermediate and longer distances and TVA appropriate at long distances. However, from the discussion of each of these schemes presented above, it is clear that such generalizations do not rest on the data base.

The PG curves were based upon ground level sources with measurements to 800 m (except for 3 measurements at 75 km all in a limited mixing situation). Gifford (1975) makes clear that Briggs' formulation is for elevated sources at large downwind distances (i.e. after surface impingement). Gifford (1975) adds that if plume level concentrations measurements are desired the plume spreading values for buoyant plumes (Briggs (1975)) should be used. Thus the use of the PG curves up to about 1 km in the

Table 9 Formulas Recommended by Briggs (1975) for $\sigma_y(X)$ and $\sigma_z(x)$; $10^2 < x < 10^4$m, Open-Country Conditions

Pasquill Type	σ_y,m	σ_z,m
A	$0.22x(1 + 0.0001x)^{-1/2}$	$0.20x$
B	$0.16x(1 + 0.0001x)^{-1/2}$	$0.12x$
C	$0.11x(1 + 0.0001x)^{-1/2}$	$0.08x(1 + 0.0002x)^{-1/2}$
D	$0.08x(1 + 0.0001x)^{-1/2}$	$0.06x(1 + 0.0015x)^{-1/2}$
E	$0.06x(1 + 0.0001x)^{-1/2}$	$0.03x(1 + 0.0003x)^{-1}$
F	$0.04x(1 + 0.0001x)^{-1/2}$	$0.016x(1 + 0.0003x)^{-1}$

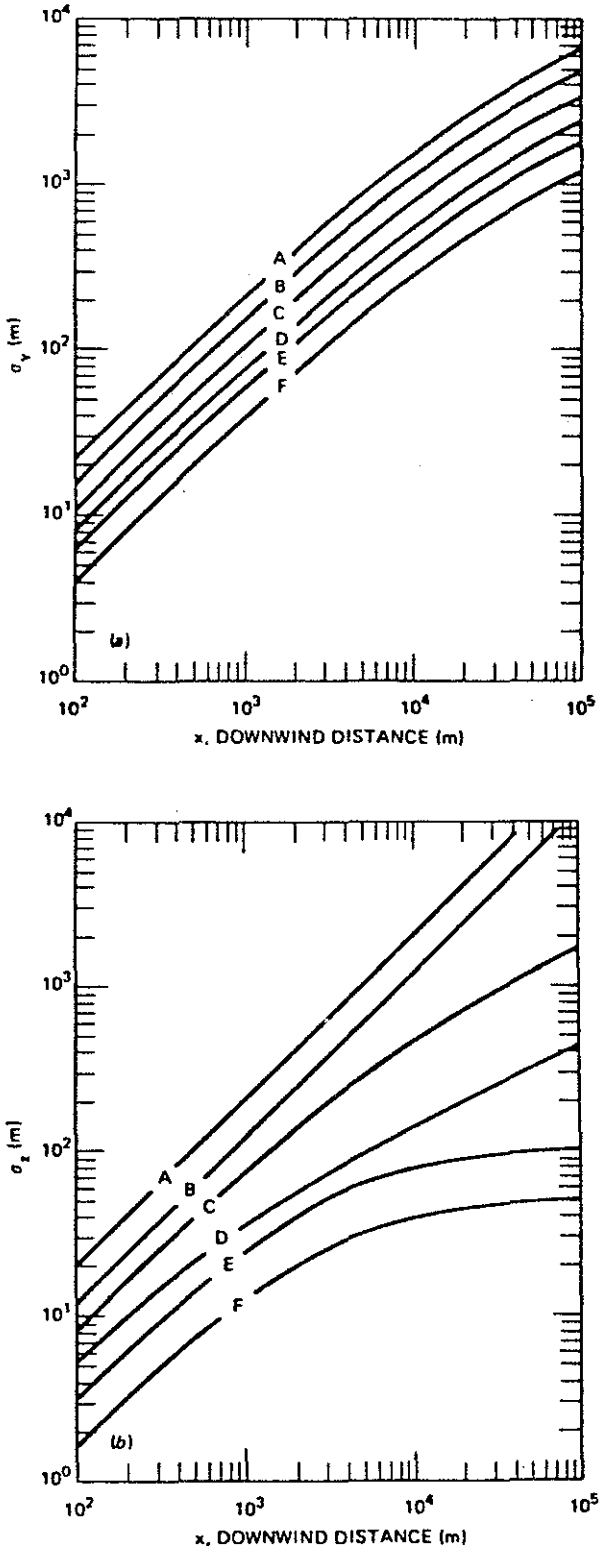

Figure 10 Curves of σ_y and σ_z based on interpolation formulas by Briggs for flow over open country as presented by Gifford (1976).

Briggs formulation is meaningless since the formulation should not be used until perhaps 1 km downwind.

The BNL curves were based on passive tracer measurements from an elevated (100 m) source. When the effects of the initial plume-induced dilution are negligible, then the BNL data base may be appropriate. However, the BNL curves were derived as a single power law at all downwind distances which is considered to be inappropriate.

The TVA curves have a measurement basis to 3.2 km downwind in neutral conditions and 16 km downwind in stable conditions. Over those ranges the TVA curves are probably quite valid. Their use at longer downwind distances is considered to be unwarranted.

Thus, it appears that the Briggs scheme is really an attempt to apply some theoretical guidance by means of Taylor's theory to the various empirical schemes. The range of downwind distances from 100 m to about 1 km should perhaps not even be presented in the Briggs scheme since the scheme is meant for use only after ground impingement. The extrapolations beyond about 16 km do not have a reliable data base and perhaps should be shown as dotted lines. The Briggs interpolation scheme has a similar power law trend with distance (from X^1 to $X^{1/2}$ at larger X) as proposed by Pasquill (1976), Draxler (1976) and as recommended by the AMS Workshop (Hanna et al. 1977). However, the transition to an $X^{1/2}$ power law occurs at a greater downwind distance in the Brigg's scheme.

4.3 THEORETICALLY BASED TYPING SCHEMES

There are a number of typing schemes which have been developed from theoretical considerations, usually being combined with field data to evaluated empirical constants or the form of universal functions. The following three sections outline the most commonly used of these theoretical schemes.

4.3.1 F.B. Smith Model Estimates of σ_z

Very few dispersion measurements have been obtained at distances greater than 10 to 20 km from the source, particularly in unstable conditions. Even at closer distances, measurements are limited to those occasions when researchers can detect the tracer substance with sufficient accuracy to have confidence in the measurements. One approach to this limitation of data is to model the turbulent flow and solve the diffusion equation numerically; see, for example, Weber (1976) for a review.

One of the most widely known models was one developed by F. B. Smith in 1973. Smith (1973, published in Pasquill 1974) used an eddy diffusivity model to solve the two-dimensional diffusion equation (i.e. lateral diffusion was not modeled). His eddy diffusivity was height dependent and is proportional to rate of turbulent kinetic energy dissipation and the predominant eddy size. The diffusion equation was then solved for different values of atmospheric stability and surface roughness. Values of σ_z were computed from the computed concentration profiles. The curves of σ_z plotted in Figure 11 were computed by R.P. Hosker (see Gifford 1976) for two values of surface roughness (Z_o = 10 cm, 100 cm) using the PG stability types. The Smith model assumes a ground level source and uniform terrain. This model is also limited by the validity of the assumptions used to determine the eddy diffusivity profile and by the assumptions of stationarity and horizontal homogeneity. The wide spread usage of the results of Smith's model is probably due to the generation of sigma values that can be used in a simple Gaussian approach.

Many other K-theory models, including three dimensional solutions; with a variety of K-specification techniques have been developed. However, in most cases these models have been restricted in use to the groups that developed them. A more detailed review of K-theory models is beyond the terms of reference of this study.

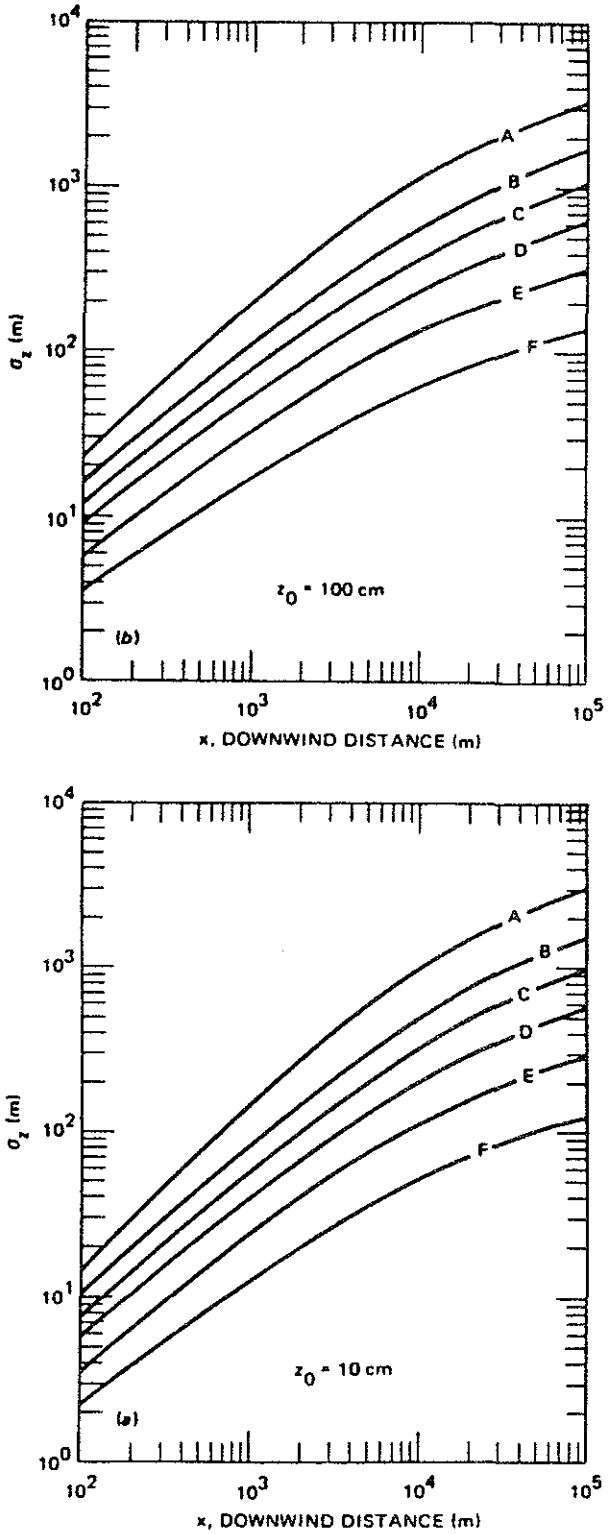

Figure 11 The sigma curves based upon the method of Smith (1973) as published in Pasquill (1974) for roughness lengths of 100 and 10 cm. These curves were generated by Hosker as reported in Gifford (1976).

4.3.2 Hay-Pasquill

A prediction scheme for σ_y was presented by Hay and Pasquill (1959) based upon Taylor's statistical theory and a Lagrangian/Eulerian assumption. Hay and Pasquill assumed that they could simulate the Lagrangian statistics required in Taylor's theory by measuring the Eulerian (fixed point) statistics over an appropriately shortened time period. They assumed in effect that the Lagrangian and Eulerian velocity autocorrelation are identical after appropriate rescaling of the time axis, i.e.

$$R_E(t) = R_L(\beta_t t) \tag{4.2}$$

where R_E and R_L are the Eulerian and Lagrangian velocity autocorrelation functions and β_t is a stability-dependent constant. The value of $\beta_t = 4$ has often given good results; Pasquill (1974) recommends $\beta_t i = 0.44$ where i is the intensity of turbulence. The Hay-Pasquill scheme can be written as,

$$\frac{\sigma_y}{X} \simeq \sigma_\theta \left(\tau, \frac{x}{\overline{U}\beta_t} \right) \tag{4.3}$$

where σ_y is the standard deviation of the crosswind displacements of the particles at a downwind distance, X.

σ_θ is the standard deviation of the wind direction

τ, $\frac{x}{\overline{U}\beta_t}$ are subscripts used to denote that the standard deviation is obtained by forming averages of the wind direction over moving intervals $\frac{x}{\overline{U}\beta_t}$ and using the values so obtained over a duration τ equal to the duration of release of the material or the duration of sampling which ever is shorter (i.e. a frequency band-limited estimate of σ_θ).

β_t is the ratio of the Lagrangian to Eulerian integral scales.

Note that the Hay-Pasquill approach requires on-site measurements of wind direction fluctuations.

Csanady (1973 p.80) comments that the success of the Hay-Pasquill formulation in real world situations indicates that it is "more important to allow for the actual, nonstationary character of atmospheric turbulence, than to have accurate information on the Lagrangian correlation coefficient".

4.3.3 Pasquill's Modification of Taylor's Statistical Theory

4.3.3.1 Pasquill's Universal Functions. Pasquill (1971) and (1976) showed that if the height variations of the lateral wind component are neglected, then Taylor's statistical theory leads to

$$\sigma_y = \sigma_v T f_1 (T/t_L) = \frac{\sigma_v X}{U_e} f_1 \left(\frac{X}{U_e t_L}\right) \qquad (4.4)$$

where f_1 is a universal function of the dispersion time T and the Lagrangian integral time scale, t_L, and where U_e is the effective advection speed of the plume. The function f_1 was not specified by theory. It depends upon the shape of the Lagrangian autocorrelation function and has the limits

$$f_1 = 1 \qquad \text{for small T} \qquad (4.5)$$
$$f_1 = \left(\frac{2t_L}{T}\right)^{1/2} \qquad \text{for large T}$$

in accordance with the X^1 and $X^{1/2}$ limits for Taylor's statistical theory. Equation (4.4) has often been re-arranged into the form

$$\frac{\sigma_y}{\sigma_\theta X} \simeq f_1 \left(\frac{X}{U_e t_L}\right) \qquad (4.6)$$

A similar expression can be written for the vertical component of spread (see Draxler 1976) where f_2 is used for the universal function of t_L/T. However, for vertical spread, the specification of the advection speed causes some problems due to the usual vertical gradient of the wind speed.

4.3.3.2 Draxler's Approach. Draxler (1976) presented one variation of the use of the above form of Taylor's theory. Draxler reviewed a wide variety of passive diffusion data from ground-based and elevated sources. The data sets used by Draxler did not include measurements of the Lagrangian integral time scale. Thus, Draxler adopted a different normalization time scale, T_i, the time required for f_1 to drop to 0.5. Draxler suggested the following forms for f_1 and f_2 based upon an empirical fit to the data,

$$f_1 = f_2 = \frac{1}{1 + 0.90\ (T/T_i)^{0.5}} \qquad (4.7)$$

If the large-T limits of Draxler's formulation and of Taylor's theory are compared, then

$$T_i = 1.64\ t_L \qquad (4.8)$$

The above formulation for f_1 and f_2 was not valid for vertical diffusion from a ground source in unstable conditions and for vertical diffusion from an elevated source in stable conditions. For vertical dispersion from an elevated source in stable conditions, Draxler suggested

$$f_2 = \frac{1}{1 + 0.945\ (T/T_i)^{0.806}} \qquad (4.9)$$

Draxler's formulations lead to a scatter of f_1 with a range of about $\pm$ 50%.

Draxler found that there was considerable scatter in the specification of T_i as a function of stability and height within each diffusion class (e.g. horizontal dispersion for an elevated site in stable conditions). He suggested mean values of T_i for each diffusion class. Note, however, that the best estimate for T_i should be determined at each site; otherwise systematic errors may result.

Draxler found that his normalization time, T_i, was 1000 seconds for horizontal diffusion for elevated sources for all stability classes. This finding is surprising since the integral scale is tied to the V-spectral peak which is known to vary considerably with stability (Kaimal et al. 1972). This discrepancy may reflect the difference between an integral scale determined from true 3-dimensional turbulence and an effective integral scale which includes contributions from quasi 2-dimensional horizontal eddies.

4.3.3.3 Pasquill's (1976) Formulation. In an EPA review study, Pasquill (1976) reviewed data from several studies and recommended the following practical formulation. Equation (4.6) was simplified to

$$\frac{\sigma_y}{\sigma_\theta X} = f(x) \qquad (4.10)$$

where f is a function only of downwind distance. Pasquill suggested the following values for f(x)

x(km)	0.1	0.2	0.4	1	2	4	10	>10
f(x)	0.8	0.7	0.65	0.6	0.5	0.4	0.33	$0.33\ (10/x)^{1/2}$

where σ_θ is expressed in radians averaged over the sampling time of interest and for the height at which $\bar{U}$ is specified.

Pasquill (1976) suggests that the above formulation will lead to predictions that are "mostly within a factor of 1.5 at short range and 2.0 at long range". Note that no allowance has been made in this simplified procedure for any variations of σ_v with height or of the product $U_e t_L$, where U_e is the wind speed at the height of the σ_θ measurement and t_L is the Lagrangian integral time scales.

The above Draxler and Pasquill (1976) formulations have been recommended by the AMS Workshop on Stability Classifications and Sigma Curves (Hanna et al. 1977), as a replacement for the Pasquill-Gifford curves whenever the data base is available. This direct specification in terms of σ_θ permits allowance for the large site-to-site variations of σ_θ due to roughness effects (Weber 1976).

5. CHARACTERISTICS OF THE DATA SOURCES

5.1 DATA SOURCES AND THE NEED FOR DATA VALIDATION

This study was primarily directed toward the interpretation and analysis of measurements of SO_2 distribution and associated meteorological parameters. The measurements examined were those measurements made during the three intensive field studies of March 1976, February 1977 and June 1977. The data from the network of ground SO_2 monitors were not used. This study attempted to relate the observed elevated distribution of SO_2 to the meteorological and source characteristics. In this way, the adequacy of the various formulations for the specification of plume disperison parameters could be analyzed in a detailed manner. The measurements used in this report are listed in Table 10.

Each of the data sources listed in Table 10 has unique characteristics which must be considered prior to usage in the text of specification schemes. The sampling and averaging characteristics inherent in each system and the subsequent analysis procedures produced a wide variety of measures of the plume. It is important to allow for these differences or to be sure that the differences are minimal before consolidating the entire data set. One of the major sources of discrepancies between the different data sets was in the calculation of the plume sigma values. The noise removal techniques and the allowance (or non-allowance) for secondary displaced sources were not standard. It is a strong recommendation that in any subsequent field study, detailed planning discussions be undertaken prior to the field study and after the field study to ensure comparable analysis procedures are adopted by all groups. A considerable amount of data scatter and systematic discrepancies is believed to have originated from the diversity of analysis procedures.

Table 10 Measurements used for this study

Measurement Technique	Field Trips: March 1976	Field Trips: February 1977	Field Trips: June 1977	Principal Investigator and Affiliation
SO_2:				
Plume Photography	X	X	X	Fanaki, AES
Helicopter		X		Lugis, AES
LIDAR			X	Hoff, AES
COSPEC	X		X	Hoff, AES
Aircraft	X		X	Davison, INTERA
Meteorology:				
Minisonde	X	X	X	Fanaki, AES
Tethersonde	X	X	X	Mickle, AES
Aircraft	X		X	Davison, INTERA

5.2 METEOROLOGICAL DATA SOURCES

Data from four systems were used to define the meteorological parameters affecting the effluent plume. These primary systems were the minisondes, the tethersonde, the instrumented aircraft, and to a more limited extent, the bivane. There were other meteorological sensors at the site but for this study the data from them were not used extensively. The acoustic sounder (Kerman and Turner 1978) provided a qualitative description of the many details of the stability structure in the lower atmosphere. However, there were no quantitative measurements presented which were considered by the present authors to be superior to the minisonde or tethersonde data. The acoustic sounder may prove to be a very useful tool in the monitoring of mixing heights; however, for the present study the data were not applicable. The Delta-T sonde (Kerman and Turner 1978) was a temperature difference sensor whose primary purpose appeared to be associated with attempts to quantify the data from the acoustic sounder.

5.2.1 Minisondes

The minisonde operational procedures for the March 1976 and February 1977 field studies have been described by Walmsley et al. (1978) and Fanaki et al. (1978b). The procedures apparently had few changes between the March and February field trips (and presumably for the June 1977 field study).

In all field trips two or three sites were used for simultaneous minisonde releases. The data supplied consisted of graphs and hard-copy print-outs of smoothed temperature and wind profiles.

A major problem was encountered in the use of the minisonde data. Occasionally there were minisonde records which were clearly incorrect. For example, there were several cases in which there were significantly super-adiabatic lapse rates for hundreds of

meters, and alternating changes in the whole boundary layer wind speeds by as much as 5 m/sec between sites or at a single site over a period of a few hours (June 22 1977, 1730-2130 MST). At first this problem was attributed to the "locking-on" to an incorrect slope by the smoothing routine adopted by Walmsley et al. Since the uncertainties attributed to data points increased with height, it was clear that the smoothing routine adopted could generate a straight line whose slope might be determined by the local slope at some critical height. There were no unsmoothed processed data to permit an evaluation in a specific case as to whether an unrealistic profile was generated by a problem in the smoothing routines.

After extensive discussions with Dr. F. Fanaki and his colleagues at AES, the analysis procedure actually used was clarified. The procedure outlined by Vickers (1976) and included in the minisonde data report was an early version of the analysis routines. The actual procedure used was very similar to the one recommended by Thyer (1962) which involves the calculation of rays from each theodolite with the balloon position assumed to lie along the shortest connecting line between the rays.

Dr. Fanaki suggested (personal communications) that the minisonde problems were primarily due to the occasional missing of data from one of the theodolites. In this case an assumed rise rate could be incorrect leading to superadiabatic lapse rates and unreasonable wind profiles. He argued that the smoothing techniques themselves should not have caused a problem for typical plume heights.

For the purpose of this study, the procedure adopted was to ensure that any given minisonde profile was consistent with other profiles taken earlier and later and at all sites in the AOSERP study region. For cases in which one or more profiles appeared to be inconsistent (such as June 22 1977 in the late afternoon and evening) a best estimate of the profile was made

upon the basis of what appeared to be meteorologically reasonable. In addition, minisonde profiles were re-examined for times when the observed plume sigma values in a typing scheme appeared to have large scatter from the expected values. Although there is a danger in biasing the results by a more critical examination of only a part of the data, it did provide a means of ensuring that large discrepancies from the typing schemes were not due to obviously inappropriate assignments of stability classes due to minisonde uncertainties.

The minisonde system like all other measurement systems has inherent sampling characteristics which lead to unavoidable statistical uncertainties in the measurements. The theodolites were sampled every 30 seconds. Thus winds were computed based upon 30-second separations of balloon position, equivalent to 30-second integrations of the actual balloon motions. For typical balloon rise rates of 2 m/sec, the wind (and temperature) vertical resolution is limited to 60 m by sampling restrictions. An averaging period of 30 seconds will remove only a portion of the wind direction and speed fluctuations leaving the estimate of the mean wind quite uncertain. Quantitatively, the averaging period will remove the wind speed and direction variance contributions from shorter period fluctuations in the wind spectra. However, the estimate of the mean wind will be affected by the remaining larger scale eddies which will have introduced statistical uncertainties in the mini-sonde wind estimate. For a typical wind speed of, say, 8 m/sec, the averaging length scale associated with each wind sample is about 250 m. For a height of 250 m, then, the normalized wave number is 1. This averaging period is very small compared to the time scale of the peak of the turbulent spectrum (see Panofsky (1973 p.169). Thus most of the turbulent eddies can still contribute to the statistical uncertainty of that single wind value. A rough estimate of $\sigma_u/\bar{U}$ is about 0.2 in strong winds (Shelland 1968) as reported by Pasquill (1974 p.84). Thus a

statistical uncertainty of typically 20% is associated with each minisonde data point. Clearly the magnitude of the uncertainty will depend upon stability and the details of the spectra of the horizontal wind components. For more unstable situations, an increase in low frequency spectral magnitude will cause a significantly greater uncertainty.

Averaging procedures can improve upon the statistical uncertainties inherent in the minisonde sampling. The best way is to have multiple minisondes and perform an ensemble average. In this way the vertical resolution is maintained. A possible alternative to multiple minisondes is the averaging over several data points on a single minisonde flight. If a running average is made over, say, 5 data points, (150 seconds, about 300 m in the vertical, and about 1200 m of horizontal distance for $\overline{U}$ = 8 m/sec), then a normalized frequency of about 0.2 is obtained. If the normalized frequency is treated as an Eulerian frequency, then it is still larger than the frequency of the spectral peak (Panofsky 1973 p. 169). There will be an improvement but a considerable statistical uncertainty remains. A further consideration is that the minisonde measurement is not strictly an Eulerian measurement since the minisonde advects with the wind as it rises. Any tendency towards the measurement being Lagrangian in form will further deteriorate the statistical reliability of the measurement.

Measurement errors could be another major source of uncertainty. The Askania theodolites used in the program have angular resolutions of 0.1° (Walmsley et al. 1978). However, as Walmsley et al. point out, the smoothing routines will tend to minimize the effects of these randomly distributed sampling errors.

One of the primary data outputs from the minisonde is the height of a limited mixing region. For this application, the statistical sampling restrictions are not as serious since the

height of the inversion interface will tend to be fairly stable except for the possible presence of internal gravity waves with the Brunt-Vaissala frequency. The lack of a second theodolite, however, will have a serious impact upon the estimation of the mixing height.

In summary, then, the minisonde data base is an extremely important source of data for stability classifications. It has inherent statistical sampling limitations which tend to be very important (≃ 20%) for estimations of wind speed in the mixed layer. The averaging procedures adopted by AES could generate monotonic segments which might be misleading; however some averaging is necessary to remove the sampling errors especially at larger elevations. The occasional lack of segments of data from the second theodolite could lead to very misleading profiles which could be detected only with access to the original field data sheets.

5.2.2 Tethersonde

The tethersonde system flown during the three intensive field studies was the system described by Mickle and Davison (1974), a modification of an original design by Klein and Bourke (1967). The tethersonde system was operated in either a profiling or fixed level mode and so could provide time-averaged statistics at heights above the physical stack height of the GCOS powerhouse stack. Details of the package and discussion of the data have been presented by Mickle et al. (1978).

Mickle et al. (1978) demonstrated the importance of sampling time on the wind speed. They reported that the 10-minute means of wind speed were found to vary up to factors of two over periods of 1 hour in both stable and neutral conditions. They suggested that extraction of wind information from profile data at hourly intervals and application of these data for intermediate times may "at best be no better than a factor of two". The

tethersonde data showed that,over 10-minute periods, the standard deviation of wind speed averaged 0.1 of the mean and often was much larger. If allowance is made for the additional variance contribution for time scales larger than 10 minutes, then the previous estimate of 20% uncertainty for minisonde winds is seen to be reasonable compared to the on-site tethersonde measurements. The conclusion by Mickle et al. that the profile uncertainties are as large for stable as for neutral conditions is somewhat surprising. Perhaps the uncertainties are associated with topographical effects which may be more important at heights less than the effective stack height for the GCOS powerhouse plume.

The profiling speed of the tethersonde was 0.3 m/sec. Rough calculations show that even with this slow profiling speed, the vertical interval over which data must be analyzed in order to remove the effects of eddies smaller than the spectral peak is typically 200 m (a time scale of about 10 minutes). These approximate calculations are qualitatively supported by the variability of the 10-minute averages reported by Mickle et. al.

In summary, the tethersonde system provided significantly more reliable profiles than the minisonde due to the inherent sampling characteristics of the systems. In addition, the tethersonde provided fixed level statistics which firmly documented the uncertainty associated with applying a single minisonde profile for the entire hour between minisonde flights. The fixed level statistics themselves could be used for plume spread non-dimensionalization. Unfortunately, the height range of the tethersonde measurements was often restricted to below the effective stack height.

Several of the typing schemes required estimates of wind direction fluctuations, σ_θ. There were three sources of data for σ_θ estimates: The aircraft values, the tethersonde wind direction fluctuation data $\sigma_\theta$and the tethersonde wind speed fluctuation

data $\sigma_u/\overline{U}$. A comparison with the aircraft values (for roughly equivalent averaging times) showed that the aircraft values agreed fairly well with the tethersonde $\sigma_u/\overline{U}$ values (see Table 11). For the selection of σ_θ, preference was given to the tethersonde $\sigma_u/\overline{U}$ values. This procedure may have led to slightly larger σ_θ values for stable conditions due to the asymmetry of the eddies. However, since the averaging time of 10 minutes often corresponded to a length scale somewhat less than the downward distance of many of the observations, this effect is probably not too significant. A further discussion is presented during the comparison of sigma values to the typing schemes.

5.2.3 Instrumented Aircraft

The meteorological measurements available from Intera's instrumented aircraft have been described in Davison et. al. (1977) and Davison and Grandia (1978). In brief, the measurements are made on the principal of measuring the wind with respect to a moving platform by means of gust probes and then removing the effects of platform motion which is sensed by a series of accelerometers and gyroscopes. Such a system has been used by many research groups (NCAR, NAE, University of B.C., etc.) and is a well established technology. However, the system has limitations due to accumulated measurement uncertainties and to drift problems in the gyroscopes. Perhaps the best validation of the system is the reproducibility of measurements and consistent trends in the vertical or with time (see, for example, Davison and Grandia 1978, Figure 36 and 48). Analysis blocks were usually 60 seconds long with linear detrending prior to variance computations. The aircraft speed was much greater than the wind speed. Thus the aircraft measurements can be considered to be similar to an Eulerian measurement. For a flight speed of about 60 m/sec, the large wavelength sampling limit is about 3600 m regardless of wind speed. The sampling

Table 11 A comparison of aircraft and tethersonde wind fluctuation data from 1977.

Date	Aircraft σ_θ	Tethersonde $\sigma_u/\bar{u}$	Tethersonde σ_Θ
June 19 AM	0.11	0.10	0.27
June 19 PM	0.18	0.17	0.41
June 22 early eve	0.13	0.11	0.27

interval leads to a non-dimensional frequency of about 0.1 sec^{-1} for typical plume heights and is roughly equivalent to an Eulerian sampling of 6 to 10 minutes depending upon wind speed. Often the statistics from runs at several heights within a particular meteorological region (e.g. early, mixed layer) were combined to give ensemble averages of up to 10 or more segments which were then used to non-dimensionalize the observed plume spread.

In the grouping of aircraft horizontal wind standard deviations, it was often assumed that the two components σ_v and σ_u were equivalent. At the small wavelengths, this assumption is undoubtedly valid. In a mixed layer it is widely accepted that the horizontal "eddies" are nearly horizontally isotropic (Panofsky 1973 p.168). This approximation was indeed confirmed by comparison measurements in orthogonal directions in the field. However, for stable conditions the eddies tend to be more elongated in the downwind direction, and so for a frequency band-limited sampling, there may be a difference between the lateral and longitudinal standard deviations. However, if most of the turbulent spectral contributions are sampled, then the assumption of equality of the standard deviations is probably valid. The sampling wavelength of 3600 m should include most of the spectral range which can affect the plume over the downwind range of plume sampling (about 3 to 10 km). However there probably was not any spectral gap between these measurement scales and larger scales. Mickle et al. (1978) mentioned the high degree of variability in the 10-minute average values. Thus the horizontal wind speed standard deviations calculated by the aircraft (or the tethersonde) cannot be considered as stable averages with respect to changes in averaging time. Fortunately, the 1-minute aircraft analysis blocks and the 10-minute tethersonde analysis blocks correspond to length scales typical of most of the aircraft and helicopter plume sampling downwind distances.

The aircraft system, then, had more serious measurement accuracy and noise problems than the other meteorological sensors but could improve significantly the statistical uncertainties inherent in the minisonde and to a lesser extent in the tethersonde data.

5.2.4 Bivane

Bivane measurements were made intermittently from the top of a 150 m meteorological tower at the Lower Syncrude site beside the Athabasca River. The base of the tower had an elevation of about 240 m MSL meaning that the bivane intrument was located at about 390 m MSL. This compares with the altitude of the top of the GCOS powerhouse stack of 366 m MSL. The data made available to this study were recorded on a 3-channel paper strip recorder during four time periods: November 1976, January/February 1977, July 1977 and November 1977. Only the February 1977 data coincided with an intensive field study. These February data were analyzed by Fanaki et al. (1978b) in terms of standard deviations over 30 minute intervals calculated after various pre-smoothing intervals of 10, 25, 50 and 100 seconds.

It was hoped that the present study could utilize the bivane data as analyzed by Fanaki et al. to test the Hay-Pasquill approach at further downwind distances. However only two helicopter sigma values could be so tested; it was decided that such a very limited comparison would not be worthwhile.

5.3 SO_2 DATA SOURCES

The primary objective of this study was to devise a practical scheme for the specification of Gaussian sigma diffusion parameters. The data base for plume dispersion was that provided by the three intensive field studies of March 1976, February 1977 and June 1977. The characteristics of each of the sampling systems are described below. Particular emphasis is directed towards the sampling and averaging characteristics inherent in each system and

towards the analysis techniques adopted by each researcher. The differences between Eulerian and relative dispersion, the effects of averaging times and the concept of representative sampling were discussed in Chapter 3. In the following sections, these ideas are applied to each of the plume measurement systems.

There are two data sources which were not used in this study. Syncrude Canada Ltd. sponsored a dispersion analysis program in 1977 which involved plume photography and airborne plume traverses. A preliminary report (Slawson et al. 1978) was kindly made available by Mr. Svenn Djurfors of Syncrude. However, since the data was newly collected and had not been fully analyzed, it was requested that these data not be used in the present study. These data, however, may be very helpful in subsequent validation studies of numerical models, if procedures for access to the data can be arranged.

There is a series of ground monitors of SO_2 which are mostly long term exposure cylinders distributed throughout the AOSERP study region. This data source will be of use in validating climatological dispersion models. However, they are not too useful for the purposes of specifying plume geometry as a function of environmental conditions for specific case studies. Hence these data were not used in the present study.

5.3.1 Plume Photography

5.3.1.1 Plume Photo Data Set. A photographic study of plume rise and vertical dispersion was undertaken by the Atmospheric Environment Service under the direction of Dr. F. Fanaki. Data was collected in each of the three AOSERP field trials; March 1976, February 1977 and June 1977. The experimental details, as abstracted from Fanaki et al. (1978a and 1978b), are outlined below. Complete details are contained in that report.

The camera was set up in a position to view the plume and the camera film plane was oriented parallel to a mean wind

direction abstracted from the Lower Syncrude minisonde. Photographs of the plume were then taken every 15 seconds for about 10 minutes. Quoting Fanaki et al., "the time-mean path of the plume was then determined by superimposing several photographs and tracing the plume outlines or by using time-average photographs of the plume".

Although the report does not specify, it is assumed that the height of the plume was then taken as the centerline of the time-mean path of the plume. Values of the vertical dispersion coefficient (σ_z) were estimated from the plume width by Fanaki et al. by assuming that the concentration of SO_2 at the visual edge of the plume was equal to one-tenth that of the plume centerline For a Gaussian plume this implies that

$$\sigma_z (x) = \frac{D_z}{4.3} (x) \qquad (5.1)$$

where D_z is the observed plume width and σ_z is the computed Gaussian sigma value. The approximation involved in the use of the above equation are discussed below,

For this report Dr. Fanaki has provided plume height data from the three field experiments, March 1976, February and June 1977. Plume dispersion data were available only from the February and June field trips. These data cover the downwind distance ranges from 200 m to a maximum of 1600 m, a range which is very important for specifying the important initial dilution stages of plume dispersion.

5.3.1.2 Geometry of Possible Errors in the Plume Rise Measurement. Analysis of photographic data has a long history of usage by workers in atmospheric diffusion. See for example Hogstrom (1964), the summary by Gifford (1968) or the discussion in Fanaki et al. (1978a). A thorough discussion of the errors inherent in single-camera measurement of plumes is contained in Halitsky (1961).

Some of his conclusions are incorporated into the following discussion and that paper should be referred to for further details.

Errors in evaluation of plume heights or widths result when the planes of the camera film and the plume are not parallel. The error in the calculated height resulting from the adoption of an incorrect plume bearing can be expressed as (see Figure 12)

$$\frac{Z}{Z_m} = 1 + X_m \quad B(\cot \alpha - \cot \theta)^{-1} \qquad (5.2)$$

where Z is the correct plume height, Z_m and X_m are the calculated height and downwind distance, B the perpendicular distance between the camera lens and the assumed plume axis, $90-\theta$ is the angle between B and the observed point of the plume and α is the angle between the actual and assumed plume trajectories. For details of the development of (5.2) see Appendix 1. Representative errors in plume rise are tabulated in Table 12 for different values of X_m/B, α and θ. Note that these errors are for the height above the ground elevation of the camera. The relative error in plume rise above stack height will be larger since this correction is applied to the measured height before the stack height is subtracted.

5.3.1.3 Camera Orientation Uncertainties.

There were two possibilities for determining camera orientation for the plume photography. One method was to use the wind profile as measured during a preceding minisonde ascent. A second method was to make a visual estimate of the plume direction of travel.

Observations of a minisonde ascent required about 10 to 15 minutes and processed profiles would have been at least one hour old so that time trends in the wind direction could become important. In a statistically stationary atmosphere the typical sampling error of wind direction in the mixed layer would be approximately 10°.

Variation of the mean wind direction with height in the boundary

Plan View:

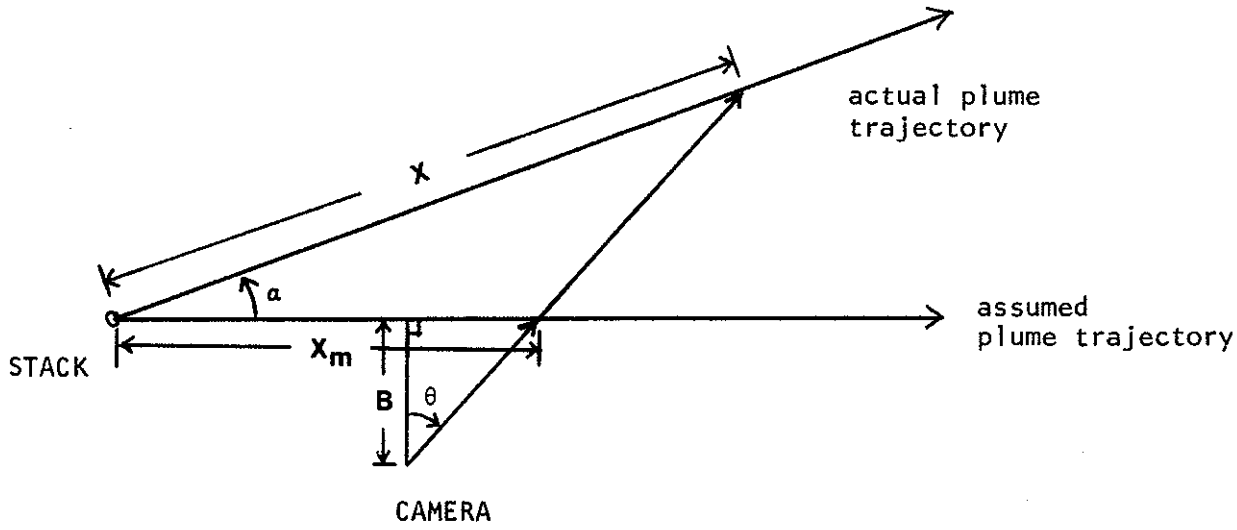

Vertical View:

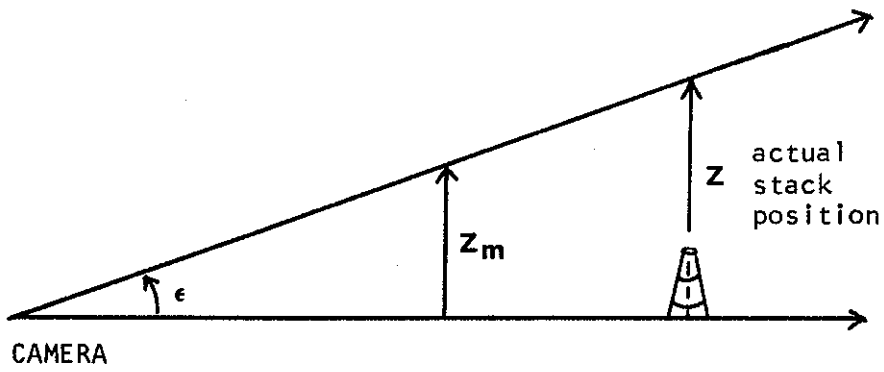

Figure 12 The geometry of single-camera plume photography for an error in the assumed plume trajectory.

Table 12 The relative size of errors resulting from an incorrect assumption of plume trajectory, as a function of the angular and spatial geometry of the measurement. The angles and lengths have been defined on Figure 12.

$\frac{X_m}{B}$	α (degrees)	Θ (degrees)	$\frac{X}{X_m}$	$\frac{Z}{Z_m}$
2	15^o	45^o	1.41	1.73
		60^o	1.22	1.46
	10^o	45^o	1.23	1.43
		60^o	1.13	1.39
	5^o	45^o	1.06	1.18
1	15^o	45^o	no change for $\frac{X_m}{B}$ change	1.37
		60^o		1.23
	10^o	45^o		1.22
		60^o		1.20
	5^o	45^o		1.09
0.5	15^o	45^o		1.18
		60^o		1.12
	10^o	45^o		1.11
		60^o		1.10
	5^o	45^o	no change	1.05

layer causes an additional problem since the appropriate plume bearings can not be determined until the plume heights are calculated. Abstraction of wind direction profiles showed that about half of the data times had wind shears exceeding 10^{o}/100 m in the layer of plume rise. A conservative estimate for the resulting uncertainty in wind direction or plume bearing is then approximately 5^{o}. Note that this error is additive to the statistical error discussed above. Thus the estimates of the average wind direction based upon minisonde data would be typically 10^{o} or more in error.

A visual estimate of the plume direction by a skilled observer able to look at the plume from two perspectives is probably as reliable as an estimate based upon a single minisonde. The visual estimate permits an averaging over the length of the plume removing some of the statistical uncertainty of a single minisonde ascent. However, the presence of wind direction shear still introduces a significant problem in selecting any representative single wind direction.

In summary, camera mis-alignment could result from (1) initial uncertainty in the determination of the correct plume orientation, (2) a shift in the mean wind direction during the observation period, (3) fluctuations in the wind direction about a stationary mean during the observation period and (4) variation of wind direction with height over the depth of plume rise.

5.3.1.4 Evaluation of the Plume Photography Analysis Techniques. There would be errors associated with the plume photography measurements themselves. Fanaki et al. (1978a) indicated that photographs were taken about every 15 seconds for 10 minutes. Thus the fluctuations in wind direction and speed over 10 minutes can be averaged out. The difference between the mean wind direction over this 10 minutes interval and the assumed wind direction (for camera orientation) is the value α in the error estimates of Table 12. Fluctuations in wind speed will cause variations in the plume rise.

However, averaging of all the photographs will tend to give a plume rise value appropriate to the wind speed encountered by the plume in that particular 10 minute interval. The assumed wind speed estimate from the minisonde, however, may be significantly different. Thus uncertainties in the mean wind direction will lead to errors in the estimates of plume rise and thickness; uncertainties in the mean wind speed will lead to improper nondimensionalization for comparison with theory and typing schemes.

The use of the 10% criterion is fairly wide-spread but has little justification. The early diffusion experiments at Porton and Cardington in England in the 1920's and 1930's used the 10% criterion to define the plume width. However, in these experiments, actual concentrations were measured and the 10% criterion was a convenient measure which was not related to visual cloud width.

A fairly widespread technique for photographic analysis was presented by Gifford (1957); see also Pasquill (1974 p. 215) and Gifford (1968 p. 103). In this technique it is assumed that the visual edge represents some threshold integrated concentration along the line of sight. At a sufficiently long downwind distance this concentration level (or isopleth) would eventually close as represented in Figure 13. If the plume is Gaussian then,

$$(\sigma_z^2)_{max} = 1/2\ r^2_{max} \tag{5.3}$$

where r_{max} is the maximum visible radius. The value of σ_z at other downwind distances can be expressed as

$$\sigma_z^2 = \frac{r^2}{2} \left[\ln\left(\frac{e\ r^2_{max}}{2\sigma_z^2}\right) \right]^{-1} \tag{5.4}$$

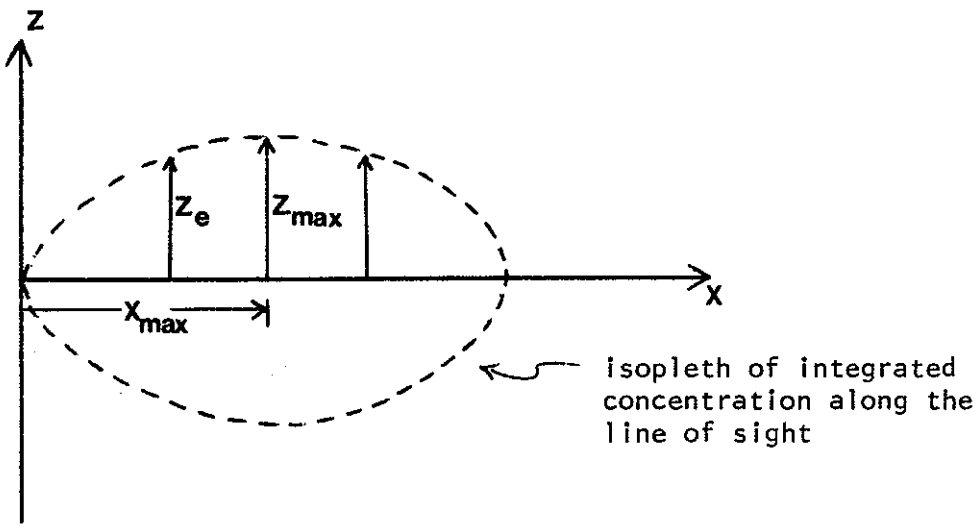

Figure 13 A highly schematic visual plume outline determined by limiting isopleth of integrated concentration along the line of sight. The marked variables appear in Gifford's (1957) equation discussed in the text.

Here e is the exponential constant and r is the half-thickness at the downwind distance at which σ_z is to be evaluated. Hogstrom (1964) used essentially this method to determine σ values in his study of smoke puff dispersion. Although the above procedure is much more rigorous then the 10% criterion, it also requires the detection of the maximum plume thickness. For many practical industrial applications, the presence of complicating features such as inversions, and simply the large downwind distance needed to reach the maximum visible thickness preclude the use of Gifford's approach. In such situations, the adoption of a 10% criterion has the strength of common usage even if it is clearly a rough approximation.

It is appropriate to now consider the physical implications of assuming a 10% criterion. Near the source, the plume will probably have a distribution closer to that of a "top-hat" profile rather than a Gaussian. At these small downwind distances, the plume boundary is a region of a very large concentration gradient. A second moment standard deviation for a top hat profile of total thickness, D, is given by

$$\sigma_z = \frac{D}{3.5} \tag{5.5}$$

The adoption of the 10% criterion would lead to a different value of σ_z (20% smaller); however, the approximation is not too serious. After further dispersion time, the concentration distribution would approximate a truncated Gaussian. If the visible boundary represents a constant threshold integrated concentration, then the position of the visible boundary will correspond to a changing ratio of the centerline concentration. Eventually the isopleth would close, as in Gifford's representation. Thus the calculated σ_z values using the 10% criterion would represent increasingly larger percentages of the centerline concentration with increasing distance. The downwind change in these calcuated σ_z values would

then not increase as rapidly as the second moment standard deviation; they would eventually begin to decrease with distance. Thus the 10% criterion can only be used over a limited range of downwind distances and may give inaccurate estimates of the X-dependence of σ_z.

In a practical application such as in AOSERP, the visible plume boundary is probably not a simple constant integrated concentration. Pasquill (1974 p.167) comments that "the real meaning of the boundary of the smoke, however, unequivocally this may be recognized, is open to some doubt". The selection of plume boundaries will depend partly on observers bias, contrast with the background, etc. Also the concentration at the visual upper and lower boundaries may vary, particularly when plume rise is inhibited by an inversion or by a stable boundary layer. This makes it difficult to use Gifford's approach without careful control over the data reduction process.

Probably the potential for underestimating the values of σ_z is greatest at the shortest distances $X < 400$ m and the longer distances $X > 800$ m. These limitations must be considered when attempting to use the plume photography data in evaluating initial dispersion.

5.3.2 COSPEC

A summary of the experimental techniques used for the COSPEC measurements at AOSERP has been presented by Fanaki et al. (1978). Some additional considerations of the instrumental response characteristics and of the accuracy of the geometric interpretations have been presented by Millan and Hoff (1977) and Millan (1976). In brief, the COSPEC is a passive remote sensor sensitive to the absorption of ultraviolet radiation by SO_2. In the AOSERP field programs, the COSPEC was used in a vertically pointing mode and the amount of SO_2 absorption was measured during transects of the plume in a vehicle along the available road network or in a boat along the Athabasca River. The transects were not, in general,

perpendicular to the plume axis; however, the errors associated with the geometric projections of the plume sections have been considered carefully by Millan (1976).

5.3.2.1 Effects of Wind Shear on the COSPEC Measurements

Since the COSPEC is a vertically integrating measurement system, the effect on the sigmas for a tilted plume due to wind shear effects was examined. The first stage was to verify that the sigma values for the COSPEC would be the same as for an in-situ measurement through the plume centerline (by an aircraft, for instance) for an idealized Gaussian plume. The next stage was to compare the sectionings for a tilted ellipse.

A Gaussian plume cross-section in the Y-Z plane can be represented by

$$X\ (Y,Z) = \frac{Q}{2\Pi\ \sigma_y\ \sigma_z u} \quad \exp\left(-\frac{y^2}{2\sigma_y^2} - \frac{z^2}{2\sigma_z^2}\right) \tag{5.6}$$

where the coordinate axis is centered on the plume center-line. Vertically integrating we have

$$\chi_c = \int_o^\infty X(Y,Z)\ dZ = \frac{Q}{2\Pi\ \sigma_y\ \sigma_z u}\left[\exp\frac{-Y^2}{2\sigma_y^2}\right]\int_o^\infty \frac{-Z^2}{2\sigma_z^2}\ dz \tag{5.7}$$

where χ_c is the COSPEC integrated concentration. The only y-dependence in (5.7) is in the term in square brackets and it is clearly the same as for the original Gaussian (5.6). The Gaussian formulation permits a separation of variables, and so for a Gaussian plume (no shear distortion) the COSPEC σ_y values should be identical to an in-situ measurement at plume centerline.

In the presence of a direction shear in the wind with height, the plume will appear to be tilted in the Y-Z plane. Dispersion at a given level will also be enhanced due to the interaction of the vertical turbulent fluctuation and the wind shear as discussed in Chapter 3. The Gaussian plume should not be viewed as being rotated in the Y-Z plane in the presence of shear distortion. The dispersion at a given level will be the same (actually larger) as the plume in a non-shear situation. It is thus more appropriate to view the plume as a series of thin slices in the Z-direction having been horizontally displaced (in the Y-direction) with height as shown in Figure 14. As can be seen in the Figure, an in-situ measurement through the centerline would shown no difference. However the vertically integrating measurement of the COSPEC will show a slightly larger σ_y value. Also the maximum integrated concentration through the center of gravity of the plume will be less since the integration line will pass through the center of gravity (COG) of only the middle slice of the plume. At all other heights, an off-axis concentration value will be sampled. The magnitude of this shear displacement effect will tend to increase with downwind distance after the transition of the plume from its self-preserving initial stage. Note that the use of the larger COSPEC value of σ_y for a shear distorted plume in a Gaussian model would lead to under-estimation of the concentrations. In terms of a Gaussian distribution the distribution could be approximated as:

$$\chi = \frac{Q}{2\pi\,\sigma_y\,\sigma_z\,\overline{U}} \exp\left[-\frac{1}{2}\left(\frac{Y - \overline{Y}\,(Z)}{\sigma_y}\right)^2\right] \exp\left[-\frac{1}{2}\left(\frac{Z - H}{\sigma_z}\right)^2\right] \qquad (5.8)$$

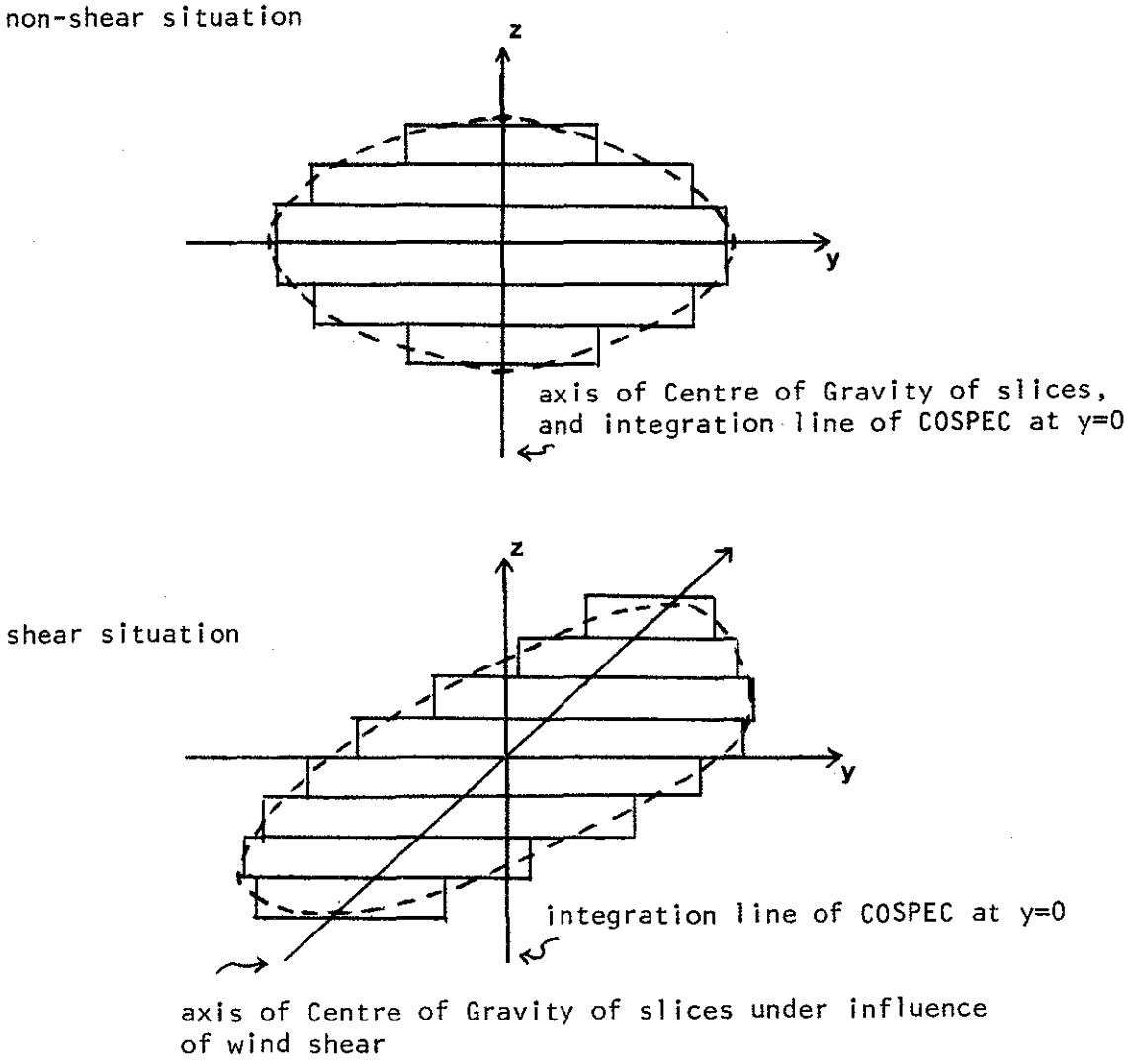

Figure 14 The effect of wind shear on plume cross-sectional shape.

where $\overline{Y}(z) \simeq \tan(\alpha(z))\ X$. This would also correct for the displacement of the maximum ground level concentration from the plume centerline.

The presence of vertical mixing through the height of the plume centerline will tend to minimize this distortion effect. In a mixed layer, the strong shears cannot exist and so the distortion of the plume is small. During fumigation by a distorted plume, the previously generated distortion will tend to generate a wider distribution reflecting the earlier COSPEC σ_y. However, for testing of disperion formulations, the COSPEC σ_y values may be anomalously large in stable shear conditions.

5.3.2.2 Effects of Multiple Sources. Because the COSPEC vertically integrates, it cannot differentiate between plumes at different heights. At GCOS the main powerhouse plume generated most of the SO_2. For 1976, the total emissions of SO_2 could be considered as coming from 3 sources (Shelfentook (1978):

Steam plant (powerhouse stack)	79000 metric tons
Sulphur recovery (incinerator stack)	9300 metric tons
Flare stacks	4680 metric tons

Since the flare stacks effluents were intermittent, the flare stacks on a given occasion could represent a more significant source than the annual average would suggest. Nevertheless, the powerhouse stack can be expected to dominate the total SO_2 and should dominate a vertically integrating measurement from the COSPEC. This conclusion is different from the interpretation of the multiple peaks presented by Hoff for the June COSPEC data. The present authors are convinced that the observed fluctuations of the COSPEC traces represent the puffiness of the main plume as are visible in plume photographs.

5.3.2.3 Relative and Eulerian Dispersion Measured by the COSPEC. The individual COSPEC traverses were averaged by Hoff et al. (1978) in two ways to produce estimates of both relative and Eulerian dispersion. As discussed earlier relative dispersion is dispersion with respect to the centerline. Thus averaging of the COSPEC traverses making the COG's coincident, generates an approximation of the time averaged relative dispersion. The averaging of the COSPEC traverses with distances along each traverse measured in a fixed Eulerian frame of reference generates on approximation of the time-averaged Eulerian dispersion (what Pasquill (1974) refers to as "time-averaged dispersion"). Thus the COSPEC data permits a critical examination of the difference between relative and Eulerian dispersion. Since the helicopter and aircraft measured relative dispersion and dispersion models usually work with Eulerian dispersion, this comparison is very significant.

Note that since the COSPEC operates in a traversing mode, a single traverse has no averaging time associated with it. The averaging of several traverses represents an ensemble average of essentially instantaneous traverses. The only way to have time-averaging associated with a given traverse is to smooth the profile data. The time base of the smoothing function could then represent an averaging interval. Relative dispersion (without smoothing) measured by a COSPEC does not depend upon the speed of the traverse.

The March 1976 COSPEC data included tabulation of both ensemble-averaged relative dispersion and ensemble-averaged Eulerian dispersion. (The relative dispersion was referred to as "pseudo-Lagrangian" by Hoff et al.). For downwind distances of 3.6 to 4.0 km, the differences in the calculated σ_y values were

$$\sum_{i=1}^{6} \left(\frac{(\text{Eulerian})_i - (\text{Relative})_i}{(\text{Eulerian})_i} \right) = 0.07 \qquad (5.9)$$

the standard deviation of the samples was 0.05; the computed standard deviation of the population of mean differences was 0.02. These data suggest that for downwind distances greater than about 3 or 4 km, the averaged relative dispersion is similar to the averaged Eulerian dispersion under the neutral and stable meteorological conditions represented in the COSPEC measurements.

The COSPEC data from the June 1977 field study included plots of relative and Eulerian dispersion. Qualitatively there were few marked differences between the two types of averaging. Individual traverses, on the other hand, showed significant differences (up to a factor of 2) in σ_y values from either of the averaged cross-sections at a downwind distance of 3 km. Thus, it appears that a major problem especially in unstable conditions, is to obtain representative values of relative mixing. Obtaining representative values is probably more important than the differences between relative and Eulerian averaged distributions. Photographs showing the "puffiness" of the plume make this conclusion understandable.

The COSPEC data can provide numerical values for the range of bearings of the center-of-gravity (COG). Although the tabulated values (available for March 13 and 15 case studies) refer to the integrated plume, they are reasonable estimations of the main plume COG variation. For the 8 runs of March 13, the range of COG hearings was 6.8° with the maximum difference between adjacent runs (10 minutes apart) being 6.3°. For the 14 runs of March 15, the range of COG hearings was 18.8°, occurring for adjacent runs. The range of COG bearings within the four 1/2 hour analysis period on March 15 were 18.8°, 12.2°, 3.4° and 6.4°. The 1/2 hour average COG bearings varied by 3.0°. The above values for fluctuations of plume bearing suggest that an uncertainty of at least 5° to 10° can be expected for the angular direction assumed for plume photography.

5.3.2.4 Summary of the Characteristics of the COSPEC Data. The characteristics of the COSPEC sigmas have been discussed in the preceding sections. The essential conclusions are:

(a) There is, in general, little systematic difference between the average relative dispersion profile and the average Eulerian profile. However, there are often significant differences for individual traverses.

(b) There are probably some instances of multiple source effects especially for ground level concentrations close to the plant (e.g. on the Athabasca River). However, some of the effects ascribed to multiple sources may be due to break-up of the main plume in summertime convective conditions.

(c) The integrating nature of the COSPEC means that directional shear will generate a larger COSPEC σ_y than that measured from an elevated plume traverse.

(d) The two effects of multiple sources and shear effects limit the usefulness of the COSPEC in the determination of appropriate σ_y values for some meteorological situations. However the COSPEC is undoubtedly an effective sensor for estimating total mass flux if sufficient traverses can be made to obtain representative values.

5.3.3 LIDAR Data

5.3.3.1 Outline of the Data Set and Analysis Technique. The AES used a mobile research laser (LIDAR) to observe the GCOS plume in the June 1977 field study. Results of this experiment are contained in a draft report by Hoff and Froude (1978). This is the first experimental use of the AES system and based on this first effort it is obvious that this instrumental system will be an exciting research tool for studying atmospheric dispersion.

The plume was scanned by setting a fixed azimuth angle and stepping the elevation angle between shots. Each back-scattered signal was sampled 500 times for a minimum sampling spacing of 1.5 m; the digitized values were recorded on magnetic tape for later processing. Each complete scan required 3 to 5 minutes to complete.

During an operation period three to six sequential scans were obtained. Eulerian averages of the plume geometry plus estimates of the variability in the dispersion over the sampling periods were obtained from the series of sequential scans.

Sigma values were computed by Hoff and Froude using the second order technique, i.e.

$$V_{y,n} = \sum_{j=1}^{N} \sum_{i=1}^{500} S_{i,j} Y_i^n / \sum_j \sum_i S_{i,j} \qquad (5.10)$$

where N is the number of shots per scan, $S_{i,j}$ is the digitized signal, n is the moment number and Y_i is the horizontal projection of the scan. The lateral dispersion coefficient is then computed from

$$\Delta_y = (V_{y,2} - V_{y,1}^2)^{1/2} \cos \sigma \qquad (5.11)$$

where σ is the slant angle. Similar expressions can be written for the vertical coefficients. Hoff and Froude analyzed 58 scans from which 13 Eulerian averages were calculated.

5.3.3.2 Characteristics of LIDAR Sampling and Averaging. The type of sampling involved in a LIDAR needs to be examined carefully. The LIDAR return is equivalent to a virtually instantaneous traverse of the plume at a particular slant angle. The absolute position of the return is known and so the measurement is a true Eulerian measurement. A problem arises in that consecutive shots are looking at a changed plume, an effect which is particularly important very close to the stack. Thus the irregularities of the plume cross-section shown in the Hoff and Froude paper is not surprising. The 3 to 5 minutes required to scan the plume does not represent an averaging time. The plume data is of a discontinuous, instantaneous nature. Only by performing running averages over a number of different elevation angles is there any

averaging of the concentration isopleths. The calculation of the plume statistics such as COG and the sigma values has a type of implicit averaging. Clearly, if the changes in elevation angle between consecutive shots are small, then there is a repeated sampling of effectively the same part of the plume. Nevertheless, since a scan took between 3 and 5 minutes, with perhaps 10 or 15 shots per scan, this pseudo-averaging in terms of overlapping cannot be large. Each scan should be interpreted as essentially an instantaneous view of the plume. The interpretation of the "scan average" from 3 to 6 scans must also be examined carefully. In terms of sampling theory, the scan average could only represent a true time average if there were no aliasing in the sampling. The plume clearly had a significant variability in structure and so aliasing is present. The scan average could still approximate a time-averaged distribution if there were sufficient scans to adequately represent the distribution of possible plume forms. Three to six scans is only marginally adequate. Thus, the scan average is only a rough approximation to the time-averaged plume distribution. It may under or over estimate the true time-averaged values.

Hoff and Froude suggested that the 3rd moment, skewness, of the distribution was a measure of the effects of wind shear. As discussed in a previous chapter there are three effects of wind shear: a change in the plume centerline trajectory with height, a distortion of the plume cross-sectional shape and enhanced lateral dispersion at all levels due to the interaction of shear and vertical mixing. They apparently are referring to the second effect: the distortion of the plume cross-sectional shape. However, a uniform shear which distorts the plume cross-sectional shape does not change the skewness from zero. The vertically integrated concentration profile in the Y-direction is still symmetric and so the Y-skewness is zero. The observed skewness could arise from a number of effects including the non-uniformity of the direction shear and secondary sources. However, it is important to recognize that a small skewness does not indicate a lack of wind direction shear.

5.3.3.3 Problems in the Weighted Averages of Sigmas. The Eulerian average σ_e of a sequence of scans can be expressed as:

$$\sigma_{y,e}^2 = \left(\sum_i^N W_i \sigma_{y,i}^2 + \sum_{i=1}^N W_i \Delta y_i^2 \right) \Big/ \sum_i W_i \qquad (5.12)$$

where N is the number of individual averages, $\sigma_{y,i}$ represents the individual estimate of relative dispersion for the i^{th} scan, W_i are the weights if total concentrations vary between plume sequences and Δy_i^2 represents the variance of the plume centerline (in this case of the center of gravity). It is apparent that the Eulerian average cannot be less than the weighted average of the relative sigma values and also that $\sigma_{y,e}^2$ must be greater than or equal to the minimum value of the $\sigma_{y,i}^2$. However, in data sequence 5, 10 and 13 in the paper by Hoff and Froude the quoted Eulerian averages are less than the minimum estimate of the relative dispersion. For this reason the individual sigma values in the present review study have been averaged to obtain average relative sigma values.

Some additional comments on the data set are outlined in Table 13 in terms of the scan average (SA) number utilized by Hoff and Froude. For the reasons outlined in Table 13 SA 3 will not be used in this analysis, the 1350 scan in SA 6 was deleted before averaging and SA 7 was split into two parts, SA 7A includes the 1631 to 1706 scans and SA 7B includes the 1715 and 1720 scans. The average values presented by Hoff and Froude were not used due to inconsistencies in them. Instead, averages from the individual scans were computed (generating average relative sigmas and not average Eulerian sigmas) and are listed in Table 14.

5.3.3.4 Problems in the Magnitudes of the Sigma Values. It appears that the computed sigma values for the LIDAR data are very large compared to the distance from the centerline to the position having a concentration of 10% of centerline concentration. Ten YZ plots (in the scanning plane) are available in Hoff and

Table 13 Comments on the individual scan averages of the LIDAR Data using the same numbering system for the data as in Hoff and Froude (1978).

Scan Average # 1	Plume rise and sigma values are very small. One possible explanation is that the LIDAR was looking at a secondary source.
Scan Average #2	The plume bearing changed from 241° to 187°, a 54° shift in wind direction in 50 minutes. This caused σ_{ye} to be very much larger than any individual scan σ_y.
Scan Average # 3	There was a large variation in computed plume rise, from 223 m to 87 m; also the calculated downwind distance varied from 1317 m to 1731 m. These data should not be used.
Scan Average # 4	Eulerian plume rise is 3 m higher than any individual scan plume rise. The range of x distances was 781 m to 1160 m.
Scan Average # 5	The scan average σ_y was less than any of the individual scan σ_y.
Scan Average # 6	One scan has an x value of 957 m while the other two were less than 700 m; the values for the 957 m downwind distance were not used. The sigma values were very large.
Scan Average # 7	A sharp change in the calculated plume rise occurred between 1706 and 1715 LST. Scan Average 7 was divided into two groups.
Scan Average # 8, # 9	No comments.
Scan Average # 10	The scan average value of σ_y was less than that of any individual scan σ_y. Plots of YZ scan planes suggest that σ_y were overestimated based upon the plume isopleths.
Scan Average # 11	Plots of YX plane suggest that σ_y was overestimated.
Scan Average # 12	The scan average downwind distances was less than any individual scan value.
Scan Average # 13	The scan average value of σ_y was less than any individual scan σ_y.

Table 14 A summary of the LIDAR data as presented by Hoff and Froude (1978) with recalculated average relative dispersion sigma.

SA#	DATE	TIME BEGIN SCAN (MST)	TIME END SCAN (MST)	# OF SCANS	X DISTANCE (m)	PLUME HEIGHT (m)	REL $\bar{\sigma}_y$ (m)	REL $\bar{\sigma}_z$ (m)
1	17	1048	1100	4	217	$52^{+}_{-}11$	$40^{+}_{-}7$	$28^{+}_{-}11$
2	18	0525	0615	5	251	$186^{+}_{-}7$	$94^{+}_{-}12$	$73^{+}_{-}8$
3	-	-	-	-	-	-	-	-
4	21	0915	0924	5	920	$129^{+}_{-}12$	$114^{+}_{-}20$	$60^{+}_{-}7$
5	21	1048	1105	4	685	$192^{+}_{-}32$	$112^{+}_{-}17$	$95^{+}_{-}28$
6	21	1350	1410	2	676	$609^{+}_{-}32$	$275^{+}_{-}74$	$351^{+}_{-}98$
7A	22	1631	1706	5	441	$200^{+}_{-}20$	$91^{+}_{-}17$	$92^{+}_{-}41$
7B	22	1715	1720	2	424	$107^{+}_{-}18$	$90^{+}_{-}11$	$67^{+}_{-}13$
8	22	1922	1959	4	484	$70^{+}_{-}18$	$118^{+}_{-}40$	$58^{+}_{-}23$
9	22	2037	2101	5	83	$33^{+}_{-}5$	$34^{+}_{-}5$	$13^{+}_{-}3$
10	22	2123	2145	6	472	$95^{+}_{-}10$	$101^{+}_{-}22$	$38^{+}_{-}8$
11	23	0454	0506	3	487	$114^{+}_{-}33$	$138^{+}_{-}25$	$63^{+}_{-}19$
12	23	0530	0553	7	939	170	180	80
13	23	0602	0610	2	1319	168	308	80

Froude report. The plots show relative concentration isopleths (10%, 40% and 70%) as well as the computed COG and computed σ_y values. In almost all cases the range of $2\sigma_y$ is about equal to or greater than the widths of the 10% concentration contours. For a Gaussian plume, the width of the 10% concentration isopleth would represent 4.3 σ. Obviously the plumes are not strictly Gaussian but a factor of two difference in the sigmas is difficult to explain on the basis of non Gaussian shape. A similar although perhaps not as severe a problem appears to exist for the σ_z values.

The second moment technique can overestimate sigma values if there is background noise or there are secondary sources. Hoff and Froude present several Y-Z plane graphs of normalized concentrations isopleths which clearly show the existence of small secondary peaks isolated from the major plume. It is also clear from these plots that the plume was often very non-Gaussian making it difficult to decide how the calculated sigmas relate to the equivalent Gaussian distribution. The fluctuations observed are perhaps not too surprising considering the small downwind distance of measurement (typically less than 1 km). Thus, part of the discrepancy between the second moment sigma values (especially σ_y) and the 10% isopleth may be related to the inadequacy of the sampling to generate realistic isopleths. However, the size of the discrepancy (a factor of over 2) suggests that a proper noise limiter has not been used prior to the calculation of the second moments, in order to eliminate the contribution of non-plume (in fact non-main-plume) signals to the plume statistics.

The inclusion of data from all levels in the computation of σ_y is an important feature of the LIDAR σ_y calculations. The procedure used for the calculation of σ_y for the LIDAR effectively vertically integrates prior to the calculation of σ_y. Thus the LIDAR data has been analyzed as if it were COSPEC data and some of the advantages of the vertical resolution provided by the LIDAR have been lost.

The error in the calcuation of σ_z due to extraneous signals contributions to the variance may be much smaller than for σ_y. The LIDAR scan is limited in the vertical; thus the ratio of Z to Y distances included in the computation would, perhaps, be of the order of 1:5. Also, in the vertical, some of the back-scattered signal lies close to the plume centerline and may not have caused a significant error in σ_z. In stable conditions, the effect of different plume rises for the main and secondary sources may result in significantly larger calculated values of σ_z than would result for each plume considered separately. The calculated values in such cases would tend to be larger than any realistic dispersion theory would predict.

5.3.4 Helicopter

5.3.4.1 Summary of the Helicopter Data. During the February 1977 field study, a helicopter was used to obtain in-situ estimates of the plume dispersion coefficients (Fanaki et al. 1978). The instrumentation consisted of a Sign-X SO_2 analyser (the same as for the aircraft measurements) with the output recorded on a strip chart recorder. Calibration of the Sign-X system was checked in the field using standard cylinders of nitrogen and SO_2. A summary of the plume sigma values are presented in Table 15; the sigma values were calculated from a Gaussian assumption as discussed below. The following sections outline the limits of confidence and the characteristics of these helicopter sigma values.

5.3.4.2 Discussion of the Techniques Used for the Derivation of the Helicopter Sigma Values. As outlined in Fanaki et al. (1978b p.114), the sigma values were solved using isopleths and a Gaussian formulation:

Table 15 A summary of the helicopter derived plume sigma values. These data appeared in Table VI of Fanaki et al. (1978b)

Date	Time (LST)	Distance from Stack (km)	σ_y m	σ_z m
Feb 5, 1977	0840-0910	8.0	630	43
	0935-1000	30.6	650	31
Feb 6, 1977	1435-1455	0.8	290	66
	1525-1605	16.9	1500	91
Feb 10, 1977	1020-1030	0.8	440	31
	0950-1005	9.7	1400	28
	0830-0920	30.4	2200	20
Feb 11, 1977	1430-1450	2.0	470	83
	1500-1530	12.0	680	81
	1550-1600	28.8	1000	84

$$\chi = \frac{Q}{2\Pi \sigma_y \sigma_z \bar{U}} \exp\left(\frac{-Y^2}{2\sigma_y^2} - \frac{(Z-H)^2}{2\sigma_z^2}\right) \quad (5.13)$$

At a given concentration $\chi = C$,

$$\frac{Y^2}{2\sigma_y^2} + \frac{(Z-H)^2}{2\sigma_z^2} = \ln \frac{Q}{2\Pi \sigma_y \sigma_z \bar{U} C} \quad (5.14)$$

At $Z = H$, for $\chi = C$, call $Y = Y_c$ (isopleth boundary in the Y-direction),

$$Y_c^2 = 2\sigma_y^2 \ln \frac{Q}{2\Pi \sigma_y \sigma_z \bar{U} C} \quad (5.15)$$

At $Y = 0$, for $\chi = C$, call $Z = Z_c$ (isopleth boundary in the z-direction),

$$Z_c^2 = 2\sigma_z^2 \ln \frac{Q}{2\Pi \sigma_y \sigma_z \bar{U} C} \quad (5.16)$$

The area, A, enclosed by the isopleth will be ellipse of area $\Pi Y_c Z_c$ can be written,

$$A = 2\Pi \sigma_y \sigma_z \ln \frac{Q}{2\Pi \sigma_y \sigma_z \bar{U} C} \quad (5.17)$$

With the inputs of source strength (Q), wind speed ($\bar{U}$), and the area enclosed by a given concentration isopleth, then one can solve for $\sigma_y \sigma_z$ and then σ_y and σ_z separately.

The above technique of estimating the plume sigmas is equivalent to using the mass flux to back out the sigmas except that one is not so sensitive to edge contributions to the mass flux. The mass flux computations presented by Davison et al. (1977) and Davison and Grandia (1978) typically showed variations of 25% attributed mainly to wind uncertainties and coarseness of

sampling. Note however that $\overline{U}$ was allowed to be a function of height in those calculations of mass fluxes, rather than a single value as in these helicopter derivations.

The technique used for the helicopter data adds the uncertainty associated with obtaining representative plume geometry measurements to the uncertainty of the Gaussian formulation of Q, and, perhaps most importantly, of selecting the appropriate $\overline{U}$. Thus the uncertainties in the sigma values derived from the helicopter data are at least 25%. Closer to the stack (less than about 2 or 3 km) where it is very difficult to obtain representative isopleths due to the puffiness of the plume, the uncertainties are probably larger.

A limited repeatability check on the concentration profiles during plume traverses demonstrated a disturbing lack of repeatability (Figure 15 taken from Figure III.19 to III.21 in Fanaki et al. 1978b). The runs at 8 km (about 0900 on February 5) were made under very stable conditions as shown by the minisonde profiles and by the very small σ_z values which apparently decreased from 8 to 30.6 km downwind (measurement error or time change). The runs at 16.9 km (about 1340 on February 6) were still made under stable conditions but in the presence of a strong wind speed shear with height. The lack of reproducibility suggests the presence of waves or perhaps variations in plume rise associated with fluctuations of wind speed. For such vertical thin plumes, changes of centerline height of only 50 m could markedly change the concentration profile for a given flight. The presence of dual peaks for the first flight at 16.9 km suggests a possible wave phenomenon. The presence of changes in local plume height with time and the limited vertical extent of the plume impacts significantly upon the mass flux and area technique of calculation sigmas. The unavoidable uncertainty in σ_z calculation in such stable circumstances is transferred by this calculation technique

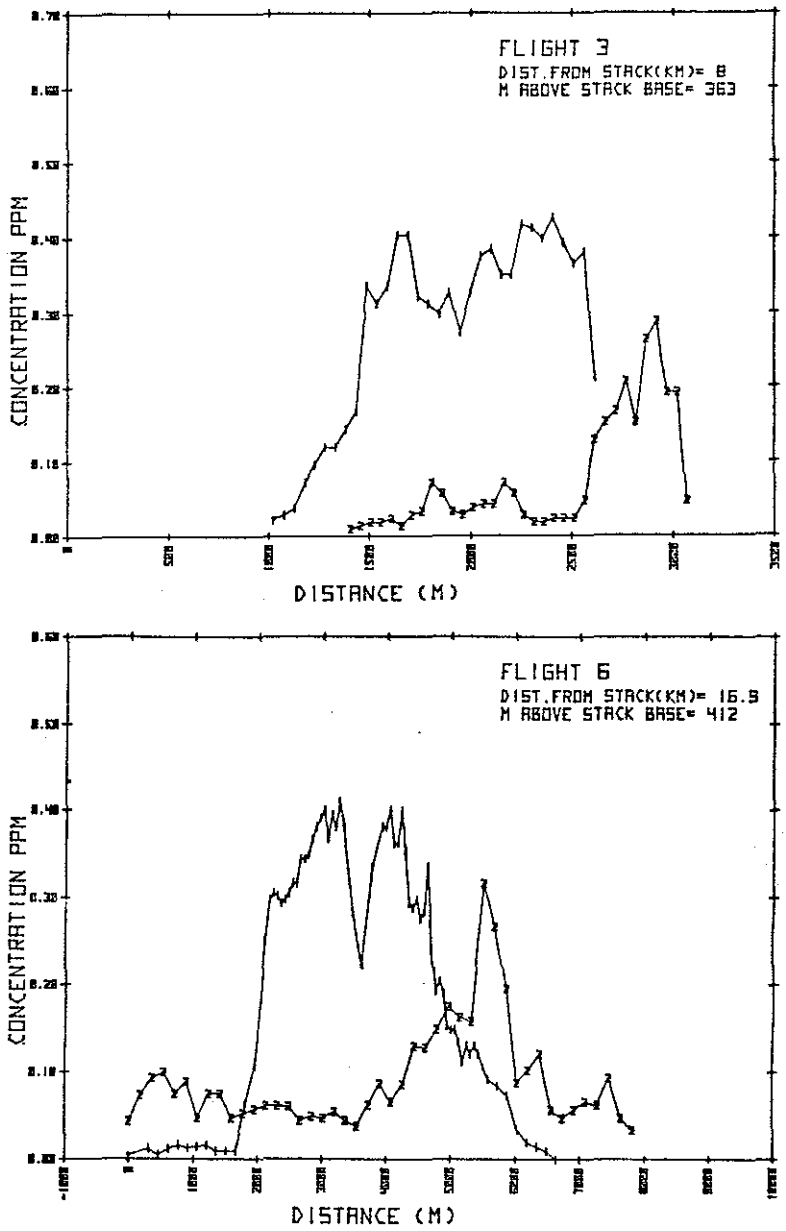

Figure 15 Samples of repeated helicopter traverses of the main plume showing the problem of obtaining representative samplings from Fanaki et al. (1978b).

into the value for σ_y. It would have been much better to have calculated σ_y based upon the single run with the greatest peak or integrated concentration.

In several of the plume profiles, there appears to be a systematic distortion of the plume shape. The plume isopleth sketches shown in Figure 16 strongly suggest a systematic error in the assumed plume location. Flight information was not provided. However, if adjacent flights were flown in opposite directions (i.e. an ordered progression of increasing or decreasing flight altitudes), then such a confusing isopleth pattern could result from systematic position reference errors. There are a variety of possible causes: systematic errors in the visual positioning with respect to the ground, a small chart recorder speed error, a systematic error in the adopted helicopter speed either due to sensor malfunction or improper allowance for the differences between indicated and absolute air speeds, etc. The plume cross-sectional isopleths presented in Fanaki et al. appear to be systematically slice-shifted as shown in the bottom part of Figure 16. Note that the area generated by the slice-shifted cross section is virtually the same as the cross section representing relative disperion where the centers of mass of each traverse are aligned vertically. Thus the sigma values generated by the area technique were not sensitive to this apparent systematic positioning error.

The calculated sigma values from the helicopter data represent relative not time-average Eulerian dispersion. The length of time required to measure the plume distribution is irrelevant to the type of dispersion being measured. Variations of plume structure and location during measurements merely increase the irregularity of the plume. There is no time averaging involved other than in the response time of the sensor.

The experimental technique used in obtaining the helicopter data may have confused time changes of wind direction with directional

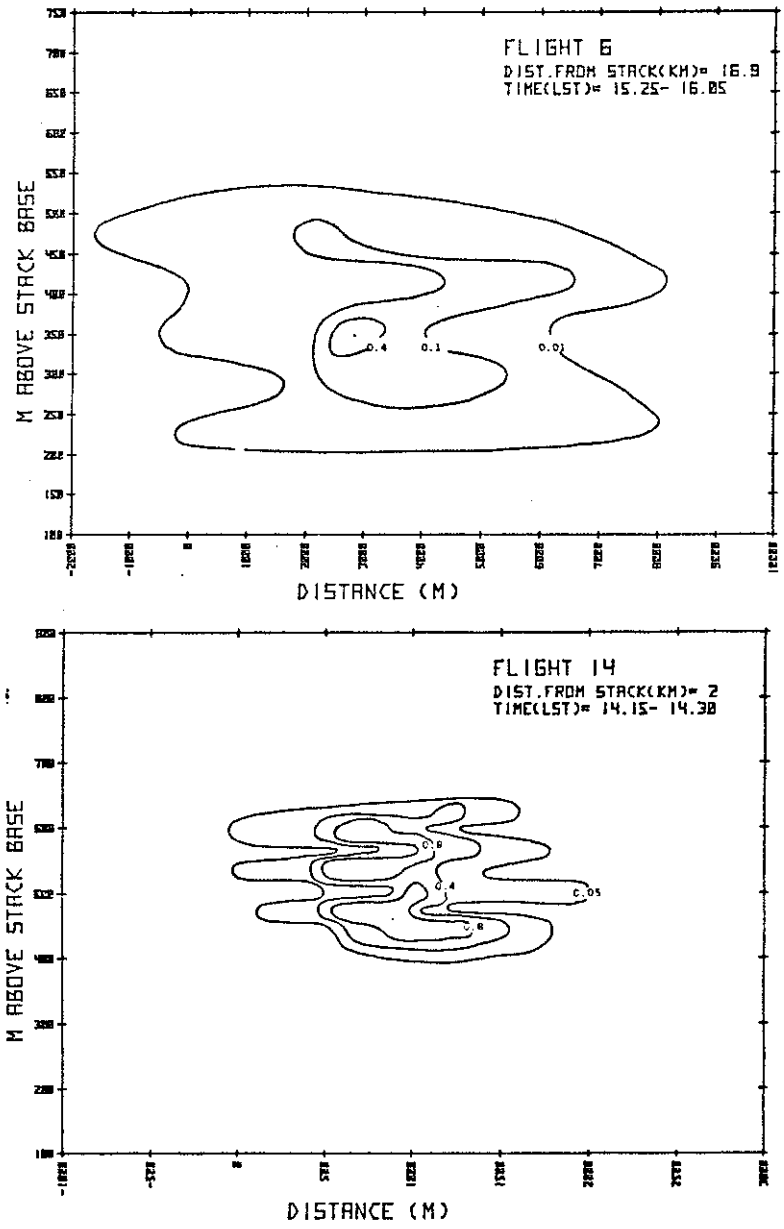

Figure 16 a. Examples of the plume cross sectional isopleth drawings obtained by Fanaki et al. from helicopter data.

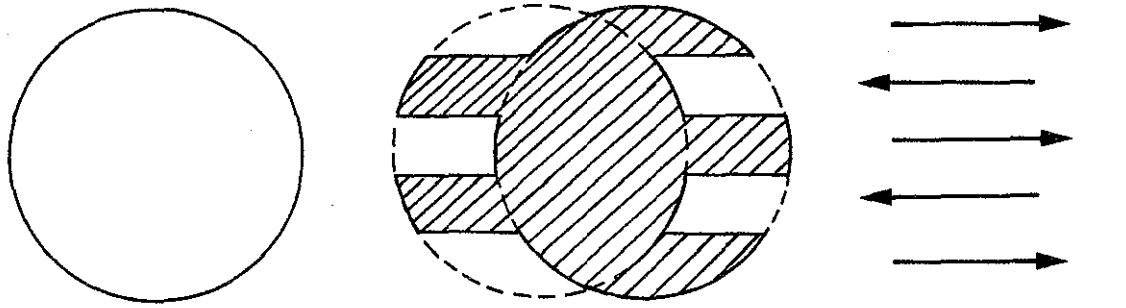

Figure 16 b. The interpretation of the isopleths of Figure 16 a in terms of a slice-shifted cross-section due to positioning uncertainty. The arrows represent the assumed alternation of flight direction as the helicopter systematically increased or decreased its height; the directions of flight may be opposite to those shown depending upon the cause of the systematic shifting.

shear effects in the vertical. If the plume was sampled at monotonically increasing or decreasing altitudes as suggested by Figure 16, then any slow time change of the wind direction may have been interpreted as a systematic wind direction change with height. Any apparent tilting of the plume cross section with height from the measured SO_2 concentration might actually be only a time-dependent meander of the plume. In such a case, however, the plume cross sectional area would not be significantly changed and so the computed sigma values would be unaffected.

In summary, the helicopter sigma values represent relative dispersion values. Because of the calculational technique used, the sigma values probably have a large degree of uncertainty (perhaps 25% or more). There is evidence of systematic positioning errors which generated a slice-shifted profile but this does not affect the calculated sigma values. A technique of monotonically increasing or decreasing flight levels may have led to an ambiguity between temporal changes or meanders in wind direction and vertical shear in the wind direction.

5.3.5 Aircraft

A summary of the experimental techniques used for the aircraft measurements have been presented in Davison et al. (1977) and Davison and Grandia (1978). A brief summary is presented here, along with the rationale for a reassessment of some of the σ_y values from the aircraft measurements.

5.3.5.1 Instrumentation and Measurement Procedures

The instrumentation for SO_2 measurement from the aircraft was a Sign-X SO_2 Analyser. Air samples were ducted into the Sign-X during traverses of the plume. Thus the aircraft measurements represent in-situ measurements of relative dispersion. Two problems were evident in the Sign-X measurements. The first was adsorption

of SO_2 onto the intake tubing. The effect of adsorption was to occasionally generate a slower fall-off of the SO_2 concentration. Since the effect did not directly scale with concentration (humidity being another controlling parameter) no systematic inverse filter function was applied to the data. A more detailed discussion of the adsorption effect has been presented by Lusis (1976). The second problem with the Sign-X system was a floating baseline. During the course of the flights, the voltage baseline (for clean air entering the intake tube) gradually increased. A noise limiting procedure was adopted to eliminate this problem. However, there were probably instances when the noise limiter and base line correction procedures were inadequate, especially when the plume traverse did not exhibit large concentrations.

The measurement procedure was to fly vertically stacked traverses in a racetrack pattern at two downwind distances. The height of the traverses were decided in the field based upon the plume structure and were staggered (e.g. high, low, high, low). The staggering of the heights and the flying of a given height at two downwind distances before going to another height were both attempts to be able to determine the significance of lack of stationarity. Lack of stationarity turned out to be a significant problem especially in the June field study. Analysis of the various data sets in this project, particularly of the minisonde and tethersonde data, demonstrated that lack of stationarity was probably a major problem for every measurment technique during the three intensive field studies.

5.3.5.2 Review and Reconsiderations of Analysis Techniques. The aircraft SO_2 measurements were used to generate both σ_y and σ_z and the plume rise.

The σ_y values were estimated for each traverse using both a second moment technique and an area technique. The area

technique consisted of integrating the concentration along the traverse, finding the center-of-mass, and then finding the distance on each side of the center-of-mass such that the integral from the center-of-mass to that distance included 34% of the total integrated area. For a Gaussian distribution, this technique would generate the correct sigma values. It was hoped that this technique would minimize the effects of displaced peaks coming from secondary sources. Small displaced peaks could have a major effect upon a second moment technique.

The above technique may have lead to inappropriate sigma values for a significantly non-Gaussian plume cross section. A non-Gaussian plume cross section could have arisen in a variety of ways: secondary sources, inadequate noise removal, instrument response limitations, and statistical variations inherent in a single realization of the plume crosssection.

The effects of multiple sources which were often very noticeable on the isopleth sketches could lead to inappropriate sigma values. In most situations, the centerline of the secondary sources was at a lower elevation than the centerline of the main powerhouse stack. Thus the seemingly paradoxical situation would arise where the computed sigma value for the main plume centerline concentration might be much less than the computed sigma value at lower levels where the multiple plume effects were more important. Thus the inappropriately computed sigma values at non centerline heights did not affect the adopted sigma values for the main plume.

The calculation procedures were designed to minimize the effects of electrical noise and drift in the sensor system. The technique of baseline selection (see Davison et al. 1977) was probably adequate for traverses with large concentrations, but perhaps was not appropriate for low concentration measurements. Thus for low concentrations, some of the sigma values previously

presented are irrelevant. However, these low concentrations were usually at the fringes of the plume and so generally did not affect the adopted main plume sigma value.

The instrument response limitations were probably not treated adequately. Undoubtedly there were situations in which the slow falloff of concentration was due to adsorption of SO_2 onto the walls of the inlet tubing (Lusis, 1976). In such high concentration situations, the previous sigma values were probably too large. An alternative way of estimating sigmas in such conditions would be to assume a Gaussian distribution and compute the sigma by means of ratioing the maximum observed concentrations. A 10% criterion could possibly be used; however to avoid fall-off problems, it would be better to use $\pm$ 0.607 of the peak value which would correspond to $\pm$ 1 sigma of a Gaussian distribution. This procedure for the determination of sigma for a smooth distribution with an obviously incorrect response problem was adopted for the revised aircraft sigma values presented below.

The importance of transient fluctuations within a single plume sampling was clear from the June 1977 COSPEC data (Fanaki et al. 1978c). Although the ensemble-averaged relative and Eulerian integrated profiles from the COSPEC usually were similar, individual traverses often showed marked differences from either averaged quantity. The variation within the population of plume profiles was much greater than the systematic differences between the means of the relative and Eulerian plume profiles. Thus obtaining a representative sample appears to be more important than whether relative or Eulerian averaging is done for downwind distances greater than a couple of kilometers. Consecutive COSPEC traverses at 3 km downwind (June 18) showed markedly different shapes and maxima (factor of 2). This variation existed in spite of the vertical integration inherent in the COSPEC. Thus, the calculation of a sigma value based upon the plume width at a concentration

corresponding to a certain fraction of the maximum concentration might not lead to repeatable sigma values. The fluctuations found in the June COSPEC data are probably not due to variations associated with secondary sources because the secondary sources of SO_2 are not very large compared to the main stack. The COSPEC data indicate that significant variability of a non-Gaussian nature is found for any given plume traverse. Thus the non-Gaussian nature of the aircraft traverses (where the smoothing effects of the vertically integrating nature of the COSPEC are not present) is probably due in many cases to the fluctuating, non-Gaussian nature of the main plume itself. If this interpretation is correct, then the calculation of a sigma value based upon a fraction of the peak concentration may be inappropriate except for highly regular and concentrated plumes (when instrument response limitations appear to be important).

All of the previous aircraft lateral sigma values (σ_y) have been reconsidered based upon the previous discussions. The cases for which there were clear instrumental adsorption effects were changed as outlined above (0.607 of peak concentration corresponding to $\pm \sigma_y$). To partially compensate for the statistical sampling problem, data for runs not quite on the centerline were considered. In this way, the representativeness of the adopted σ_y values could be improved. The data used were from the appendices of the two previous aircraft reports: Davison et al. (1977), and Davison and Grandia (1978). A summary of all aircraft σ_y values together with the rationale for any changed values is presented in Table 16.

Table 16 Revised aircraft σ_y values and characteristics

Flight Time	Downwind Distance (km)	σ_y old (m)	Modified (m)	Particulars
1976:				
March 10 (1430-1630)	1.6	1025	800	Run 5 had Gaussian shape with σ_y=790m even though slightly below centerline; it appears that dispersion was less just above centerline.
	6.4	4010	-	The centerline was not located adequately. The runs have very irregular structure, some noise problems, and possibly secondary source effects.
	14.5	2300	900	The plume appears to have an hourglass shape in the YZ plane with fanning above the centerline on a stable region and turbulent mixing below the centerline; the adopted value is probably not the best value for a Gaussian model but is a best estimate for the centerline thickness.
March 11 (0800-0930)	1.6	1150	520	The centerline was missed based upon concentrations at 3.2 km downwind. If the main peak in Run #5 is representative, then abstraction from a peak value leads to $\sigma_y \simeq 520$ m. Actual centerline value probably larger.
	3.2	890	500	Absorption effect was probably significant for Run 11. Additional data from Runs 9 and 10 support revised value.
	6.4	1180	600	Runs 7 and 8 have absorption effects. Runs 4 and 6 suggest larger values≃1000m but have lower concentrations. The values at 1.6, 3.2 and 6.4 km suggest a mitral expansion to about 500m with slow additional changes at centerline height.
March 11 (1400-1530)	3.2	1540	750	The traverses all support a strong hourglass-shaped profile on the YZ plane. This shape cannot be reasonably simulated by a Gaussian profile.

continued...

Table 16. Continued.

Flight Time	Downwind Distance (km)	σ_y old (m)	Modified (m)	Particulars
				Note that a IOSPEC would have measured a larger σ_y (perhaps 1000m).
	8.0	2230	2000	The original value was based upon run which appears to have multiple peaks. Runs 8, 10, 12 and 14 all support a value close to 2000m.
March 12 (1430-1605)	4.8	2130	2100	There were convective conditions with small wind direction variation clear through the region of plume rise. Thus the multiple peaks are assumed to be from a single source; Runs 10 and 12 would require a secondary source on opposite sides of the main plume.
	11.3	3840	3200	Runs 7 and 9 were used for the modified value.
March 15	3.2	302	300	No changes, but data has uncertainty of at least 50m.
(0800-0850)	8.0	472	470	
1977:				
June 19 (0830-0945)	3.2	1570	1100	Removal of possible baseline noise reduces value for Run 1 to $\sigma_y \approx 1250$m. Runs 7 and 11 suggest a lower value; photographs suggest some variability to be expected.
	8.0	2120	1200	Previous value based upon Run 2, when allowed for baseline problem and consider Run 6 then smaller value is more realistic.
June 19	3.2	-	-	No reliable value due to convective generated data scatter. The adopted value is still uncertain; however it is thought that some of the previous contribution to the sigma may have been due to a baseline problem due to the low maximum concentration on Run 4.
(1415-1610)	8.0	3700	2500	

continued ...

Table 16. Concluded.

Flight Time	Downwind Distance (km)	σ_y old (m)	Modified (m)	Particulars
June 20	3.2	501	500	No change
(1130-1230)	8.0	725	725	No change
June 20	3.2	528	530	No change
(1230-1340)	8.0	970	970	No change
June 22	3.2	375	-	The σ_y data at 3.2km applies to later time period.
(1915-2130)	8.0	340	340	No change
June 22	3.2	375	375	No change
(2145-2245)	8.0	480	450	Compensation for adsorption effects and consideration for other Runs suggests slightly lower σ_y value.

5.4 COMPARISON OF PLUME SIGMA VALUES FROM DIFFERENCE MEASUREMENT TECHNIQUES

5.4.1 Rationale and Data Base

A meaningful evaluation of sigma typing schemes requires that the test data be internally comparable. The characteristics of each of the sensor systems used at AOSERP for plume sigma measurements were described in the previous sections. In the following sections, simultaneous data sets are compared to ensure that any systematic differences are identified where possible. Unfortunately, there were very few good case studies for instrument comparisons. Partly the problem lies in the inherent practical limitations of each sensor to a limited range of downwind distances. However, there was a lack of a systematic attempt to generate a data set for sensor intercomparison. In addition, there was a wide variety of analysis techniques used which further increased the inhomogeneity of the data population.

All times of simultaneous measurements for each pairing of sensor systems are presented in Table 17. As can be seen, only three pairings, all involving plume photography, have a significant amount of data for comparison. These three pairings are discussed in the subsequent sections. The immersion sensors (helicopter and aircraft) generally operated at much greater downwind distances than covered by the plume photography. Note also that plume photography generated no σ_y values for comparisons.

The aircraft - COSPEC comparison consisted of only a very limited amount of data. The aircraft was finishing an early morning case as the COSPEC began. The aircraft terminated the mission because of changing conditions (start of fanning) and so no useful comparison can be made.

Table 17 Data base for sensor system comparisons, 1976 and 1977.

Sensor System Pairs	Approximate Overlapping Analysis Times
Helicopter-Photography	Feb 5 (0900), Feb 6 (1500)
	Feb 10 (1000), Feb 11 (1500)
Aircraft-COSPEC	March 15 (0830)
Aircraft-Photography	March 10 (1540), March 11 (1500)
	June 19 (0930, 1430)
	June 20 (1100, 1340)
	June 22 (2130)
LIDAR-Aircraft*	June 22 (1900,2245)
LIDAR-COSPEC*	June 18 (0600)
LIDAR-Photography	June 17 (1100), June 18 (0600),
	June 21 (0545, 1400)
	June 22 (1700, 2100)
	June 23 (0500, 0600)

* No overlapping downwind distances.

5.4.2 Helicopter-Photography σ_z Comparison

The simultaneous sigma values generated by the helicopter and photography provide a reasonable data base for comparison. Although, most of the helicopter data were taken at much greater downwind distances, a meaningful comparison can be made. The intercomparison data base together with the spatial and temporal separations are presented in Table 18.

The February 5 comparison shows little change of the photographic data with time. Note that if a wind speed of 6 m/sec is assumed, then the plume material at 30.6 km left the stack about 85 minutes earlier. The comparisons are within experimental uncertainties (see also Figure 17).

The February 6 data show significant differences between the helicopter and plume photography values at the same 0.8 km downwind (see also Figure 17). Unless the plume is exceedingly steady, reliable helicopter σ_z values at 0.8 km will be difficult to obtain because of statistical inhomogeneities in the plume at that downwind distance. Sufficiently accurate altitude measurements from the helicopter may be difficult to obtain for such narrow plumes. The discrepancy is probably not due to a temporal change since the σ_z values for plume photography decreased compared to the hour previous to the helicopter sampling.

The apparent decrease of σ_z with distance for the helicopter data for the February 10 comparison is clearly a stationarity effect. The plume photography σ_z value temporally coincident with the 0.8 km helicopter value is 42 m compared to 31 m for the helicopter value. This is good agreement considering the statistical sampling and position recovery uncertainties of the helicopter system.

The February 11 intercomparison demonstrates the importance of the integral of the mixing effects for larger downwind distances. For an average wind speed of perhaps 4 m/sec, the plume material

Table 18 Nearly simultaneous σ_z values from the helicopter and photography systems. For each day, the times (MST) have been listed chronologically to emphasize both the spatial and temporal separations of the data. All data from 1977.

Data Times	Plume Photography σ_z (m)				Helicopter σ_z (m)		
Feb 5							
Downwind Distance(km)	0.6	0.7			8.0		30.6
Times:							
0830	36	36					
0840-0910					43		
0935-1000							31
1120	38	38					
Feb 6							
Downwind Distances (km)	0.6	0.7	0.8	0.9	0.8		16.9
Times:							
1330	36	40	42	42			
1420	27	27	-	-			
1435-1455					66		
1525-1605							91
Feb 10							
Downwind Distances (km)	0.6	0.7	0.8		0.8	9.7	30.4
Times:							
0845	31	33	33				
0830-0920							20
0930	37	37					
0950-1005						28	
1020-1030					31		
1030	40	42	42				
Feb 11							
Downwind Distances (km)	0.6	0.7	0.8		2	12.0	28.8
Times:							
1410	82	86	86				
1430-1450					83		
1500-1530						81	
1515	49	47	55				
1550-1600							84

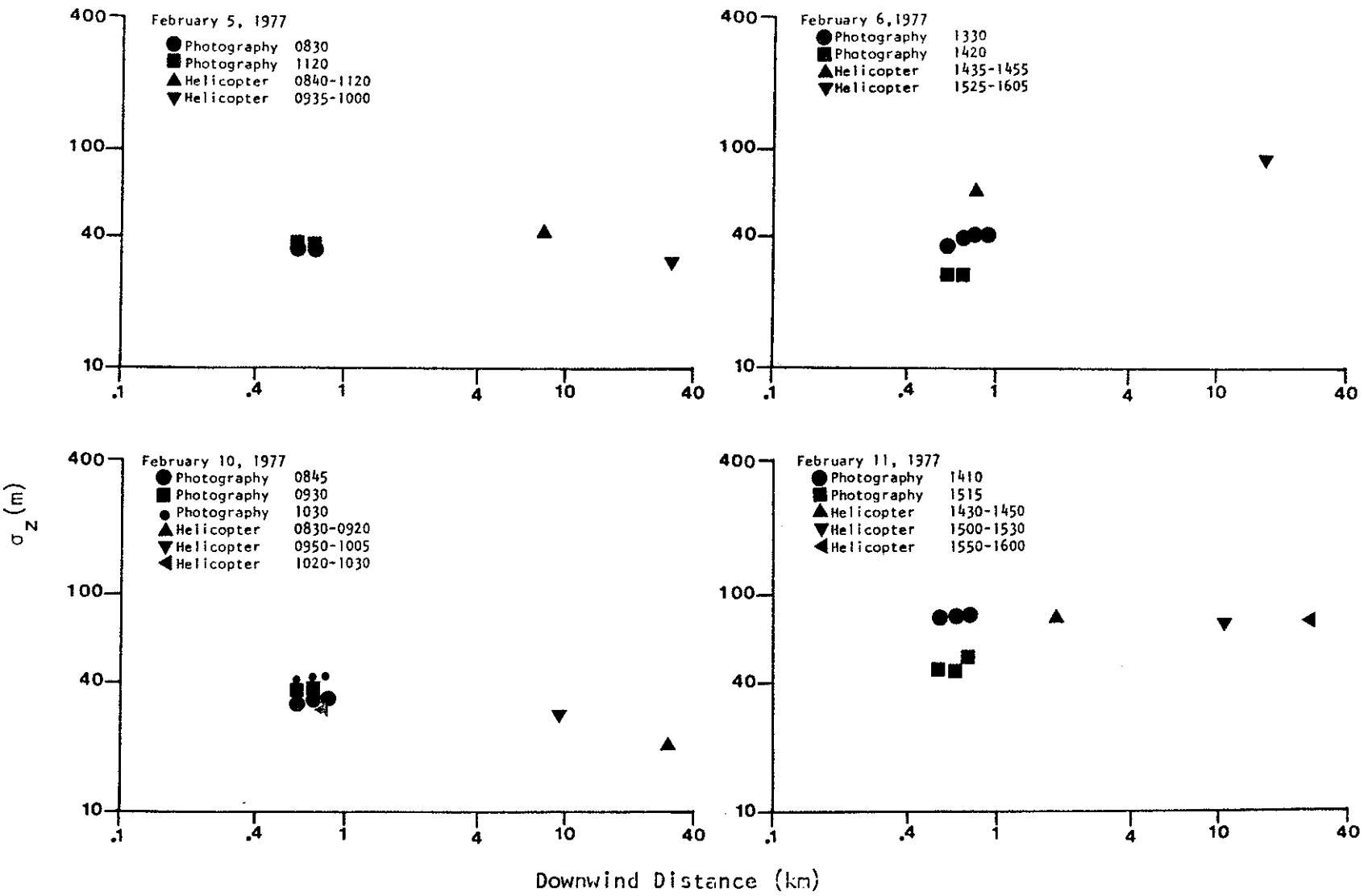

Figure 17. Helicopter and plume photography σ_z comparison.

sampled at 12 and 29 km downwind left the stack at about 1425 and 1400 MST respectively. Thus the initial plume spread may have been largely established at the time of the earlier plume photography. The plume geometry at a given downwind distance reflects the history of its mixing. The current environmental mixing parameters may be appropriate for parameterization of the current sigma values only in stationary conditions and when environmental mixing has dominated the effects of source generated initial dilution.

In summary, the observed discrepancies reflect the level of experimental error. For the very narrow plumes of these four case studies, the helicopter data could not generate values of σ_z with sufficient certainty to detect any systematic discrepancies less than perhaps 50%.

5.4.3 Aircraft-Photography σ_z Comparison

The aircraft and photography data do not overlap in downwind distances but can still be used to estimate any systematic discrepancies. Values for the plume photography σ_z for the March 1976 field trip were not available as functions of both time and downwind distance. Thus, a detailed comparison for σ_z values could only be done for the June 1977 field study. A comparison of plume rise could be done for both field studies. The σ_z values are compared in Table 19 and are then plotted in Figure 18 for each of the case studies.

There appears to be a systematic discrepancy between the two sets of data. In all cases, the plume σ_z values level off or begin to decrease beyond a downwind distance of 1 km. In the discussion of plume photography data, this type of behaviour was anticipated due to the limitations of the 10% criterion used by Fanaki et al. (1978a) to define the σ_z value.

On the morning of June 19 there was a trapping inversion present and the plume photography and aircraft values agreed

Table 19 Nearly simultaneous σ_z values from the aircraft and photography systems . All data are from 1977; times are in MDT.

Data Times	Plume Photography σ_z (m)							Aircraft σ_z (m)	
Downwind Distances (km)	0.4	0.6	0.8	1.0	1.2	1.4	1.6	3.2	8.0
June 19 A.M.									
0830-0940								78	77
0930	31	29	49	51	55	51	53		
June 19 P.M.									
1345	27	38	55	71	87	84	75		
1430	22	22	24	29	31				
1415-1610								270	260
June 20									
1100	26	27	37	42	40	40	42		
1130-1340								170	175
1340	22	49	57	62	60	66	66		
1430	20	22	27	37	38	40	40		
June 22									
1730	49	62	64	64	64	60	64		
1950-2130									200
2030	37	46	44	58	62	64			
2130	20	29	35	31	33	33	33		
2140-2300								50	90

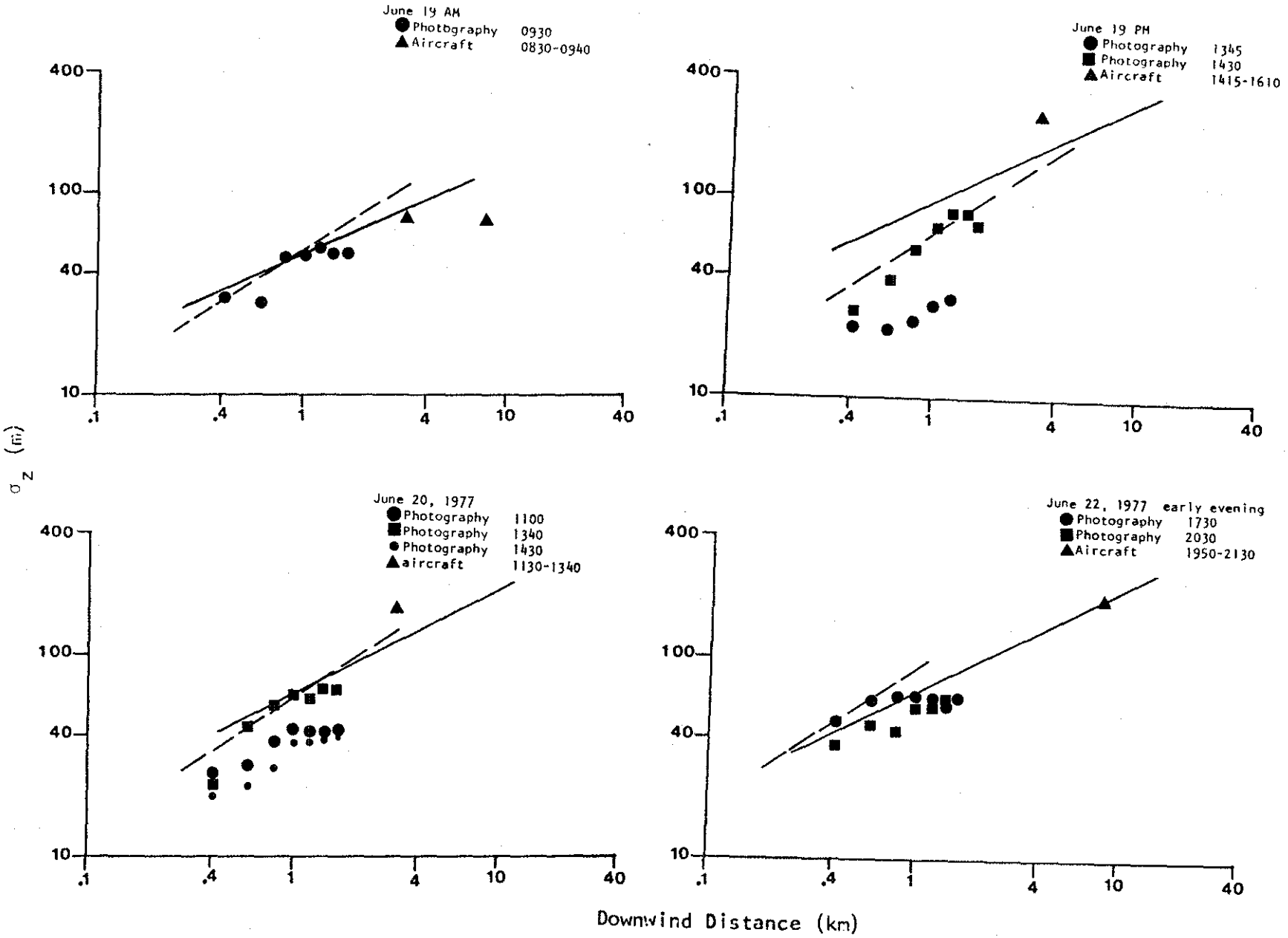

Figure 18. Aircraft and plume photography σ_z comparison.

Continued...

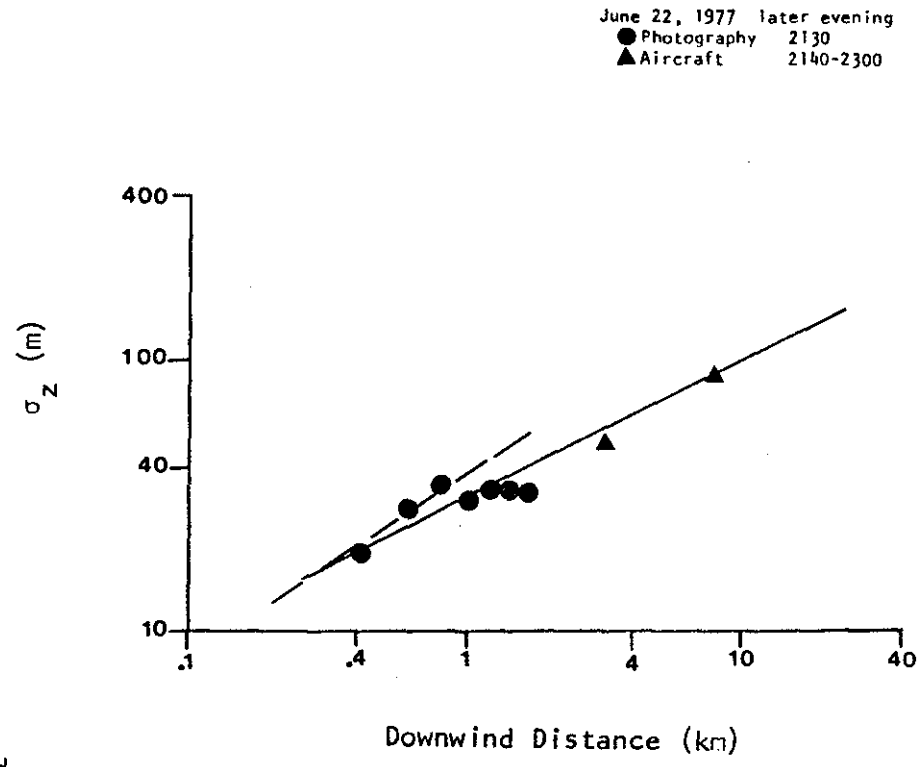

Figure 18. Concluded.

reasonably well if the plume photography drop-off beyond 1.2 km is ignored.

The afternoon of June 19 had vigorous mixing with no limiting inversion affecting the plume. The aircraft values, particularly at 3.2 km, probably were not statistically reliable due to the large variance of the plume position. The plume photography run at 1430 appears to have given σ_z values which were much to small. This could be due to either a wind direction error or difficulty in reliably perceiving the edge of the plume in such convective situations. Note the drop-off of plume photography σ_z values beyond 1.2 km.

The run on June 20 shows considerable change in the plume photography σ_z values. The increase in photographic σ_z values from 1100 MST to 1340 MST is in accordance with the observed increase in turbulence noted by Davison and Grandia (1978) from 1130 to 1340. However, the decreased photographic σ_z values at 1340 are probably not due to a turbulence structure change since runs 21 and 22 of the aircraft study at about 1340 showed no decrease in turbulence levels. Because of the lack of stationarity the aircraft σ_z values may not be too accurate. However, the values extrapolate reasonably well from the plume photography values at 1340.

The June 22 runs are reasonably consistent. Both aircraft and plume photography show the decrease in σ_z as evening progresses. Again the levelling-off of the plume photography σ_z values is probably not real.

5.4.4 LIDAR-Photography Comparison

The LIDAR and plume photography were the only two systems which had a substantial overlap in the range of downwind distances observed. The LIDAR sigma values appeared to be too large particularly for σ_y, based upon the plots presented by Hoff and Froude

(1978) as discussed in a previous section. The plume photography could be used for comparing plume rise and σ_z values. A comparison of plume rise should establish whether any discrepancy is based upon the geometry of projection of the plume photography or whether it is due to the different techniques of σ_z calculation.

5.4.4.1 Plume Rise Comparison

The data base for plume rise comparison is presented in Table 20 with graphic plots presented in Figure 19. Except for the cases of June 17 and June 21, the plume rises compare very favourably indeed. The June 17 case showed considerable variation within the plume photography runs. The minisonde data indicated that there were very light winds in the region of plume rise at 0900 becoming steady at about 6 m/sec by 1300. The light and variable winds may have contributed to uncertainty in the plume photography. When the LIDAR plume rise value is normalized by $\overline{U}$ $F^{-1/3}$, there is a large discrepancy from Briggs (1975) prediction suggesting that the LIDAR value may be in error. The discrepancy for the June 21 case is not nearly as large as for the June 17 case. The winds were steady at about 6 m/sec with no unusual features. The plume photography plume rise values are unaffected by the 10% assumption and appear to be well-behaved. The discrepancy of about 110 m (over 50% of the LIDAR value) is unresolved. In summary then, 5 of the 7 cases of plume rise measured by plume photography and LIDAR compared very closely.

5.4.4.2 σ_z comparison. The σ_z values measured by plume photography and the LIDAR can now be compared. The data base of the comparison is presented in Table 21 and the graphic comparisons are shown in Figure 20. The LIDAR σ_z values except for the June 17 case are consistently larger than the plume photography σ_z values. If the June 17 case is ignored, then the average ratio of the LIDAR σ_z

Table 20. A comparison of Plume rise estimates from plume photography and LIDAR

Data Times	Plume Photography ΔH (m) for Downwind Distance (m) of								LIDAR ΔH (m)	X(m)
	200	400	600	800	1000	1200	1400	1600		
June 17										
1015	396	494	541	561						
1048-1100									52	199
1100	139	161	176	176						
1300	169	290	353	380						
June 18										
0500	192	274	314	357						
0525-0615									186	251
0600	161	235	274	302						
June 21										
0545	106	169	227	274	314	325	345	365		
0543-0627									209	1254
June 21										
1400-1410									607	676
1400	533	584	698	792	941					
June 22										
1630	67	149	141	133	141					
1631-1720									153	432
1730	90	141	145	141	149					
1922-1959									76	483
2030	63	110	129	141	157					
2037-2101									42	82
2130	51	71	98	118	133					
2123-2145									100	472
June 23										
0500	63	94	118	129	137					
0454-0506									123	487
0600	118	122	137	129	141					

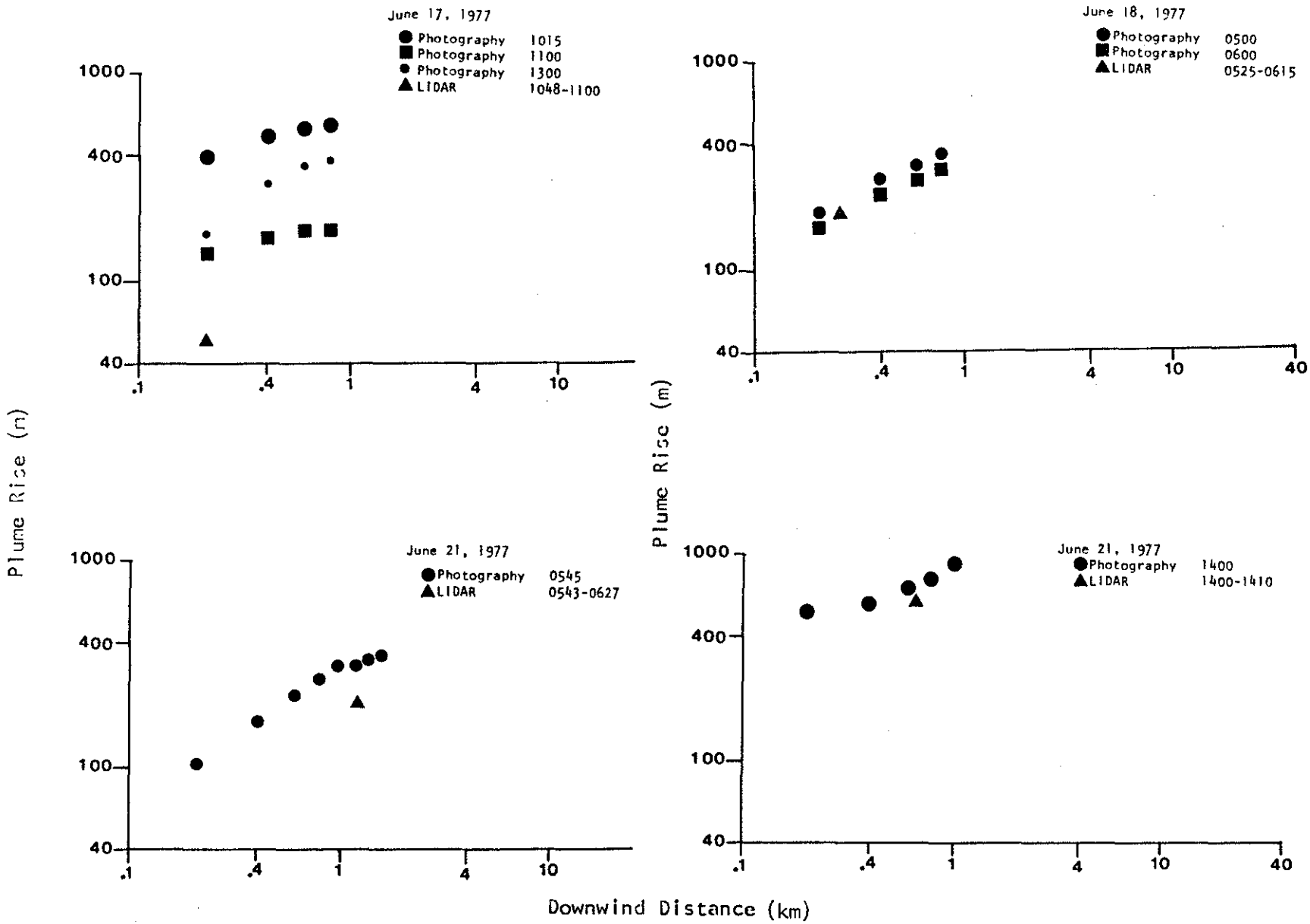

Figure 19. LIDAR and plume photography plume rise (ΔH)

Continued...

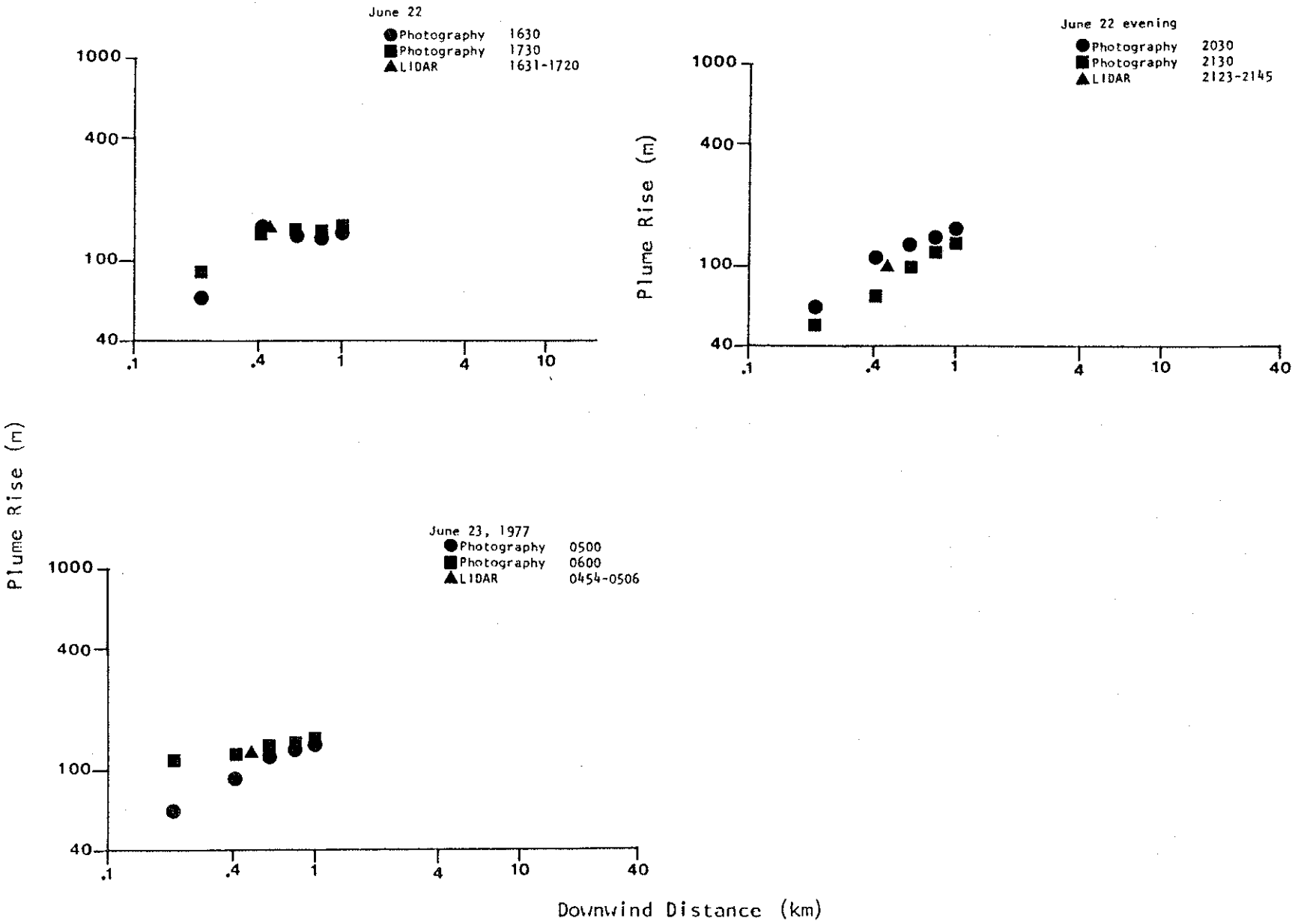

Figure 19. Concluded.

Table 21 A comparison of σ_z measurements by plume photography and the LIDAR, 1977, MDT.

Data Times	Plume photography σ_z (m) for Downwind Distances (m) of							LIDAR	
	200	400	600	800	1000	1200	1400	σ_z (m)	X (m)
June 17									
1015	49	60	64	71					
1048-1100								29	199
1100	33	46	46	42					
1300	37	62	78	87					
June 18									
0500	37	55	57	60					
0525-0615								69	251
0600	33	60	73	73					
June 21									
0545	24	38	51	58	62	64	64		
0543-0627								72	1254
June 21									
1400	37	55	73	78	93				
1400-1410								308	676
June 22									
1630	42	73	75	84	100				
1631-1720								85	432
1730	24	49	62	64	64				
1922-1959								57	483
2030	18	37	46	44	58				
2037-2101								13	82
2130	9	20	29	35	31				
2123-2145								38	472
June 23									
0500	15	26	31	31	31				
0454-0506								63	487
0600	33	37	40	42	40				

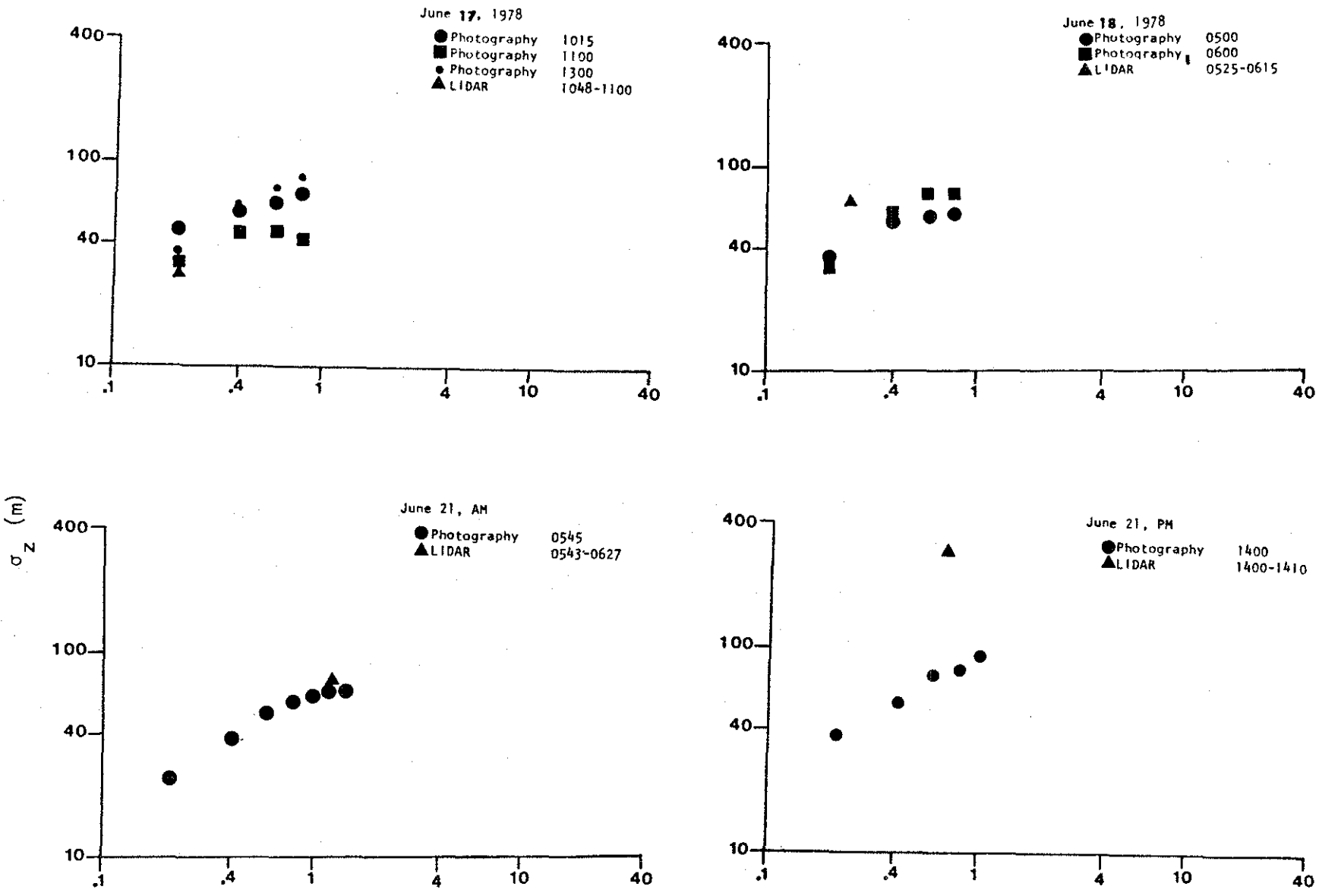

Figure 20. LIDAR and plume photography σ_z comparison.

Continued...

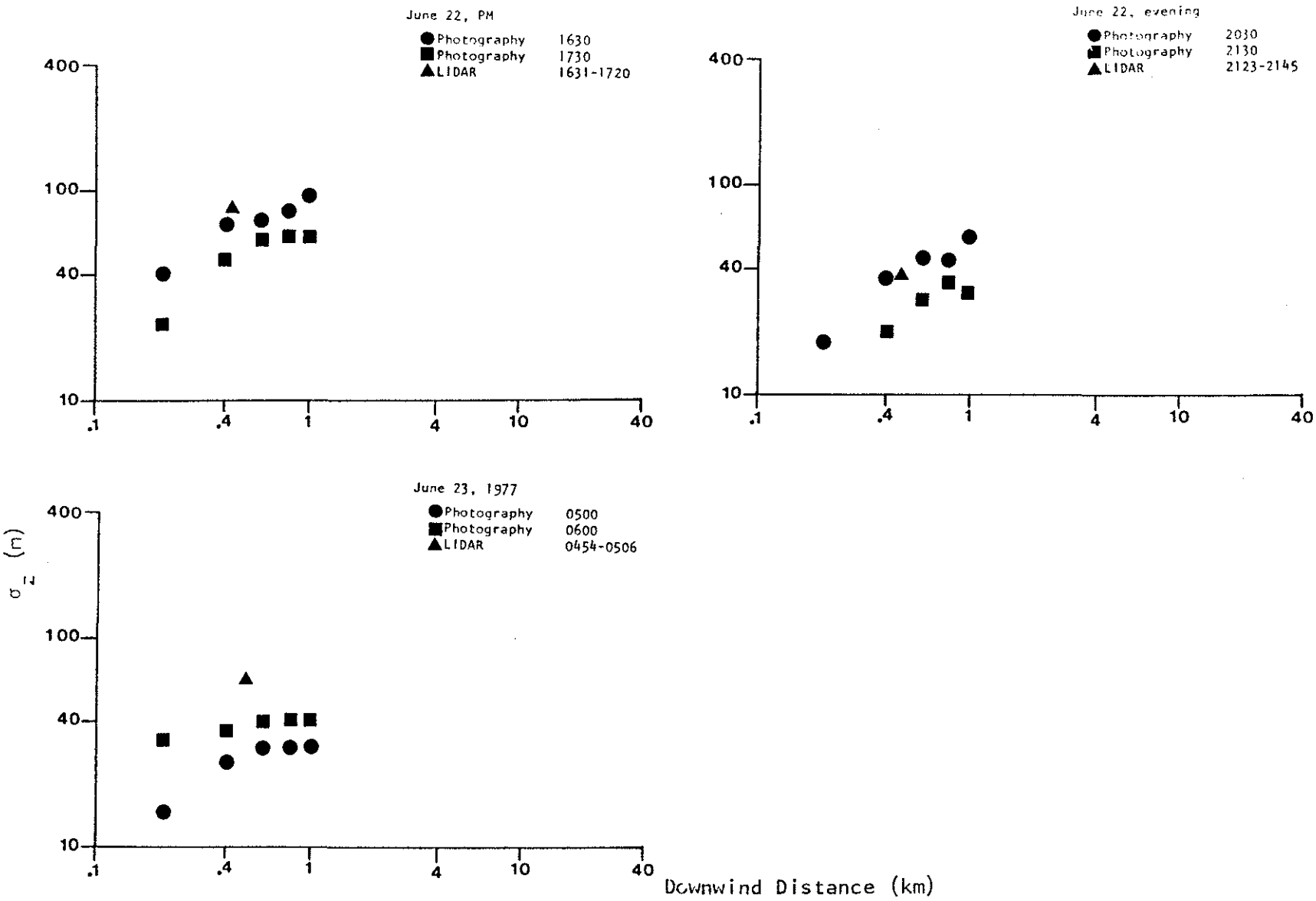

Figure 20. Concluded.

value to the plume photography σ_z value is 2.0; if the one large discrepancy of June 21 evening is ignored, then the ratio becomes 1.4.

The reason for the discrepancy appears to be due to a problem in the analysis of the LIDAR data. As discussed in the LIDAR section, the sigma values, particularly σ_y, were very large compared to the isopleths shown. It was suggested at that time, that an inadequate baseline noise filter could have generated extraneously large sigma values. A similar problem had been found for some of the aircraft σ_y values.

Part of the discrepancy may be due to the uncertainties associated with the use of the 10% criterion for σ_z specification for plume photography. However, most of the LIDAR photography comparisons are at a downwind distance where these effects are hopefully small.

The discrepancies are probably not due to geometric projection errors since the plume rise values compared fairly well. The June 17 case had a clear unresolved discrepancy with a much smaller estimate of plume rise for the LIDAR. However for σ_z, the differences for the June 17 were small, which is consistent with the rest of the data set if we assume a geometric error increased all the size scales of the plume photography for June 17 (or decreased all the LIDAR length scales). The June 21 AM case followed a similar pattern with the plume rise for the LIDAR being much smaller than, and the σ_z value being closer to, the plume photography value. Thus, if we normalized all the length scales in terms of plume rise, the LIDAR σ_z values for all cases would be much larger than the plume photography values.

The LIDAR/aircraft and LIDAR/COSPEC data provide no overlapping range of downwind distances. Thus they cannot be used to critically evaluate the validity of the LIDAR data.

5.4.4.3 Rejection of the LIDAR Sigma Values. It appears that the LIDAR data as presented by Hoff and Froude (1978) have overestimated the plume sigma values. This conclusion is based upon three criteria. Firstly, the sigma values drawn on the LIDAR isopleth sketches suggest that the σ_y values are twice as large as what the 10% criterion would generate assuming a Gaussian distribution. Secondly, the COG drawn on the LIDAR isopleths often appears off-centered (particularly in the lateral direction) compared to the isopleths; this indicates significant contribution to the sigma calculation from regions not appearing on the isopleth sketches (either real secondary sources, or noise). Thirdly, the plume photography σ_z values confirm the above suggested overestimates of LIDAR sigmas even though the plume rise values agree well indicating that few geometric errors are present. It is probable that the reason for the large sigma values is due to an inadequate baseline noise filter. A similar problem was present for some of the aircraft data which necessitated modification of results for this report.

The LIDAR sigma values will not be used for subsequent analysis in this report. This decision was made reluctantly since the LIDAR is a very promising instrument.

6. COMPARISON OF SIGMA MEASUREMENTS WITH SPECIFICATION SCHEMES

The previous chapters have presented the background necessary for a meaningful comparison of the measured plume sigma values to the various specification schemes. Both the theory of plume dispersion and the results of previous studies clearly indicate that there are two fundamentally different stages of dispersion. The first stage is source-dominated, the second is environmentally dominated. An analysis of how well the various specification schemes fit the AOSERP data base for the two stages of dispersion are presented in the following sections.

6.1 SOURCE-DOMINATED STAGE OF DISPERSION

The theory and measurement bases for adopting a source-dominated stage of dispersion were presented earlier. The plume radius and hence the plume sigma values were shown to be intimately connected to the plume rise since entrainment of ambient air by the plume determines both rise and radius. The source-dominated region of dispersion typically was expected to occur to downwind distances of 1 or 2 km with considerable variation depending upon the strength of the environmental mixing. The analysis of the March 1976 and February 1977 plume photography σ_z values presented by Fanaki et al. (1978a, 1978b) showed that environmental scaling did not appear to work, in agreement with the above concept of a source-dominated stage of dispersion.

The AOSERP data base for an analysis of the source-dominated stage of dispersion is mainly the plume photography data. The plume rise data as well as the σ_z data have been examined in some detail in order to assess the applicability of the theory to the AOSERP region. An analysis of plume rise has the additional advantage of removing the uncertainties of the 10% criterion used in the σ_z calculations. Ratioing of σ_z to plume rise can remove some of the geometric and wind speed uncertainties in comparison with the theory. In the following sections, plume rise and then σ_z are compared to theory. Some conclusions can then be drawn as to

the specification of the plume geometry in the source-dominated region of dispersion.

6.1.1 Plume Rise Analysis

The uncertainties in the plume photography data discussed earlier in some detail prompted the adoption of selection criteria for data to be used in subsequent analysis. The data were rejected if:

(a) Wind profile information was not available within one hour of the data collection time,

(b) The wind direction turning extracted from the appropriate mini-sonde profile exceeded 10^{o}/100 m,

(c) There was non-zero plume rise at X = 0 when the wind speed exceeded 2 m/s at stack height and

(d) The differences in wind speeds extracted from simultaneous mini-sondes exceeded 2 m/s and could not be resolved.

Data were also not used if the maximum downwind distance, X, was less then 1 km. This criterion was adopted to avoid biasing the data towards small X values. Use of these criteria left approximately 4 data times from March, 4 from February and 22 from June. About one half of the data were rejected because of excessive wind turning with height. After further consideration it was decided to use neutral data only from June (only 3 neutral data points were left in the March and February data) and the stable data only from February and June. The rejection of the March data was partly due to the lack of suitable σ_z values for analysis. Since one of the primary purposes of the plume rise analysis was to test the theory for application to σ_z specification, there was some advantage to keeping the plume rise and σ_z data sets equivalent.

The average normalized plume rise for neutral conditions is plotted as a function of X in Figure 21. Also shown are the range of extreme and the standard deviation of the population of similar means (i.e. standard deviation of the data set divided by

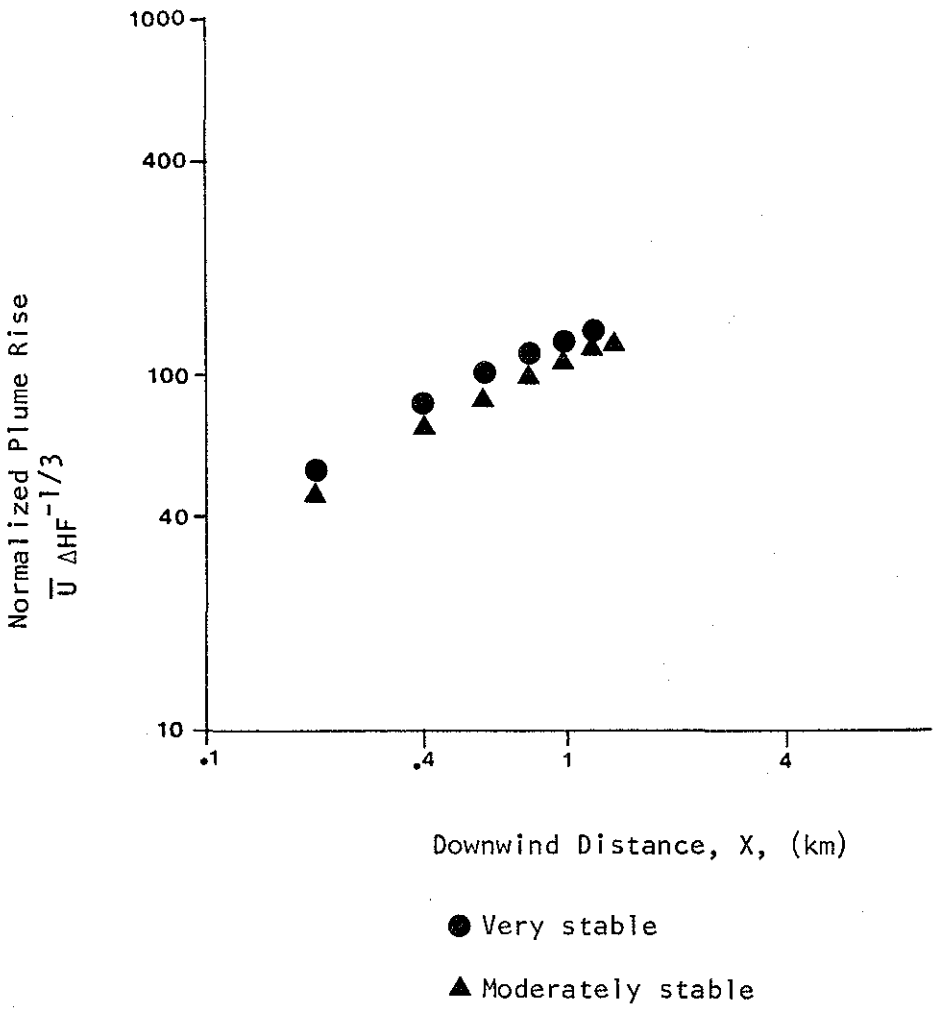

Figure 22. Normalized plume rise for the two classes of stable conditions.

The two stability classes gave virtually identical curves since the elevated wind speeds were higher for the very stable class. The Briggs curve is shown in Figure 23 with the combined stable normalized plume rise observations. It can be seen that the Briggs curve tends to overestimate the plume rise if $\beta = 0.6$ is used. The neutral plume rise suggested a coefficient of 1.4 (corresponding to $\beta = 0.74$). This value of β reduces the predicted values by about 15% and reduces the discrepancies by about one half.

The maximum plume rise is predicted at a downwind distance corresponding to $\omega' t = \Pi$. For a wind speed of about 8 m/sec and for a modified Brunt-Vaissala frequency, ω', of about 0.013 sec^{-1} (the average values for all the stable cases), the maximum plume rise is predicted to occur at about 1.9 km downwind from the source. The average stable plume rise values are seen to be continuing to rise to the limit of the plume photography data; however there is some indication of a levelling-off at a lower height than predicted by theory. Considering the simplications in the theory, it is encouraging that the theory and measurements agree as well as they do.

6.1.2 Analysis of Plume Photography σ_z Data

6.1.2.1 Comparison of Plume Spread to Plume Rise. Most theoretical studies of plume rise and initial dilution have related the plume radius r, to the plume rise ΔH by

$$r = \beta \Delta H \qquad (6.2)$$

as discussed in Chapter 3. There have been many observations supporting this relationship, however the proportionality constant, β, has a very wide range of values (see Chapter 3 and Briggs 1975 p. 73 ff). Undoubtedly part of the problem is the difficulty in defining the plume radius.

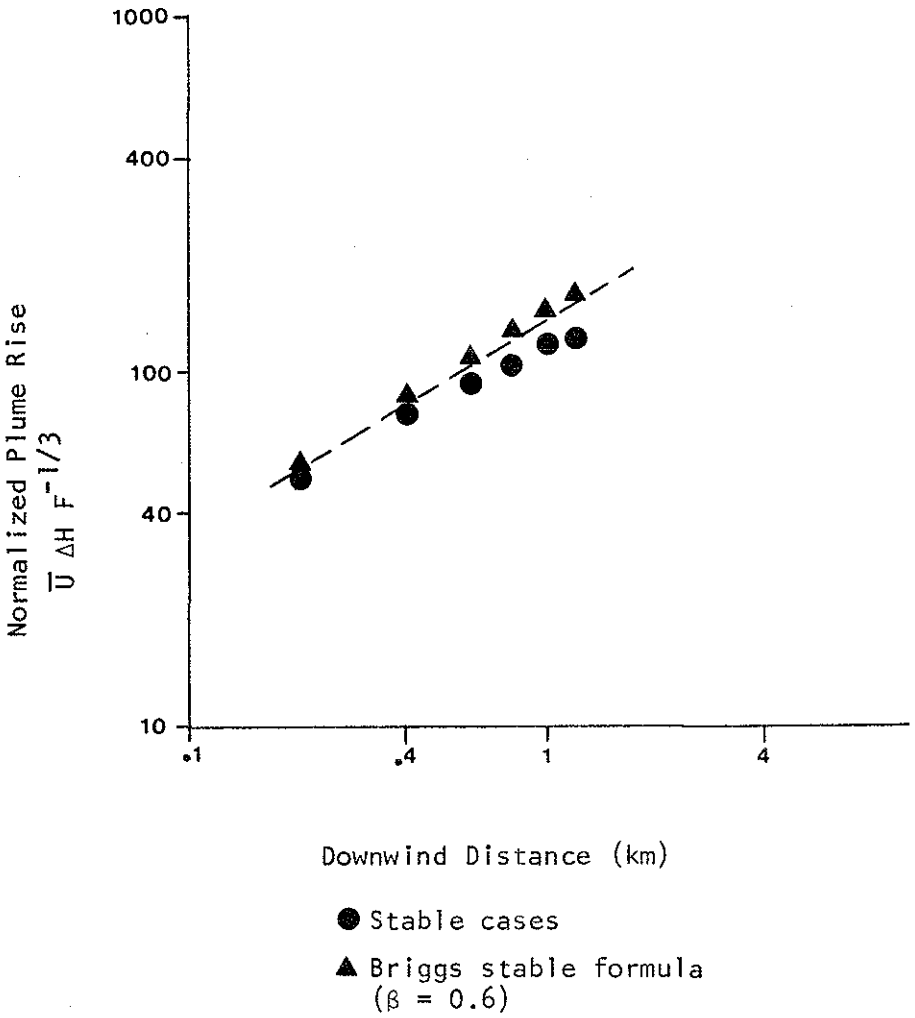

Figure 23. A comparison of the normalized plume rises for stable and neutral conditions with the Briggs formula for stable conditions. The dashed line is the best fitting $X^{2/3}$ line for neutral conditions over the downwind range of 600-1400 m.

In theoretical models, the plume is represented as a distinct entity with a boundary. Such an approximation is necessary to make the problem more tractable. For real plume observations, the boundary of the plume is less certain. If the plume has a dynamic circulation as suggested by Briggs (1975, p.74), then a boundary has some physical meaning. However, visual observations of plumes and the concentration patterns presented by Hoff and Froude in their LIDAR analysis suggest that any such organization is probably masked in most cases by the more turbulent fluctuations. The plume photography observations define a visual plume boundary; how much plume material is left outside this boundary is not clear particularly at larger downwind distances. The adoption of a 10% criterion for the plume boundary implies a Gaussian distribution which is again very different than both the well-mixed plume of the theories and Briggs' vortices.

The plume photography data provide a means of testing the relationship between visual plume radius and plume rise (6.2). Since the plume photography σ_z values are simple fractions of visual plume thickness, then a plot of σ_z versus plume rise can be used to estimate β in (6.2). Because ratios are being considered, many of the geometric errors associated with incorrect estimates of wind direction in the plume photography analysis are minimized. In Figure 24, the observed values of σ_z and plume rise, ΔH, for the June study, are compared for downwind distances of 400 and 1000 m. Although there is considerable scatter the value of $\beta = 0.5$ as suggested by Briggs (1969) is seen to be reasonable, but appears to underestimate the visible radius especially for small plume rises. The value of $\beta = 0.6$ suggested by Briggs (1975) for the "effective" plume radius matches most of the data somewhat better than $\beta = 0.5$. The adoption of a linear curve is analytically simple; however, the data in Figure 24 suggest that a power law of perhaps $\sigma_z \simeq (\Delta H)^{2/3}$ would fit the data better. A variety of physical processes could be speculated to explain such a reduced power law. For example, large plume rises might occur when there is large scale support for a region of uplift which might lead to larger plume rises with less of a shear in the vertical motion components.

(a)

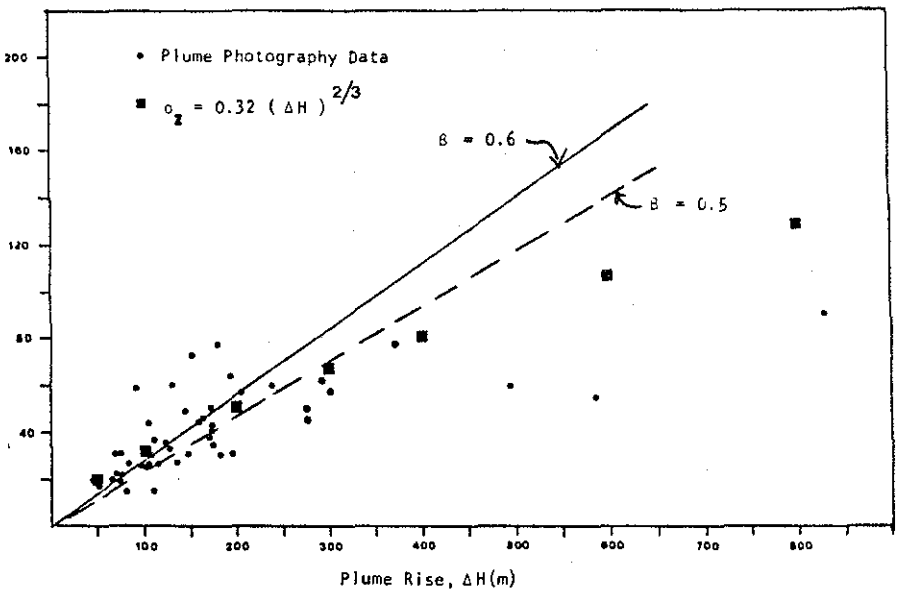

(b)

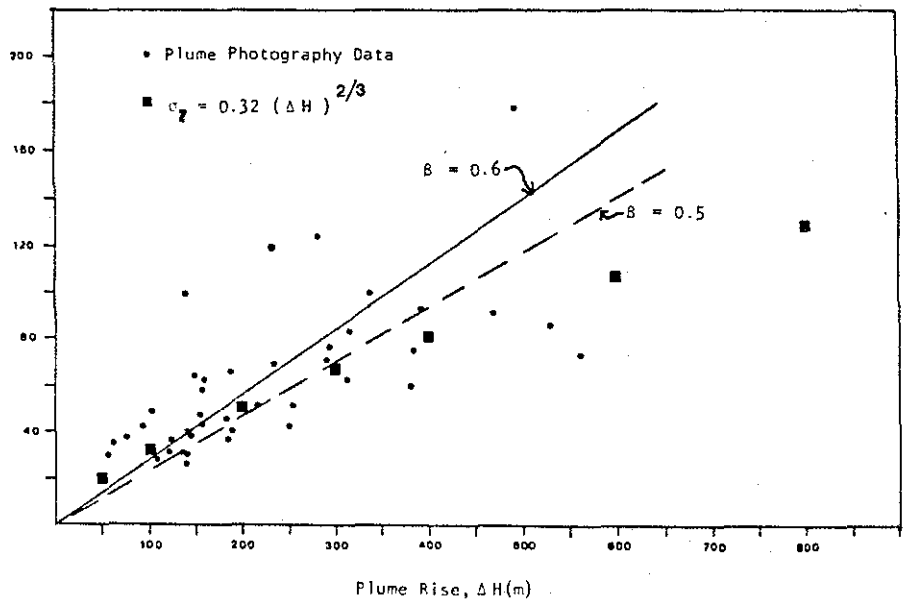

Figure 24 A comparison of plume rise and σ_z at downwind distances of (a) 400 m and (b) 1000 m.

6.1.2.2 Dimensionless Vertical Plume Spread. The specification of plume spread in the source-dominated region will involve a relationship with plume rise as discussed in the previous section. Thus it is appropriate to express the vertical plume spread in dimensionless terms analogous to the plume rise specifications discussed earlier. If we adopt Briggs suggested value of $\beta = 0.5$ for the visual plume radius, and use the 10% criterion adopted by Fanaki et. al (1978), then

$$\sigma_z \simeq 0.42 \; F^{1/3} \, \bar{U}^{-1} \; X^{2/3} \qquad (6.3)$$

The numerical coefficient would be 0.54 if $\beta = 0.6$ had been used in equation (6.2). Although (6.3) has several dubious assumptions, it should provide a reasonable analysis framework.

The equation (6.3) can be recast to form a normalized vertical plume spread, (for $\beta = 0.5$),

$$\bar{U} \, \sigma_z F^{-1/3} \simeq 0.42 \; X^{2/3} \qquad (6.4)$$

The neutral data from June 1977 (15 cases) has been plotted in Figure 25 and the agreement with theory is quite good. The drop-off at large downwind distances is a result of adopting the 10% criterion for the analysis of the plume photography as discussed in the previous chapter.

The stable σ_z data appeared to present some discrepancies between the June and February data sets. These are the same data times as analyzed for plume rise where no such discrepancy was found. Another problem was that the February σ_z data usually extended only to 600 m downwind from the source; whereas the June data extended to typically 1200 m. Thus combining the two sets of data could introduce an anomalous change in the slope of σ_z with distance. The discrepancy is perhaps not real because of the limited number (9) of data sets used. The average normalized stable σ_z values are presented in Figure 26. Also included are "theoretical"

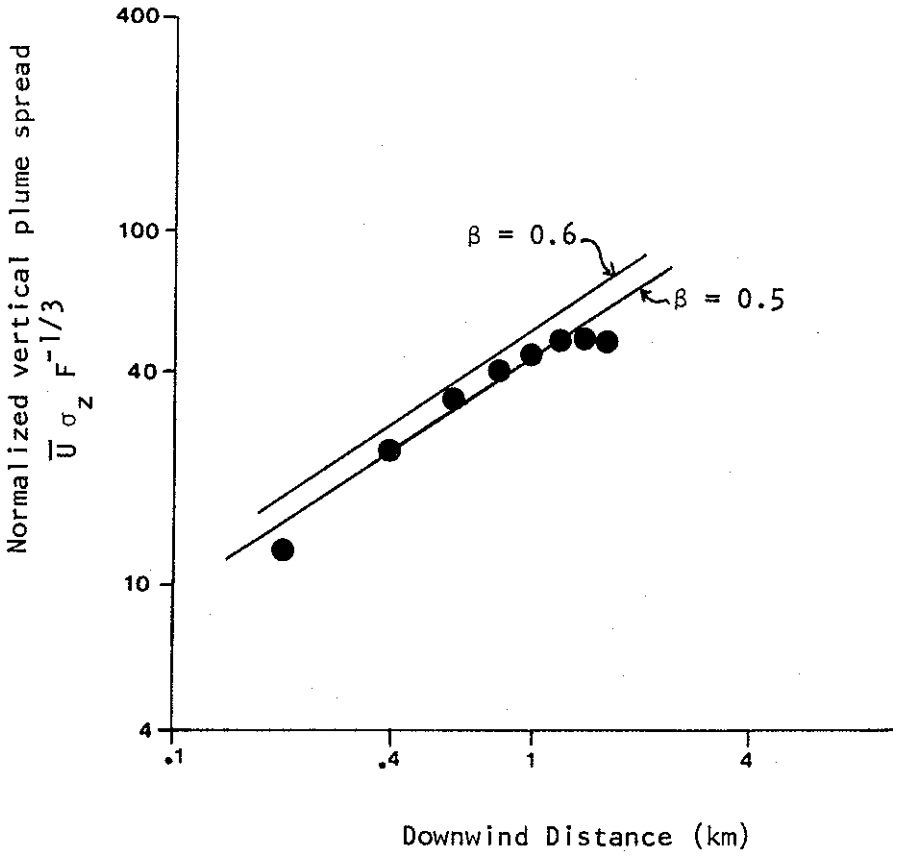

Figure 25. Normalized vertical plume spread, $\bar{U}\ \sigma_z\ F^{-1/3}$, as a function of downwind distance for neutral stability cases. The two lines correspond to equation (6.5).

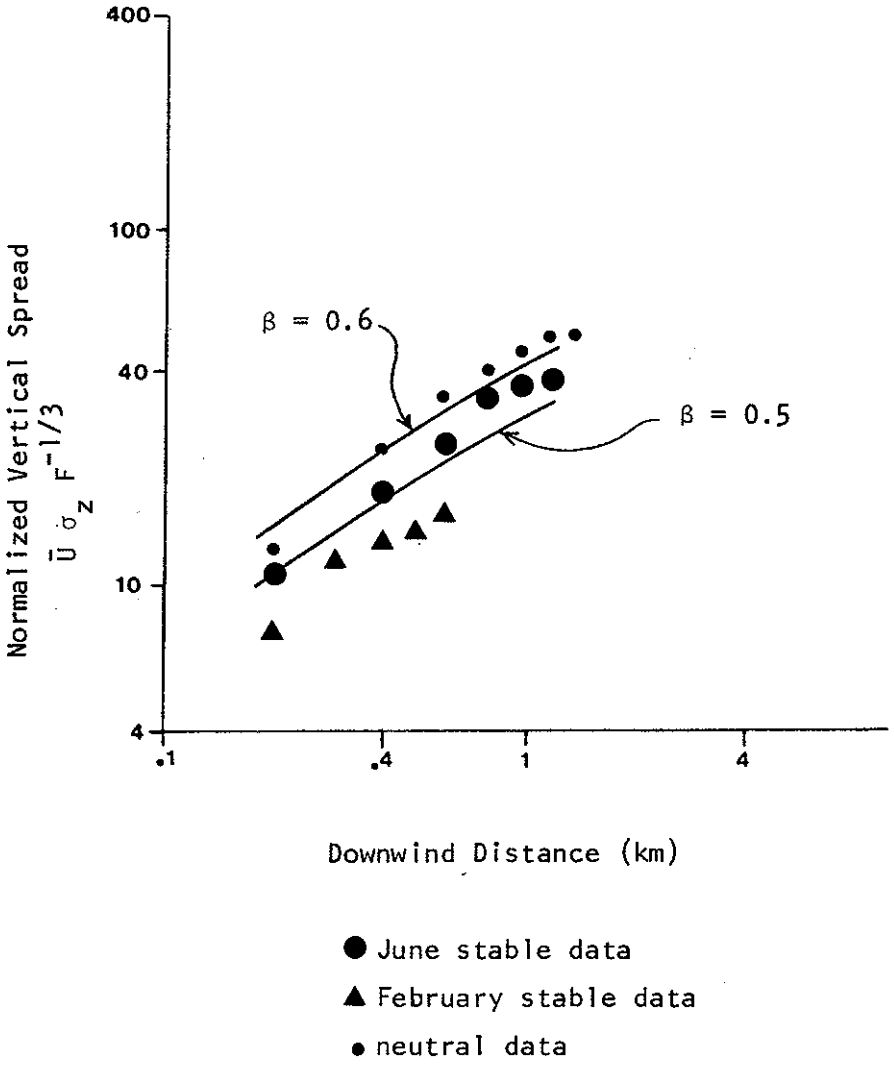

Figure 26. Normalized vertical plume spread, $\bar{U}\,\sigma_z\,F^{-1/3}$, as a function of downwind distance for stable conditions. The lines represent predictions from a stable plume rise theory (6.1) combined with an assumed relationship between plume rise and thickness (6.3).

lines based upon the stable plume rise expression (6.1) and the assumed relationship between plume rise and thickness (6.2).

The relationship between plume rise and thickness (6.2) clearly has physical limitations for a stable situation. After the point of maximum plume rise in stable conditions, the height of the plume centerline may oscillate. Clearly the physics of turbulent mixing would not permit such oscillations of plume thickness (unless there were longitudinal accelerations of the whole plume cross section). Equation (6.2) can really be applied only during the initial stages of plume rise. The conservation models of plume rise often have problems near the point of maximum plume rise due to the physical failure of the closure hypotheses. In the classic Morton, Taylor and Turner (1956) model, the closure technique is the assumption that the entrainment velocity is proportional to the vertical velocity. A negative entrainment rate or even a zero entrainment rate is not physical. The turbulence responsible for mixing will be non-zero throughout the rise; if it ever becomes extremely small then the subsequent generation of turbulence by the velocity shear is minimal (Telford 1966).

For practical purposes, however, the relationship (6.2) is probably useful until the transition to environmentally dominated turbulence.

6.1.3 Ratio of Lateral to Vertical Spread

The specification of the lateral plume spread during the initial source-dominated stage of dispersion is not well known. Most data for industrial plumes close to the source have been derived from plume photography. There is good documentation of lateral dispersion for tracer studies; however, the application of this data to the source-dominated region is not appropriate. Theoretical studies have usually dealt with a plume having a circular cross section and have predicted the growth of the plume's radius.

The LIDAR isopleth plots (Hoff and Froude 1978) permit an estimate of the ratio, σ_y/σ_z, during the initial dilution stage.

The five scans for case study of June 18 at about 0530 at a downwind distance of 230 m suggest a σ_y/σ_z ratio of about 1.4. The other early morning case study, June 23 at 0500 at a downwind distance of 490 m, also suggests a σ_y/σ_z ratio of about 1.4. The early evening case study of June 22 at a downwind distance of 466m (very weak turbulence with a surface radiation inversion beginning to form) suggests a ratio of about 1.5. Based upon this limited data set a tentative value for the ratio, σ_y/σ_z, in the source dominated region is 1.4. However, it is noted that large scale meandering particularly in stable conditions could significantly increase the time-averaged values of σ_y/σ_z.

6.2 ENVIRONMENTALLY DOMINATED STAGE OF DISPERSION

The previous section has shown that the plume sigma values at downwind distances of typically less than 1 km can be predicted reasonably well, at least on an average, based upon the ideas of source-dominated dispersion. In this section, the data for downwind distances greater than 1 km are compared to the various sigma specification schemes discussed in Chapter 4.

The average data fit is compared for each of the schemes together with a discussion on the suitability for individual case studies. The more commonly used empirical schemes are considered first and then the more theoretically based schemes are discussed.

6.2.1 Data Set

The plume photography data and LIDAR data were clearly in the source-dominated region for at least most of the measurements. Some of the further downwind measurements say between 1 and 1.6 km may have sometimes been in the environmentally dominated region, but the σ_z values at these distance may have been suspect as discussed earlier. Thus all the plume photography data have been discussed in the previous section on source-dominated dispersion. Most of the data from the other sources were far enough downwind that environmental mixing was dominant. Some helicopter data was obtained at 0.8 km downwind but in these cases, statistical sampling problems were probably important as discussed in Chapter 5 and so these data points have not been considered further.

The data set remaining for comparison with the sigma typing schemes for environmentally dominated mixing is summarized in Table 22.

6.2.2 Goodness-of-fit for Empirical Sigma Typing Schemes

In the following sections, the empirical typing schemes tested are the Pasquill Gifford scheme (with three techniques of stability class selection), the TVA scheme, the BNL scheme and Brigg's scheme. Cramer's scheme was shown in Chapter 4 to be similar in form to the theoretical schemes based on Taylor's theory and will be discussed with those schemes in a later section.

6.2.2.1 Pasquill-Gifford Scheme. Three techniques were tested for the selection of the Pasquill-Gifford (PG) stability types. The Turner classification was used with wind speeds estimated for plume height from the minisonde and tethersonde data. The equivalent wind speeds at a height of 10 m were estimated using a power law extrapolation down to 10 m from the minisonde profiles and were then used in Turner's classification. Finally, the temperature lapse rate over the region of plume rise was used for stable cases together with the U.S. NRC procedures outlined in Chapter 4.

The data fit to the PG curves for winds at plume height is summarized in the histograms of Figure 27 where the abscissa scale indicates the difference of the observed to predicted sigma value in terms of numbers of stability classes. Perfect agreement would occur if all the data were within ± 1 stability classes of the predicted class. A comparison of each data set to the curves is shown in Figure 28 (for σ_y) and Figure 29 (for σ_z).

On the average, the PG scheme with winds at plume height tends to underestimate the observed σ_y values. The underestimation of σ_y is more serious closer to the stack which may be due to a combination of multiple sources contaminating the observed σ_y values and of the lack of consideration of initial dilution by the

Table 22 Data set for testing of the sigma specification schemes for environmentally dominated mixing

Field Trip	Sensor	Number of Valid Data Points	
		σ_y	σ_z
March 1976	Aircraft	11	12
	COSPEC	2	-
February 1977	Helicopter	8	8
June 1977	Aircraft	10	9
	COSPEC	4	-

Notes:

1. The number of data points for the helicopter data set does not include the 2 data runs at 0.8 km downwind of the stack.
2. The COSPEC data runs in June have been grouped according to meteorological condition.

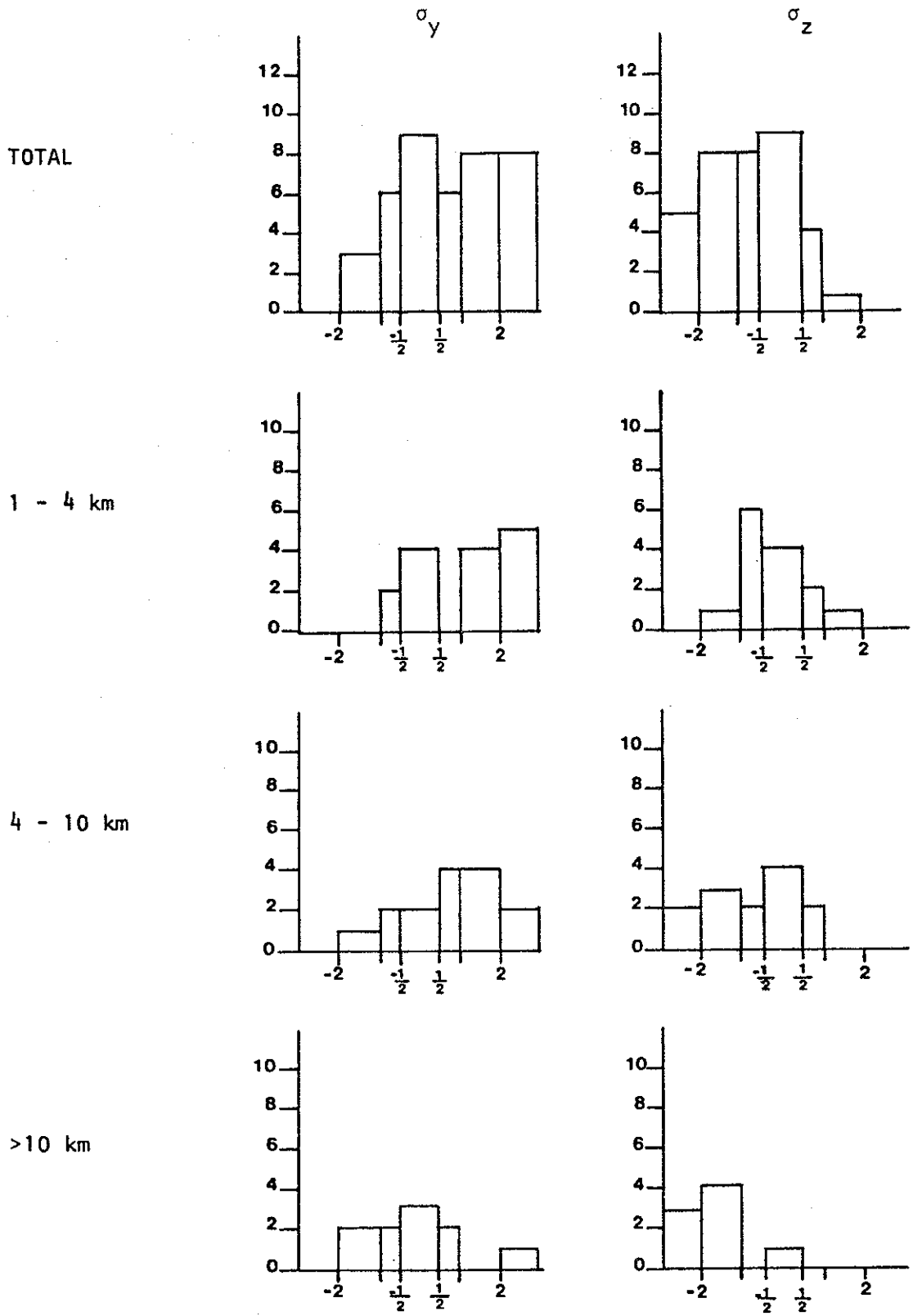

Figure 27 Goodness-of-fit histograms for the Pasquill-Gifford curves with stability classes chosen using Turner's method and using wind speed at plume height. The abscissae represent the sizes of discrepancies in terms of number of classes. The ordinate represents the frequency of occurrence ($\frac{1}{2}$ class widths have been multiplied by two to conserve number density).

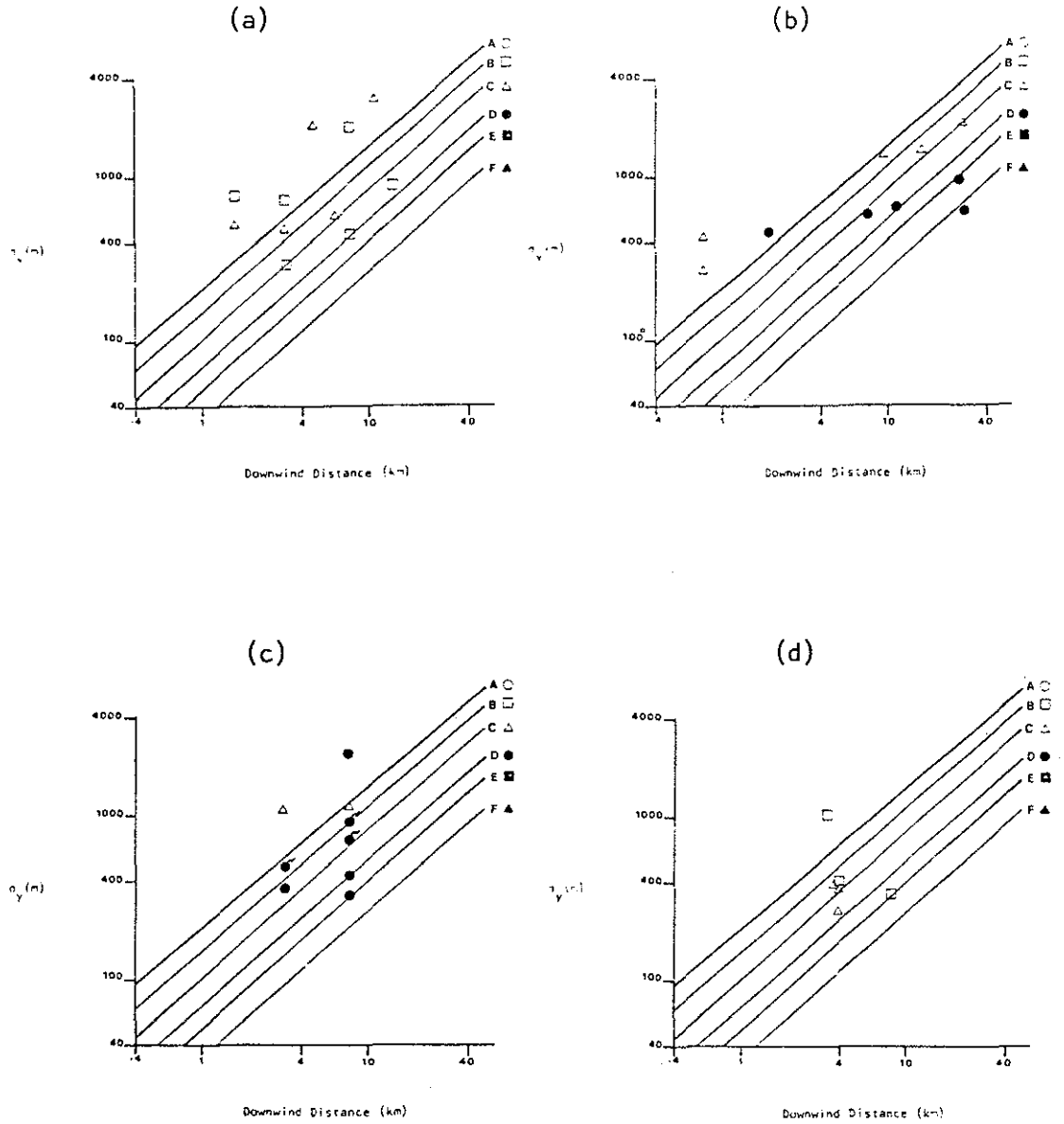

Figure 28 The Pasquill-Gifford y - curves with the Turner stability scheme (plume height winds) for (a) March 1976 aircraft, (b) February 1977 helicopter, (c) June 1977 aircraft, (d) March, June COSPEC. A tail on the symbol means ½ class less stable.

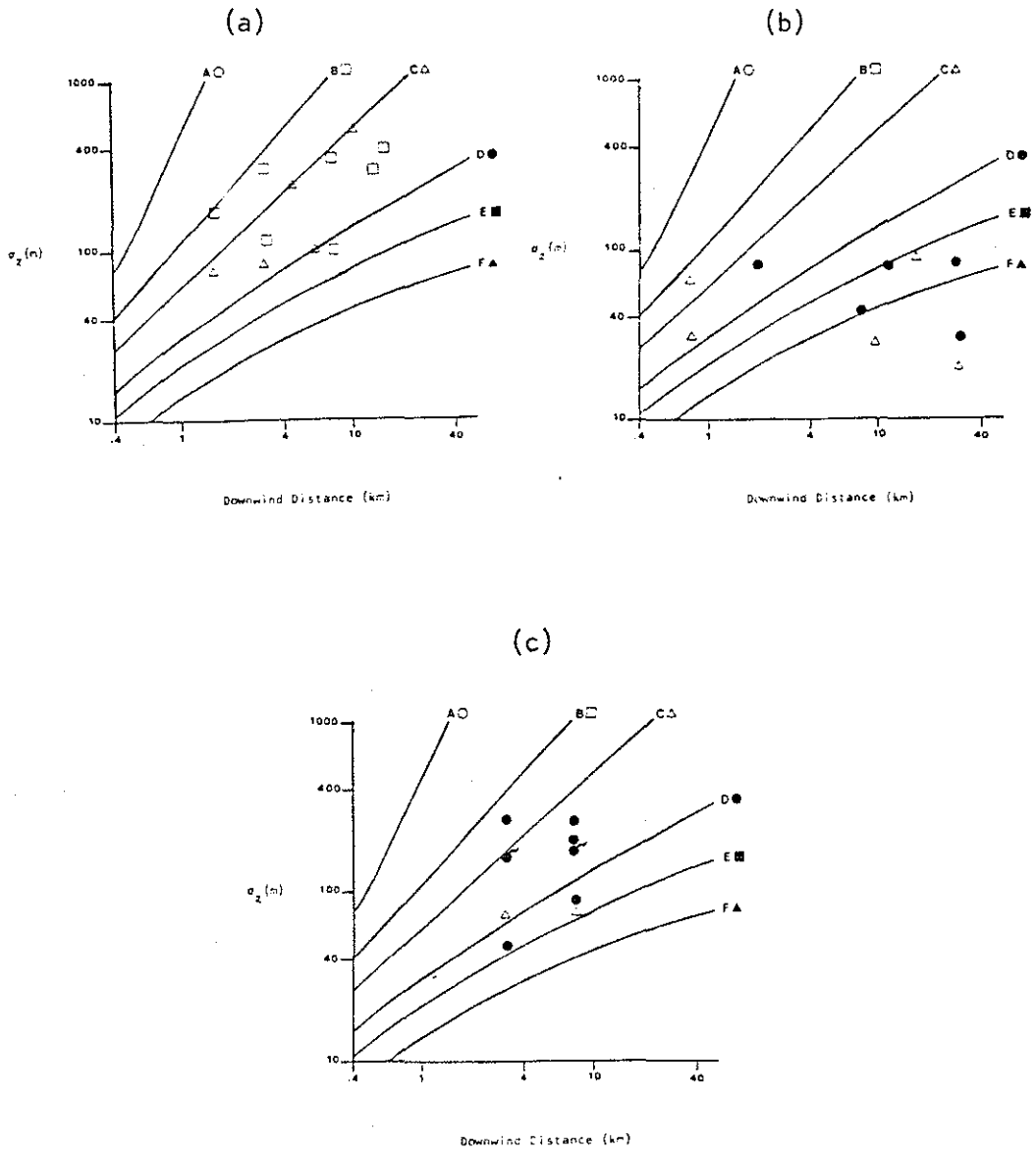

Figure 29 The Pasquill-Gifford z - curves with the Turner stability scheme (plume height winds) for (a) March 1976 aircraft, (b) February 1977 helicopter, (c) June 1977 aircraft. A tail on the symbol means $\frac{1}{2}$ class less stable.

PG scheme. Further from the source, the PG σ_y curves appear to be increasing faster than the observed data; this is not surprising since the PG curves do not agree with the $X^{1/2}$ behaviour predicted by Taylor's statistical theory at large distances.

The PG σ_z curves give fairly good agreement with observation except at downwind distances greater than 10 km. This lack of agreement at long range is largely due to the helicopter data from February. The PG-Turner scheme predicts C and D stabilities for daytime conditions even with slight solar insolation. However, in the presence of very low sun angles and fairly large regions of high albedo due to snow cover, the plume very often remains in a stable layer which has very little vertical mixing. In such situations, beyond the source-dominated mixing region, the σ_z values tend to increase very slowly and the PG curves tend to overestimate σ_z.

The corresponding curves for 10 m winds are shown in Figures 30, 31 and 32. There are few changes except for the June aircraft data. This result is not surprising since for slight radiation, found for almost all cases in the March and February field trips, only C and D stability classes are available. For the June field study, however, there were several shifts of more than one stability class, due to the decreased wind speeds calculated for a height of 10 m. The change in wind speed does not improve the situation for the cold-season cases when the PG scheme tends to overestimate σ_z, in particular beyond the source-dominated region. The lapse rate classification scheme for the PG curves is summarized in Figure 33, 34 and 35. The σ_z specification appears to be improved over the Turner scheme discussed above. Presumably this is due to more realistic specifications in the winter situations. Also, the summer estimates are improved due to better estimations of whether the plume is in or above a mixed region. Note, however, that the elevated lapse rate specification scheme cannot distinguish neutral from convective conditions. For σ_y, the lapse rate scheme appears to significantly underestimate the observed σ_y

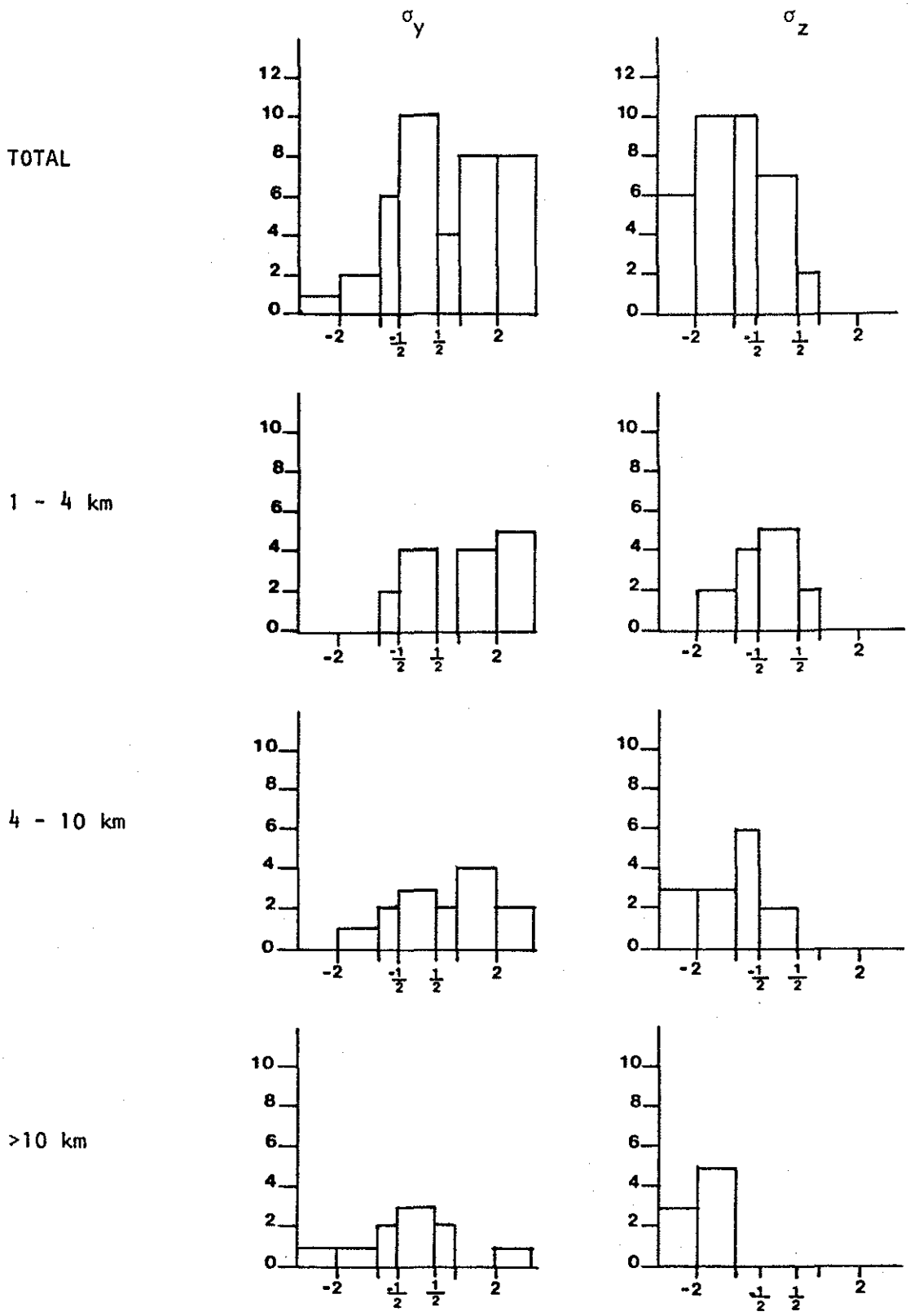

Figure 30 Goodness-of-fit histograms for the Pasquil-Gifford curves with stability classes chosen using Turner's method and using 10 m wind speeds extrapolated downward from minisonde/tethersonde winds. The meanings of the abscissae and ordinates were described below Figure 27.

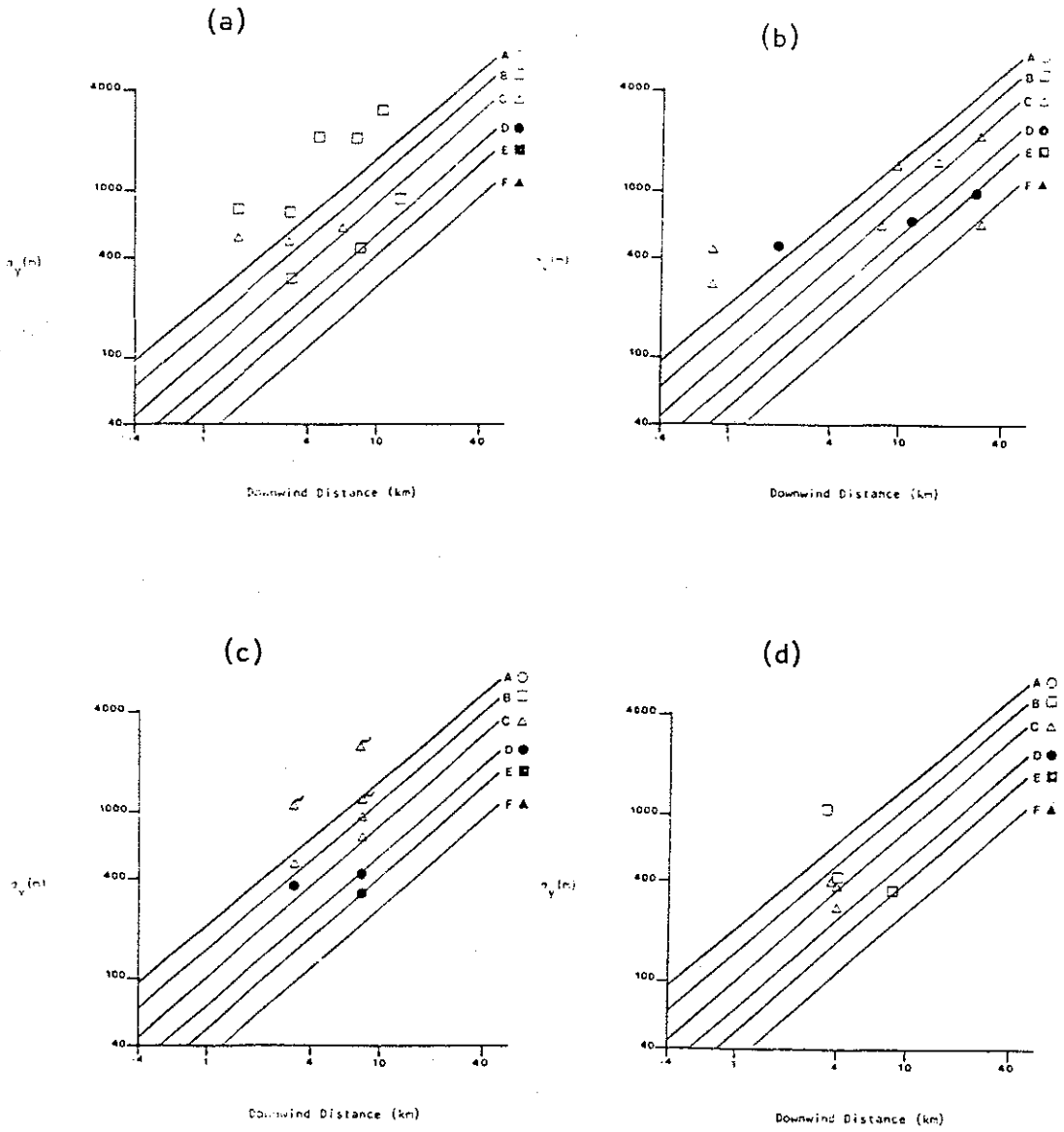

Figure 31 The Pasquill-Gifford y - curves with the Turner stability scheme (10 m winds) for (a) March 1976 aircraft, (b) February 1977 helicopter, (c) June 1977 aircraft, (d) March, June COSPEC. A tail on the symbol means $\frac{1}{2}$ class less stable.

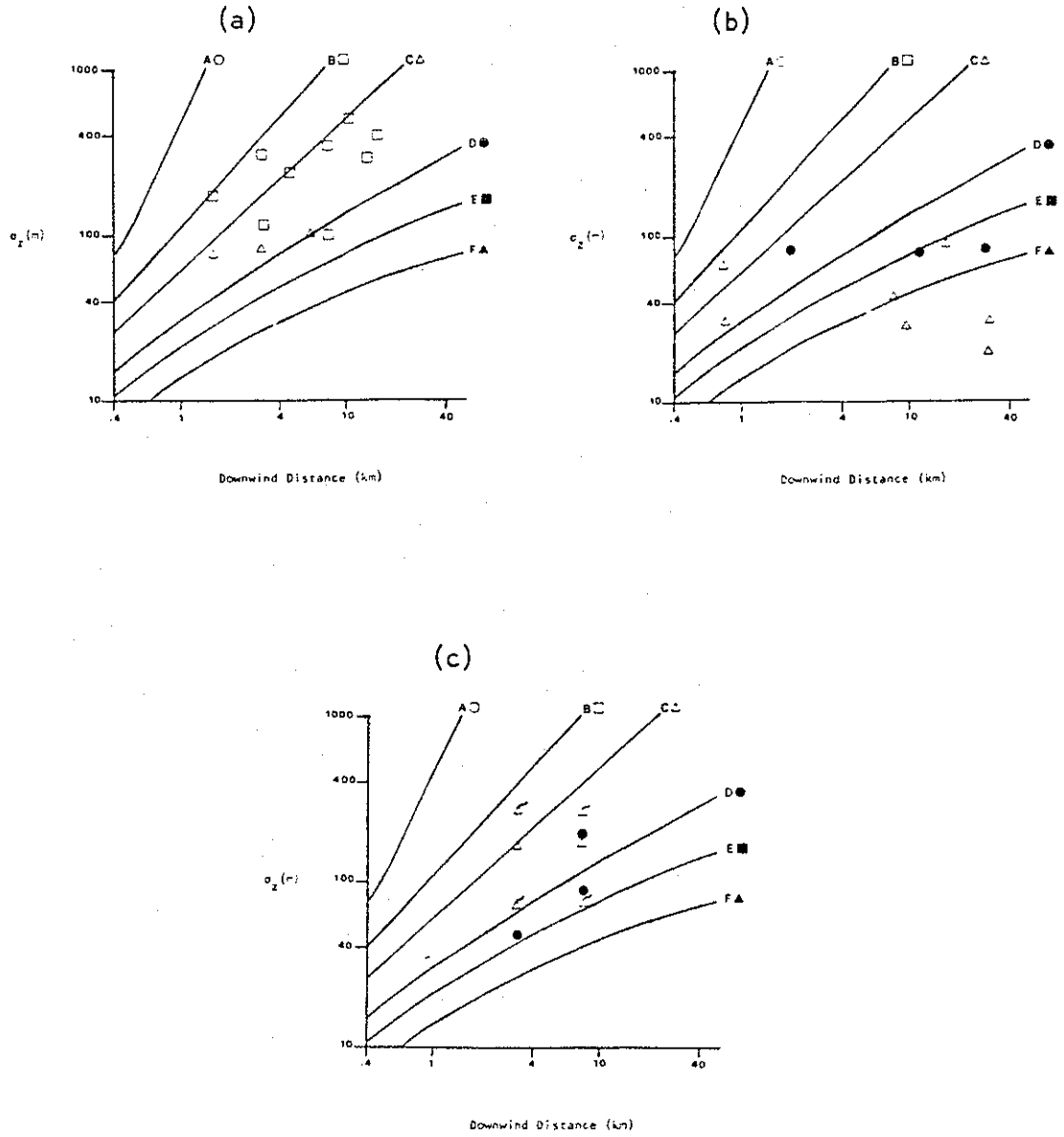

Figure 32 The Pasquill-Gifford z - curves with the Turner stability scheme (10 m winds) for (a) March 1976 aircraft, (b) February 1977 helicopter, (c) June 1977 aircraft. A tail on the symbol means $\frac{1}{2}$ class less stable.

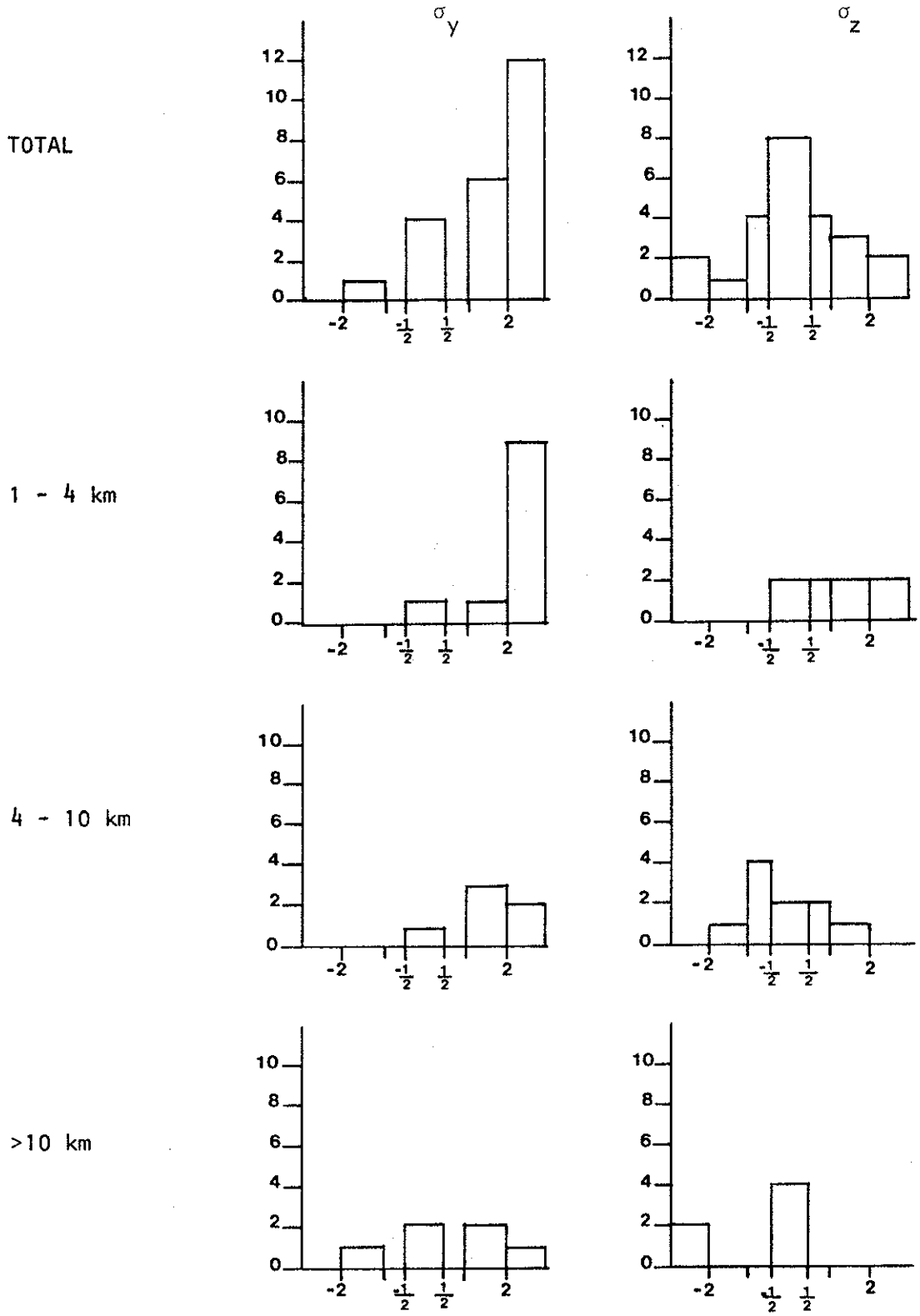

Figure 33 Goodness-of-fit histograms for the Pasquill-Gifford curves with stability classes chosen from an elevated temperature profile (US NRC method) for stable cases. The abscissae represent the sizes of discrepancies in terms of number of classes. The ordinate represents the frequency of occurrence ($\frac{1}{2}$ class widths have been multiplied by two to conserve number density).

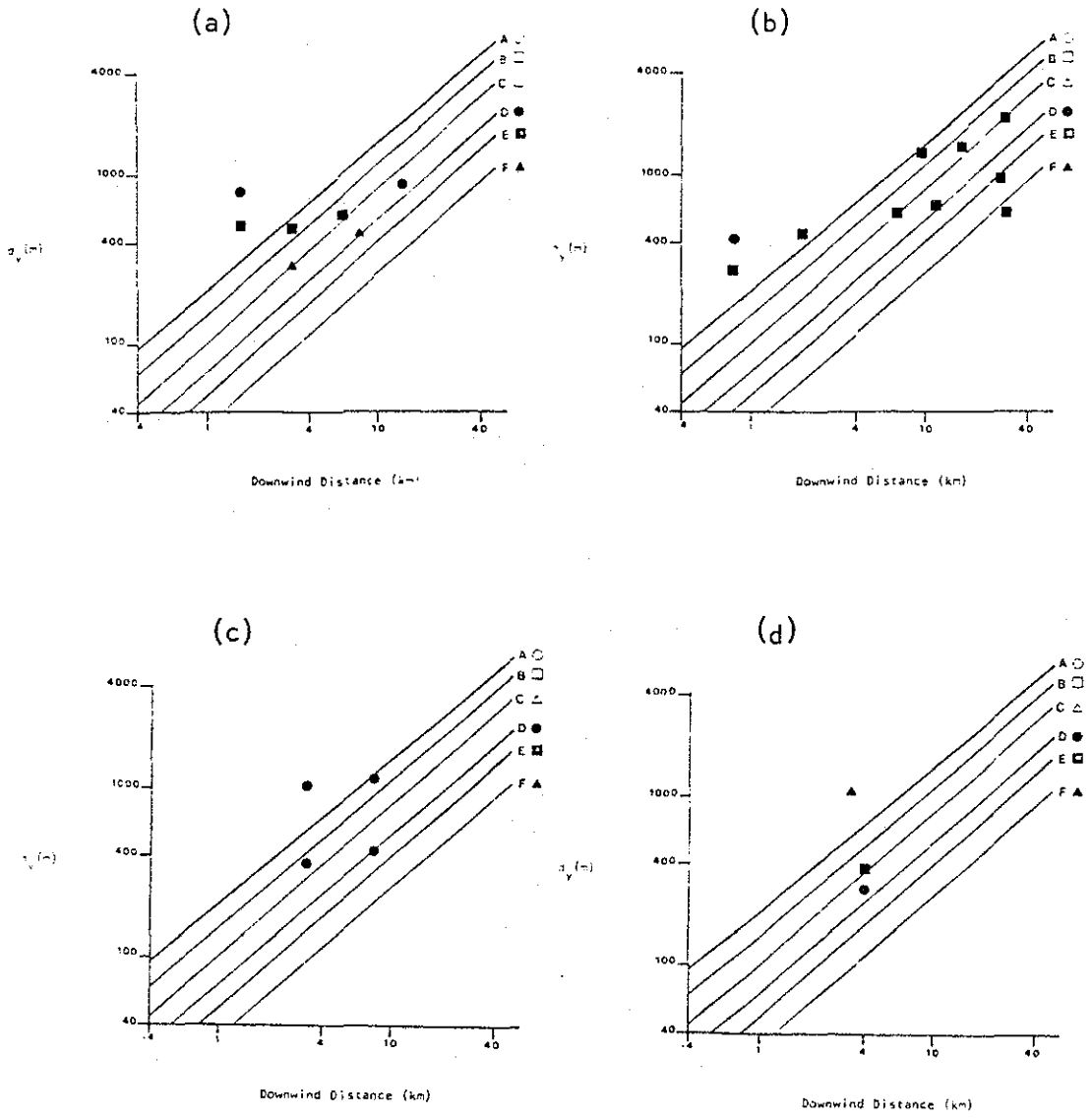

Figure 34 The Pasquill-Gifford y - curves with the NRC lapse rate stability scheme (plume height winds) for (a) March 1976 aircraft, (b) February 1977 helicopter, (c) June 1977 aircraft, (d) March, June COSPEC. A tail on the symbol means $\frac{1}{2}$ class less stable.

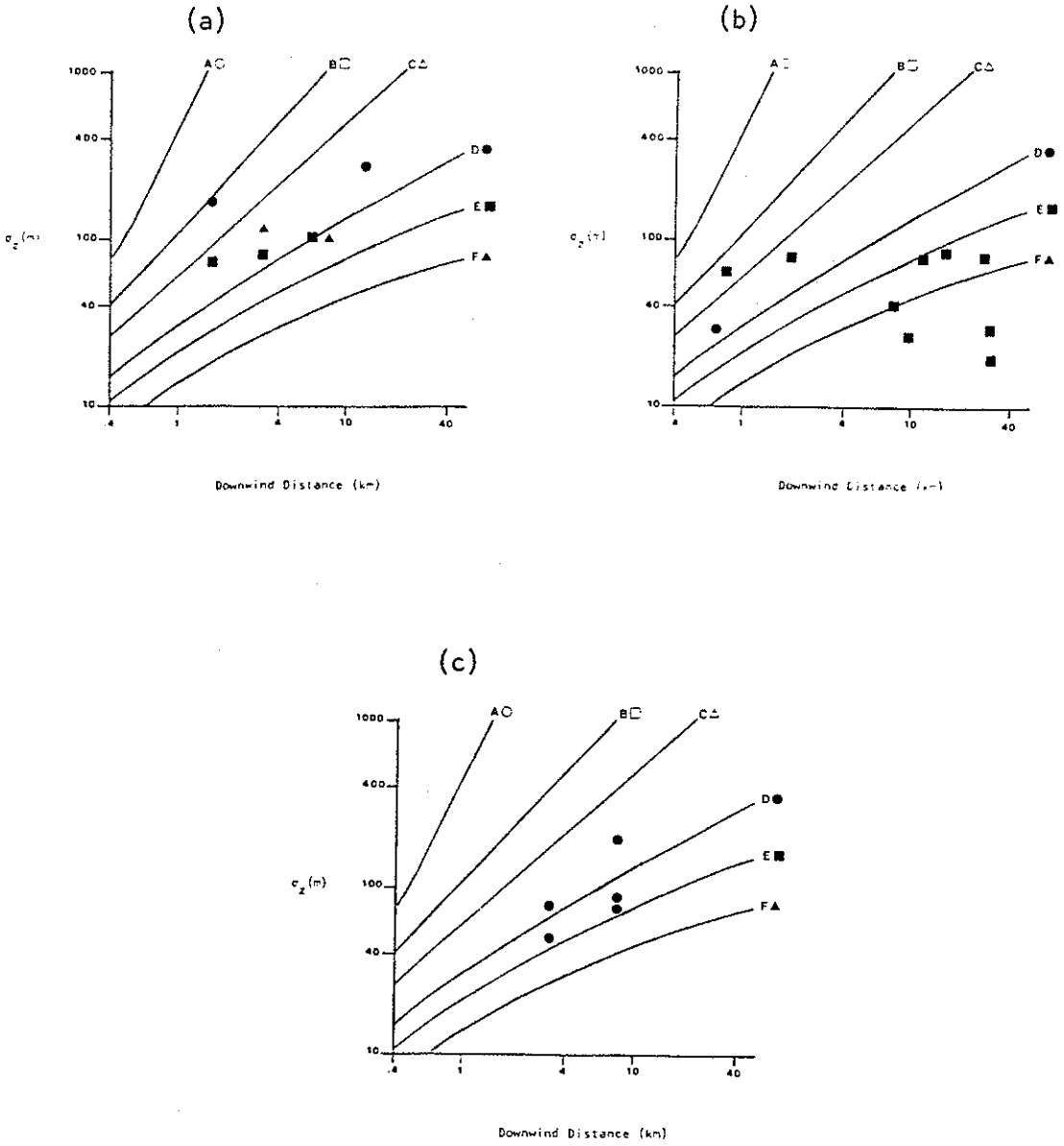

Figure 35 The Pasquill-Gifford z - curves with the NRC lapse rate stability scheme (plume height winds) for (a) March 1976 aircraft, (b) February 1977 helicopter, (c) June 1977 aircraft. A tail on the symbol means $\frac{1}{2}$ class less stable.

values close to the source (less than 4 km). This occurs for data from all of the sensor systems.

In summary, the PG system has some obvious shortcomings, some of which would be rather easily overcome in an application to the AOSERP region. An elevated lapse rate over the region of plume rise with compensation for initial dilution could lead to reasonable estimates of σ_z. The meteorological scheme (Turner scheme) is inappropriate in the winter for σ_z. The σ_y curves tend to underestimate the observed values except at large distances downwind. This result suggests that there tends to be enhanced dispersion in the AOSERP region compared to the PG estimates. The disagreement at large downwind distances is due to the failure of the PG curves to recognize the $X^{1/2}$ behaviour at long range. Thus the PG curves tend to significantly underestimate σ_y close to the source (due to possible multiple source effects, source-dominated dispersion and underestimation of environmental mixing) and tend to increase too quickly with increasing distance.

6.2.2.2 TVA Scheme. The goodness-of-fit for the TVA scheme is summarized in Figures 36, 37 and 38. As discussed in Chapter 4, the TVA curves are based upon helicopter traverses of real industrial plumes to downwind distances of 3.2 km for neutral conditions and 16 km for stable conditions. The stability classes are based upon an elevated lapse rate and so neutral and convective conditions cannot be distinguished.

The agreement between the predicted and observed σ_z values is good. The discrepancies occur largely in the comparisons with the March aircraft data. In these cases the observed values are larger than predicted. Part of the problem may lie in the uncertainties associated with the observed data. Secondary sources may have increased the σ_z values. In addition, the aircraft height information has uncertainties of probably $\pm$ 20 m at the best. Variations in wind speed may have caused changes in the height of the plume during observations which would have increased the

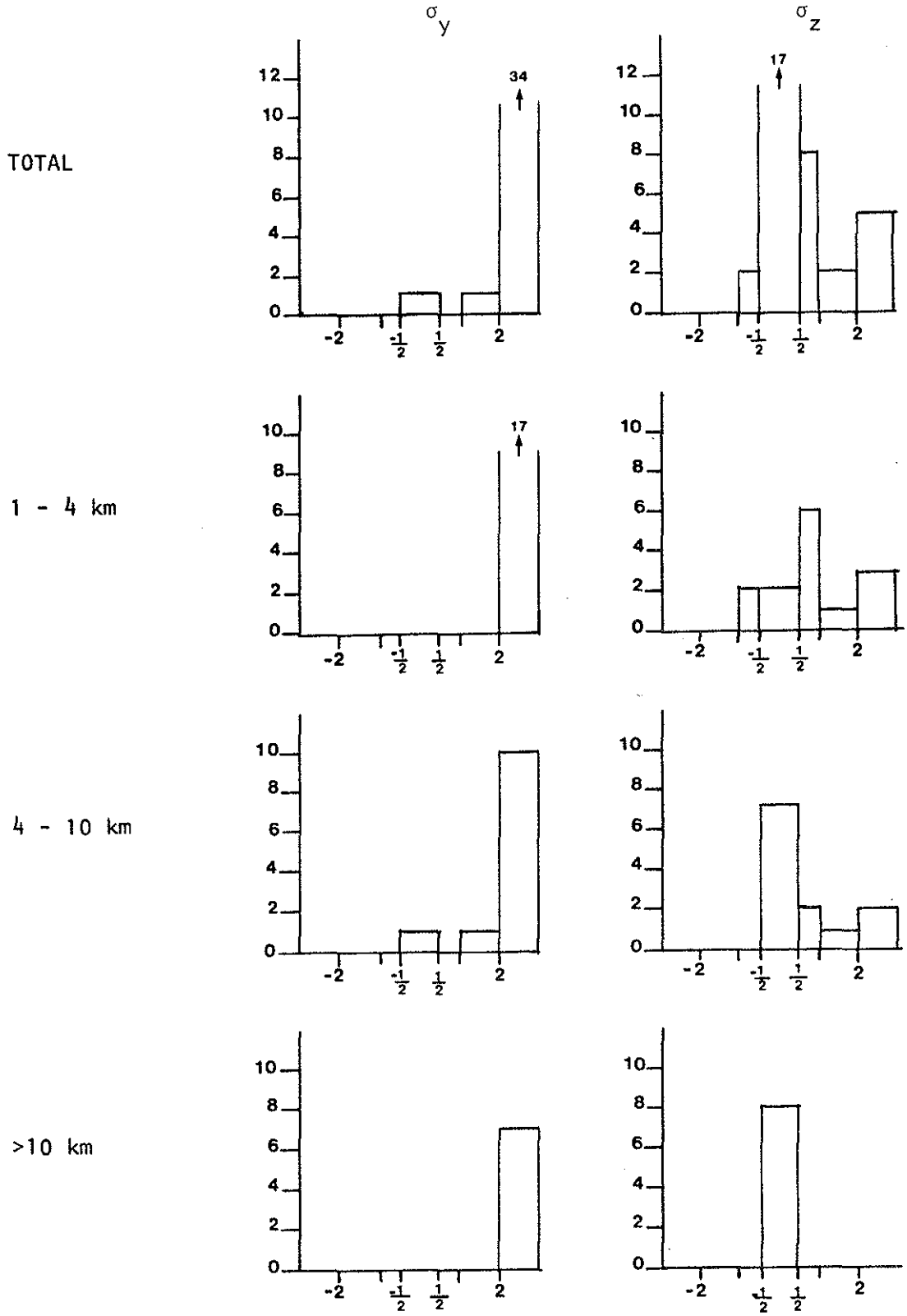

Figure 36 Goodness-of-fit histograms for the TVA scheme. The abscissae represent the sizes of discrepancies in terms of number of classes. The ordinate represents the frequency of occurrence ($\frac{1}{2}$ class widths have been multiplied by two to conserve number density).

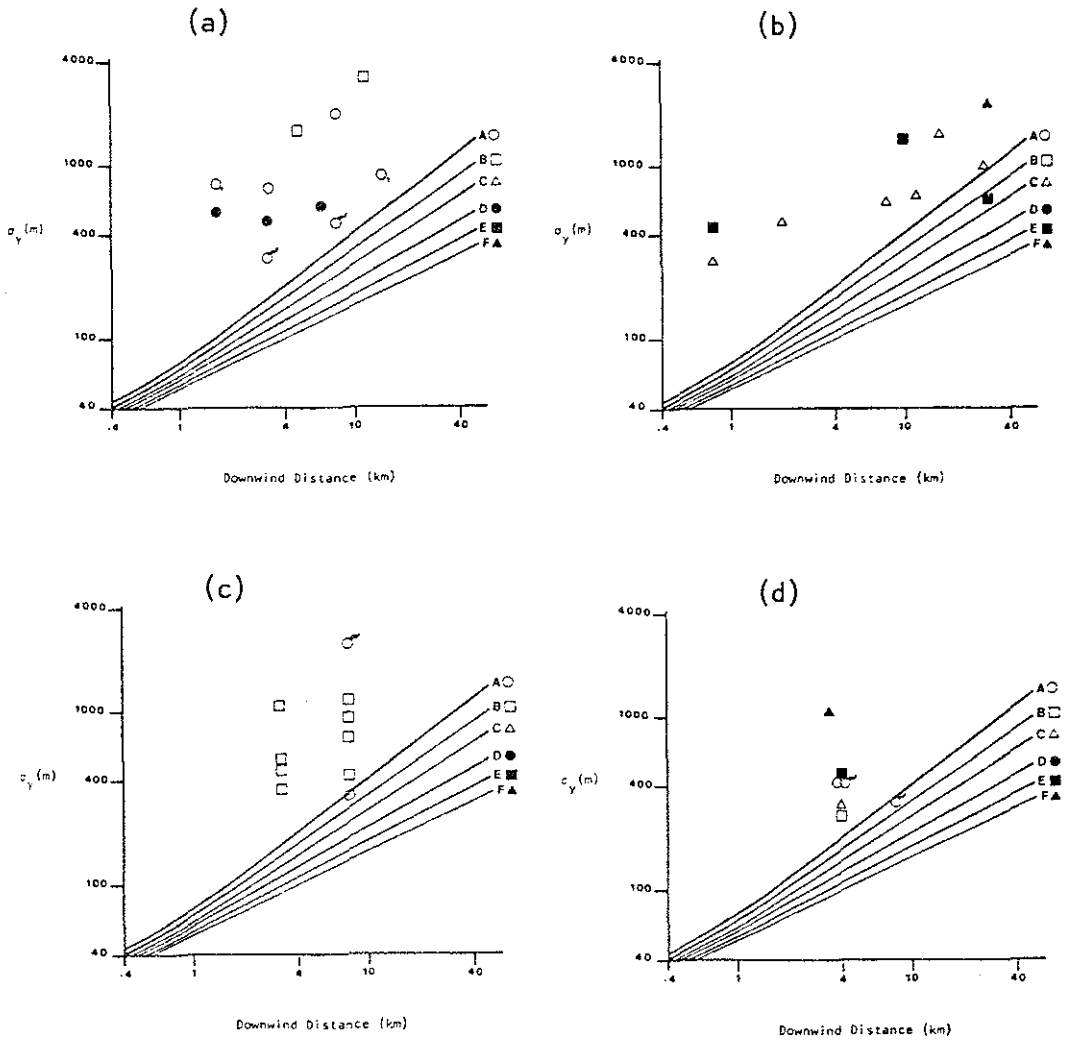

Figure 37 The TVA y - curves for (a) March 1976 aircraft, (b) February 1977 helicopter, (c) June 1977 aircraft, (d) March, June COSPEC. A tail on the symbol means $\frac{1}{2}$ class less stable.

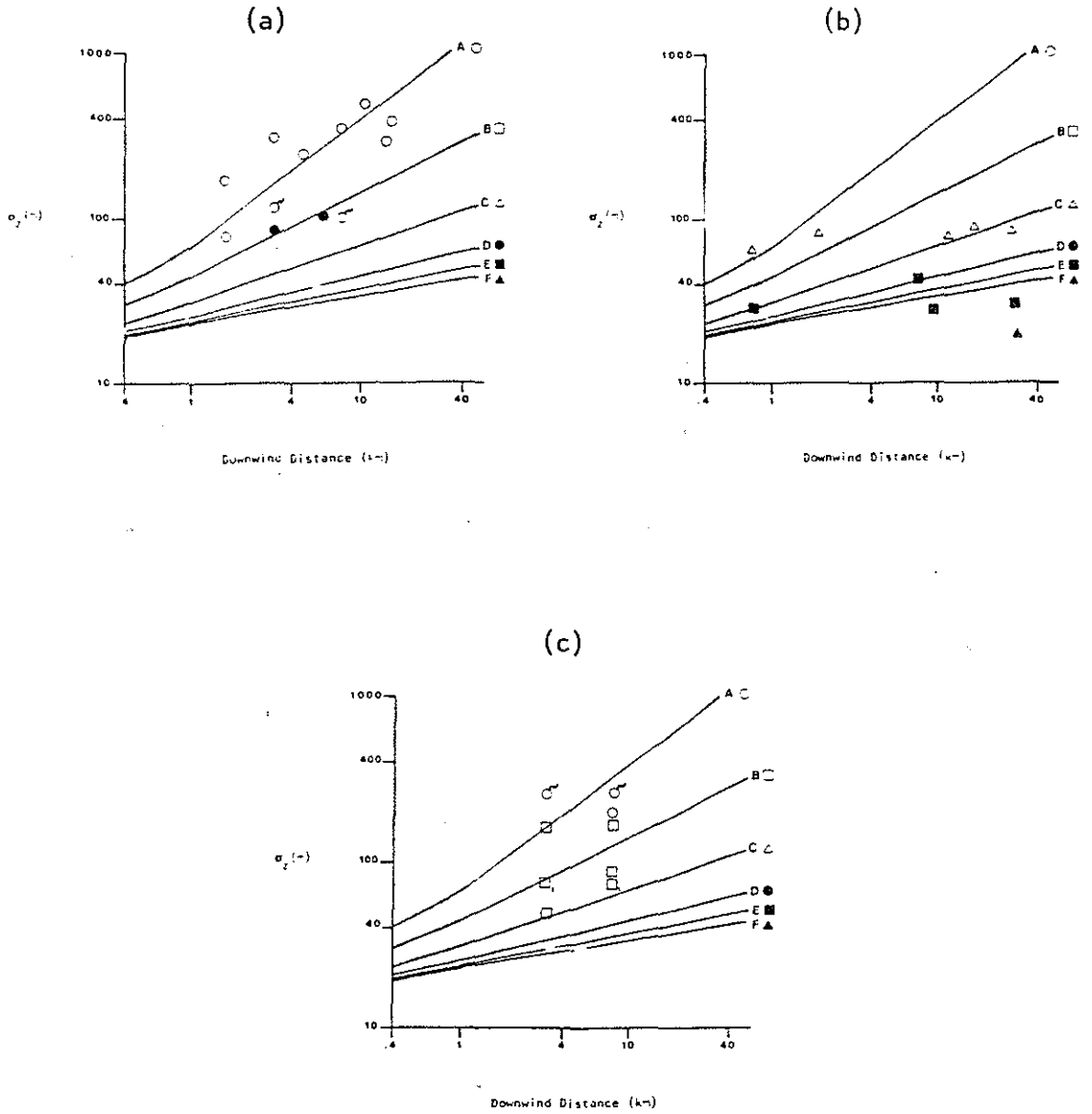

Figure 38 The TVA z - curves for (a) March 1976 aircraft, (b) February 1977 helicopter, (c) June 1977 aircraft. A tail on the symbol means ½ class less stable. Subscript 1 indicates a trapping inversion.

uncertainties associated with constructing a representative plume thickness estimate. It must also be noted that these same measurement problems (except possibly for secondary sources) would have been encountered in the TVA study suggesting that the low values predicted for σ_z may be quite uncertain. For the helicopter data, reasonable experimental uncertainties were assumed for the runs showing small σ_z values. Agreement was considered to be met if the predicted values lay within these reasonable error limits. The separation of classes D, E and F for the TVA σ_z curves over the TVA measurement range of 1 to 16 km. is considered to be negligible compared to any reasonable estimate of experimental errors.

The TVA σ_y curves appear to systematically underestimate the observed σ_y values for all sensor systems (aircraft, helicopter, COSPEC), by about a factor of 3. The March aircraft data appear to be separated properly using the TVA stability scheme. However, the June aircraft data show considerable scatter for the same stability class. The helicopter and COSPEC data do not separate well. The systematic discrepancy from the TVA results is not too surprising since it is well known that for a given stability class, the size of the wind direction fluctuations, which are the mixing mechanism generating the dispersion, is very site specific (Weber 1976). The scatter of σ_y for the June aircraft data under the same stability class is not too surprising since the TVA scheme cannot distinguish neutral from convective conditions nor can it evaluate the strength of the mixing if neutral.

In summary, the TVA scheme can probably work well for stable conditions for σ_z. However very little test data were obtained for unstable conditions when the TVA σ_z estimates may be inappropriate due to the inability to separate neutral and convective conditions. The TVA σ_y estimates are markedly smaller than observed, presumably due to site specificity for the TVA σ_y curves. The typing scheme itself is only acceptable for stable conditions.

6.2.2.3 BNL Scheme. The BNL predictions are compared to observations in Figures 39, 40 and 41. In general the BNL scheme appears to predict σ_y reasonably well except it sometimes underpredicts. The predicted values of σ_z were greater than observed.

Part of the problem with the σ_z discrepancy may originate in height differences in the determinants of vertical and horizontal mixing. Close to the surface, the vertical mixing may be dominated by mechanical mixing and so the relationship between vertical spread and horizontal wind fluctuations may be fairly good. However for elevated plumes with effective stack heights of several hundred meters, the vertical mixing may be less closely tied to horizontal wind fluctuations. In stable conditions, quasi two-dimensional eddies may generate quite large σ_θ values. The BNL scheme does not distinguish the spectral size of the eddies. Consequently, a fairly large σ_θ may exist together with quite small vertical velocity fluctuations in stable conditions. This would lead to predictions of a less stable stability class and hence predictions of σ_z which are too large. The discrepancies with the BNL σ_z predictions may also be affected by the limited data set used for testing. If there were more unstable or at least fully mixed boundary layers, then the agreement for σ_z might have been better.

The σ_y values appeared to agree with predictions fairly well; although there was some scatter. Part of the scatter may have been associated with the frequent lack of good σ_θ data for stability scheme selection. The procedure adopted for stability class selection for cases with questionable σ_θ data was described in Chapter 4. However, there were, in addition, some serious discrepancies in the different estimates of σ_θ itself and $\sigma_u/\overline{U}$. These have been discussed at the end of the tethersonde section in Chapter 5, where it was shown that the aircraft values tended to agree with the tethersonde $\sigma_u/\overline{U}$ values. Several orthogonal runs made by the aircraft (Davison and Grandia 1978) showed that, for many situations, there were no statistically significant differences

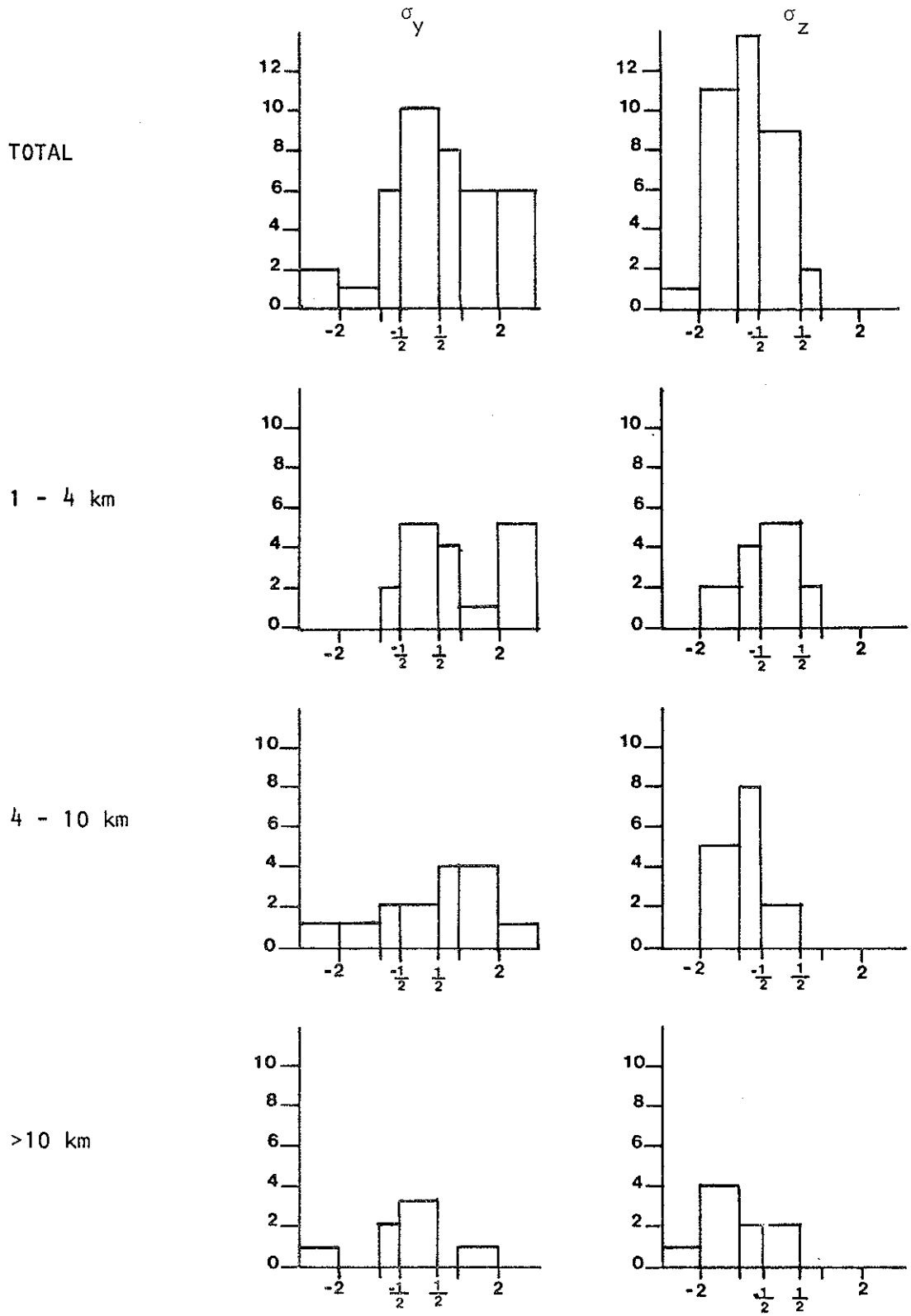

Figure 39 Goodness-of-fit histograms for the BNL scheme. The abscissae represent the sizes of discrepancies in terms of number of classes. The ordinate represents the frequency of occurrence, ($\frac{1}{2}$ class widths have been multiplied by two to conserve number density).

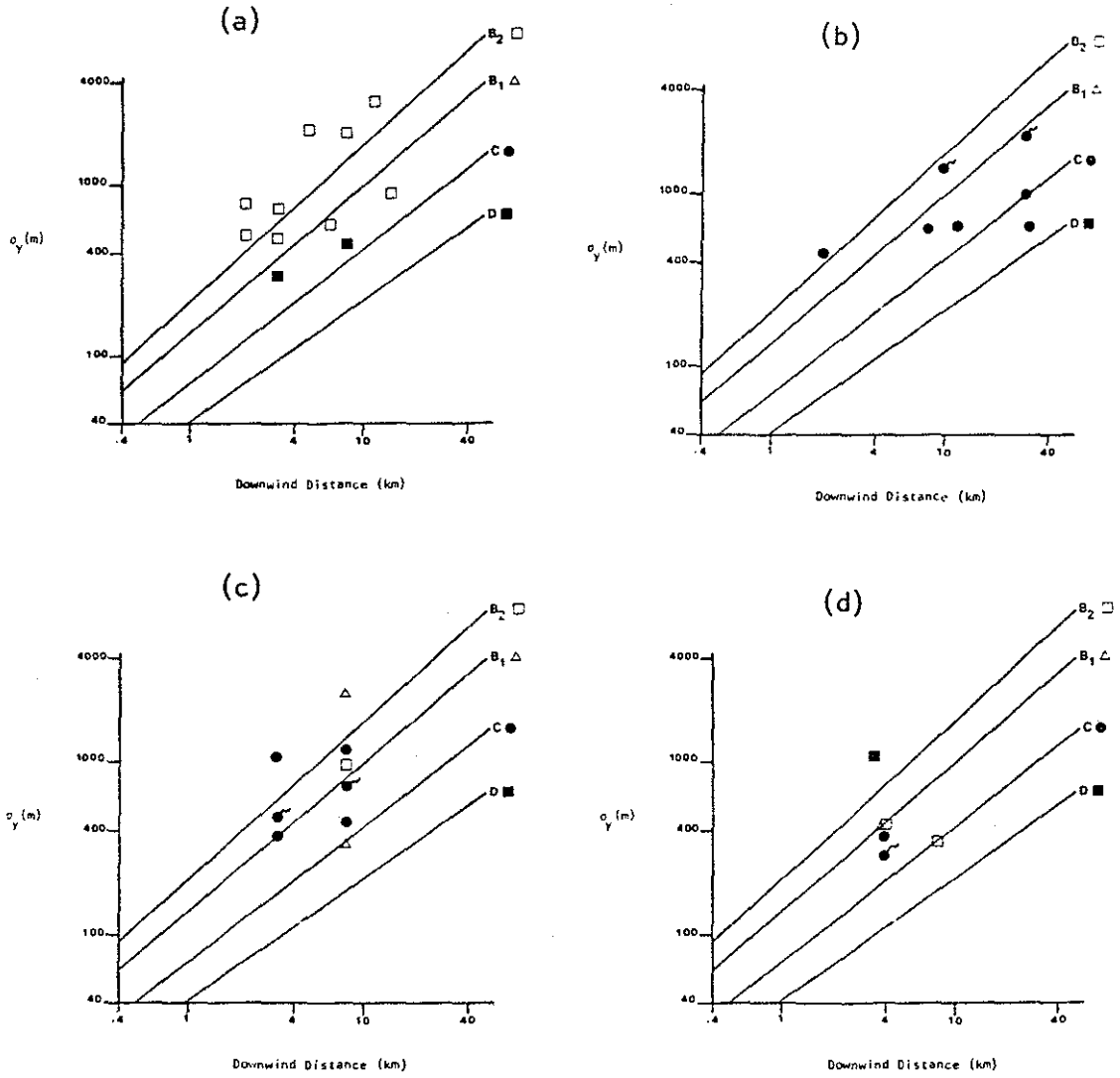

Figure 40 The BNL y - curves for (a) March 1976 aircraft (b) February 1977 helicopter, (c) June 1977 aircraft, (d) March, June COSPEC. A tail on the symbol means $\frac{1}{2}$ class less stable.

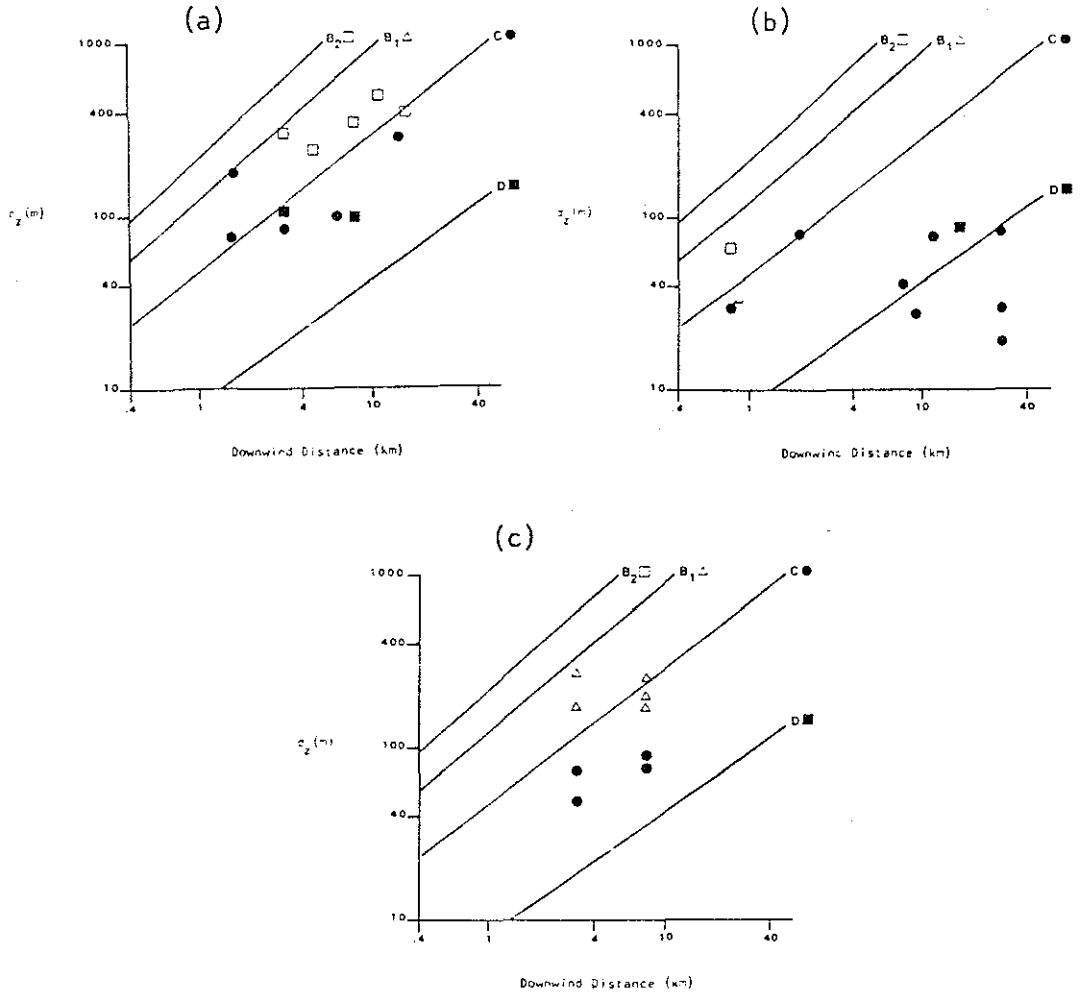

Figure 41 The BNL z - curves for (a) March 1976 aircraft, (b) February 1977 helicopter, (c) June 1977 aircraft. A tail on the symbol means $\frac{1}{2}$ class less stable.

between σ_u and σ_v. Nevertheless, there is some uncertainty for some of the adopted σ_θ values.

The σ_y values tend to be underestimated closer to the source but not farther away from the source. This distance dependence of the discrepancies may reflect the difference in the power law adopted for the BNL curves compared to the change towards $X^{1/2}$ predicted by Taylor's statistical theory as discussed in Chapter 4.

In summary, the BNL curves do not appear to be suitable for σ_z predictions. The σ_y predictions appear reasonably good when all downwind distances are averaged. However, the adoption of a single power law dependence for the σ_y curves is probably incorrect. The separation by σ_θ is reasonable but may suffer from some uncertainties in the σ_θ data.

6.2.2.4 Briggs' Scheme. The Briggs' interpolation scheme is compared to the observed sigma values in Figures 42, 43 and 44. The Briggs scheme was described in Chapter 4. It is an interpolation scheme using the PG, TVA and BNL curves together with some influence of Taylor's theory. The stability classifications are based upon the Turner modification of the Pasquill meteorological scheme. For this study the plume height winds were used.

A comparison with the results for the PG scheme show that the Briggs scheme for this data set presents virtually no improvement. The estimates of σ_z from the Briggs scheme are perhaps not quite as good as the PG estimates. However, the data base is quite small for such a generalization. Since the Briggs scheme utilizes the same stability classifications as Pasquill's meteorological scheme modified by Turner, the same problems of winter stable conditions exist for the Briggs scheme as discussed above for the PG scheme.

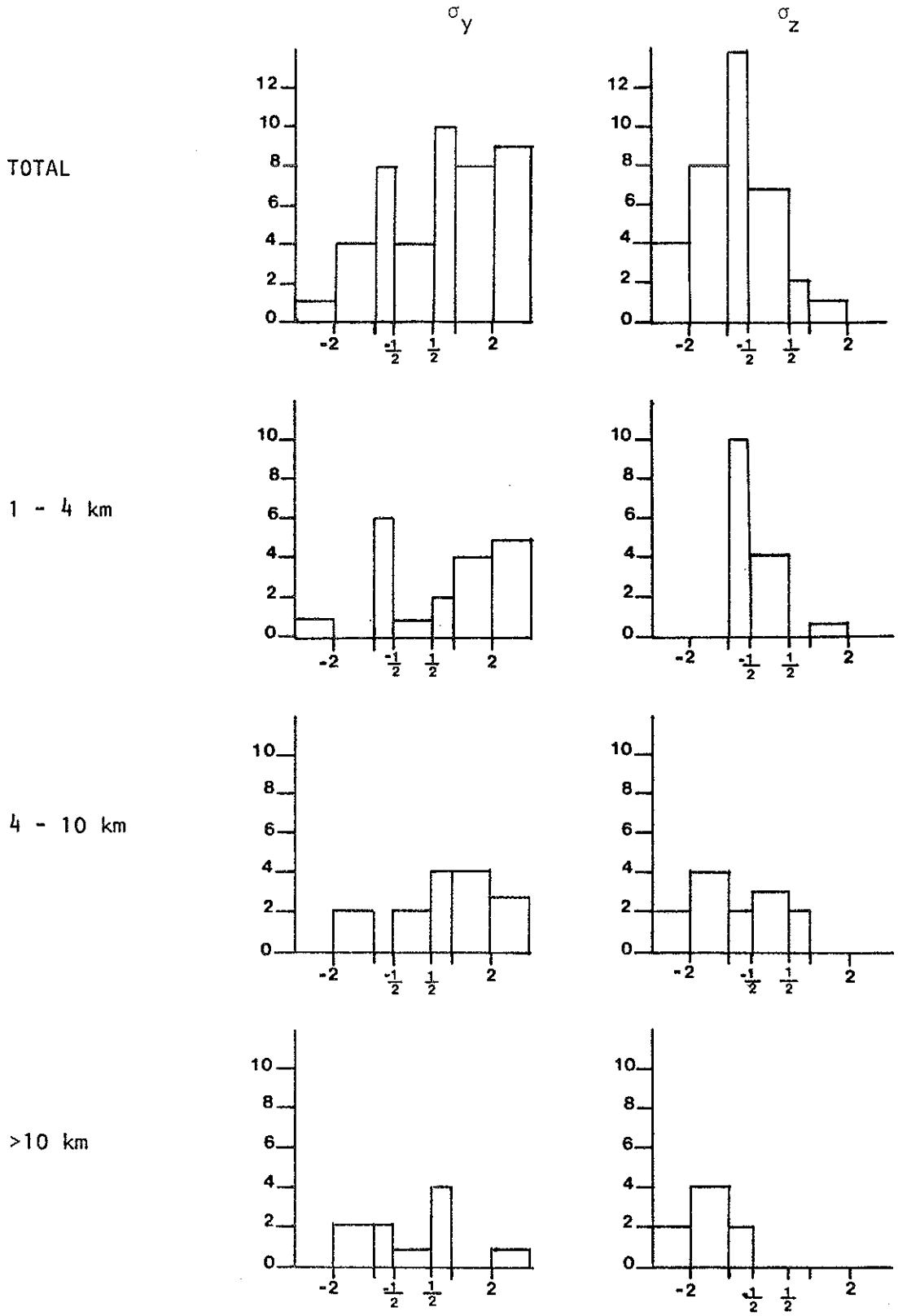

Figure 42 Goodness-of-fit histograms for the Briggs interpolation scheme. The abscissae represent the sizes of discrepancies in terms of number of classes. The ordinate represents the frequency of occurrence ($\frac{1}{2}$ class widths have been multiplied by two to conserve number density).

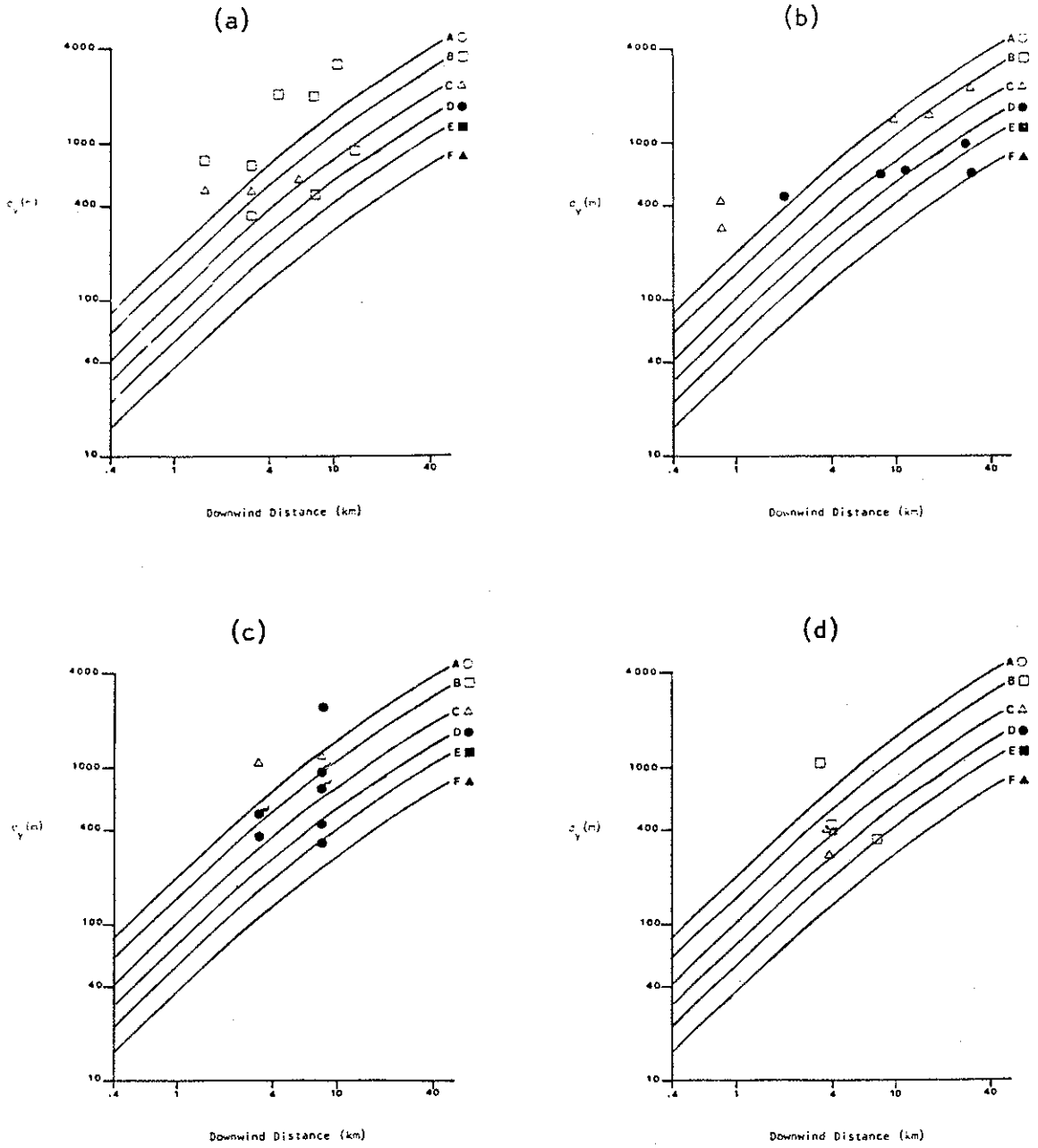

Figure 43 The Briggs y - curves for (a) March 1976 aircraft, (b) February 1977 helicopter, (c) June 1977 aircraft, (d) March, June COSPEC. A tail on the symbol means ½ class less stable.

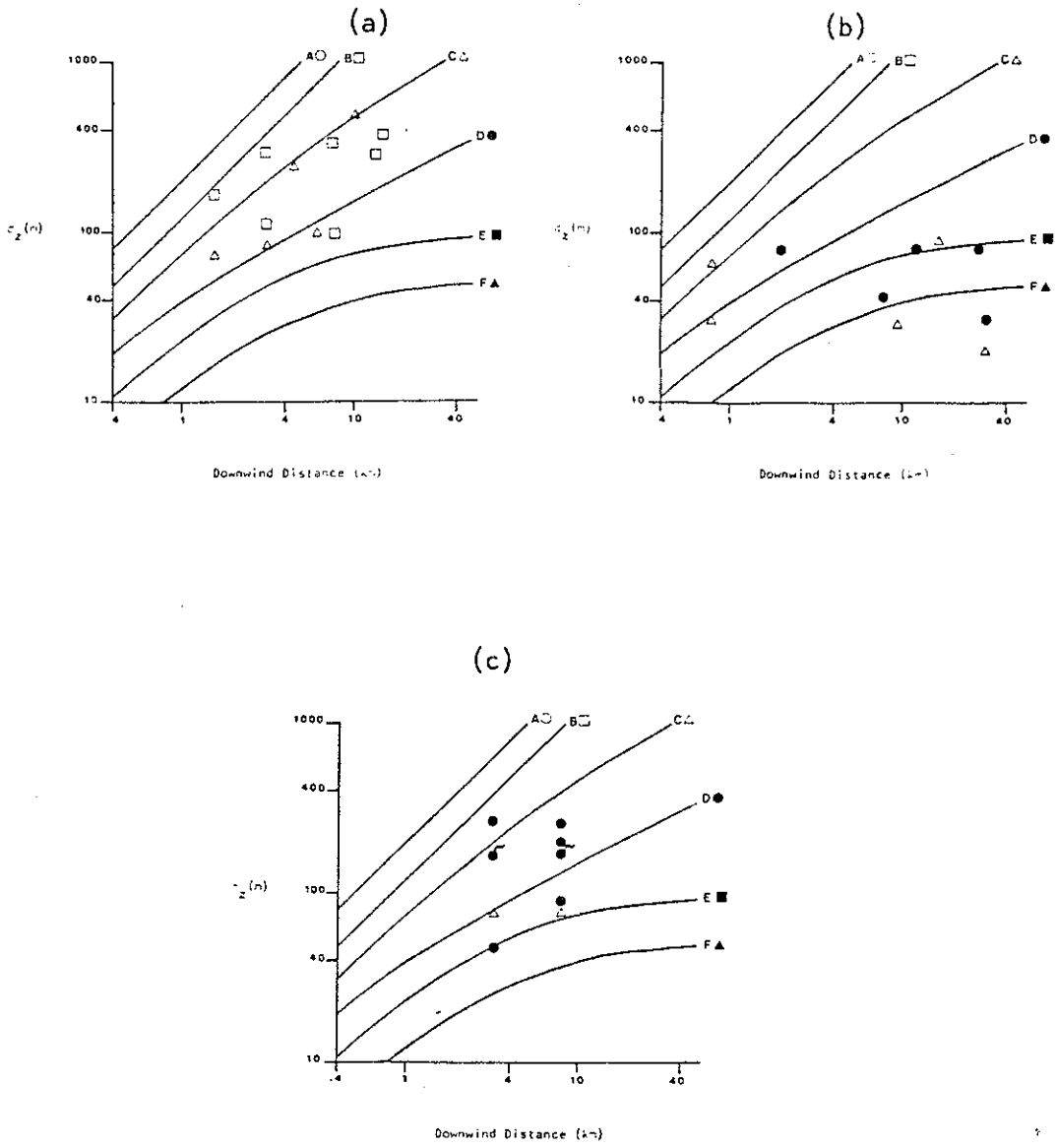

Figure 44 The Briggs z - curves for (a) March 1976 aircraft, (b) February 1977 helicopter, (c) June 1977 aircraft.

6.2.3 Goodness-of-fit for More Theoretically Based Sigma Typing Schemes

In the following sections, the theoretically based sigma typing schemes are compared to the data. F. B. Smith's specification scheme for σ_z is discussed first. Then the σ_y specification schemes based upon Taylor's statistical theory are discussed; these schemes include Pasquill's 1976 scheme, Cramer's scheme, and Draxler's scheme.

6.2.3.1 F. B. Smith's σ_z Typing Scheme. Smith's scheme (as described in Chapter 4) is based upon a two-dimensional eddy diffusivity model for a ground source and uses the Pasquill stability classes. For this study, two values of roughness were used, z_o = 10 cm and z_o = 100 cm; the curves had been computed for these roughness lengths by R. P. Hosker in Gifford (1976). The comparison of the σ_z predictions to the observed values are shown in Figures 45, 46 and 47.

The Smith scheme appears to overestimate the observed σ_z values. Since the Pasquill meteorological system is used to specify the stability class, the problem may lie more in the stability classification than in the curves themselves. As discussed previously for the PG curves and for the BNL curves, the Pasquill stability classes can be very misleading for winter situations. For an elevated source in the AOSERP region, the plume may remain in a stable layer for considerable periods especially in the winter in the presence of snow and low sun angle. The largest discrepancies occur for the helicopter data (February) and for stable cases (or limited mixing) in the other March and June studies.

This scheme is particularly important since it has been adopted by the Environmental Protection Services of Alberta Environment (Alberta Environment 1978). We strongly recommend that if Pasquill stability classes are to be used, then a seasonal allowance be made to account for changed albedo conditions due to snow cover.

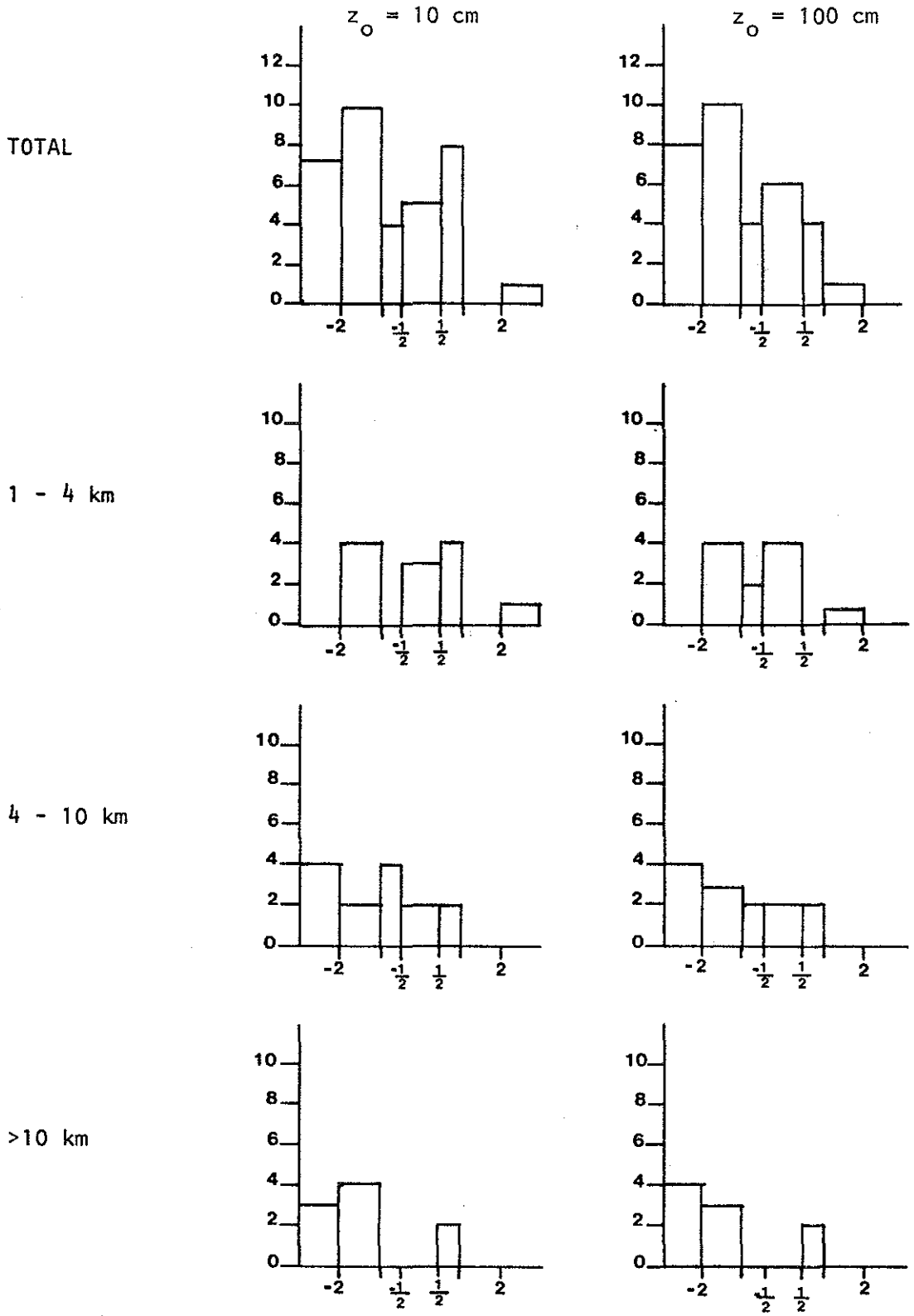

Figure 45 Goodness-of-fit histograms for the Smith σ_z specification scheme for roughness lengths of 10 and 100 cm. The abscissae represent the sizes of discrepancies in terms of number of classes. The ordinate represents the frequency of occurrence ($\frac{1}{2}$ class widths have been multiplied by two to conserve number density).

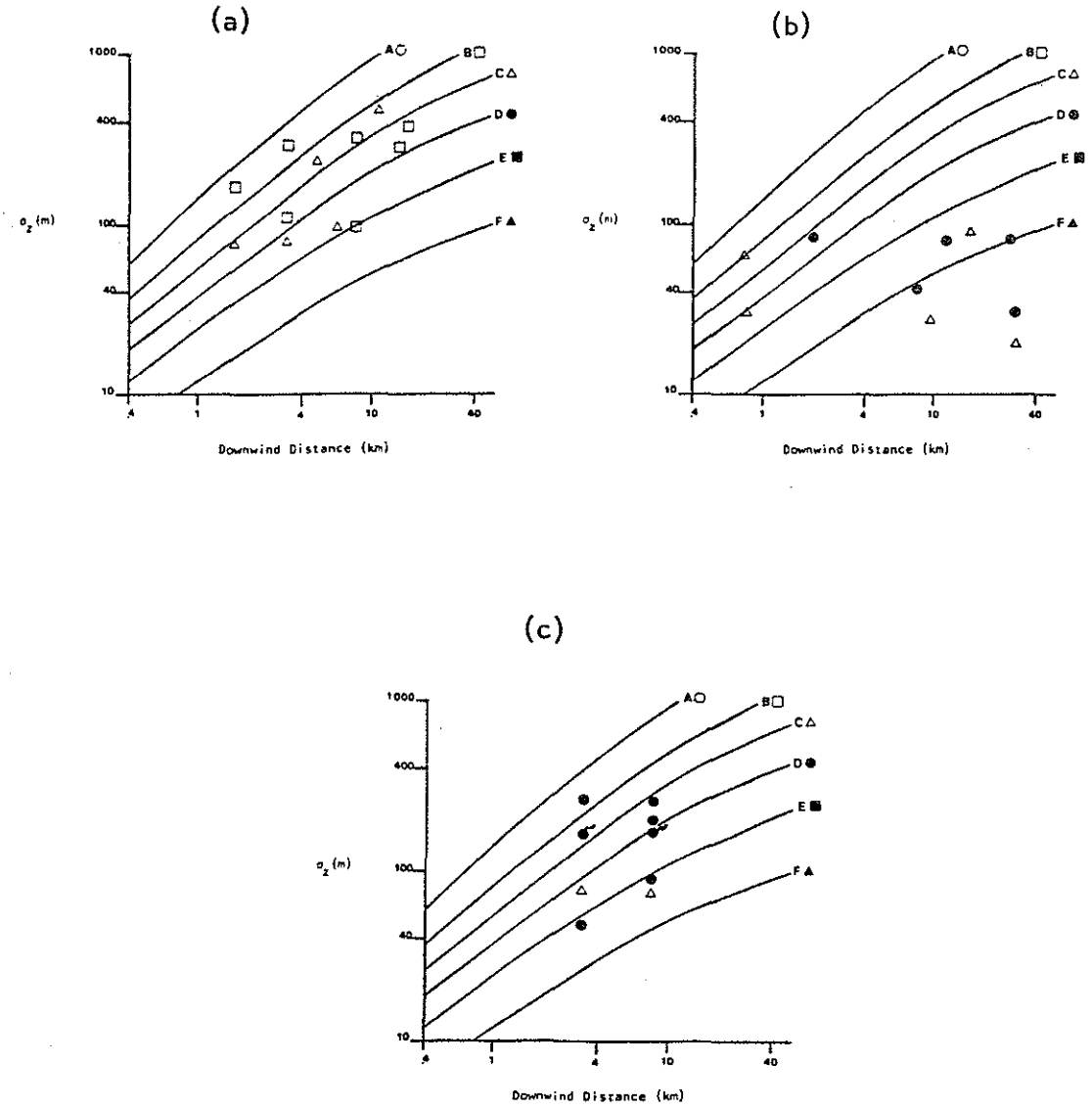

Figure 46 The Smith curves for z_o = 10 cm for (a) March 1976 aircraft, (b) February 1977 helicopter, (c) June 1977 aircraft. A tail on the symbol means $\frac{1}{2}$ class less stable.

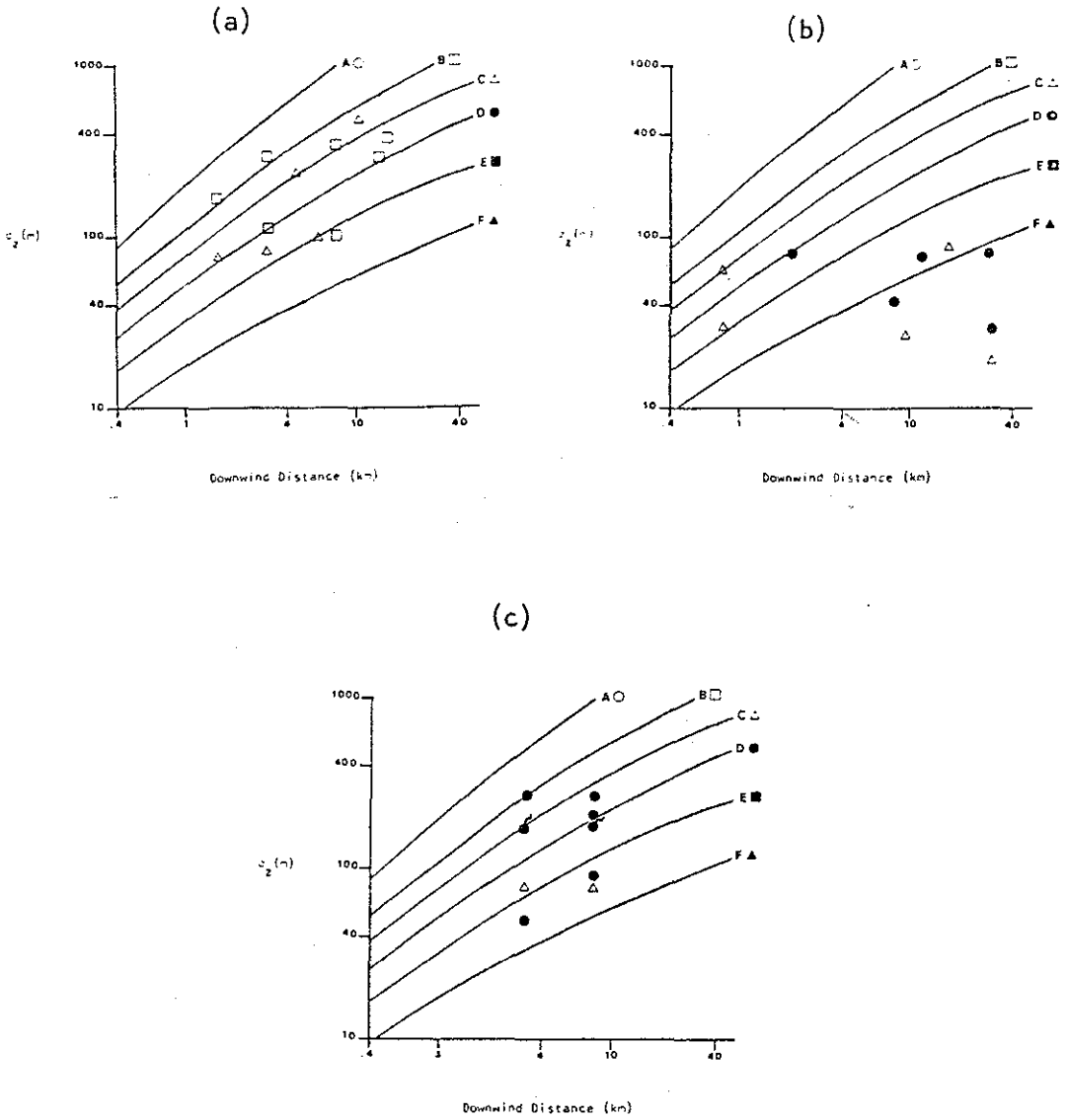

Figure 47 The Smith curves for z_o = 100 cm for (a) March 1976 aircraft, (b) February 1977 helicopter, (c) 1977 aircraft. A tail on the symbol means $\frac{1}{2}$ class less stable.

6.2.3.2 Pasquill 1976 Method. The Pasquill 1976 method of σ_y specification is a simplification of Taylor's statistical theory. As outlined in Chapter 4, Pasquill's method is very easy to use if σ_θ data are available but the simplification can be expected to lead to some scatter.

Figure 48 shows the observed normalized σ_y values compared to the Pasquill prediction. The ratio of predicted to observed is shown in Figure 49 in a logarithmic plot. The observed helicopter data is consistently larger than the predicted values by about a factor of 3. The aircraft values agree more closely; although they may average about 25% larger than predicted. Considering the uncertainties in the σ_θ values, the agreement for the aircraft data is generally satisfactory. The discrepancy for the helicopter values may be associated with the sigma calculation technique used for the helicopter data. As discussed in Chapter 5, the sigma calculation technique for the helicopter involved a Gaussian assumption and a mass flux computation which could lead to large measurement errors in the observed σ_y values. The large normalized σ_y values close to the source (small ratios in Figure 49) may be due to the low levels of environmental mixing for some of the stable February helicopter runs. For these runs close to the stack, the σ_y value may have been significantly increased by the source-dominated stage of mixing.

In Figure 50 is shown some of the data used by Pasquill (1976) to generate his estimates of the function f(x). Also shown in Figure 50 are the normalized AOSERP aircraft data. As can be seen the scatter of the AOSERP aircraft data sets are similar to other data sets used to generate the values for f(x). The helicopter data set appears to have a larger discrepancy.

The three large values for the June aircraft data all occurred on the June 19 runs, (at about 0900 and 1500 MDT). The observed σ_θ values for the tethersonde were over a factor of two larger than the aircraft values and the tethersonde $\sigma_u/\bar{u}$ values (see also Table 11). Thus part of the discrepancy may have been

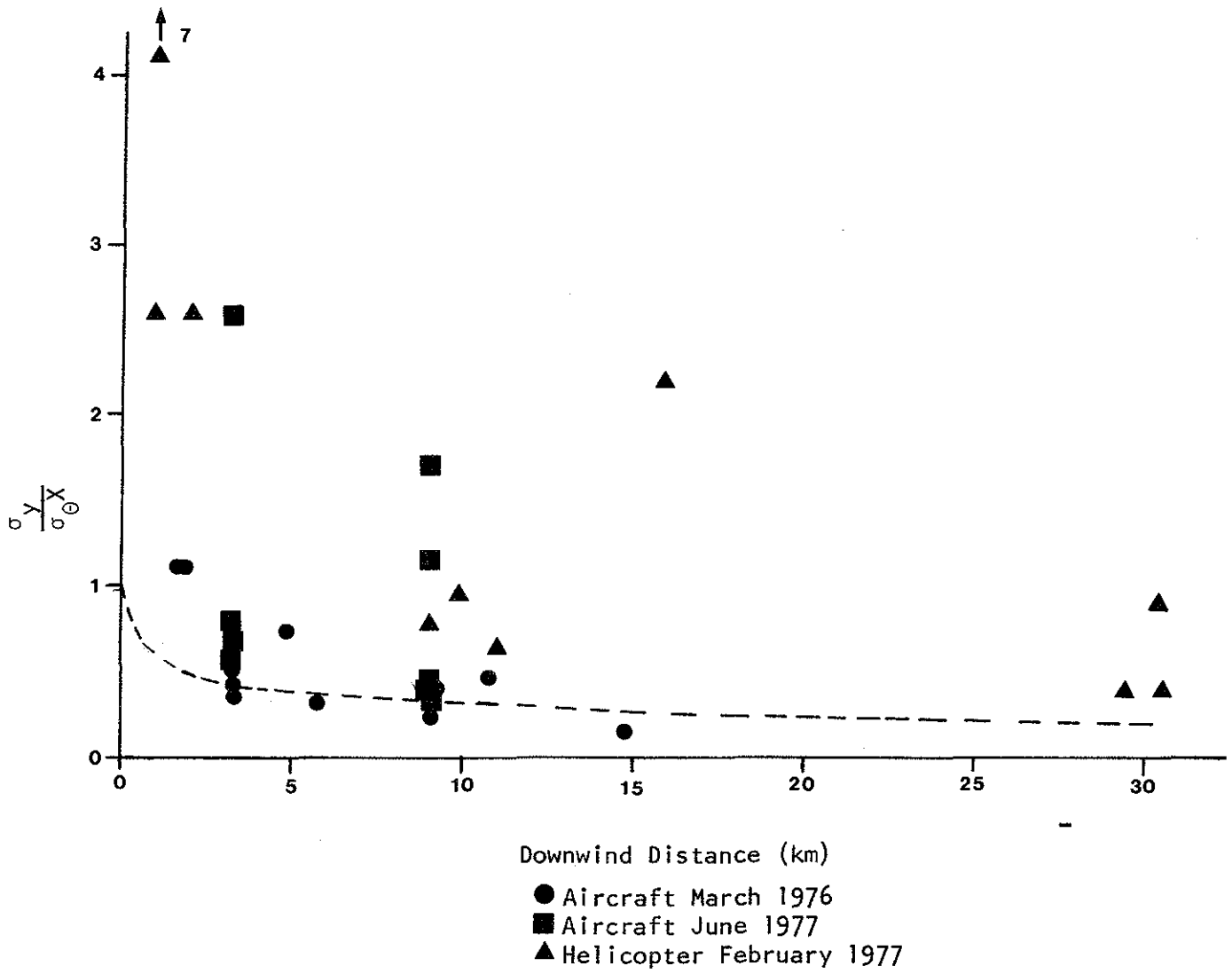

Figure 48. Normalized lateral plume spread (σ_y) values compared to the predictions of Pasquill (1976)

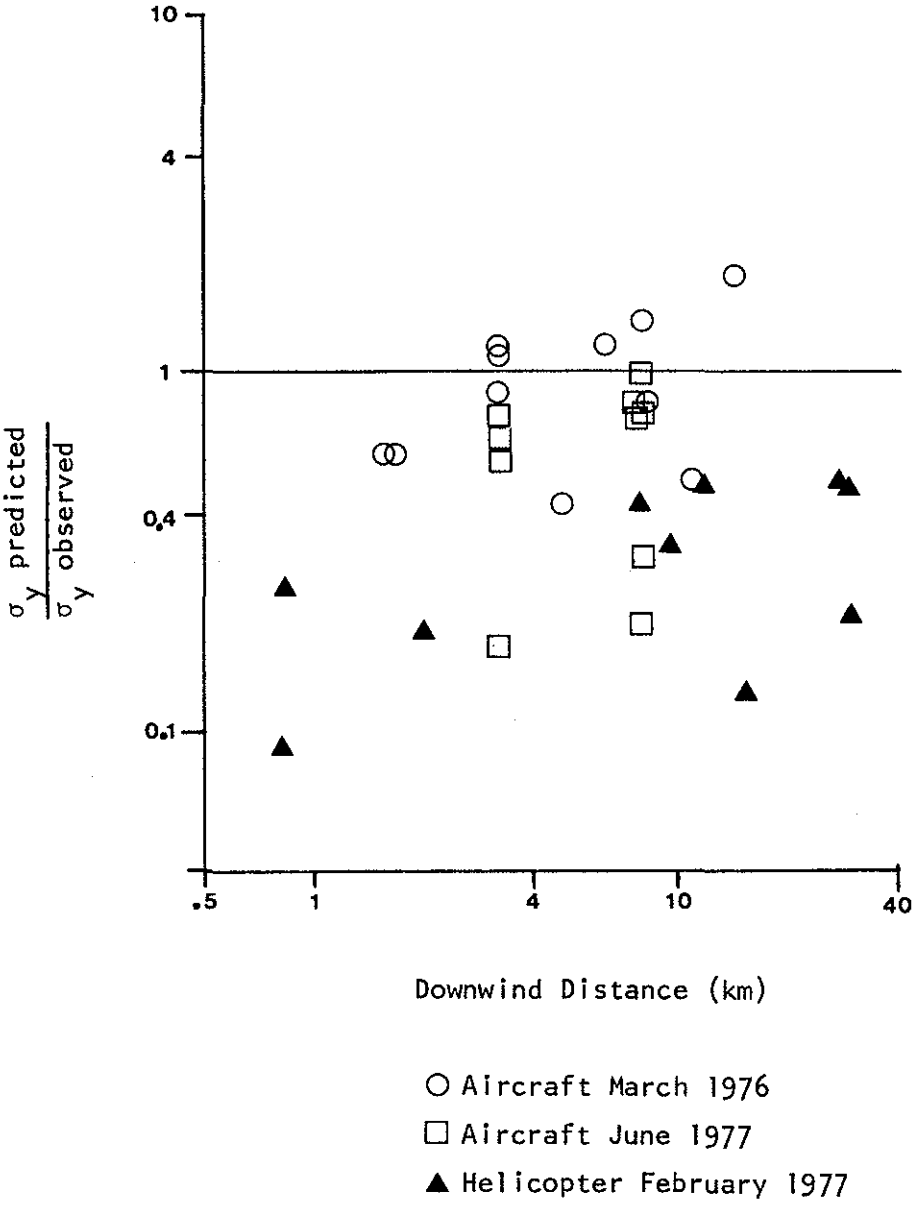

Figure 49. The ratio of predicted to observed σ_y values for the Pasquill 1976 scheme.

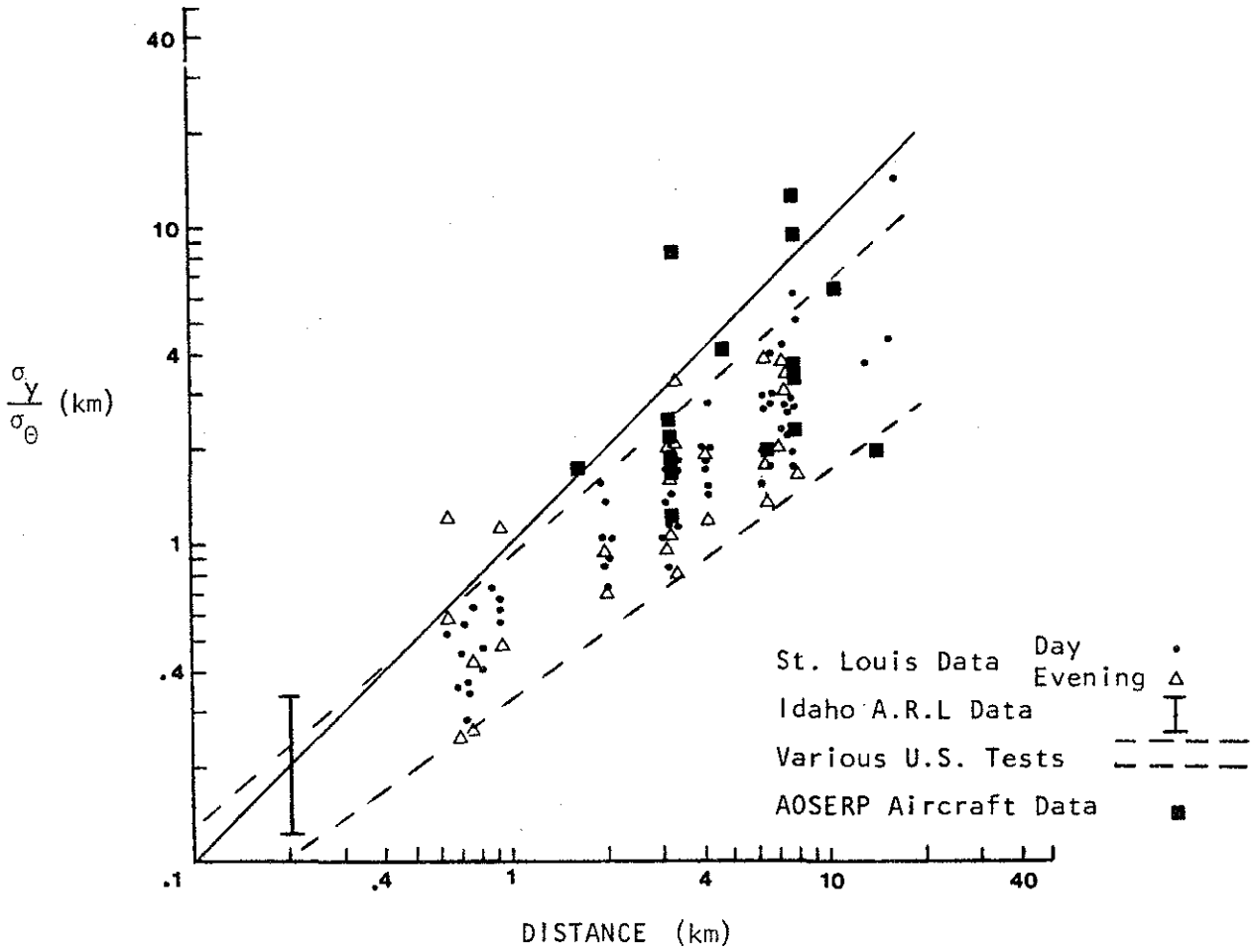

Figure 50 A comparison of the data spread for the AOSERP data set with other data sets used by Pasquill (1976) to generate the f(x) function values.

due to the adopted σ_θ values (aircraft values). However, the magnitude of the σ_y values was somewhat suspect since the 8.0 km values (1200 m) was only slightly larger than the 3.2 km values (1100 m). If only the central peaks of the concentration distributions were considered, then the σ_y values would have been about half as large giving good agreement. It was previously thought that the distributions reflected the natural variability of the plume. However, possibly secondary sources resulted in anomalous σ_y values for these three data points.

The systematic difference for the aircraft data (about 25%) may be a site-specific effect. In the simplifications of the Pasquill 1976 system (see Chapter 4), it was implicitly assumed that $U_e\ t_L$ was a constant, where U_e is the effective wind speed and t_L is the Lagrangian integral time scale. However, the integral scale may be expected to vary with stability and probably roughness. Thus Pasquill's values of f(x) could probably be improved for application to the AOSERP region.

Pasquill's formulation at long dispersion times is given by

$$\frac{\sigma_y}{\sigma_\theta X} = 0.33 \left(\frac{10}{X}\right)^{1/2} \qquad \text{for } X > 10 \text{ km} \qquad (6.5)$$

When Taylor's statistical theory is compared to (6.5), then the Pasquill (1976) formulation leads to

$$U_e\ t_L = 0.54 \text{ (km)} \qquad (6.6)$$

If we adopt a wind speed of 5.4 m/sec then

$$t_L \simeq 100 \text{ (sec)} \qquad (6.7)$$

and using $\beta \simeq 4$,

$$t_E \simeq 25 \text{ (sec)} \qquad (6.8)$$

$$\ell_E \simeq 135 \text{ (m)} \tag{6.9}$$

where ℓ is the integral length scale and where subscript E refers to Eulerian integral scales. The above value of the Eulerian integral length scale is similar in magnitude to the values estimated by Davison and Grandia (1978) for the June aircraft data. In that study, variations of ℓ_E were coincident with changes in the plume sigma values (case of June 22). Thus there are significant approximations in the Pasquill 1976 simplification of Taylor's theory which may be important for specific case studies. However the Pasquill system does have the significant advantage of being easy to use in a practical situation.

6.2.3.3 Cramer's Scheme. As discussed in Chapter 4, Cramer's empirical scheme can be formulated as a variation of the Pasquill 1976 scheme where

$$\frac{\sigma_y}{\sigma_\theta x} = f(x) = x^{p-1} \tag{6.10}$$

Cramer specified empirical values for the coefficient p based upon measurements to 800 m. Figure 51 shows the ratio of observed to predicted σ_y values. As can be seen the discrepancies are significantly larger than for the Pasquill 1976 formulation discussed in the preceding section.

The Cramer system does not agree with the long dispersion time limits of Taylor's theory. In addition it is unit dependent; the right hand side of (6.10) is dimensional, the left is not. Since the values for the exponent, p, are case specific, a single theoretical line cannot be plotted for comparison with the normalized σ_y data. The values of p are reasonably consistent with Taylor's theory considering the distances downwind over which the observations of the passive tracer was made. However, the curves are considered to be inappropriate for elevated releases from industrial stacks.

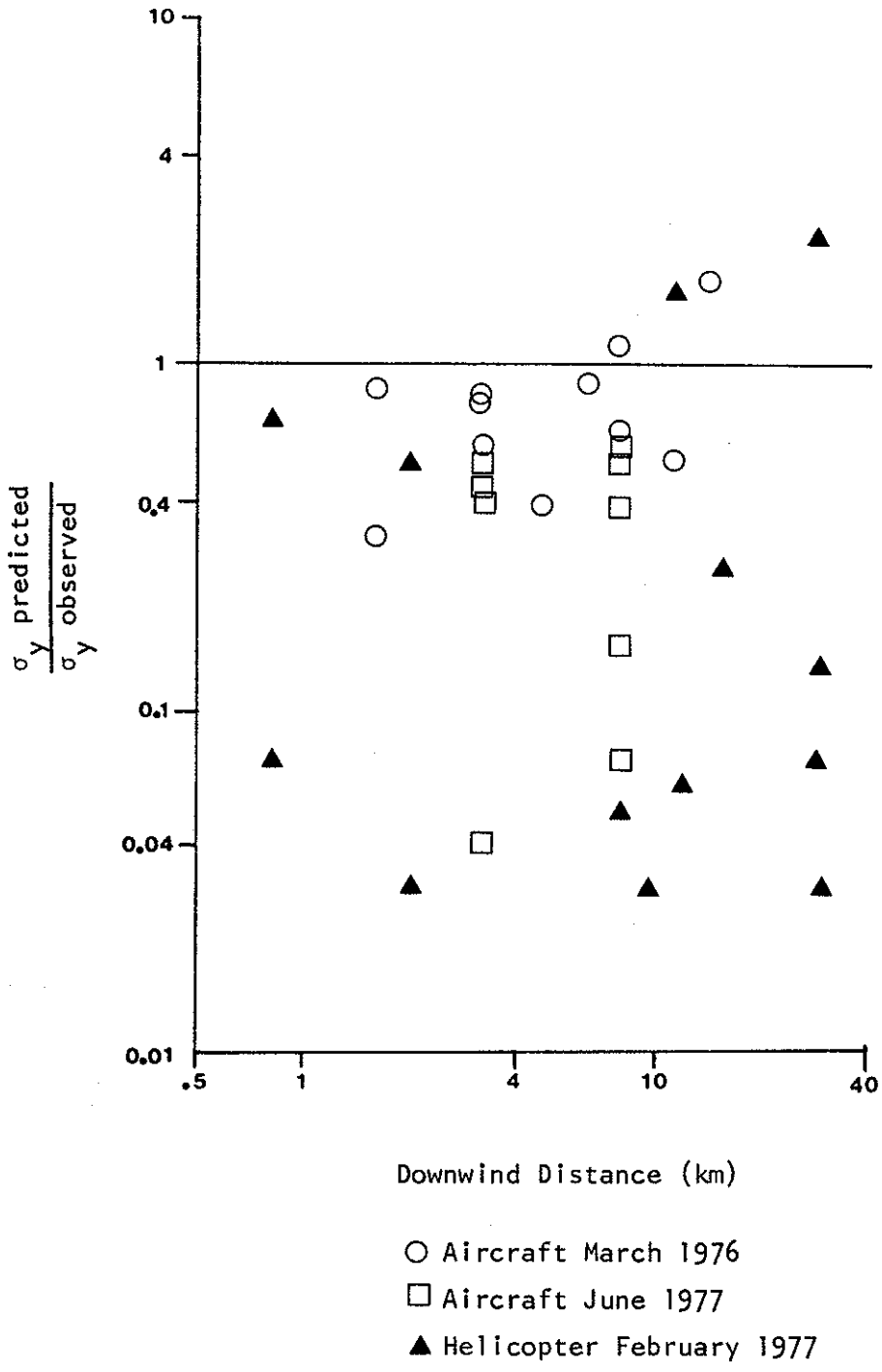

Figure 51. Comparison of observed plume spread, σ_y, to the values predicted by Cramer's technique using σ_y estimates of wind direction fluctuations, σ_θ, from the tethersonde or aircraft when available.

6.2.3.4 Draxler's Scheme. Draxler's scheme is a variation of Pasquill's universal functions relating to Taylor's statistical theory. As outlined in Chapter 4, Draxler adopted an alternative time scale to the Lagrangian integral time scale to non-dimensionalize the total dispersion time and generated estimates of a particular form of Pasquill's functions f_1 and f_2. Using Draxler's recommended values for the time scale normalization factor, T_i = 1000 seconds, then f_1 becomes

$$f_1 = \frac{1}{1 + 0.90 \left(\frac{T}{T_i}\right)^{1/2}} = \left[1 + 0.0285\ T^{1/2}\right]^{-1} \qquad (6.11)$$

where T is total dispersion time.

The ratio of the predicted to observed σ_y values for Draxler's scheme are shown in Figure 52. The agreement appears to be slightly better than for Pasquill's formulation especially for many of the helicopter values. However, a 20% to 25% reduction in the Pasquill f(x) values would make the agreements comparable.

About 75% of the values are within a factor of two of the predicted values. Considering the uncertainties associated with both the σ_y and σ_θ measurements, the agreement is acceptable.

Draxler showed that for long dispersion times, his normalization time, T_i, could be related to the Lagrangian integral time scale, t_L, by

$$T_i \simeq 1.64\ t_L \qquad (6.12)$$

For his adopted value of T_i = 1000 seconds, and for $\bar{U}$ = 5 m/sec, this leads to an Eulerian integral length scale, ℓ_E, of about 750 meters. This value of ℓ_E is much larger than predicted by Pasquill's (1976) formulation and is also larger than the values estimated by Davison and Grandia (1978) for the AOSERP area. Note too that Draxler's value of T_i is unchanged for all stability

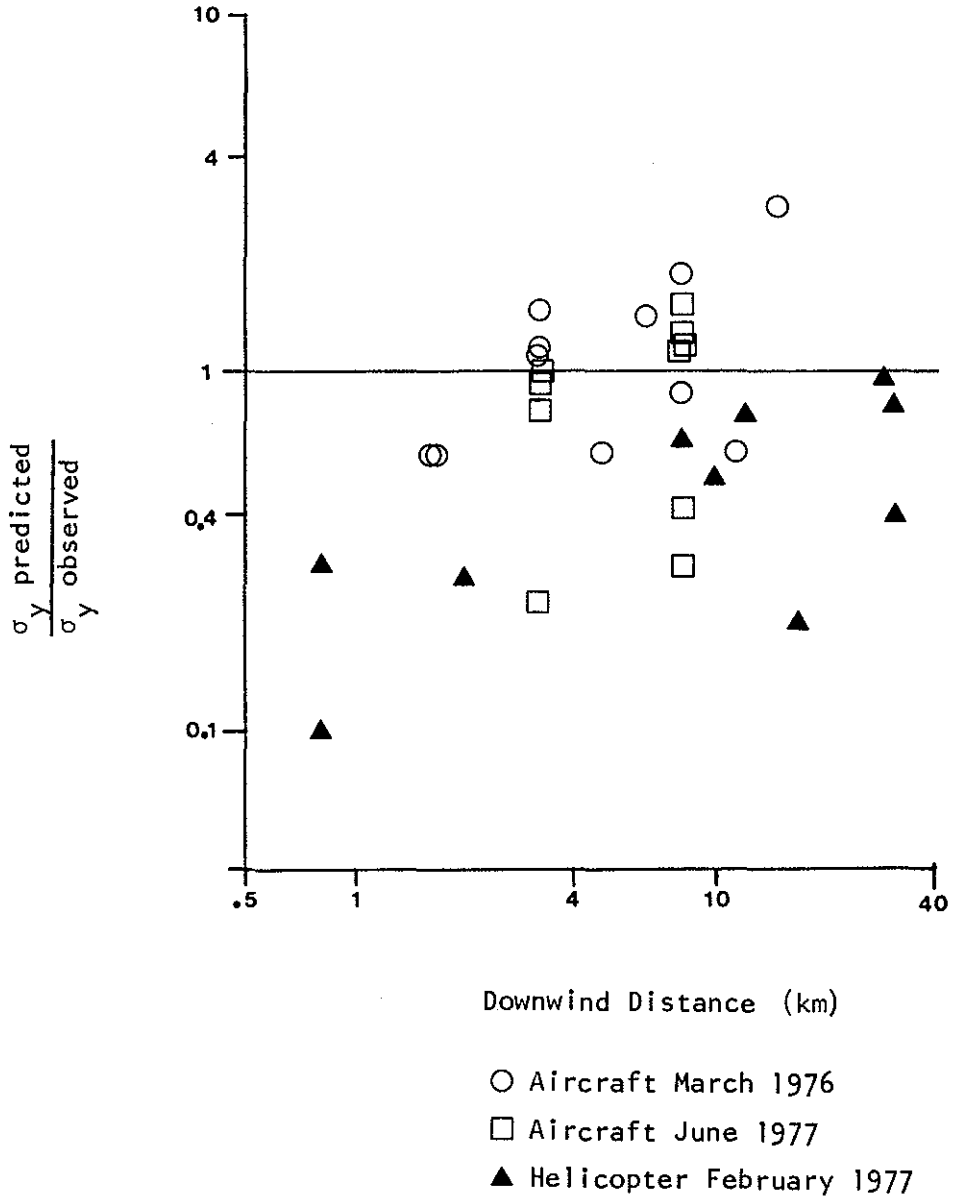

Figure 52. Comparison of observed plume spread, σ_y, to the values predicted by Draxler's formulation using estimates of wind direction fluctuations, σ_θ, from the tethersonde and aircraft.

conditions. This constancy of the implied Lagrangian integral time scale is perhaps unrealistic but may be necessary for a practical scheme in spite of the scatter it may introduce into the fit.

Draxler's scheme tends to predict slightly larger values than the Pasquill 1976 scheme. The difference depends upon wind speed since the Pasquill formulation is tied to downwind distance and the Draxler scheme to dispersion time. Discrepancies of almost a factor of two can occur for longer dispersion times. The present data set does not permit an adequate evaluation of which procedure is better; although the Pasquill f(x) values should be increased by about 20% to 25%.

7. DISCUSSION OF SHEAR EFFECTS

There are three types of shear effects as discussed in Chapter 3. The first two effects are the centerline displacement and the distortion of the plume cross-sectional shape. These two effects are routinely observed. However, they do not significantly affect the magnitude of the appropriate sigma values. The sigma values are influenced by shear only in the presence of vertical mixing. This interaction of vertical mixing with the wind shear produces shear-enhanced dispersion. In Chapter 3, Smith's (1965) theory for shear-enhanced dispersion was discussed and typical downwind distances required for significant shear effects were estimated. In the following sections, some very approximate means are used to estimate the shear contributions to lateral spreading for the observation case studies. The implications for a practical scheme of sigma specification are then discussed.

7.1 OBSERVED SHEAR-ENHANCED LATERAL DISPERSION

The observed plume sigma values permit an approximate evaluation of the effect of shear on the σ_y values. From Chapter 3, we may write,

$$\sigma_s^2 \approx \frac{1}{6} \left(\frac{\tan \alpha}{\Delta Z} \right)^2 \sigma_w^2 \; t_{wL} \; T \; X^2 \qquad (7.1)$$

where σ_s^2 is the shear contribution to the lateral plume spread variance σ_y^2

α is the turning angle over a vertical depth ΔZ

σ_w^2 is the variance of the vertical velocity

t_{wL} is the Lagrangian integral time scale for vertical motions

T is dispersion time

X is downwind distance.

To be able to proceed further approximations must be made for the vertical turbulence terms, σ_w and t_{wL}. It was decided to utilize the long dispersion time limit of Taylor's theory for homogeneous turbulence which predicts

$$\sigma_z^2 \simeq \sigma_w^2 \, 2t_{wL} \, T \qquad (7.2)$$

Although (7.2) is a very rough approximation, it is probably reasonable if vertical spread is not limited and if conditions are reasonably homogeneous in the vertical. Uniformly stable conditions over the plume depth probably are suitable for the application of (7.2). In such cases, (7.1) becomes

$$\sigma_s \simeq 0.29 \, \frac{\tan \alpha}{\Delta Z} \, \sigma_z X \qquad (7.3)$$

Equation (7.3) was used for all of the helicopter and aircraft data. Although some of the assumptions in its derivation may be questionable it should indicate the importance of shear effects. Calculations of the shear effects are presented in Tables 23, 24 and 25.

The numerical values for shear effects need to be viewed with some caution. For the morning run of March 11 at X = 6.4 km, the computed shear effects were large. The σ_y values could also be explained by the turbulent mixing effects in terms of Pasquill's 1976 formulation. If both shear and turbulent effects acted as predicted, then the observed σ_y value would have been about twice as large as observed. For such discrepanies, the reliability of each estimate needs to be evaluated. It is suggested that the estimates have the following order of reliability (most reliable first) (i) observed σ_y value (ii) turbulent mixing effect in terms of Pasquill's 1976 formulation (iii) approximate shear estimate in (7.3).

For the afternoon run of March 11, large σ_z values were observed in the presence of strong shear. It is improbable that there could be such a strong direction shear in the presence of strong vertical mixing.

A review of the other values in Tables 23, 24 and 25 indicate that shear effects are occasionally important. Note that

Table 23 An estimate of the importance of shear effects for the aircraft data from the March 1976 field study

Date	Time (MST)	X (km)	σ_y (m)	σ_z (m)	Wind Direction Change (deg./100m)	σ_s (m)	$\frac{\sigma_s}{\sigma_y}$	$\left(\frac{\sigma_s}{\sigma_y}\right)^2$
March 10	1431-1633	1.6	800	170	*			
		14.5	900	190				
March 11	0817-0928	1.6	520	77	15	96	0.2	0.03
		3.2	500	84		210	0.4	0.18
		6.4	600	103		514	0.9	0.73
March 11	1306-1533	3.2	750	306	15 [2]	763	~1.	~1.
		8.0	2000	339		2100	~1.	~1.
March 12	1430-1603	4.8	2100	246	7.6 [1]	443	0.2	0.04
		11.3	3200	488		2070	0.65	0.42
March 15	0800-0850	3.2	300	116	~0.	~0.	~0.	~0.
		8.0	470	100	~0.	~0.	~0.	~0.

1. Most of the turning occurred in the lower 300 m above stack height so shear effect is only calculated for 4.8 km.

2. Estimates of shear term suggested that σ_z decreased with downwind which is impossible; the presence of large shear with strong vertical mixing is unlikely.

* The wind direction variation very large, impossible to get an accurate estimate; also this is a limited mixing case.

Table 24 An estimate of the importance of shear effects for the helicopter data from the February 1977 field study.

Date	Time (MST)	X (km)	σ_y (m)	σ_z (m)	Wind Direction Change (deg./100m)	σ_s (m)	$\frac{\sigma_s}{\sigma_y}$	$\left(\frac{\sigma_s}{\sigma_y}\right)^2$
Feb 5	0840-0910	8.0	630	43	11.	190	0.3	0.09
	0935-1000	30.6	650	31	15.	740	>1	>1
Feb 6	1435-1455	0.8	290	66	~0.	~0.	~0.	~0.
	1525-1605	16.9	1500	91	5.	386	0.3	0.07
Feb 10	1020-1030	0.8	440	31	14.	18	0.0	0.0
	0950-1005	9.7	1400	28	25.	370	0.3	0.07
	0830-0920	30.4	2200	20	24.	790	0.4	0.13
Feb 11	1430-1450	2.0	470	83	30.	280[1]	0.6	0.35
	1500-1530	12.0	680	81	~0.	~0.[2]	~0.	~0.
	1550-1600	28.8	1000	84	~0.	~0.	~0.	~0.

1. The approximations used for shear estimation are probably not valid at only 2 km downwind from the source.

2. Plume rose fairly quickly to attain a constant level in a layer of nearly constant wind direction.

Table 25 An estimate of the importance of shear effects for the aircraft data from the June 1977 field study

Date	Time (MST)	X (km)	σ_y (m)	σ_z (m)	Wind Direction Change (deg./100m)	σ_s (m)	$\frac{\sigma_s}{\sigma_y}$	$\left(\frac{\sigma_s}{\sigma_y}\right)^2$
June 19	0828-0935	3.2	1100	78	7	86	0.11	0.01
		8	1200	77	7	213	0.1	0.01
June 19	1415-1600	8	2500	260	3.5	360	0.1	0.02
June 20	1130-1230	3.2	500	170	12	330	0.7	0.4
		8	725	175	12	848	~1	~1
June 20	1230-1340	3.2	530	170	8	220	0.4	0.2
		8	970	175	8	566	0.6	0.3
June 22	1915-2130	8	340	200	~0.	~0.	~0.	~0.
June 22	2145-2245	3.2	375	50	~0.	~0.	~0.	~0.
		8	480	90	~0.	~0.	~0.	~0.

the shear and turbulence contributions combine for the variance of the lateral spread (σ_y^2) and so the squared ratio $(\sigma_s/\sigma_y)^2$ is the estimate of the significance of shear effects. The validity of adopting a σ_y specification based upon just the turbulent contribution can be estimated from

$$\left[1 - \left(\frac{\sigma_s}{\sigma_y}\right)^2\right]^{1/2}$$

The helicopter data showed only one value which was dominated by shear effects in spite of the presence of large wind direction shears. This emphasizes the importance of the interaction between vertical mixing and shear in the development of shear-enhanced dispersion. As noted by Pasquill (1974 p.165), the important cases of shear-enhanced dispersion may exist for only moderate shear conditions. Thus distortion of the plume shape is not a good measure of the importance of shear effects on plume sigma values.

There were several normalized plume spread values in the discussion of the specification schemes of Pasquill and Draxler which showed major discrepancies from the predicted values. In particular, the June 19 aircraft values were much larger than predicted. The values in Table 25 show that these discrepancies cannot be explained in terms of shear. The helicopter case studies had only a single case of important shear effects and so their discrepancies with the Pasquill and Draxler schemes are also not due to shear effects.

7.2 IMPORTANCE OF SHEAR EFFECTS FOR AOSERP

The importance of shear effects depends upon the downwind distance of concern. The theoretical estimates of Chapter 3 and the observed values discussed above suggest that shear-enhanced dispersion can be neglected for at least 5 km and probably 10 km downwind of the source. Beyond 10 km, the effects of shear-enhanced dispersion may be important for some situations. For

practical purposes, shear can be neglected for well mixed boundary layers and probably for very stable situations. The effects of shear-enhanced dispersion should be considered for downwind distances of 10 km or larger in moderately stable conditions.

An approximate evaluation of shear effects is provided by equation (7.3). The inputs required are estimates of the wind turning over the plume depth and of the plume σ_z values.

The turning of wind angle with height may be important in the determination of the region eventually affected by significant ground level concentrations. The most marked wind turning will generally exist for very stable situations; however in these cases, ground impingement would probably occur only after the mixing height has risen to plume height. Thus the location of the surface regions subjected to fumigation episodes would be influenced by the wind shear prior to the fumigation. The areal extent and concentrations of the fumigation episode may be influenced by the amount of shear-enhanced dispersion in the stable layer prior to fumigation. The above generalizations suggest that Gaussian or other types of dispersion models which do not permit wind turning with height may over-estimate the time-averaged concentrations for fumigation episodes.

8. DIRECTIONAL DEPENDENCE OF THE SIGMA VALUES

Sigma values may have a directional dependence due to differences in the topography or surface characteristics as a function of direction. In Section 3.3. a brief review of very preliminary work reported by Davison et al. (1977) and Davison and Grandia (1978) was presented. A systematic examination of spatial variability of the turbulent mixing characteristics has not yet been undertaken in the AOSERP region. However, an evaluation of the directional dependence of the observed sigma values should indicate whether major directional differences exist.

Figure 53 presents a polar plot of the logarithm of the ratios of predicted to observed σ_y values using the Pasquill 1976 specification scheme. Figure 53 presents the same data as Figure 49 except that the data is plotted as a function of plume heading not downwind distance. A point outside the 1. circle (i.e. a value greater than 1) corresponds to a σ_y value larger than predicted. The very limited data base for Figure 53 does not permit definitive conclusions regarding directional dependence of the sigma values. The three large aircraft σ_y values for June 19 (heading of 320°) tend to suggest that there might be greater dispersion towards that direction (down the Athabasca River). However, for both the June 19 afternoon flight and the June 20 flight (also with a plume heading of 320°), turbulence levels along the plume trajectory (roughly along the river valley), were compared with turbulence runs about 5 miles east of the river valley (Davison and Grandia 1978 p.109). In all four cases (two heights, on each of two days), the turbulence levels were slightly larger along the runs east of the river valley than along the river valley itself. Thus, the three large June aircraft values along a heading of 320° probably do not mean that there is enhanced dispersion along that direction. In summary, there is no strong evidence of any significant directional dependence for the sigma values for the main plume.

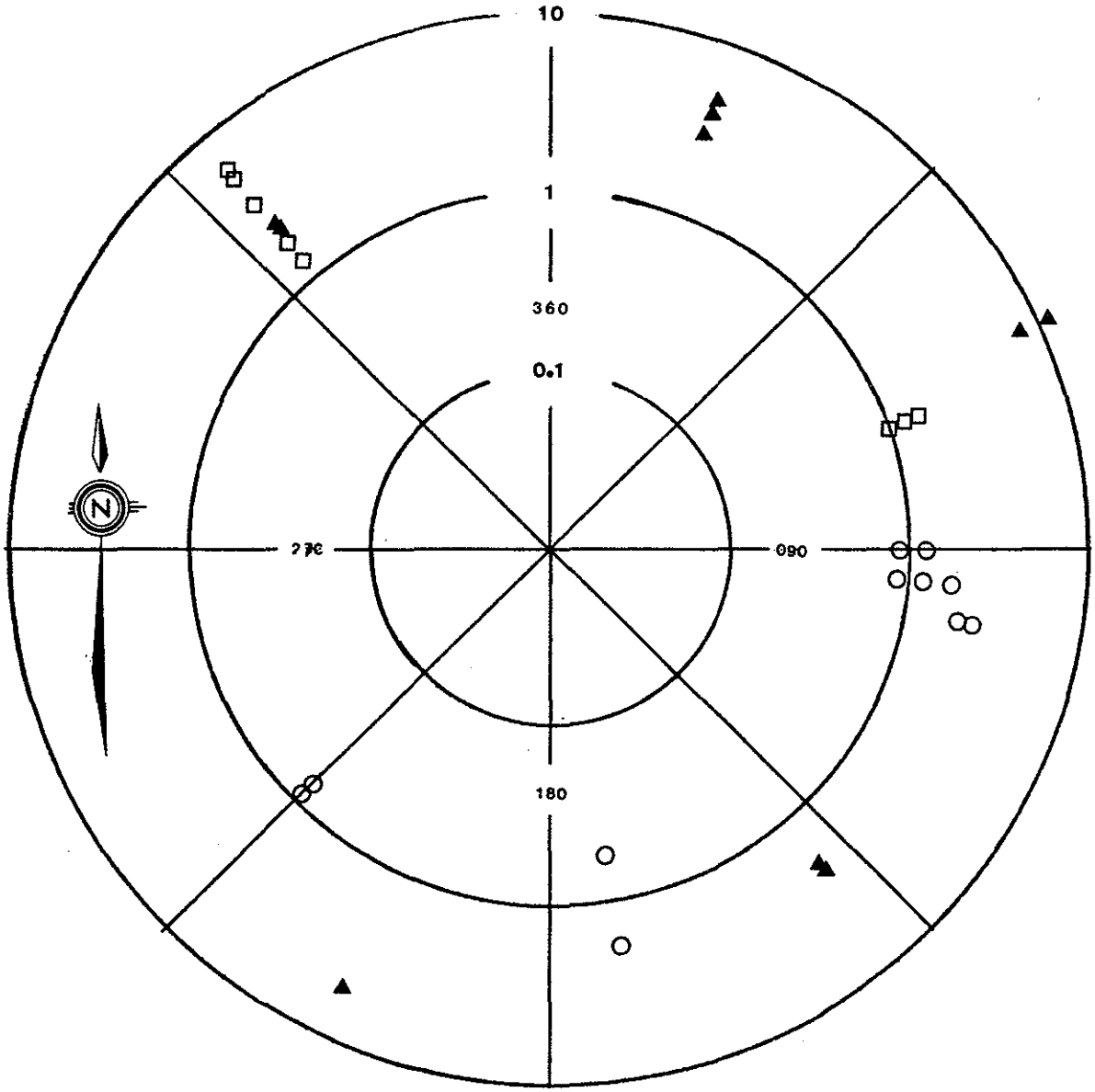

○ Aircraft, March 1976
□ Aircraft, June 1977
▲ Helicopter, February 1977

Figure 53. Directional dependence of the sigma values. The logarithm of the ratio of predicted to observed σ_y values are shown as a function of observed plume bearing. The Pasquill (1976) classification scheme was used for the predicted σ_y values

9. RECOMMENDED PROCEDURES FOR THE SPECIFICATION OF THE PLUME SIGMA VALUES

One of the major objectives of this study was to develop a useful procedure for the specification of sigma values. The following sections outline a recommended procedure. It must be re-emphasized that the data base was often not sufficient to come to definite conclusions. A continuing reassessment of the best procedure is recommended based upon continuing measurements, model results and theoretical developments both in the AOSERP region and elsewhere.

9.1 LIMITATIONS OF TYPING SCHEMES

The optimum sigma specification scheme depends to a considerable extent upon the use of the predicted results. For long-term environmental loading, considerable errors can be accepted for individual cases so long as the averages over a season, perhaps, are reasonable. However, for regulatory uses, it is important that the extreme values be accurately predicted even if this requires a greater real time data input.

If most concern is concentrated on the regions of maximum ground level concentrations close to the source, then the sigma specification scheme needs to be accurate over a range of downwind distances of perhaps 1 to 3 or 4 km. If accumulated dosage over a wider region is of concern then a larger range of downwind distances is of concern and shear effects may have to be adequately handled.

The data base in this study permitted an evaluation of sigma typing schemes for a few tens of case studies. Measurements were available of the physical plume geometry and the associated meteorological conditions. Thus, this data base was best suited for an evaluation of specific case studies and not of long term averages.

The data were concentrated in two ranges of downwind distances, from near the stack to about 1 km downwind, and from about 3 km to about 10 km downwind, with a few measurements at

30 km. Thus, dispersion beyond 10 kms could not be evaluated adequately; this is the range where shear effects might be expected to dominate on occasion. The range between 1 and 3 km presented problems for the sensor systems used in the field studies and so reliable data is sparse. However, this range of distances is typical of the transition to environmentally controlled dispersion (the sigma transition) and is also not atypical of the distance of maximum ground level concentrations for a mixed atmosphere. Thus sigma specification over this range must rely significantly upon interpolation of data with some guidance from theoretical formulations and experimental results from elsewhere.

Limitations of data sets and of the resultant recommended sigma typing schemes, as mentioned above for the AOSERP data base, have often been outlined by the developers of the various schemes. Unfortunately, such stated limitations are often ignored and many schemes have been applied to situations for which they are inappropriate.

9.2 SUMMARY OF RECOMMENDED FORMULATIONS

The diffusion process has two distinct phases: a source-dominated phase and an environmentally dominated phase.

9.2.1 Source-Dominated Phase

In the source-dominated phase, the dynamics of plume rise and growth of plume radius are connected. The plume rise formulation is considered first. The plume rise, ΔH, in neutral conditions is

$$\Delta H = C_1 F^{1/3} U^{-1} X^{2/3} \qquad (9.1)$$

where F is the source buoyancy flux (3.11) and where the coefficient $C_1 \simeq 1.6$ (Briggs 1975). The AOSERP photography data suggests $C_1 \simeq 1.4$. The value of C_1 found by various groups has a range of 1.2 to 2.6 (Briggs 1975). In stable conditions,

plume rise is given by (Briggs (1975)

$$\Delta H = F^{1/3} U^{-1} \left[\frac{3U^2}{\beta^2 (\omega')^2} (1 - \cos \omega' t) \right]^{1/3} \quad (9.2)$$

where t is dispersion time, ω' is the modified Brunt-Vaissala frequency (3.2.5) and where Briggs recommends $\beta = 0.6$. This value of β tends to over-estimate the observed plume rise. Using a value of $\beta = 0.74$ (consistent with $C_1 = 1.4$ in (9.1)) gives better agreement.

The plume radius, r, during the source-dominated region is related to plume rise, ΔH, in many theoretical developments by

$$r = \beta \Delta H \quad (9.3)$$

where β is the same constant as appears in (9.2) and implicitly in C_1 in (9.1). Using the AOSERP plume photography data taken by Fanaki, and assuming a Gaussian distribution and the 10% criterion (following Fanaki), then

$$r \simeq 2.15 \sigma_z \quad (9.4)$$

and a good fit for neutral conditions is given by

$$\sigma_z \simeq 0.23 \Delta H \quad (9.5)$$

where ΔH is given by (9.1). The numerical coefficient in (9.5) would imply $\beta = 0.55$ if (9.4) is accepted.

For stable conditions (9.5) appears to provide a reasonable fit using (9.2) for the plume rise in stable conditions. However, the stable data from February suggests a smaller coefficient in (9.5). There is some evidence (Figure 24), that a better fit is given by

$$\sigma_z = 0.32\ (\Delta H)^{2/3} \qquad (9.6)$$

The linear relationship in (9.5) is reasonable for average values but appears to underestimate σ_z for small ΔH values and to overestimate σ_z or large ΔH values at a given downwind distance. There may be some question as to the validity of the 10% criterion used for the photography data analysis; however, it is not clear how any systematic error from the 10% criterion could produce a fit given by (9.6) at a given distance. The adoption of the linear relationship of (9.3) is a closure assumption in models, not a theoretical prediction. The adoption of (9.5) is tentatively recommended because of wide-spread usage and the success of plume rise models which incorporate the linear closure assumption.

There is very little available data for estimating σ_y in the source-dominated stage of dispersion. Most theoretical models treat the plume as circular. The LIDAR data suggest

$$\sigma_y \simeq 1.4\ \sigma_z \qquad (9.7)$$

which can be adopted as a tentative value. There undoubtedly will be a dependence in (9.7) on the magnitude of large scale eddies particularly in stable conditions. The expressions for σ_z and σ_y given by (9.5) and (9.7) and using (9.1) and (9.2) for plume rise estimates should be used to downwind distance of the sigma transition point.

The downwind distance to the sigma transition point (when environmental mixing dominates) is difficult to predict in a practical scheme. The physics of the transition, (the equality of the plume and environmental dissipation levels), appears very reasonable. However, the accurate specification of dissipation inside the plume and in the environment in a practical scheme is difficult. The typical values estimated in Chapter 3 (Table 3) suggested a sigma transition at 1 or 2 km downwind from the source. The adoption of a constant value of 1 km is a tentative approximation.

9.2.2 Environmentally Dominated Phase

The lateral plume spread, σ_y, is best predicted by variations of Taylor's statistical theory. The Draxler scheme appears adequate; the values for f(x) in Pasquill's 1976 scheme should be increased by about 20 or 25%. The recommendation for the adoption of the schemes of Draxler and of Pasquill 1976 is the same as that of the AMS Workshop on Stability Classifications and Sigma Curves, reported by Hanna et al. (1977).

The TVA curves are recommended for σ_z specification in stable conditions. In convective conditions, Draxler's scheme is tentatively recommended. The Draxler scheme for σ_z specification in convective conditions could not be adequately tested with the available data. However, it is consistent with Taylor's theory and with a fairly extensive data base. The success of the Draxler scheme for σ_y encourages its adoption for σ_z in neutral-convective conditions when the TVA stability classification scheme is inadequate. Draxler's scheme for σ_z in convective conditions is

$$\sigma_z = \sigma_w \, t \, f_z \tag{9.8}$$

where

$$f_z = \left[1 + 0.90 \, (t/T_i)^{1/2} \right]^{-1} \tag{9.9}$$

where t is the total dispersion time and where T_i is the normalization constant for which Draxler recommends a value of 500 seconds for vertical diffusion from an elevated source.

For distances beyond about 10 km, shear-enhanced dispersion should be allowed for by

$$\sigma_y^2 = \sigma_{yt}^2 + \sigma_{ys}^2 \tag{9.10}$$

where σ_{yt} is the contribution from turbulent mixing as specified

by the Pasquill-1976 or Draxler schemes and where σ_{ys} is the shear contribution given by

$$\sigma_{ys} \simeq 0.29 \frac{\tan \alpha}{\Delta Z} \sigma_z X \qquad (9.11)$$

where α is the wind turning over the vertical distance ΔZ (of plume depth) and X is downwind distance. Equation (9.11) was presented in Chapter 7 as (7.3) and follows the development of Smith (1965).

9.3 DATA REQUIREMENTS AND APPROXIMATIONS

In order to predict plume rise to use the recommended sigma specification schemes, certain data must be measured directly or estimated.

The lapse rate in the region of plume rise and the occurrence and strength of any inversion which is limiting the mixing must be known. It is recommended that minisondes be released once or twice a day and be used in conjunction with improved mixing height models such as have been recently developed, for example, by Kumar (1978b) at Syncrude Canada Ltd. It must be emphasized that accurate mixing height information is vital for realistic plume modeling results. If the plume rises above the mixing height, then the ground level concentrations will be very low. If only long-term average concentrations are needed, the necessity of routine minisondes can be relaxed. However, a mixing height climatology would still be highly desirable.

The prediction of σ_z by the TVA scheme in the environmentally dominated region requires a temperature lapse rate. The meteorological tower at the Lower Syncrude site may give anomalous stability estimates in stable conditions due to the valley effects. A minisonde temperature profile (updated by a model perhaps) is desirable. A back-up system of perhaps 3 temperatures sensors over the upper 50 m of the tower is worthwhile. Data from temperature sensors on meteorological booms on the main industrial stacks may be useful; however there may be significant interference problems from the stacks themselves.

A minisonde could also give an estimate of the wind profile. Wind estimates are necessary for both plume rise and all the recommended sigma schemes. A wind speed sensor on the meteorological tower (or on the industrial stacks) could be used together with power law extrapolations to higher levels. The extrapolation of wind speed to higher levels would not always be suitable in stable conditions. However, in such stable conditions, the main plume would probably not be mixing down to the ground until fumigation, by which time the extrapolation techniques would be reasonably valid.

The determination of the effects of shear-enhanced dispersion require a wind direction profile obtainable from a minisonde.

The Draxler and the Pasquill 1976 schemes both require estimates of the wind direction fluctuations, σ_θ. A directional vane on the meteorological tower could give reasonable estimates if $\sigma_v = (\overline{U}\ \sigma_\theta)$ is assumed constant with height (Panofsky 1973). Again the wind speed is needed for the extrapolation to obtain σ_θ at plume height. If the plume is in a stable layer aloft and the σ_θ measurement is in the mixed layer then rough estimates of σ_θ for the Draxler or Pasquill 1976 schemes can be had from the BNL relationships between σ_θ and lapse rate/wind characteristics as presented earlier in the discussion of the BNL scheme in Chapter 4. The BNL curves themselves are <u>not</u> recommended. Although such estimates of σ_θ from the BNL table are very approximate, the spreading of the plume will be of less concern if it remains in the elevated stable layer above the mixed layer. Once the plume is in the mixed layer, the mixed layer σ_θ obtainable from tower measurements will be applicable.

If the plume is in the mixed layer in convective conditions and if σ_θ measurements are unavailable, then results of free convection theory can be used to estimate σ_θ. Such estimates require that the heat flux be measured from the meteorological tower. In this situation

$$\sigma_\theta = \frac{\sigma_v}{\overline{U}} = 0.6 \frac{w_*}{\overline{U}} \tag{9.12}$$

where

$$w_* = \left(\frac{g}{T} Q_o Z_i \right)^{1/3} \tag{9.13}$$

where T is temperature, Q_o is the surface heat flux and Z_i is the height of the inversion. The coefficient of 0.6 in (9.12) is following a review by Panofsky (1978). The surface heat flux could be measured directly using eddy correlation techniques on the bivane and temperature sensor signal outputs on the meteorological tower or estimated from solar radiation and albedo estimates; (a validation study might be necessary for this latter technique). An estimate of Q_o can also be made solely from the elevation angle measurements from the bivane on the meteorological tower as outlined below (9.14).

Draxler's approach for σ_z specification in unstable conditions requires estimates of the standard deviation of the vertical velocity, σ_w. Direct measurements from a bivane on the top of the meteorological tower at lower Syncrude would probably be adequate when combined with the free convection result to scale the tower measurement to plume height (following Panofsky 1978):

$$\sigma_w \simeq 1.33 \left(\frac{g \; Q_o \; Z}{T} \right)^{1/3} \tag{9.14}$$

where Z is the height and other quantities are as defined below (9.13). Note that with the bivane measurement of $\sigma_w = (\overline{U} \, \sigma_e)$, where σ_e is the standard deviation of the elevation angle), an estimate of the heat flux can be made if we assume free convective scaling is valid. The height, Z, in (9.14) may have to be chosen carefully. If the wind is from the West, for instance, the effective height at the top of the Lower Syncrude tower may be approximately the height above the Mildred Lake airstrip.

In summary, the recommended meteorological sensors are:

(a) a bivane at the top of the 150 m meteorological tower

(b) minisonde launch twice per day

(c) 3 temperature sensors spaced along the top 50 m of the tower (useful but not necessary if minisondes are used).

The tower at Supertest Hill or one of the large industrial stacks with a meteorological instrument boom could be used in lieu of the 150 m tower at Lower Syncrude. With the above instrumentation properly interfaced to a recording and analysis system, routine estimates of the plume sigma values could be made. The number of minisondes might need to be increased until an adequate numerical model for estimating mixing heights is operational.

10. RECOMMENDATIONS

10.1 PRIORITIES

The priority of the unresolved problems is determined by the priorities of desired air quality model outputs. It is recommended that the results of the user-survey study presently underway be incorporated with the results of the present study to ensure that the important time and space scales of interest can be handled by the recommended sigma specification scheme outlined in Chapter 9. In addition, the priorities of the unresolved problems in the sigma specification scheme and the need for additional intensive field studies should be revised, as necessary, based upon the user survey results.

10.2 MEASUREMENTS ON A CONTINUOUS BASIS

The data requirements for the routine specification of plume sigmas were outlined in some detail in the previous chapter. It is recommended that tower-based bivane and temperature data be collected, processed and digitally recorded. The existing 150 m meteorological tower at the Lower Syncrude site is adequate. Alternative (or back-up) installations could be located at the tower on Supertest Hill or on a meteorological instrument boom on any of the larger industrial stacks. It is suggested that the real time data be processed to produce 10-minute averages and standard deviations of wind speed, azimuth and elevation angles, temperature, and the product of elevation angle and temperature.

Routine minisondes are highly recommended in order to determine the temperature and wind profiles and most important, the mixing height and strength of inversions. The frequency of the minisonde flights would depend upon the adequacy of the mixing height models to predict the necessary input for plume rise and sigma estimates. Initially, it is recommended to

proceed with twice daily minisonde flights perhaps at early to mid-morning and then in late afternoon. The timing of the flights may be changed depending upon whether a monitoring of the climatology or a predicting of conditions in time for application of supplementary emission controls is desired.

A development of a mixing height and dispersion climatology is highly recommended. In order to assess long-term environmental loading in a reasonably accurate way, the existing climatological data should be applied to the recommended sigma schemes to generate a sigma climatology. The climatological dispersion model (CDM) results may have fulfilled this requirement already. However, the CDM results are only as good as the data and adopted formulations. It is considered to be worthwhile to review the CDM assumptions and input data to ensure the results are adequate for the intended purposes. The mixing height is a crucial determinant of ground level concentrations as has been emphasized by Dr. Christie of AES. A continuing minisonde program appears to be the only viable way to generate the mixing height climatology until accurate numerical models of mixing height have been validated.

10.3 INTENSIVE FIELD STUDIES

A number of unresolved problems have been identified in this study. The priority of the problems depends to a considerable extent upon the priorities of the desired air quality outputs. However a preliminary ranking can be attempted.

Determination of mixing height with respect to plume rise is probably the most important area of uncertainty. No reliable procedures for estimating ground level concentrations can be developed without acceptable mixing height and plume rise formulations. The plume rise predictions appear to be in reasonable shape when the stability and wind charactertistics of the boundary layer are known. Thus, it is the prediction of boundary layer

profiles and in particular, of mixing height which needs attention. One of the objectives of any future intensive field study should be the generation of a data set for the improvement and validation of mixing height models. Ideally the mixing height models should be able to predict the temperature profile given routine meteorological inputs. The more easily obtainable meteorological inputs may include solar radiation surface albedo, season (for an estimate of evaporation and transpiration effects), cloud cover, tower level winds, etc. The routine minisondes recommended above should provide a reasonable data set for development of the mixing height model. However, a series of more frequent minisondes possibly combined with tethersonde and plume rise observations is recommended at the stage of model validation.

The existing plume sigma data base is weakest at the downwind distances typical of maximum ground level concentrations. One of the reasons for this is that plume photography data have been concentrated in the region of maximum plume rise (less then about 1 km) and the immersion sensors have concentrated in the region where statistical sampling problems are less severe (typically greater than 3 km). Especially in mixed and unstable conditions, the region between 1 and 3 km downwind of the source is very important. It is recommended that any future intensive field study concentrate on the downwind range of 1 to 5 km with special consideration given to the inherent sampling problems and with detailed co-ordination between the immersion sensing and photographic systems.

A possible uncertainty which has not been discussed previously is the interaction of the plume material with the surface vegetation. Gaussian models treat the surface as a perfectly reflecting surface. This approximation may be reasonable during the biologically dormant season. However, during the active growing season, the work of Martin and Barber (1971) suggests

that this assumption is not valid. Actively transpiring vegetation may absorb a very large fraction of the ground level SO_2. If this is the case for certain seasons in the AOSERP region, then the lower boundary in numerical dispersion models should perhaps be treated as an absorbing surface. The virtual image sources used in the Gaussian models would then have to be very significantly changed. Ground level concentrations predicted by classical Gaussian models might be as much as a factor of 2 too large. It is recommended that this problem be resolved through either a literature research or detailed near-surface concentration gradient measurements prior to model validation studies.

10.4 CO-ORDINATION OF FIELD STUDIES

Improved co-ordination of any future field study is strongly recommended. It is recommended that detailed plans be developed for co-ordination of measurements by all sensor systems prior to the field study to ensure an overlapping of measurement times and an optimum selection of measurement downwind distances. It is recommended that the measurements in the field be very closely co-ordinated with clearly defined authority vested in a scientific co-ordinator who will make on-site decisions based upon a previously accepted set of priorities. The selection of data for detailed processing should be made on the basis of the overall data quality for that case study and not on the basis of data quality for an individual sensor system.

The processing techniques for sigma computations should be standardized. The definitions of sigmas may have to be somewhat different depending upon the sensor characteristics. However, alternative ways of calculating sigmas should be intercompared on a test set of data to ensure that sigma values from the different sensor systems can be treated together as a single population of statistics without systematic discrepancies.

A case study approach should be implemented for the discussion of the results. All data should be applied to the specific problems and objectives of the study. The chapters of the overall report should reflect the various study objectives not the sensor systems.

11. CONCLUSIONS

This study has consisted of a detailed review and assessment of the AOSERP plume sigma data base and an application of that data base to a variety of widely used typing schemes in order to derive a useful procedure for predicting the plume sigma values. The following conclusions summarize the study:

(a) A review of the theory and previous experimental results of plume rise and dispersion showed that diffusion from an industrial stack should be treated as a 2-stage process: a source-dominated stage and an environmentally dominated stage.

(b) The transition from the source-dominated to the environmentally dominated stages, the sigma transition, probably occurs when the plume and environmental dissipation rates are equal. Beyond the sigma transition point, the concept of plume entrainment is inappropriate. The sigma transition point, although clear theoretically, is difficult to specify accurately in practise. Typically it occurs at about 1 or 2 kms downwind from the stack but closer to the stack in vigorously convective situations.

(c) A review of the theoretical and experimental bases of commonly used sigma specification schemes showed that many of these schemes have been extrapolated far beyond the range of supporting measurements. These extrapolations are often inconsistent with theory and with other typing schemes.

(d) The AOSERP data base from the three intensive field studies were critically reviewed.

The review showed that there were few times with multiple sensor overlappings of analyzed data; so that the advantages of having simultaneous measurements were often lost.

The techniques of calculating plume sigma values were not standardized between groups; so that unnecessary discrepancies between data sets were generated.

There were problems in baseline removal and noise filtering; these were corrected for the aircraft data by modifying some of the previous σ_y values; the sigma values from the LIDAR data could not be used.

There were uncertainties in the adoption of the 10% criterion for plume photography analysis which probably generated systematic errors in σ_z close to the stack and beyond about 1 km downwind of the stack.

There were some major inconsistencies in the minisonde data which were probably due to the use of an assumed rise rate when data from only one theodolite were available; comparisons of minisondes for all sites and for times before and after the time of interest were essential to ensure a proper estimate of the wind and temperature profiles.

The tethersonde data may have a systematic error in the σ_θ estimates; the σ_θ estimates were often much larger than $\sigma_u/\overline{U}$ from the tethersonde; the aircraft values for roughly equivalent averaging times tended to agree with the $\sigma_u/\overline{U}$ estimates.

(e) All sensors which traverse the plume are measuring relative dispersion; there is no averaging time associated with such

a measurement. Confusion on this point is common in the literature.

(f) A review and analysis of wind direction shear effects showed that wind direction shear has three distinct effects upon a plume: change in the bearing of the plume as it rises, distortion of the plume cross-sectional shape, and shear-enhanced dispersion.

(g) Shear-enhanced dispersion may sometimes be a dominant determinant of the plume σ_y value for downwind distances of about 10 km and greater. Vertical mixing in conjunction with shear produces shear-enhanced dispersion. The most important shear effects appeared to occur for moderate levels of shear. Very large shears were usually associated with very weak vertical mixing and often had only a small degree of shear-enhanced dispersion.

(h) In the source-dominated region, plume rise and σ_z could be specified fairly well using the procedures recommended by Briggs (1975). There were uncertainties in the σ_y/σ_z ratio, but a tentative value of 1.4 is recommended based upon a very limited data set.

(i) In the environmentally dominated phase of dispersion, σ_y was best estimated using the Pasquill-1976 or Draxler formulations. These schemes involve σ_y specification in terms of the wind direction fluctuation standard deviation, σ_θ, and are modifications of Taylor's statistical theory. The predictions of the Pasquill 1976 scheme should be increased by about 20 to 25%.

(j) In the environmentally dominated stage of dispersion, σ_z is estimated adequately in stable conditions by the TVA scheme. In connective conditions, the Draxler scheme is tentatively recommended.

(k) A practical procedure was outlined for obtaining the input data required for the recommended sigma specification schemes. The recommended data sources were a tower bivane and temperature system, combined with routine minisondes.

(l) There was no obvious direction dependence shown by the normalized σ_y values. However this result is tentative due to the limited data set.

(m) The adequacy of sigma specification schemes is determined by their intended use. Specific case study predictions, as in a regulatory application, may require accurate estimates for extreme environmental conditions and case-specific meteorological data. Predictions of annual seasonal loadings, in contrast, may not be significantly adversely affected by anomalous predictions if they average out. For long-term loadings, a climatological average of the meteorological dispersion determinants, not specific data, is required. A clearer definition of the priority of model uses is required. The direction of future research efforts should be guided accordingly.

(n) Determination of mixing heights is very important for air quality modeling. Further improvements, validation and implementation of a mixing height model used in conjunction with minisondes is strongly recommended.

(o) The major areas of uncertainty were identified as: prediction of mixing heights and lapse rates, the plume geometry in the range of 1 to 3 km downwind, the specification of plume geometry in the vertical in unstable conditions, and the significance of surface absorption of SO_2 upon ground level concentrations.

This study provided a first synthesis and critical review of the air quality data set generated by AOSERP. It provided an evaluation of the various schemes for estimating the dispersion coefficients for use in a Gaussian model. Some of the dispersive mechanisms such as initial dilution and shear have been reviewed and specific procedures for handling them have been recommended. Although some of the specific data interpretations, recommendations and conclusions may need to be modified in the light of future research, it is felt that this study will serve as a major resource for numerical modeling and other future air quality studies undertaken in the AOSERP study region.

12. REFERENCES CITED

Alberta Environment. 1978. Guidelines for plume dispersion calculations. Standards and Approvals Division, Environmental Protection Service of Alberta Environment. 108 pp.

Blackman, R. B. and J. W. Tukey. 1959. The measurement of power spectra. Dover, New York. 190 p.

Briggs, G. A. 1964. A smoke plume rise theory. Preliminary Report, Atmospheric Turbulence and Diffusion Laboratory, Oak Ridge, Tenn.

Briggs, G. A. 1969. Plume rise. US AEC, Oak Ridge, Tennessee. 81 pp.

Briggs, G. A. 1975. Plume rise predictions. In D. A. Haugen (Ed.), Lectures on Air Pollution and Environmental Impact Analyses. Amer. Met. Soc., Boston. p. 59-111.

Bringfelt, B. 1969. A study of buoyant chimney plumes in neutral and stable atmospheres. Atmos. Env., 3: 609-623.

Brown, R. M., L. Cohen, and M. E. Smith. 1972. Diffusion measurements in the 10-100 km range. JAM 11: 323-334.

Brown R. M. and P. Michael. 1974. Measured effect of shear on plume dispersion. In Symp. on Atm. Diff. and Air Pollution, Santa Barbara. Amer. Met. Soc., Boston. P. 246-250.

Calder, K. L. 1965. On the equation of atmospheric diffusion. QJRMS 91: 514-517.

Carpenter, S. B., T. L. Montgomery, J. M. Leavitt, W. C. Colbaugh, and F. W. Thomas. 1971. Principal plume dispersion models: TVA power plants. JAPCA 21: 491-495.

Caughey, S. J. and C. J. Readings. 1974. The vertical component of turbulence in convective conditions. In Turbulent diffusion in environmental pollution, Advances in Geophysics, 18A. Academic Press. New York and London. p. 125-130.

Corrsin, S. 1974. Limitations of gradient transport models in random walks and in turbulence. In Turbulent diffusion in environmental pollution. Adv. in Geophysics, 18A, Academic Press, New York and London. p. 25-60.

Cramer, H. E. 1957. A practical method for estimating the dispersal of atmospheric contaminants. Proc. of First Nat. Conf. on App. Met. Soc., Hartford, Conn. p. C-33 to C-55 (information from Gifford 1976 .)

Cramer, H. E., F. A. Record and H. C. Vaughan. 1959. The study of the diffusion of gases or aerosals in the lower atmosphere. AFRCL Tech. Report No. 59-207. 33p.

Cramer, H. E., G. M. Desanto, R. K. Dumbauld, P. Morgenstern, and R. N. Swanson. 1964. Meteorological prediction techniques and data system. Report GCA-64-3-G prep. for Geophysical Corp. of America, Bedford, Mass. (Information from Islitzer and Slade 1968 .)

Csanady, G. T. 1969. Diffusion in an Ekman Layer. J. Atmos. Sci. 26: 414-426

Csanady, G. T. 1973. Turbulent diffusion in the environment. D. Reidel. Dordrecht, Netherlands. 248 pp.

Davison, D. S., C. C. Fortems, and K. L. Grandia. 1977. Plume dispersion measurements from an oil sands estraction plant, March 1976. Prepared for AOSERP by Intera. AOSERP Report 13. 195 pp.

Davison, D. S. and K. L. Grandia. 1978. Plume dispersion measurements from an oil sands extraction plant, June 1977. Prepared for AOSERP by Intera. Project ME 2.3.2. 194 pp.

Deardorff, J. W. and G. E. Willis. 1975. A parameterization of diffusion into the mixed layer. J. Appl. Met. 14: 1451-1458.

Draxler, R. R. 1976. Determination of atmospheric diffusion parameters. Atm. Env., 10: 99-105.

Egan, B. 1975. Turbulent diffusion in complex terrain. In D. A. Haugen (Ed.), Lectures on Air Pollution and Environmental Impact Analyses. Amer. Met. Soc., Boston. p. 112-135.

Fanaki, F., compiler. 1978a. Meteorology and air quality winter field study in the AOSERP study area, March 1976. Prepared for AOSERP by Atmospheric Environment Service. AOSERP Report 27. 249 pp.

Fanaki, F., compiler. 1978b. Alberta oil sands environmental winter study, February 1977. Draft of report prepared for AOSERP prepared by Atmospheric Environment Service. Project ME 1.5.2 and ME 3.5.1. 135 pp.

Fanaki, F., compiler. 1978c. Meteorology and air quality summer field study in the AOSERP study area, June 1977. Preliminary draft prepared for AOSERP by Atmospheric Environment Service.

Gifford, F. A. 1957. Relative atmospheric diffusion of smoke puffs, J. Met., 14: 410-414.

Gifford, F. A. 1961. Use of routine meteorological observations for estimating atmospheric dispersion. Nucl. Safety, 2: 47-51.

Gifford, F. A. 1968. An outline of theories of diffusion in the lower layers of the atmosphere. In D. H. Slade (Ed.), Meteorology and atomic energy. USAEC. NTIS Report TID-24190 TID-24190. US Department of Com., Springfield, Virginia. p. 65-116.

Gifford, F. A. 1975. Atmospheric dispersion models for environmental pollution application. In D. A. Haugen (Ed.), Lectures on Air Pollution and Environmental Impact Analysis. Amer. Met. Soc., Boston.

Gifford, F. A. 1976. Turbulent diffusion-typing schemes : a review. NUC Safety 17: 68-86.

Halitsky, J. 1961. Single camera measurement of smoke plumes, Int. J. Air and Water Poll. 4: 185-198.

Hanna, S. R., G. A. Briggs, J. Deardorff, B. A. Egan, F. A. Gifford and F. Pasquill. 1977. AMS workshop on stability classification schemes and sigma curves - summary of recommendations. Bulletin American Met. Soc., 58: 1305-1309.

Hay, J. S. and F. Pasquill. 1959. Diffusion from a continuous source in relation to the spectrum and scale of turbulence. In F. N. Frankiel and P. A. Sheppard (Eds.). Advances in Geophysics. Vol. 6, Academic Press, New York. p. 345-365.

Herbert, G. A. 1971. Energy profiles of small-scale wind fluctuations. In I. Van derHoven (Ed.), Atmospheric transport and diffusion in the planetary boundary layer. NDAA Tech. Memo. ERL ARL-32, 10-17. (Information from Briggs 1975 .)

Hino, M. 1968. Maximum ground level concentration and sampling time. Atm. Env. 2: 149-166.

Hoff, R. and F. Froude. 1978. LIDAR observation of plume dispersion in northern Alberta. Draft of paper submitted to Atmos. Environment.

Hoff, R., M. Millan, and A. Gallant. 1978. In F. Fanaki, comiler. 1978a. Meteorology and air quality winter field study in the AOSERP study area. March 1976. Prepared for AOSERP by Atmospheric Environment Service. AOSERP Report 27. p. 92-123.

Hogstrom, U. 1964. An experimental study on atmospheric diffusion. Tellus 16: 205-251.

Holland, J. Z. 1953. A meteorological survey of the Oak Ridge area: final report covering the period 1948-1952. US. AEC Report ORO-99, Weather Bureau, Oak Ridge, Tennessee. (Information from Islitzer and Slade 1968 .)

Islitzer, N. and D. Slade. 1968. Diffusion and transport experiments. In D. H. Slade (Ed.), Meteorology and atomic energy, USAEC. NTIS Report TID-24190. US Dept. of Com., Springfield, Virginia. p. 117-188.

Kaimal, J., J. Wyngaard, Y. Izumi, and O. Cote. 1972. Spectral characteristics of surface-layer turbulence. QJRMS 98: p. 563-589.

Kaimal, J. C., J. C. Wyngaard, D. A. Haugen, O. Cote, Y. Izumi, S. J. Caughey, and C. J. Readings. 1976. Turbulence structure in the convective boundary layer. JAS 33: 2152-2169.

Kerman, B. and H. E. Turner. 1978. An application of acoustic sounding to the estimation of mixing depth and vertical plume spread in the Alberta oil sands area. In F. Fanaki, compiler, 1978a. Meteorology and air quality in the AOSERP study area, March 1976. Prepared for AOSERP by Atmospheric Environment Service. p. 22-47.

Klein, G. and R. Bourke. 1967. An audio modulated tethersonde package for detailed micrometeorological sounding. JAM 6: 707-716.

Kumar, A. 1978a. Pollutant dispersion in the planetary boundary layer. Syncrude Canada Ltd. Prof. Paper 1978-1.

Kumar, A. 1978b. Numerical modeling of the development of the thermal boundary layer near a synthetic crude oil plant. Syncrude Canada Ltd. Prof. Paper 1978-4.

Lenshow, D. H. 1970. Airplane measurements of planetary boundary layer structure. JAM 9: 874-884.

Lumley, J. and H. Panofsky. 1964. The structure of atmospheric turbulence. Interscience, a div. of Wiley & Sons, New York, London, and Sidney. 239 pp.

Lusis, M. A. 1976. The effect of sample humidity on the response characteristics of SO_2 and NO_x analyser systems. Report ARQA 31-76, Atmospheric Chemistry Division, Atmospheric Environment Service, Downsview, Ontario.

Martin, A. and F. Barber. 1971. Some measurements of loss of atmospheric sulphur dioxide near foliage. Atm. Env. 5: 345-352.

Mickle, R. and D. S. Davison. 1974. Results from sea trials of a new boundary layer tethersonde package. Paper at 8th Congress of CMOS, York University, Toronto.

Mickle, R., L. Guise - Bagley, and W. Kobelka. 1978. Tethersonde. In Fanaki, F., compiler. 1978a. Meteorology and air quality winter field study in the AOSERP study area, March 1976. Prepared for AOSERP by Atmospheric Environment Service. AOSERP Report 27. p. 11-21.

Millan, M. 1976. A note on the geometry of plume diffusion measurements. Atm. Env. 10: 655-658.

Millian, M. and R. Hoff. 1978. Remote sensing of air pollutants by correlation spectroscopy: instrumental response characteristics. Submitted to Atm. Env.

Monin, A. S. 1965. Structure of an atmospheric boundary layer. IZV. ANSSSR, Ser. Atm. and Oceanic Phys. 1: 3,258. (Information from Pasquill 1974 .)

Montgomery, T. L., S. B. Carpenter, W. C. Colbaugh and F. W. Thomas. 1972. Results of recent TVA investigations of plume rise. JAPCA 22: 779-784.

Morton, B. G., I. Taylor, J. S. Turner. 1956. Turbulent gravitational convection from maintained and instantaneous sources. Proc. Roy. Soc. (London), Ser. A. 234: 1 - 23.

Panofsky, H. 1978. Matching in the convective planetary boundary layer. JAS. 35: p. 272-276.

Panofsky, H. 1973. Tower micrometeorology. In D. A. Haugen (Ed.), Workshop on micrometeorology. Amer. Met. Soc., Boston. p. 151-176.

Pasquill, F. 1961. The estimation of the dispersion of windborne material. Met. Mag. 90: 33-49.

Pasquill, F. 1969. The influence of turning of the wind with height on crosswind diffusion. Phil. Trans. Roy. Soc. London, 265: 173-181.

Pasquill, F. 1971. Atmospheric dispersion of pollution - Presidential Address. QJRMS 97: 369-395.

Pasquill, F. 1974. Atmospheric diffusion. Ellis Horwood. Chichester, U.K. 429 p.

Pasquill, F. 1975. The dispersion of material in the atmospheric boundary layer - the basis for generalization. In D. A. Haugen (Ed.), Lectures on Air Pollution and Environmental Impact Analyses. Amer. Met. Soc., Boston. p. 1-34.

Pasquill, F. 1976. Atmospheric dispersion parameters in Gaussian plume modelling. Part II. Possible requirements for change in the Turner Workbook values. U.S. EPA Report EPA - 600/4-76-030b. Research Triangle Park, North Caroline. 12 pp.

Randerson, D. 1972. Temporal changes in horizontal diffusion parameters of a single nuclear debris cloud. JAM. 11: 670-673.

Richards, J. M. 1963. Experiments on the motions of isolated cylindrical thermals through unstratified surroundings. Int. J. Air Water Pollut. 7: 17-34.

Saffman, P. G. 1962. The effect of wind shear on horizontal spread from an instanteneous ground source. QJRMS. 88: 382-393.

Shelfentook, W. 1978. An inventory system for atmospheric emissions in the AOSERP study area. Prep. for AOSERP by SNC Tottrup. AOSERP Report 29, 58 pp.

Shelland, H. C. 1968. Results of some recent special measurements in the United Kingdon relevant to wind loading problems. Proc. Int. Symp. on Wind Effects on Buildings and Structures. Ottawa. University of Toronto Press. Information from Pasquill 1974 .)

Singer, I. A. and M. E. Smith. 1966. Atmospheric dispersion at Brookhaven National Laboratory. Int. J. of Air and Water Poll. 10: 125-135.

Slawson, P. and G. Csanady. 1967. On the mean path of buoyant, bent-over chimney plumes. JFM 47: 33-40.

Slawson, P. and G. Csanady. 1967. On the mean path of buoyant, bent-over chimney plumes. JFM 47: 33-40.

Slawson, P. and G. Csanady. 1971. The effect of atmospheric conditions on plume rise. JFM 47: 33-40.

Slawson, P., G. Davidson, W. McCormick and G. Raithby. 1978. A study of dispersion characteristics of the GCOS plume. Prep. for Syncrude Canada Ltd., Edmonton. 112 pp.

Smith, F. B. 1965. The role of wind shear in horizontal diffusion of ambient particles. QJRMS, 91: 318-329.

Smith, M. 1968. Recommended guide for the prediction of the dispersion of airborne effluents. Amer. Soc. of Mech. Eng. New York. 84 pp.

Sutton, O. G. 1953. Micrometeorology. McGraw Hill, New York, Toronto and London. 333 pp.

Taylor, G. I. 1953. Dispersion of soluble material in solvent flowing slowly through a table. Proc. Royal Soc. London A. 219:186. (Information from Pasquill 1974 .)

Telford, J. W. 1966. The convective mechanism in clear air. JAS 23: 652-665.

Tennekes, H. and J. Lumley. 1972. A first course in turbulence. MIT Press. Cambridge Mass. 300 pp.

Thompson, M. D., M. C. Wride, and M. E. Kirby. 1978. Ecological habitat mapping of the AOSERP study are: phase 1. Prep. for AOSERP by Intera. AOSERP Report 31. 176 pp.

Thyer, N. 1962. Double theodolite pibal evaluation by computer. JAM 1: 66-68.

Turner, D. B. 1970 (revised). Workbook of atmospheric dispersion estimates. U.S. EPA, Research Triangle Park, N.C. 84 pp.

US Nuclear Regulatory Commission. 1972. NRC Regulatory Guide 1.23. (Information from Islitzer and Slade 1968 .)

Vickers, G. 1976. A method for determining smoothed wind and temperature profiles from minisonde data. Unpublished manuscript, Atm. Env. Serv., Toronto. 21 May 1976.

Walmsley, J., A. Arnold and G. Vickers. 1978. Minisonde. In F. Fanaki, compiler, 1978a. Meteorology and air quality winter field study in the AOSERP study area, March 1976. Prep. for AOSERP by Atmosphere Env. Serv. p. 5-10.

Weber, A. 1976. Atmospheric dispersion parameters in Gaussian plume modeling, Part I. Review of current systems and possible future developments. US EPA Report No. EPA - 600/4-76-030a. Research Triangle Park, N.C. 58 pp.

13. APPENDIX

13.1 ERROR ANALYSIS OF PLUME RISE AND σ_z FROM PLUME PHOTOGRAPHY

The objective of this error analysis is to obtain expression for the actual downwind distance and plume height compared to the assumed values (i.e. measured ones) in terms of the geometry of the measurement. The analysis is based upon the geometry as outline in the plane view and the vertical view of the plume shown in Figure 54.

The first stage is the calculation of the true camera-plume separation for an assumed direction error of α, and for a plume sighting at an angle Θ from the plume axis (angle $90^{o} - \Theta$ from the perpendicular to the plume).

W_m = assumed distance from the camera to the plume centerline = $B/\sin \Theta$ (A.1)

W = real distance from the camera to the plume centerline

= $W_m + V/\sin \Theta$

= $(B + V)/\sin \Theta$ (A.2)

If Z is the true vertical extent for a given subtended angle, ϕ, and if Z_m is the assumed vertical extent (as shown in Figure 54,

Plan View:

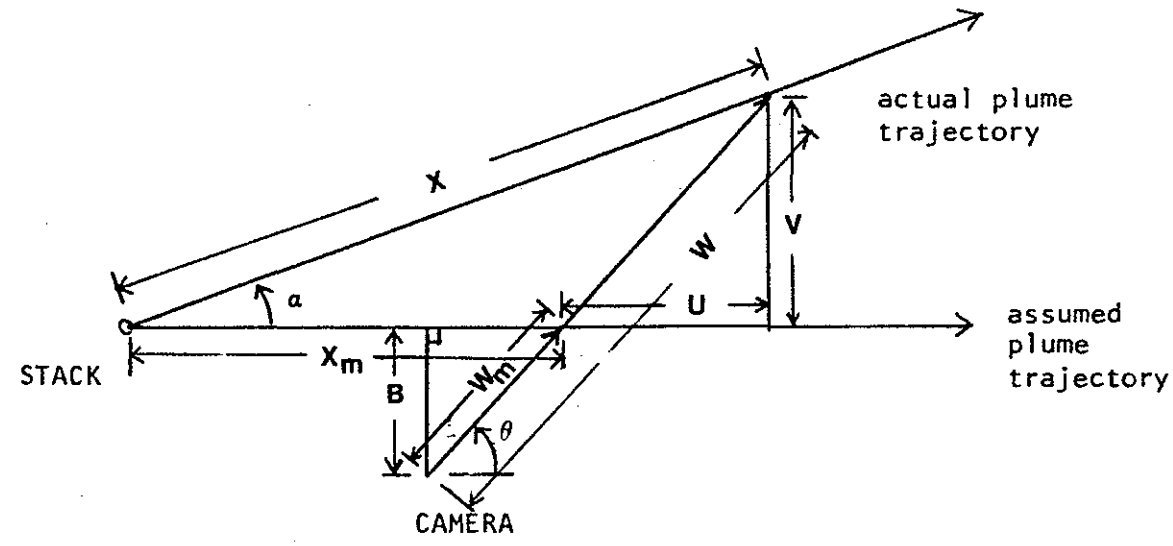

Vertical View:

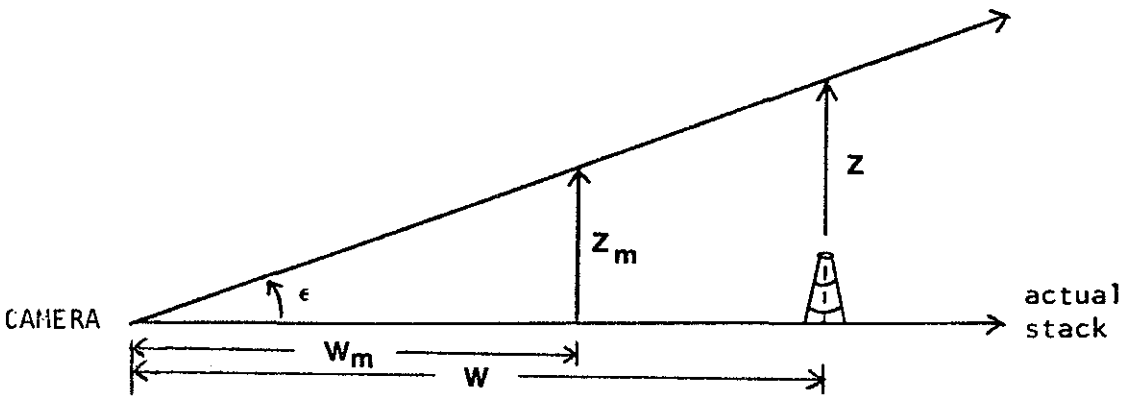

Figure 54. Plan and vertical views of the geometry of plume photography measurement errors.

then,

$$\frac{Z}{Z_m} = \frac{W}{W_m} = \frac{B + V}{B} \tag{A.3}$$

but,

$$V = X \sin \alpha \tag{A.4}$$

Therefore X must be expressed in terms of X_m, α, Θ to solve for the errors in the vertical given by (A.3). From the geometry shown in Figure 54,

$$X \cos \alpha = X_m + U \tag{A.5}$$

$$X \sin \alpha = V \tag{A.6}$$

$$V = U \tan \Theta \tag{A.7}$$

and so,

$$X \cos \alpha = X_m + \frac{V}{\tan \Theta}$$

$$= X_m + \frac{X \sin \alpha}{\tan \Theta} \tag{A.8}$$

$$X_m = X \left(\cos \alpha - \frac{\sin \alpha}{\tan \Theta} \right) \tag{A.9}$$

$$\frac{X}{X_m} = \left(\cos \alpha - \frac{\sin \alpha}{\tan \Theta} \right)^{-1}$$

$$= \left[\sin \alpha \, (\cot \alpha - \cot \Theta) \right]^{-1} \tag{A.10}$$

Replacing X in (A.4) and V in (A.3),

$$\frac{Z}{Z_m} = \frac{B + X \sin \alpha}{B} = 1 + \frac{X \sin \alpha}{B} \qquad (A.11)$$

$$\frac{Z}{Z_m} = 1 + \frac{X_m \sin \alpha}{B\left(\cos \alpha - \frac{\sin \alpha}{\tan \Theta}\right)} \qquad (A.12)$$

or

$$\left[\frac{Z}{Z_m} = 1 + \frac{X_m}{B\ (\cot \alpha - \cot \Theta)} \right] \qquad (A.13)$$

The size of the errors due to errors in the angles and distances involved in the plume photography have been evaluated in Chapter 5 (Table 12).

14. AOSERP RESEARCH REPORTS

1.		AOSERP First Annual Report, 1975
2.	AF 4.1.1	Walleye and Goldeye Fisheries Investigations in the Peace-Athabasca Delta--1975
3.	HE 1.1.1	Structure of a Traditional Baseline Data System
4.	VE 2.2	A Preliminary Vegetation Survey of the Alberta Oil Sands Environmental Research Program Study Area
5.	HY 3.1	The Evaluation of Wastewaters from an Oil Sand Extraction Plant
6.		Housing for the North--The Stackwall System
7.	AF 3.1.1	A Synopsis of the Physical and Biological Limnology and Fisheries Programs whithin the Alberta Oil Sands Area
8.	AF 1.2.1	The Impact of Saline Waters upon Freshwater Biota (A Literature Review and Bibliography)
9.	ME 3.3	Preliminary Investigations into the Magnitude of Fog Occurrence and Associated Problems in the Oil Sands Area
10.	HE 2.1	Development of a Research Design Related to Archaeological Studies in the Athabasca Oil Sands Area
11.	AF 2.2.1	Life Cycles of Some Common Aquatic Insects of the Athabasca River, Alberta
12.	ME 1.7	Very High Resolution Meteorological Satellite Study of Oil Sands Weather: "A Feasibility Study"
13.	ME 2.3.1	Plume Dispersion Measurements from an Oil Sands Extraction Plant, March 1976
14.		
15.	ME 3.4	A Climatology of Low Level Air Trajectories in the Alberta Oil Sands Area
16.	ME 1.6	The Feasibility of a Weather Radar near Fort McMurray, Alberta
17.	AF 2.1.1	A Survey of Baseline Levels of Contaminants in Aquatic Biota of the AOSERP Study Area
18.	HY 1.1	Interim Compilation of Stream Gauging Data to December 1976 for the Alberta Oil Sands Environmental Research Program
19.	ME 4.1	Calculations of Annual Averaged Sulphur Dioxide Concentrations at Ground Level in the AOSERP Study Area
20.	HY 3.1.1	Characterization of Organic Constituents in Waters and Wastewaters of the Athabasca Oil Sands Mining Area
21.		AOSERP Second Annual Report, 1976-77
22.		Alberta Oil Sands Environmental Research Program Interim Report to 1978 covering the period April 1975 to November 1978
23.	AF 1.1.2	Acute Lethality of Mine Depressurization Water on Trout Perch and Rainbow Trout
24.	ME 1.5.2	Air System Winter Field Study in the AOSERP Study Area, February 1977.
25.	ME 3.5.1	Review of Pollutant Transformation Processes Relevant to the Alberta Oil Sands Area

26.	AF 4.5.1	Interim Report on an Intensive Study of the Fish Fauna of the Muskeg River Watershed of Northeastern Alberta
27.	ME 1.5.1	Meteorology and Air Quality Winter Field Study in the AOSERP Study Area, March 1976
28.	VE 2.1	Interim Report on a Soils Inventory in the Athabasca Oil Sands Area
29.	ME 2.2	An Inventory System for Atmospheric Emissions in the AOSERP Study Area
30.	ME 2.1	Ambient Air Quality in the AOSERP Study Area, 1977
31.	VE 2.3	Ecological Habitat Mapping of the AOSERP Study Area: Phase I
32.		AOSERP Third Annual Report, 1977-78
33.	TF 1.2	Relationships Between Habitats, Forages, and Carrying Capacity of Moose Range in northern Alberta. Part I: Moose Preferences for Habitat Strata and Forages.
34.	HY 2.4	Heavy Metals in Bottom Sediments of the Mainstem Athabasca River System in the AOSERP Study Area
35.	AF 4.9.1	The Effects of Sedimentation on the Aquatic Biota
36.	AF 4.8.1	Fall Fisheries Investigations in the Athabasca and Clearwater Rivers Upstream of Fort McMurray: Volume I
37.	HE 2.2.2	Community Studies: Fort McMurray, Anzac, Fort MacKay
38.	VE 7.1.1	Techniques for the Control of Small Mammals: A Review
39.	ME 1.0	The Climatology of the Alberta Oil Sands Environmental Research Program Study Area
40.	WS 3.3	Mixing Characteristics of the Athabasca River below Fort McMurray - Winter Conditions
41.	AF 3.5.1	Acute and Chronic Toxicity of Vanadium to Fish
42.	TF 1.1.4	Analysis of Fur Production Records for Registered Traplines in the AOSERP Study Area, 1970-75
43.	TF 6.1	A Socioeconomic Evaluation of the Recreational Fish and Wildlife Resources in Alberta, with Particular Reference to the AOSERP Study Area. Volume I: Summary and Conclusions
44.	VE 3.1	Interim Report on Symptomology and Threshold Levels of Air Pollutant Injury to Vegetation, 1975 to 1978
45.	VE 3.3	Interim Report on Physiology and Mechanisms of Air-Borne Pollutant Injury to Vegetation, 1975 to 1978
46.	VE 3.4	Interim Report on Ecological Benchmarking and Biomonitoring for Detection of Air-Borne Pollutant Effects on Vegetation and Soils, 1975 to 1978.
47.	TF 1.1.1	A Visibility Bias Model for Aerial Surveys for Moose on the AOSERP Study Area
48.	HG 1.1	Interim Report on a Hydrogeological Investigation of the Muskeg River Basin, Alberta
49.	WS 1.3.3	The Ecology of Macrobenthic Invertebrate Communities in Hartley Creek, Northeastern Alberta
50.	ME 3.6	Literature Review on Pollution Deposition Processes
51.	HY 1.3	Interim Compilation of 1976 Suspended Sediment Date in the AOSERP Study Area
52.	ME 2.3.2	Plume Dispersion Measurements from an Oil Sands Extraction Plan, June 1977

53.	HY 3.1.2	Baseline States of Organic Constituents in the Athabasca River System Upstream of Fort McMurray
54.	WS 2.3	A Preliminary Study of Chemical and Microbial Characteristics of the Athabasca River in the Athabasca Oil Sands Area of Northeastern Alberta
55.	HY 2.6	Microbial Populations in the Athabasca River
56.	AF 3.2.1	The Acute Toxicity of Saline Groundwater and of Vanadium to Fish and Aquatic Invertebrates
57.	LS 2.3.1	Ecological Habitat Mapping of the AOSERP Study Area (Supplement): Phase I
58.	AF 2.0.2	Interim Report on Ecological Studies on the Lower Trophic Levels of Muskeg Rivers Within the Alberta Oil Sands Environmental Research Program Study Area
59.	TF 3.1	Semi-Aquatic Mammals: Annotated Bibliography
60.	WS 1.1.1	Synthesis of Surface Water Hydrology
61.	AF 4.5.2	An Intensive Study of the Fish Fauna of the Steepbank River Watershed of Northeastern Alberta
62.	TF 5.1	Amphibians and Reptiles in the AOSERP Study Area
63.	ME 3.8.3	Calculate Sigma Data for the Alberta Oil Sands Environmental Research Program Study Area.
64.	LS 21.6.1	A Review of the Baseline Data Relevant to the Impacts of Oil Sands Development on Large Mammals in the AOSERP Study Area
65.	LS 21.6.2	A Review of the Baseline Data Relevant to the Impacts of Oil Sands Development on Black Bears in the AOSERP Study Area
66.	AS 4.3.2	An Assessment of the Models LIRAQ and ADPIC for Application to the Athabasca Oil Sands Area
67.	WS 1.3.2	Aquatic Biological Investigations of the Muskeg River Watershed
68.	AS 1.5.3 AS 3.5.2	Air System Summer Field Study in the AOSERP Study Area, June 1977
69.	HS 40.1	Native Employment Patterns in Alberta's Athabasca Oil Sands Region
70.	LS 28.1.2	An Interim Report on the Insectivorous Animals in the AOSERP Study Area
71.	HY 2.2	Lake Acidification Potential in the Alberta Oil Sands Environmental Research Program Study Area
72.	LS 7.1.2	The Ecology of Five Major Species of Small Mammals in the AOSERP Study Area: A Review
73.	LS 23.2	Distribution, Abundance and Habitat Associations of Beavers, Muskrats, Mink and River Otters in the AOSERP Study Area, Northeastern Alberta
-	--	Interim Report to 1978
74.	AS 4.5	Air Quality Modelling and User Needs
75.	WS 1.3.4	Interim report on a comparative study of benthic algal primary productivity in the AOSERP study area

76.	AF 4.5.1	An Intensive Study of the Fish Fauna of the Muskeg River Watershed of Northeastern Alberta
77.	HS 20.1	Overview of Local Economic Development in the Athabasca Oil Sands Region Since 1961.
78.	LS 22.1.1	Habitat Relationships and Management of Terrestrial Birds in Northeastern Alberta.
79.	AF 3.6.1	The Multiple Toxicity of Vanadium, Nickel, and Phenol to Fish.
80.	LS 22.3.1	Biology and Management of Peregrin Falcons (*Falco peregrinus anatum*) in Northeastern Alberta.
81.	LS 22.1.2	Species Distribution and Habitat Relationships of Waterfowl in Northeastern Alberta.
82.	LS 22.2	Breeding Distribution and Behaviour of the White Pelican in the Athabasca Oil Sands Area.
83.	LS 22.2	The Distribution, Foraging Behaviour, and Allied Activities of the White Pelican in the Athabasca Oil Sands Area.

These reports are not available upon request. For further information about availability and location of depositories, please contact:

Alberta Oil Sands Environmental Research Program
15th Floor, Oxbridge Place
9820 - 106 Street
Edmonton, Alberta
T5K 2J6